Universitat Autònoma de Barcelona

Metallacarboranes: Synthesis of Boron-Heteroatom Derivatives and Applications in Energy and Magnetism

Ana Begoña Buades Martín

Universitat Autònoma de Barcelona

Metallacarboranes: Synthesis of Boron-Heteroatom Derivatives and Applications in Energy and Magnetism

Ana Begoña Buades Martín

Doctoral Thesis
Doctoral Program in Chemistry

Supervisor: Francesc Teixidor Bombardó
Tutor: Luís Escriche Martinez

Departament de Química
Facultat de Ciències

2020

ICMAB INSTITUT DE CIÈNCIA DE MATERIALS DE BARCELONA
EXCELENCIA SEVERO OCHOA
CSIC CONSEJO SUPERIOR DE INVESTIGACIONES CIENTÍFICAS

Memoria presentada para aspirar al
Grado de Doctor por

Ana Begoña Buades Martín.
Vist i plau

Prof.Francesc Teixidor Bombardó
(Supervisor)

Luís Escriche Martinez
(Tutor)

Bellaterra, 18 de Novembre de 2020

El Prof. Francesc Teixidor Bombardó, Profesor Investigador del Consejo Superior de Investigaciones Científicas (CSIC) del Instituto de Ciencia de Materiales de Barcelona (ICMAB)

CERTIFICA:

Que Ana Begoña Buades Martín, Graduada en Química y con máster en Investigación, Desarrollo, Control e innovación de medicamentos, ha realizado bajo su dirección el trabajo de tesis que lleva por título "Metalacarboranos: Síntesis de Derivados Boro-Heteroatomo y Aplicaciones en Energía y Magnetismo" que queda recogido en esta memoria para optar al título de Doctora por la Universidad Autónoma de Barcelona.

Para que así conste y tenga los efectos correspondientes, firma este certificado en Bellaterra a 18 de Noviembre de 2020

Este trabajo de Investigación ha estado financiado por la Comisión Interministerial de Ciencia y Tecnología CICYT mediante los proyectos CTQ2013-44670-R y CTQ2016-75150-R, por la Generalitat de Catalunya con el proyecto 2014/SGR/149 y por los proyecto de la Unión Europea FP7-OCEAN-2013 y H2O2O-NMBP-13-2017 , KARDIATOOL (Grant Nº-768686).

Este trabajo de investigación tiene como miembros del tribunal a:

- *Presidenta:* Dra. Emilia Morallón Núñez, Catedrática del Departamento de Química de la Universidad de Alicante.

- *Vocal:* Dra. Hong Yan, Profesora Titular del Departamento de Química de la Universidad de Nanjing.

- *Secretario:* Dr. Jordi Faraudo Gener, Científico Titular del Institut de Ciència de Materials de Barcelona (ICMAB-CSIC).

Como miembros suplentes:

- *Suplente 1:* Dr. Gonzalo Guirado López, Profesor Titular del Departamento de Química de la Universitat Autònoma de Barcelona.

- *Suplente 2:* Dra. Maria Isabel Romero García, Profesora Titular de la Universidad de Girona

Para mi abuelo Guillermo por enseñarme la importancia del saber.

Para mi madre Martina, por enseñarme la importancia del creer.

Sin ellos nunca hubiese sido posible.

Acknowledgements

El resultado de esta tesis no podría haber sido el mismo que hoy aquí se presenta si no fuese por la aportación de algunas personas que durante estos cinco años me han ayudado a crecer tanto profesional como personalmente. A todas ellas les quiero agradecer su ayuda y apoyo.

En primer lugar, quiero agradecer al Prof. Francesc Teixidor haberme elegido para desarrollar esta tesis. Gracias por los temas propuestos, por ayudarme a desarrollarlos, pero a la vez darme la independencia necesaria para aprender por mí misma y crecer como científica. En estos cinco años he aprendido muchísimo de ti, gracias por la confianza que siempre he sentido que tienes en mí y por tus sabios consejos que sin duda me serán muy útiles en esta nueva etapa científica.

Además, quiero agradecer enormemente todo su esfuerzo y dedicación a la Prof. Clara Viñas. Gracias por estar siempre disponible, por contar conmigo para múltiples colaboraciones y por haberme ayudado siempre que lo he necesitado. Tu constante dedicación a la ciencia es un ejemplo para todos.

A la Dr. Rosario Nuñez, gracias por ser mi mami del trabajo. Siempre recordaré con mucho cariño cada vez que me reñías por como tenía la mesa, sé que para tí no ha sido fácil aguantar esa mesa desordenada 5 años, pero te agradezco que nunca fueses demasiado dura. También quiero agradecerte que siempre intentases darnos una de cal y otra de arena con la organización de múltiples actividades para mantener el grupo unido. Al Dr. Pepe Giner, gracias por toda tu ayuda, sobre todo al principio cuando me enseñaste a seleccionar cristales para poder resolverlos y mil gracias por contar conmigo para ir al sincrotrón ALBA sin duda una experiencia que me hizo muchísima ilusión.

Al director del Instituto de Ciencia de Materiales de Barcelona (ICMAB-CSIC) el Prof. Xavier Obradors por acogerme en el centro. A todo el personal de administración y mantenimiento, siempre disponibles y resolutivos, sin duda

ambos equipos sois de 10. Sin embargo, quiero agradecer de forma especial a Maria Rivera y Pietat Sierra porque habéis hecho todo lo posible por ayudarme siempre que lo he necesitado, mil gracias. También quiero agradecer a los servicios científico técnicos, tanto de la UAB como del ICMAB su ayuda y dedicación.

Al Prof. Luís Escriche de la Universidad Autónoma de Barcelona por haber aceptado la tutoría de esta tesis doctoral.

In addition, I want to acknowledge everybody that participates in some of the papers discussed in this thesis. Thank you for your contribution, with no doubt really helpful for the outcome of my work.

A Jordi Cortés, gracias a ti, nuestro laboratorio es la envidia de todos los laboratorios. Jamás vi tanto orden en un laboratorio, los productos ordenados y numerados, los cajones con dibujos…Además siempre que te he pedido que te encargases de algo me has ayudado sin dudarlo, eres fantástico.

Durante mis cinco años en este grupo he visto ir y venir a muchísimas personas, a todas ellas quiero agradecerle su aportación. A Victor Sánchez y Adnana Zaulet por haber iniciado alguno de los temas que he desarrollado en esta tesis, a Justo Cabrera por sus miles de consejos científicos y por ayudarme siempre en el laboratorio. A los compañeros con los que empecé, Flavia, Arpita, Abhishek, Ines, Mahdi y sobre todo a Isa, gracias a ti empecé esta gran aventura que hemos compartido juntas, gracias por toda tu ayuda y apoyo, sobre todo al principio cuando estaba perdidísima y gracias por compartir conmigo viajes, excursiones, cenas, deporte y mil cosas más que no caben aquí. A los que llegaron después, Lei, Isabel, Miquel, Joan, Pol, Sohini, Zheng, Jewel, specially to Zsolt for his inconditional scientific support in our common paper. Y no me olvido de dos personas que estuvieron de paso pero que fueron super importantes para mí en esta tesis. Gracias Fran por tu apoyo y largas conversaciones y mil gracias, Marcos por todo tu apoyo profesional y personal, me ha encantado coincidir contigo, nunca olvidare que me pase un congreso entero sin dormir gracias a tus ronquidos XD.

Durante toda mi estancia en el ICMAB he ido conociendo a muchísimas personas que me han aportado mil cosas diferentes, todas ellas únicas y maravillosas que no quiero dejar sin nombrar. Gracias a Juanan, Javi y Aleandro por habernos incluido en vuestro grupo tan rápidamente. Juanan, gracias por enseñarme a jugar a pádel, eres un tío 10. Javi gracias por ser mi confidente, por contar siempre conmigo y por haberme llevado al Sutton a pesar de que Natascia nos lo pusiese difícil ^^. Os recuerdo que nosotros e Isa somos los jefes fundadores de paddle + Giralda/Caleta, rituales como este han hecho mucho más llevadera la tesis. Luego llegaron Edu y Quique, que decir de vosotros…os adoro, gracias Edu por ser tan cercano y cariñoso, desde el primer momento simplemente conectamos y eres un gran amigo que espero tener siempre, ojalá hubiesen más personas como tú. Quique, has sido la alegría del grupo, mil gracias por todos esos chistes que me han hecho reír hasta morir, sin duda algunas de las arrugas de mi cara son culpa tuya XD. Gracias Francesco por todas nuestras charlas, sin duda eres una gran persona con un gran corazón muy escondido^^

Gracias al grupo Nanopto por haberme acogido a la hora de la comida y por las infinitas charlas sobre temas varios, ese break diario me ha ayudado mucho científicamente. En especial quiero agradecer a Pau, por sus findes en Llívia, para alguien como yo que vengo de Mallorca, esas noches de invierno, después de haber esquiado todo el día, delante de la chimenea con la nieve fuera es como de película, a Mayte por compartir entre otras cosas la experiencia de hacer nuestro primer muñeco de nieve, a Os, eres el único que me entiende de tu grupo XD, un millón de gracias por la gran experiencia que fue viajar a México, sin duda ha sido una de las grandes experiencias de mi vida de la que siempre tengo buenos recuerdos y sin duda no hubiese sido ni la mitad de increíble si no hubiese sido por Fendi y por ti. Leo, tú has llegado en la última etapa, pero contigo he aprendido muchísimas cosas, gracias por las largas conversaciones científicas, sin duda he aprendido muchísimo de ellas. Camilla, gracias por las mil experiencias compartidas como fiestas, viajes increíbles, findes relajantes de surf, montones de deportes nuevos… pero, sobre todo, gracias por ayudarme a aguantar al cinghiale XD, ha sido muy divertido formar equipo para reírnos de él. A Cristina, por compartir conmigo esta última etapa de escritura, por empujarme a hacer windsurf, deporte que definitivamente se ha convertido en mi favorito, por nuestros sábados de shopping y por esas largas tardes de cotilleos y confesiones,

sin duda han sido muy especiales para mí. Por último, no me olvido de la persona que ha sacado mi lado más friki estos 5 años, Martí. Contigo he aprendido tanto y de tanto… mil gracias por todas nuestras discusiones en las que yo nunca estoy de acuerdo y al final resulta que tu tenías razón, aunque yo siempre puedo acabar diciéndote: yo no lo veo así XD. Gracias por ser mi confidente, por poder hablar de todo contigo, por entenderme tan bien siempre, aunque no estés de acuerdo, eres una gran persona y te admiro muchísimo, sin duda has sido y sigues siendo una inspiración para mí.

Inoltre, non voglio dimenticarmi d'un gruppo di persone che anche se non sono delle mi grupo di lavoro, mi hanno insegnato un altro lato della vita in generale, sono conosciuti come il gruppo dell'antico kiwi. Grazzie mill per aver reso questa tesi molto piu divertente introducendomi al classico apperitivo con vermut, molto importante in certi momenti di questa tesi.

Finalmente, pero no menos importante, quiero agradecer esta tesis a una persona que apareció en mi vida durante estos cinco años y con quien ahora la comparto, Cristiano. Mil agracias por todo el apoyo incondicional que me has dado en estos años. Gracias por ayudarme a hacer los cambios que he querido hacer en mi vida y por ayudarme a saltar todas las piedras de mi camino, gracias por ser siempre de mi equipo, por aguantar mis subidas y bajadas en esta última etapa, por ayudarme con la escritura de esta tesis, sin duda sin tus consejos esta tesis no sería ni la mitad de lo que es. Además, quiero agradecerte enormemente la realización de las fotos que aparecen en esta tesis, sin duda sin tu talento no podría haber materializado mi idea.

A mi hermana Zurely, mi otra mitad, gracias por tener siempre fe ciega en mí. Gracias por tus constantes ánimos y apoyo, por siempre entenderme, por tu sonrisa que me han alegrado en los malos momentos y por tus consejos que no han sido muchos, pero han sido fundamentales. A mi madre, Martina, sin ti esto nunca hubiese ocurrido. Llegar hasta aquí no era algo trivial u obvio, requería mucho esfuerzo y sacrificio. Ahora que soy adulta y han ido pasando por mi vida distintas personas me doy cuenta de que estoy donde estoy simplemente porque he tenido a alguien como tú en mi vida que ha hecho posible lo imposible. Mil gracias por tu fuerza y apoyo incondicional que ha hecho que todo lo que he

querido en mi vida fuese posible. Pero sobre todo gracias por enseñarme que la ilusión mueve montañas, a no rendirme nunca, a confiar en mí misma y a creer que soy capaz de todo lo que me proponga en la vida.

Finalmente, quiero agradecer y dedicar esta tesis a una persona que ha sido clave en mi vida, mi abuelo Guillermo Buades. Usted es la persona que, a base de mucha perseverancia, nos ha inculcado tanto a mi como a mi hermana el amor por los libros, por aprender, por formarnos. Usted nos enseñó que el conocimiento es la llave que más puertas abre en este mundo y que es fundamental no solo para crecer profesional sino personalmente. Gracias por todos esos sermones que cuando éramos pequeñas nos aburrían pero que ahora valoramos enormemente porque sin usted en nuestro camino, nada de esto hubiese sido posible.

Manuscript Organization

De acuerdo con la normativa vigente y previa aceptación por la Comisión de Doctorado de la Universidad Autónoma de Barcelona esta memoria s presenta como compendio de publicaciones, aprobada el 26 de Octubre de 2020 con las siguientes publicaciones:

- "Electron Accumulative Molecules" Ana B. Buades, Victor S. Arderiu, David Olid-Britos, Clara Viñas, Reijo Sillanpää, Matti Haukka, Xavier Fontrodona, Marcos Paradinas, Carmen Ocal and Francesc Teixidor. *J. Am. Chem. Soc*. **2018**, 140, 8, 2957-2970 (DOI: 10.1021/jacs.7b12815)

- "Slow-spin relaxation of a low-spin S = ½ FeIII carborane complex" Ana B.Buades, Victor S. Arderiu, Lindley Maxwell, Martín Amoza, Duane Choquesillo-Lazarte, Núria Aliaga-Alcalde, Clara Viñas Francesc Teixidor and Eliseo Ruiz. *Chem. Commun*., **2019**, 55, 3825 (DOI:10.1039/c9cc01123d)

- "A fast and simple B-C bond-forming in metallacarboranes avoiding halometallacarboranes and transition metal catalysts" Ana B. Buades, Zsolt Kelemen, Victor S. Arderiu, Adnana Zaulet, Clara Viñas and Francesc Teixidor. *Dalton Trans*. **2020**, 49, 3525-3531 (DOI: 10.1039/C9DT04695J).

Motivation

The work presented in this dissertation is dedicated to the chemistry of metallacarboranes for different purposes. Chemistry is the branch of science focus on the study of the matter. This study could be focused on to know the matter behaviour or to modify it for a specific target, this dissertation includes both.

Substitution of a B-H position by other molecules permits us to modify the intrinsic properties of the metallacarborane for a specific goal. Namely, the addition of organic molecules to the metallacarborane by B-C bond formation seems to be especially difficult to obtain. Therefore, the study of general synthetic routes to the formation of B-C bonds in metallacarboranes possesses high interest for the scientific community. Chapter 1 unveil the power to combine theoretical with experimental chemistry to understand the nature of the B-C bond formation through the use of trytilbromide. The reaction of the silver salt of COSAN with trytilbromide permitted us to generate B-C bonds in metallacarboranes in few minutes avoiding the typical palladium catalyst used for the synthesis of this type of compounds up to now. The initial observation of this phenomenon prompted us to go so far with this research testing different reagents to know the scope of the reaction. In addition, the theoretical calculation permitted us to understand how and why this product had been formed.

Development of sustainable energy systems is a hot topic that prompt to the scientific community study electroactive molecules with energy applications such as solar cells, molecular electronics, artificial photosynthesis, fuel cells or water splitting. Chapter 2 and Chapter 3 describe the synthesis of metallacarborane derivatives as electroactive molecules for these types of applications. C60 or PCM structures are well known by their electron accumulative properties. However, they are known too by their low solubility in the common organic solvents, property that difficult the processability of these molecules for real applications. COSAN and FESAN are aromatic systems with a negative charge distributed by

the whole molecule that makes them electroactive molecules with high solubility in the major part of the organic solvents. Thus, the modification of these structures to make them able to accept more electrons maintaining their solubility properties was the target of this research. The synthesis and the spectroscopical and electrochemical characterization of bipyridine derivatives of COSAN and/or FESAN permits study the number of electrons able to accept in a reversible way for every product. In addition, the study of the electronic communication study between two metallic centers for compounds with two metallacarboranes per bipyridine unveils their applicability for molecular electronics. Furthermore, the synthesis of chlorinated derivatives of COSAN is an old topic. Even though it was a breakthrough due to the promising possible applications of these compounds in radiolysis or as weakly coordinating anions. The topic was losing interest due to the high difficult to synthesized the molecules and since the synthesis of the pure hexachloro COSAN in 1982 not many attempts to increase the chlorination order appear in the bibliography. However, in the last years, the electrochemical studies of the chlorinated derivatives of COSAN unveil how the addition of halogens to the COSAN skeleton modify the electrochemical properties of the products. Thus, synthesis of COSAN derivatives with more chloro in its structure will offer us the possibility to get a library of the compounds with slowly different redox potentials that permit us to select the adequate compound for a specific application. In addition, the spectroscopic and electrochemical characterization of these highly chlorinated derivatives could unveil the chemical structure and the possible electrochemical application of these compounds.

In order to demonstrate the possible real applications of the compounds developed in Chapter 3 together with the need to contribute to the scientific community in the energetic challenge, Chapter 4 study the behaviour of chlorinated derivatives of COSAN as electrocatalysts for water electrolysis. Preliminary studies base on comparing the electrocatalytic power of our compounds with the typical salts used for water splitting such as $NaSO_4$, the results unveil interesting electrochemical properties of our compounds. However, these types of systems required huge quantities of metallacarborane, that would become the system unachievable due to the high price of the metallacarboranes. Therefore, the research was focus on functionalizing graphite rods with our chloro derivatives compounds and study

their catalytic power together with their electrochemical stability to demonstrate the high potential of these compounds for water oxidation processes.

During the last decades, huge efforts have been made to develop Single-Molecule Magnets (SMM) as a qubit for quantum computing. The fabrication of these qubits by chemical synthesis permits guarantee that all the qubits are identical hence the reproducibility and the total control of the system. The research described in Chapter 5 takes advantage of the unpair electron of FESAN to study its properties as Single-Molecule Magnet (SMM). The achievement of a monocrystal able to be resolve by X-ray diffraction, was fundamental to study the magnetical properties of the molecule by theoretical calculations. In addition, the crystal power of the tetramethylammonium salt of FESAN leads the study of the relaxation time of the molecule needed to assess its applications as a qubit for quantum computing.

List of Abbreviations

3c-2e	3 centre 2 electrons
AC	Atrnative Current
AILFT	*ab initio* Ligand Field Theory
Bn	Benzyl
Bzh	Benzhydryl
cis	cisoid
COSAN	Cobaltabisdicarbollide
COSY	Correlated Spectroscopy
CSD	Cambridge Structural Database
CV	Cyclic Voltammetry
DBS	Dodecylbenzenesulfonate
DC	Direct Current
DCM	Dichloromethane
DFT	Desnsity Functional Theory
DME	Dimetoxyethane
DSC	Differential Scanning Calorimetry
DSSC	Dye Senzitizer Solar Cells
EA	Elemental Analysis
EDX	Energy-Dispersive X-ray
EINS	Electrophilic-Induced Nucleophilic Substitution
EPR	Electronic Paramagnetic Resonance
Et	Ethyl
Fc	Ferrocene
FESAN	Ferrabisdicarbollide
FT-IR	Fourier Transform- Infrared
G	Graphite
GO	Graphite Oxide

HER	Hydrogen Evolution Reaction
HSQC	Heteronuclear single quantum coherence spectroscopy
IVCT	Intervalence Charge Transfer
LSV	Linear Sweep Voltammetry
MALDI-TOF-MS	Matrix-Assited Laser Desorpption/Ionization - Time of Flight – Mass Spectra
Me	Methyl
MV	Methyl Viologen
NCS	N-Chlorosuccinimide
NMR	Nuclear Magnetic Resonance
OER	Oxygen Evolution Reaction
ORR	Oxygen Reduction Reaction
PCBM	[6,6]-phenyl-C61-butyric acid methyl ester
Ph	Phenyl
POM	Polyoxometallate
PSEPT	Polyhedron Skeletal Electron Pair Theory
PTS	*p*-toluenesulfonate
Pyr	Pyridinyl
QT	Quantum Tunnelling
RX	Halogenated Reagent
SEM	Scanning Electron Microscopy
SMM	Single-Molecule-Magnet
SQUID	Superconducting Quantum Interference Device
STM	Scanning Tunnelling Microscopy
$TBAPF_6$	Tetrabutylammonium hexafluorophosphate
TGA	Thermogravimetric analysis
THF	Tetrahydrofurane
TLC	Thin-layer chromatography
Tr	Trityl
trans	*transoid*
TS	Transition State

Table of Contents

CHAPTER ONE
Introduction to Boron Clusters

CHAPTER TWO
Fast and Simple B-C Bond Formation in COSAN

CHAPTER THREE
Metallacarborane Derivatives as Electron Acceptors

CHAPTER FOUR
Highly Chlorinated Derivatives of COSAN

CHAPTER FIVE
Chlorinated Derivatives of COSAN as Catalysts for Water Splitting

CHAPTER SIX
FESAN as Single-Molecule Magnet

CHAPTER ONE

Introduction to Boron Clusters

The first chapter focuses on to introduce the reader to the boron chemistry world since the synthesis and characterization of the first boron compound in 1912. This thesis will focus on the synthesis of metallacarborane derivatives base on COSAN and FESAN structures. This introduction will explain the structural properties of these compounds, their physicochemical properties and the characterization techniques we use to understand their structure. Finally, this chapter includes a summary of the last applications in the energy field for this type of compounds.

1.1 Historical overview

Boron compounds have been used over 4000 years since the Babylonians importing borax from the Far East as a flux for working gold. Egyptians used it for mummifying dead body, metallurgic or medicinal applications. Today, applications of borates are focused on the fabrication of glass and ceramics, detergents and bleaches, alloys and metals, fire retardants, agriculture or adhesives.[1]

Indeed, boron clusters were already known at the beginning of the XX century, the first borane synthesis was developed in 1912 by A stock.[2] We had to wait until 1943 for a clear structural characterization when H. C. Longuet-Higgins introduced the electron deficiency concept. The electron-deficient species possesses fewer valence electrons than those required for a localized bond scheme. Thus, the proposed concept suggests the existence of three centres with two electrons (3c-2e), e.g. B_3 or the bridge bonds B-H-B all obeying the Lewis concept of two electrons per bond; this and the molecular orbital theory was consistent with the high connectivity of the boranes.[3]

The possible application of some boranes as rocket fuels prompted the development in this field and led to the synthesis of pentaborane and decaborane during the last period of the Second World War.[4] As a consequence, W.N. Lipscomp received the Chemistry Nobel prize for his research about the borane structure in 1976[5] and H.C. Brown with Wittig for their research on boron and phosphorus compounds as reagents in organic synthesis in 1979.[6]

The existence of three-dimensional boron structures is a direct consequence of the boron property to make polyhedral skeletons, composed by triangular boron faces.[7] These boron clusters are classified depending on the atoms present in the structure. Boranes are clusters built by boron and hydrogen atoms, carboranes present some carbon atoms in its structure, and metallacarboranes, in addition, incorporate some metal atom.

1.1.1 Boranes

Boranes are compounds with molecular formula $[B_nH_m]^{x-}$ that are not present in nature but exist many ways to synthesize them.[8] The most important are the dimer B_2H_6, the pentaborane (B_5H_9) and the decaboranes ($B_{10}H_{14}$). These compounds are arranged in polyhedral clusters with B-H units in the vertices when present more than 5 boron atoms and their thermal stability increase with the number of boron atoms.[9] [*closo*-$B_{12}H_{12}]^{2-}$ is a significant borane with a high number of boron atoms with extraordinary stability.[10] It also presents important electronic properties due to the delocalization of the skeletal electrons on its triangular faces and magnetic properties.[11] It is a 3D aromatic compound[10-13] and has been compared with the classic organic aromaticity by Teixidor *et al* (**Figure 1.1**a).[14,15]

The formation of the 3c-2e bond is the milestone to build boron clusters. The B_2H_6 present two B-H-B bridges that connect two BH_2 units. The four B-H_t (H_t for terminal hydrogen atoms) contribute 8 e^- due to the 4 classical B-H bonds 2c-2e (**Figure 1.1**b), whereas the two B-H_b-B bridges (H_b for bridging hydrogen atoms) contribute 4 e^- to the total of 12 e^-. Lipscomb suggests for boranes with a higher number of boron atoms than two, the existence of 2c-2e bonds (B-H and B-B) and 3c-2e open and closed bonds between three boron atoms (B-B-B) or two boron atoms and one hydrogen (B-H-B).[16,17]

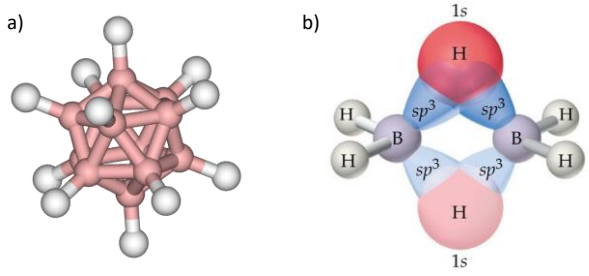

Figure 1.1. $[B_{12}H_{12}]^{2-}$ structure. B (pink) and H (white). b) B_2H_6 structure representing the 3c-2e bonds.

1.1.2 Carboranes

The formal exchange of one boron atom by one heteroatom such as C, N, O, Si, P, As, S, Se, Sb or Te,[18,19] gives an extended family of heteroboranes in which the

most studied are the carboranes, clusters with one or more carbon atoms in the skeleton.

R. E. Williams proposed in 1971 a classification of the clusters in three groups: *closo, nido* and *arachno*. The classification depends on the structural and stoichiometric properties determined by the number of vertices and available electrons. The classification follows the Wade rules and was studied by K. Wade, R. E. Williams, R. W. Rudolph and D. M. P. Mingos in 1971.[20-25]

The Polyhedron Skeletal Electron Pair Theory (PSEPT) or commonly named Wade's rules proposes that *n* B-H groups with *n* + 1 skeletal electron pairs favour a closed polyhedral structure. Each B-H group in polyhedral boranes is considered to donate two electrons for polyhedral binding. The remaining one-valence electron of the boron atom is used in the B-H bond. The rule further states that an increase of two electrons, i.e. *n* B-H groups with *n* + 2 skeletal electron pairs, lead to a *nido* arrangement of BH groups. *Nido* clusters are obtained by removal of one vertex from a *closo* structure. Addition of yet another electron pair (*n* + 3 skeletal electron pairs) changes the cluster to an *arachno* type obtained by removing two vertices from a *closo* structure.[23,26]

To know how many electrons are involved in the cluster, it is considered that every B-H group gives 2 electrons to the cluster. The hydrogen bridge contributes with one electron to the cluster and for the carboranes, every C-H or C-R contribute with three electrons to the cluster.

Carboranes with formula $[C_nB_mH_{n+m+p}]^{x-}$ namely these with two carbon atoms are the most studied and constitute the family of dicarba-*closo*-dodecaboranes with formula $C_2B_{10}H_{12}$. This structure presents three structural isomers depending on the relative positions of the carbons in the cluster. The most common is the 1,2-$C_2B_{10}H_{12}$ or *ortho*-carborane with two adjacent carbons.[27,28] The synthesis of 1,7-$C_2B_{10}H_{12}$ or *meta*-carborane (isomer with one boron atom between the two carbon atoms) was produced from the *ortho* isomer, in vacuum, at 450-500ºC by D. Grafstein and J. Dvorak in 1963.[29] In addition, 1,12-$C_2B_{10}H_{12}$ or *para*-carborane

(isomer with two boron atoms between the carbon atoms) was obtained when the temperature was increased above 600ºC (**Figure 1.2**).[30]

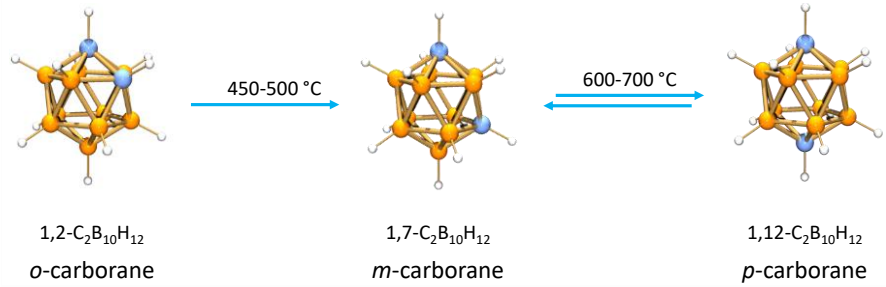

Figure 1.2. Thermal isomerization of dicarba-*closo*-dodecaborane. The nomenclature *o*-, *m*- and *p*- refers to the carbon positions. B (orange), C (blue) and H (white).

1.2 Metallacarboranes

Metallacarboranes are the family group of boron clusters with some of its boron atoms exchanged by a metal atom.[31,32] Among them are the theta shaped metallacarboranes (**θ**),[33] the most studied to date are those formed by two dicarbollide units $[1,2\text{-}C_2B_9H_{11}]^{2-}$ and a transition metal in between them such as Co^{3+}, Co^{2+}, Fe^{3+}, Fe^{2+}, Ni^{3+}, Cu^{3+}, Au^{3+}, among others.

In 1965, M. F. Hawthorne *et al*. synthesized the first **θ** metallacarborane, it was $[3,3'\text{-}Fe(1,2\text{-}C_2B_9H_{11})_2]^-$ ([**2**]$^-$), its name is ferrabis(dicarbollide)[34] but in the last decades the name FESAN for Fe SANwich has become popular and is how will be named in this thesis (**Figure 1.3**). Later the same authors published the same complexes with cobalt $[3,3'\text{-}Co(1,2\text{-}C_2B_9H_{11})_2]^-$ ([**1**]$^-$), with name cobaltabis(dicarbollide)[35] or COSAN and during the following years the group got to synthesize the metallacarboranes of Ni,[36] Cr,[37] Cu, Au and Pd (**Figure 1.3**).[38]

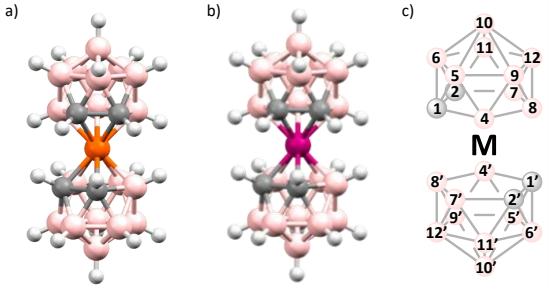

Figure 1.3. a) COSAN and b) FESAN structures, B [39], H (white), C (grey), Co (orange), Fe (purple). c) Metallacarborane vertex numbering.

The most studied θ metallacarboranes are COSAN and FESAN. This thesis will focus on these two compounds and their derivatives, studying new ways of synthesis and applications. Both structures present their metal as Co^{3+} and Fe^{3+} coordinated with two negative charges on each dicarbollide (-4 in total) hence the metallacarborane is a monoanionic compound. This negative charge is delocalized throughout the whole molecule leading to a low charge density[40] that together with the high molecular volume give to this compound high thermal and chemical stability and uncommon water behaviour.

The typical methodology to synthesize COSAN or FESAN requires the partial degradation of the *ortho*-carborane clusters to obtain the *nido* $[7,8\text{-}C_2B_9H_{12}]^-$.[34] Then a strong base as t-BuOK, NaH or n-BuLi in dry THF is used to remove the hydrogen in the bridging position, obtaining the dianionic dicarbollide $[7,8\text{-}C_2B_9H_{11}]^{2-}$.[38] Finally, the addition of dry $CoCl_2$ or $FeCl_2$ permit the complexation reaction and the later oxidation of the metal giving the metallacarborane of cobalt or iron, respectively.[34,35] However, Viñas *et al*. have recently proposed a new clean and faster methodology to synthesize COSAN in solid-state.[41]

1.2.1 Structure and aromaticity

Metallacarboranes show 3D structure with an important but complex nomenclature. The numbering of every vertex is fundamental to understand the structure and their derivatives (**Figure 1.3**c). The first studies about the synthesis of carboranes[42] and metallacarboranes[43-45] already set the basis on the vertex nomenclature as shown in **Figure 1.3**. However, it was only in 1990 when the IUPAC started to propose a unified nomenclature based on the literature also updated in 2005 and 2019.[46]

In addition, the anions COSAN and FESAN show three different conformations or rotational isomers: *cisoid* (*cis*), *gauche* or *transoid* (*trans*), represented in **Figure 1.4**. Despite that the *trans* conformation is the most energetically stable for both metallacarboranes,[47,48] it is not the most abundant according to the Cambridge Structural Database (CSD) for COSAN or FESAN derivatives. Contrarily, the most abundant is the *cis* conformation. A possible explanation can be found in Teixidor's *et al*. research. They study the conformation of the protonated salt of

COSAN in water by theoretical calculations, the study concludes that the *cisoid* rotamer is the most stable form of COSAN in water because this conformation permits a minimum of energy in contact with polar solvents[49] or ions.[47]

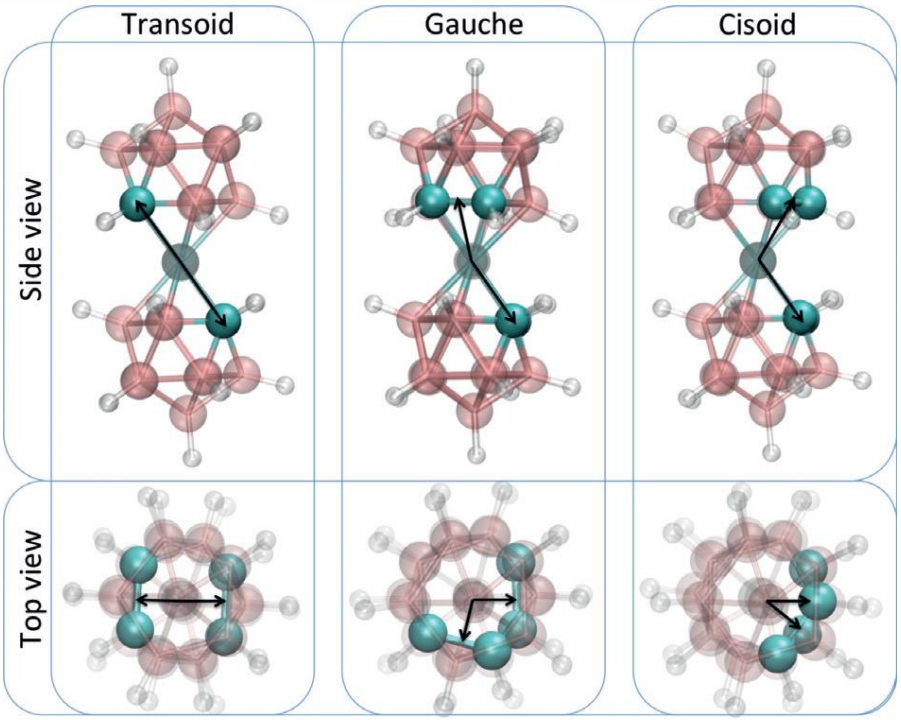

Figure 1.4. Top and side views of the atomic structure of COSAN anion in its three rotameric forms (*cis*-, *gauche*- and *trans*-). BH [39], CH (blue), Co (grey). Figure adapted from reference 49.

Since the discovery of FESAN in 1965, the metallacarboranes have been traditionally considered organometallic complexes sandwich-type and constantly compared with sandwichs as ferrocene.[34] However, the research developed by P. Baudin *et al*. suggests[33] and later the research of Teixidor *et al*. confirm that for metallacarboranes the highest intensity of the current density in a magnetic field is found inside the icosahedron of COSAN, not far from the Co atom, hence the metallacarboranes display global aromaticity whereas the metallocene present local aromaticity in the ligands.[50]

1.2.2 Characterization of metallacarboranes

* MALDI-TOF-MS for COSAN derivatives

MALDI-TOF-MS that stands for Matrix-Assisted Laser Desorption/Ionization , Time-of-Flight (TOF) mass spectroscopy (MS)[51] is a key characterization tool for COSAN derivatives in this thesis. It provides the mass as well as the molecular ratio of the distinct species derivatives of COSAN, as we proved earlier.[52] With this technique we have been able to analyse the products directly from the reaction crude with a minimum error. In addition, it is worth to specify that we did not use any matrix for COSAN derivatives because the products are stable enough and they did not discompose with the ionization laser hence they do not require the use of a matrix.

* ^{11}B-NMR Characterization

NMR is the classical characterization technique used in organic and inorganic chemistry. The characterization of COSAN and FESAN by NMR is key to analyze the structure details. ^{1}H-, ^{1}H{^{11}B}- and ^{13}C-NMR contribute very important information of the B-H and C-H vertices of the cluster. However, ^{11}B- and ^{11}B{^{1}H}-NMR provide extensive information about the derivatives, the conformation and the environment of the metallacarborane (**Figure 1.5**).[53]

- *COSAN*. ^{11}B-NMR characterization of COSAN has been widely studied because can give us information about the bonding type between the metallacarborane and the substituent, the number of substituents in the same metallacarborane and the purity of the product.

- *FESAN*. ^{11}B-NMR characterization of FESAN (Fe^{3+}) derivatives is completely dependent on its odd electron. The spectra of paramagnetic compounds display broad signals due to the effect of the unpaired electron in the relaxation time of the nucleus and very different shift range from diamagnetic compounds as COSAN. In particular, the signals for our FESAN (Fe^{3+}) compounds appear between 120 and -30 ppm or 120 and -600 ppm for the ^{1}H- or ^{11}B- NMR spectra respectively (**Figure 1.5**).

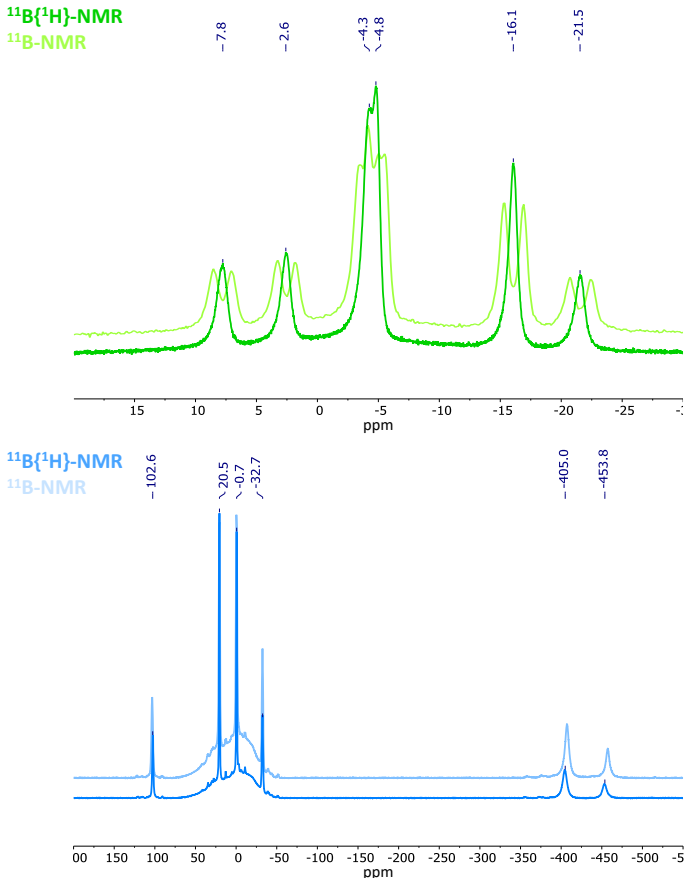

Figure 1.5. $^{11}B\{^{1}H\}$-NMR and ^{11}B-NMR of Na[COSAN] (green) and [NMe_4][FESAN] (blue).

* Crystal characterization

The crystal structure of Cs[3,3'-Co(1,2-$C_2B_9H_{11}$)$_2$] was determined in 1967; [54] however, the positions of the carbon atoms were not determined and hence the ligand orientation was not established. Later, the crystal and molecular structure of [Et_3NH][3,3'-Co(1,2-$C_2B_9H_{11}$)$_2$] was determined.[55] The crystal display a *cis* conformation with two similar distances from Co to the faces η^5-C_2B_3 (1.466 and 1.476 Å), and the metal is approximately equidistant from the boron and carbon atoms although the Co-C distances are slightly shorter than the Co-B vectors (mean values 2.046 and 2.097 Å, respectively).[56]

In addition, getting monocrystals for X-ray diffraction is more difficult for FESAN (Fe^{3+}) than for COSAN. The first crystal structure of FESAN was characterized by J.M. Forward *et al.* in 1991 and corresponded to $[Fe(C_5Me_5)_2][3,3'\text{-}Fe(1,2\text{-}C_2B_9H_{11})_2]$ that display *cis* conformation.[57]

1.3 Physicochemical Properties

Initially, the study of metallacarboranes was directed to the synthesis of as many new derivatives as possible. However, during the last decades, some research groups put their efforts into studying the physicochemical properties aiming at finding innovative applications. Thus the focus shifted to the rational design and synthesis of metallacarborane derivatives with predictable properties, targeting specific applications.

The properties of metallacarboranes include a low charge density, a big molecular volume and a great thermal and chemical stability. Moreover, they are considered hydrophobic compounds with a rigid geometry that limits the rotational movement of the molecule due to the building of dihydrogen bonds.[47,48,58-61]

* Cation effect

One of the most basic but more consistent properties of metallacarboranes is the solubility.[31] Anionic metallacarboranes as COSAN and FESAN display the property to be soluble in organic solvents and water depending on the nature of counter cation. For example the solubility of COSAN in water, at room temperature, strongly varies from Na^+, Li^+, H^+, K^+, Cs^+ and $[NMe_4]^+$, respectively: 1509 mM, 1175 mM, 846 mM, 747 mM, 1.5 mM and 0.019 mM, the last two are insoluble.[62] This property permits us to choose one or other counter cation for our metallacarborane derivatives depending on the desired application.

1.3.1 Electrochemical properties

The metal together with the charge delocalization, enabled by the aromatic 3D structure, bestows the metallacarboranes interesting electrochemical properties. The redox potential of metallacarboranes of Co, Fe, Ni, Cu, Ru, Rh, Pd and Au can be found in the literature.[63] For the scope of this thesis we will focus on the

electrochemical properties of COSAN and FESAN. On the one hand, COSAN has three accessible redox reversible processes, formally $Co^{2+/+}$, $Co^{3+/2+}$ and $Co^{4+/3+}$ at -2.64, -1.75 and 1.22 V *vs* Fc, respectively.[64] On the other hand, FESAN presents a non-reversible redox potential at 0.76 V *vs* Fc corresponding to $Fe^{4+/3+}$ and a second one reversible at -0.78 V *vs* Fc corresponding to $Fe^{3+/2+}$.[64] In addition, the relationship between redox potential and structure or, in other words, ligand nature, has been studied by several works[65-67] that demonstrate how the derivatization of COSAN or FESAN modifies their redox potentials.

Generally, the addition of functional groups such as methyl or phenyl to the carbons of FESAN causes a variation of the redox potential to more negatives values but if the substitution occurs at the boron atoms the redox potential of the derivatives is more positive than pristine FESAN redox potential (**Table 1**). However, the small number of electrochemical studies of FESAN derivatives do not permit us to establish a rule; actually, the addition of tiophenyl group lead the redox potential slightly more positive. Finally, different substituents will affect in different degree the redox potential.

Table 1. Redox potential values of FESAN derivatives.

Metallacarborane			$E_{1/2}$ (V *vs* Fc)	
M	L_1	L_2	$M^{3+/2+}$	Ref
Fe	1,2-$C_2B_9H_{11}$	1,2-$C_2B_9H_{11}$	-0.78	[64]
	1-Tioph1,2-$C_2B_9H_{10}$	1-Tioph1,2-$C_2B_9H_{10}$	-0.74	[68,69]
	1,2-Me_2-$C_2B_9H_9$	1,2-Me_2-$C_2B_9H_9$	-0.94	[70]
	1,2-Ph_2-$C_2B_9H_9$	1,2-Ph_2-$C_2B_9H_9$	-0.87	[70]
	8,9,12-Cl_3-1,2-$C_2B_9H_{10}$	8,9,12-Cl_3-1,2-$C_2B_9H_{10}$	-0.17	[71]
	8-I-1,2-$C_2B_9H_{10}$	8-I-1,2-$C_2B_9H_{10}$	-0.35	[64]

The literature about electrochemical studies of COSAN derivatives is much more extended and it is possible to propose a general tendency. Unlike the FESAN, all the substitutions in the carbon atoms of COSAN boost the redox potential of the final derivatives to more positive values than pristine COSAN. However, the addition of substituents such as methyl or phenyl groups in the boron atoms make the structure more negative (**Table 2**). Finally, the dehydrohalogenation of COSAN lead to compounds whose redox potentials are more positive than

pristine COSAN, and the number and type of halogen affect the final redox potential values.

Table 2. Redox potential values of COSAN derivatives.

Metallacarborane			$E_{1/2}$ (V *vs* Fc)		
M	L_1	L_2	$M^{3+/2+}$	$M^{2+/+}$	Ref
Co	1,2-$C_2B_9H_{11}$	1,2-$C_2B_9H_{11}$	-1.75	-2.64	[64]
	1-Tioph-1,2-$C_2B_9H_{10}$	1-Tioph-1,2-$C_2B_9H_{10}$	-1.46		[72]
	1-SEt-1,2-$C_2B_9H_{10}$	1-SEt-1,2-$C_2B_9H_{10}$	-1.45		[73]
	1-Me-1,2-$C_2B_9H_{10}$	1-Me-1,2-$C_2B_9H_{10}$	-1.69		[73]
	1-Ph-1,2-$C_2B_9H_{10}$	1-Ph-1,2-$C_2B_9H_{10}$	-1.69		[70]
	1,2-Me_2-$C_2B_9H_9$	1,2-Me_2-$C_2B_9H_9$	-1.54		[74]
	1,2-Ph_2-$C_2B_9H_9$	1,2-Ph_2-$C_2B_9H_9$	-1.68		[70]
	8-Me-1,2-$C_2B_9H_{10}$	1,2-$C_2B_9H_{11}$	-1.90		[75]
	8-Ph-1,2-$C_2B_9H_{10}$	1,2-$C_2B_9H_{11}$	-1.74		[75]
	8-Me-1,2-$C_2B_9H_{10}$	8-Me-1,2-$C_2B_9H_{10}$	-1.82		[76]
	8-Cl-1,2-$C_2B_9H_{10}$	8-Cl-1,2-$C_2B_9H_{10}$	-1.39	-2.41	[77]
	8-Br-1,2-$C_2B_9H_{10}$	8-Br-1,2-$C_2B_9H_{10}$	-1.34	-2.37	[77]
	8-I-1,2-$C_2B_9H_{10}$	8-I-1,2-$C_2B_9H_{10}$	-1.25	-2.27	[64]
	8,9,12-Me_3-1,2-$C_2B_9H_8$	8,9,12-Me_3-1,2-$C_2B_9H_8$	-1.89		[76]
	8,9,12-Cl_3-1,2-$C_2B_9H_8$	8,9,12-Cl_3-1,2-$C_2B_9H_8$	-1.01		[78]
	8,9,12-I_3-1,2-$C_2B_9H_8$	8,9,12-I_3-1,2-$C_2B_9H_8$	-0.82		[64]
	8,9,10,12-Me_4-1,2-$C_2B_9H_7$	8,9,10,12-Me_4-1,2-$C_2B_9H_7$	-1.92		[76]
	8,9,10,12-I_4-1,2-$C_2B_9H_7$	8,9,10,12-I_4-1,2-$C_2B_9H_7$	-0.68		[76]

1.4 Applications of metallacarboranes in energy

In the last decade, great concern has arisen related to environmental pollution and the global energy crisis caused by the consumption of fossil fuels. Thus, the development of materials for energy applications has become a widely studied subject and has gained importance. In this framework, metallacarborane studies have experienced the same change.

The study of metallacarboranes for energy applications started 10 years ago when Singh *et al.* introduced the possibility to use different metallacarboranes to store hydrogen. The work used different transition metals (Sc, Ti, V, Cr, Mn, Fe, Co and Ni) and structures ($C_2B_4H_6M$, $C_2B_9H_{11}M$, $C_2B_8H_{10}M_2$ and $C_4B_8H_{12}M_2$).

Theoretical calculations unveiled Sc and Ti are the best metals to hydrogen storage reaching absorption weight of 7%.[79]

Recently Fuentes *et al.* studied the properties of conducting organic polymers doped with metallacarboranes for batteries, fuel cells and supercapacitors. The study presents metallacarboranes M[**1**] (M = Cs^+, Na^+, Li^+ and H^+) and Cs[$\mathbf{Cl_x}$**-1**] (x = 2, 4 and 6) as promoters of conductivity when the medium contains sufficient amounts of ionic components and certain degree of humidity.[80-82] The study of Na[$\mathbf{Cl_4}$**-1**] reveals its properties as a mediator for boosting the stability of carbon-based aqueous supercapacitors.[83]

Finally, the nickel metallacarborane ([3,3'-Ni(1,2-$C_2B_9H_{11}$)$_2$]$^-$) has been studied as an electroactive electrolyte for Dye-Sensitized Solar Cells (DSSCs). The compound presents more efficiency than some metallic complexes of Co, Cu and the redox couple Fc/Fc^+ but not more than the I^-/I_3^- reference redox couple.[84] Later, some derivatives of the nickel metallacarborane that change the polarity, solubility and other properties were studied to favour the dye interactions.[85] In addition, another study used derivatives of COSAN (phosphate and phosphinate derivatives) bonded to the surface of the TiO_2 nanoparticles to act as a dye in DSSCs.[86]

In summary, several recent developments mainly from the application point of view, lead to promising results. These results motivated many researchers to dig deeper into the practical properties of metallacaboranes that are unveiling their other side of the coin. This thesis and the following paragraphs are the results of a though research on metallacarborane derivatives from their rational design to the study of their properties without losing sight of the possible final application in the energy sector.

1.5 References

(1) W. G. Woods, An introduction to boron: history, sources, uses, and chemistry, *Environmental Health Perspectives*, **1994**, 102, 5-11.

(2) A. Stock and C. Massenez, Borwasserstoffe, *Berichte der deutschen chemischen Gesellschaft*, **1912**, 45, 3539-3568.

(3) H. C. Longuet-Higgins and R. P. Bell, 64. The structure of the boron hydrides, *J. Chem. Soc.*, **1943**, 250-255.

(4) S. Hermanek, Boron-11 NMR spectra of boranes, main-group heteroboranes, and substituted derivatives. Factors influencing chemical shifts of skeletal atoms, *Chem. Rev.*, **1992**, 92, 325-362.

(5) W. N. Lipscomb, The Boranes and Their Relatives, *Science*, **1977**, 196, 1047-1055.

(6) H. C. Brown, *Hydroboration: with supplement, Nobel lecture, December 8, 1979*, Benjamin-Cummings Publishing Company, **1962**.

(7) H. Longuet-Higgins, Substances hydrogénées avec défaut d'électrons, *L. Chim. Phys.*, **1949**, 46, 268-275.

(8) W. N. Lipscomb, *Boron hydrides*, Dover Plublications, Inc., New York, **2012**.

(9) N. N. Greenwood and A. Earnshaw, *Chemistry of the Elements*, Elsevier, **2012**.

(10) J. Aihara, Three-dimensional aromaticity of polyhedral boranes, *J. Am. Chem. Soc.*, **1978**, 100, 3339-3342.

(11) V. Volkov and V. Ikorskii, Magnetochemistry of boron hydride structures. Empirical aspects, *J. Struct. Chem.*, **2004**, 45, 694-705.

(12) R. King, Three-dimensional aromaticity in deltahedral boranes and carboranes, *Russ. Chem. Bull.*, **1993**, 42, 1283-1291.

(13) R. B. King, Three-dimensional aromaticity in polyhedral boranes and related molecules, *Chem. Rev.*, **2001**, 101, 1119-1152.

(14) J. Poater, M. Solà, C. Viñas and F. Teixidor, π Aromaticity and Three-Dimensional Aromaticity: Two sides of the Same Coin?, *Angew. Chem. Int. Ed.*, **2014**, 53, 12191-12195.

(15) J. Poater, M. Solà, C. Viñas and F. Teixidor, Hückel's Rule of Aromaticity Categorizes Aromatic closo Boron Hydride Clusters, *Chem. Eur. J.*, **2016**, 22, 7437-7443.

(16) W. H. Eberhardt, B. C. Jr. and W. N. Lipscomb, The Valence Structure of the Boron Hydrides, *J. Chem. Phys.*, **1954**, 22, 989-1001.

(17) R. Hoffmann and W. N. Lipscomb, Boron Hydrides: LCAO—MO and Resonance Studies, *J. Chem. Phys.*, **1962**, 37, 2872-2883.

(18) R. N. Grimes, *Carboranes*, US, 3rd edn., **2016**.

(19) D. Schubert, in *Kirk-Othmer Encyclopedia of Chemical Technology*, **2011**, pp. 1-68.

(20) D. Mingos, A general theory for cluster and ring compounds of the main group and transition elements, *Nat. Phys. Sci.*, **1972**, 236, 99-102.

(21) R. Rudolph and W. Pretzer, Hueckel-type rules and the systematization of borane and heteroborane chemistry, *Inorg. Chem.*, **1972**, 11, 1974-1978.

(22) R. E. Williams, Carboranes and boranes; polyhedra and polyhedral fragments, *Inorg. Chem.*, **1971**, 10, 210-214.

(23) R. W. Rudolph, Boranes and heteroboranes: a paradigm for the electron requirements of clusters?, *Accounts Chem. Res.*, **1976**, 9, 446-452.

(24) K. Wade, in *Advances in Inorganic Chemistry and Radiochemistry*, eds. H. J. Emeléus and A. G. Sharpe, Academic Press, **1976**, vol. 18, pp. 1-66.

(25) R. E. Williams, in *Advances in Inorganic Chemistry and Radiochemistry*, eds. H. J. Emeléus and A. G. Sharpe, Academic Press, **1976**, vol. 18, pp. 67-142.

(26) E. D. Jemmis and P. N. V. Pavankumar. "Stability of polyhedral borane anions and carboranes." *Proceedings of the Indian Academy of Sciences-Chemical Sciences.* Vol. 93. No. 3. Springer India, 1984.

(27) M. M. Fein, J. Bobinski, N. Mayes, N. Schwartz and M. S. Cohen, Carboranes. I. The preparation and chemistry of 1-isopropenylcarborane and its derivatives (a new family of stable clovoboranes), *Inorg. Chem.*, **1963**, 2, 1111-1115.

(28) T. L. Heying, J. W. Ager, S. L. Clark, D. J. Mangold, H. L. Goldstein, M. Hillman, R. J. Polak and J. W. Szymanski, A New Series of Organoboranes. I. Carboranes from the Reaction of Decaborane with Acetylenic Compounds, *Inorg. Chem.*, **1963**, 2, 1089-1092.

(29) D. Grafstein and J. Dvorak, Neocarboranes, a new family of stable organoboranes isomeric with the carboranes, *Inorg. Chem.*, **1963**, 2, 1128-1133.

(30) S. Papetti and T. L. Heying, p-Carborane [1, 12-Dicarbaclovododecaborane (12)], *J. Am. Chem. Soc.*, **1964**, 86, 2295-2295.

(31) R. N. Grimes, Metallacarboranes in the new millennium, *Coord. Chem. Rev.*, **2000**, 200, 773-811.

(32) N. Hosmane and J. Maguire, in *Comprehensive Organometallic Chemistry III*, **2007**, ch. 3, pp. 175-264.

(33) P. Bauduin, S. Prevost, P. Farràs, F. Teixidor, O. Diat and T. Zemb, A Theta-Shaped Amphiphilic Cobaltabisdicarbollide Anion: Transition From Monolayer Vesicles to Micelles, *Angew. Chem. Int. Ed.*, **2011**, 50, 5298-5300.

(34) M. F. Hawthorne, D. C. Young and P. A. Wegner, Carbametallic Boron Hydride Derivatives. I. Apparent Analogs of Ferrocene and Ferricinium Ion, *J. Am. Chem. Soc.*, **1965**, 87, 1818-1819.

(35) M. F. Hawthorne and T. D. Andrews, Carborane analogues of cobalticinium ion, *Chem. Commun, (London)*, **1965**, 443-444.

(36) L. F. Warren and M. F. Hawthorne, (3)-1, 2-Dicarbollyl Complexes of Nickel (III) and Nickel (IV), *J. Am. Chem. Soc.*, **1967**, 89, 470-471.

(37) H. W. Ruhle and M. F. Hawthorne, . pi.-Dicarbollyl derivatives of chromium. Metallocene analogs, *Inorg. Chem.*, **1968**, 7, 2279-2282.

(38) M. F. Hawthorne, D. C. Young, T. D. Andrews, D. V. Howe, R. L. Pilling, A. D. Pitts, M. Reintjes, L. F. Warren Jr and P. A. Wegner, . pi.-Dicarbollyl derivatives of the transition metals. Metallocene analogs, *J. Am. Chem. Soc.*, **1968**, 90, 879-896.

(39) E. C. Santos, A. B. Pinkerton, S. A. Kinkead, P. K. Hurlburt, S. A. Jasper, C. W. Sellers, J. C. Huffman and L. J. Todd, Syntheses of nido-9,11-X2-7,8-C2B9H10− anions (X=Cl, Br or I) and the synthesis and structural characterization of N(C2H5)4[commo-3,3′-Co(4,7-Br2-3,1,2-CoC2B9H9)2], *Polyhedron*, **2000**, 19, 1777-1781.

(40) C. Masalles, S. Borrós, C. Viñas and F. Teixidor, Are Low-Coordinating Anions of Interest as Doping Agents in Organic Conducting Polymers?, *Adv. Mater.*, **2000**, 12, 1199-1202.

(41) I. Bennour, A. M. Cioran, F. Teixidor and C. Viñas, 3, 2, 1 and stop! An innovative, straightforward and clean route for the flash synthesis of metallacarboranes, *Green Chem*, **2019**, 21, 1925-1928.

(42) M. F. Hawthorne, D. C. Young, P. M. Garrett, D. A. Owen, S. G. Schwerin, F. N. Tebbe and P. A. Wegner, Preparation and characterization of the (3)-1, 2-and (3)-1, 7-dicarbadodecahydroundecaborate (-1) ions, *J. Am. Chem. Soc.*, **1968**, 90, 862-868.

(43) M. F. Hawthorne, L. F. Warren Jr, K. P. Callahan and N. F. Travers, Chemistry of bis [. pi.-(3)-1, 2-dicarbollyl] metalates. Protonation and boron substitution, *J. Am. Chem. Soc.*, **1971**, 93, 2407-2412.

(44) M. F. Hawthorne, D. C. Young, T. D. Andrews, D. V. Howe, R. L. Pilling, A. D. Pitts, M. Reintjes, L. F. Warren and P. A. Wegner, .pi.-Dicarbollyl derivatives of the transition metals. Metallocene analogs, *J. Am. Chem. Soc.*, **1968**, 90, 879-896.

(45) L. I. Zakharkin and V. N. Kalinin, Metallacarboranes, *Russ. Chem. Rev.*, **1974**, 43, 551-573.

(46) M. A. Beckett, B. Brellochs, I. T. Chizhevsky, T. Damhus, K.-H. Hellwich, J. D. Kennedy, R. Laitinen, W. H. Powell, D. Rabinovich, C. Viñas and A. Yerin, Nomenclature for boranes and related species (IUPAC Recommendations 2019), *Pure Appl. Chem.*, **2020**, 92, 355.

(47) E. J. Juárez-Pérez, R. Núñez, C. Viñas, R. Sillanpää and F. Teixidor, The Role of C–H···H–B Interactions in Establishing Rotamer Configurations in Metallabis(dicarbollide) Systems, *Eur. J. Inorg. Chem*, **2010**, 2385-2392.

(48) A. B. Buades, V. S. Arderiu, L. Maxwell, M. Amoza, D. Choquesillo-Lazarte, N. Aliaga-Alcalde, C. Viñas, F. Teixidor and E. Ruiz, Slow-spin relaxation of a low-spin S= 1/2 Fe III carborane complex, *Chem. Comm.*, **2019**, 55, 3825-3828.

(49) D. C. Malaspina, C. Viñas, F. Teixidor and J. Faraudo, Atomistic Simulations of COSAN: Amphiphiles without a Head-and-Tail Design Display "Head and Tail" Surfactant Behavior, *Angew. Chem. Int. Ed.*, **2020**, 59, 3088-3092.

(50) J. Poater, C. Viñas, I. Bennour, S. l. Escayola, M. Solà and F. Teixidor, Too Persistent to Give Up: Aromaticity in Boron Clusters Survives Radical Structural Changes, *J. Am. Chem. Soc.*, **2020**, 142, 9396-9407.

(51) J. M. Forward, D. Michael, P. Mingos, T. E. Müller, D. J. Williams and Y.-K. Yan, Synthesis and structural characterization of metallacarborane sandwich salts with tetrathiafulvalene (ttf)[M ($C_2B_9H_{11}$)$_2$][ttf](M= Cr, Fe, Ni), *J. Organomet. Chem.*, **1994**, 467, 207-216.

(52) P. González-Cardoso, A.-I. Stoica, P. Farràs, A. Pepiol, C. Viñas and F. Teixidor, Additive Tuning of Redox Potential in Metallacarboranes by Sequential Halogen Substitution, *Chem. Eur. J.*, **2010**, 16, 6660-6665.

(53) A. Zaulet, F. Teixidor, P. Bauduin, O. Diat, P. Hirva, A. Ofori and C. Vinas, Deciphering the role of the cation in anionic cobaltabisdicarbollide clusters, *J. Organomet. Chem.*, **2018**, 865, 214-225.

(54) A. Zalkin, T. E. Hopkins and D. H. Templeton, Crystal structure of Cs ($B_9C_2H_{11}$)$_2$Co, *Inorg. Chem.*, **1967**, 6, 1911-1915.

(55) L. Borodinsky, E. Sinn and R. N. Grimes, Crystal and molecular structure of (C_2H_5)$_3$NH$^+$[Co(1,2-$C_2B_9H_{11}$)$_2$], *Inorg. Chem.*, **1982**, 21, 1686-1689.

(56) I. B. Sivaev and V. I. Bregadze, Chemistry of cobalt bis (dicarbollides). A review, *Collect. Czech. Chem. Commun.*, **1999**, 64, 783-805.

(57) J. M. Forward, D. M. P. Mingos and A. V. Powell, Synthesis and magnetic studies of the metallocarborane sandwich salts [Fe(C_5Me_5)$_2$][M($C_2B_9H_{12}$)$_2$)](Me= Cr, Fe, Ni, *J. Organomet. Chem.*, **1994**, 465, 251-258.

(58) L. Ma, J. Hamdi, J. Huang and M. F. Hawthorne, Camouflaged carborane amphiphiles: synthesis and self-assembly, *Inorg. Chem.*, **2005**, 44, 7249-7258.

(59) P. Matějíček, P. Cígler, K. Procházka and V. Král, Molecular Assembly of Metallacarboranes in Water: Light Scattering and Microscopy Study, *Langmuir*, **2006**, 22, 575-581.

(60) G. Chevrot, R. Schurhammer and G. Wipff, Surfactant behavior of "ellipsoidal" dicarbollide anions: A molecular dynamics study, *J. Phys. Chem. B*, **2006**, 110, 9488-9498.

(61) J. Rak, B. Dejlová, H. Lampová, R. Kaplánek, P. Matějíček, P. Cígler and V. Král, On the solubility and lipophilicity of metallacarborane pharmacophores, *Mol. Pharm.*, **2013**, 10, 1751-1759.

(62) M. Tarrés, C. Viñas, P. González-Cardoso, M. M. Hänninen, R. Sillanpää, V. Ďorďovič, M. Uchman, F. Teixidor and P. Matějíček, Aqueous Self-Assembly and Cation Selectivity of Cobaltabisdicarbollide Dianionic Dumbbells, *Chem. Eur. J.*, **2014**, 20, 6786-6794.

(63) R. Núñez, M. Tarrés, A. Ferrer-Ugalde, F. F. de Biani and F. Teixidor, Electrochemistry and Photoluminescence of Icosahedral Carboranes, Boranes, Metallacarboranes, and Their Derivatives, *Chem. Rev.*, **2016**, 116, 14307-14378.

(64) M. Tarres, V. S. Arderiu, A. Zaulet, C. Vinas, F. Fabrizi de Biani and F. Teixidor, How to get the desired reduction voltage in a single framework! Metallacarborane as an optimal probe for sequential voltage tuning, *Dalton Trans.*, **2015**, 44, 11690-11695.

(65) A. Pombeiro, *Encyclopedia of Electrochemistry: Inorganic Electrochemistry, ed. F. Sholz and CJ Pickett*, Wiley-VCH, Weinheim, **2006**.

(66) G. Wilkinson, R. D. Gillard and J. A. McCleverty, Comprehensive coordination chemistry. The synthesis, reactions, properties and applications of coordination compounds. V. 3. Main group and early transition elements, **1987**.

(67) A. Lever, Electrochemical parametrization of metal complex redox potentials, using the ruthenium (III)/ruthenium (II) couple to generate a ligand electrochemical series, *Inorg. Chem.*, **1990**, 29, 1271-1285.

(68) Y.-K. Yan, D. M. P. Mingos, D. J. Williams and M. Kurmoo, Synthesis, structures and physical properties of bis (ethylenedithio) tetrathiafulvalenium salts of paramagnetic metallacarborane anions, *J. Chem. Soc. Dalton*, **1995**, 3221-3230.

(69) Y.-K. Yan, D. M. P. Mingos, M. Kurmoo, W.-S. Li, I. J. Scowen, M. McPartlin, A. T. Coomber and R. H. Friend, Synthesis, structure and physical properties of tetrathiafulvalenium salts of the ferracarborane complex commo-[3,3′-Fe{1-(C_4H_3S)-1,2-$C_2B_9H_{10}$}$_2$]$^-$, *J. Chem. Soc. Dalton*, **1995**, 2851-2860.

(70) L. J. Todd, in *Advances in Organometallic Chemistry*, Elsevier, **1970**, vol. 8, pp. 87-115.

(71) T. García-Mendiola, V. Bayon-Pizarro, A. Zaulet, I. Fuentes, F. Pariente, F. Teixidor, C. Viñas and E. Lorenzo, Metallacarboranes as tunable redox potential electrochemical indicators for screening of gene mutation, *Chem. Sci.*, **2016**, 7, 5786-5797.

(72) B. Fabre, E. Hao, Z. M. LeJeune, E. K. Amuhaya, F. Barrière, J. C. Garno and M. G. H. Vicente, Polythiophenes containing in-chain cobaltabisdicarbollide centers, *ACS Appl. Mater. Inter.*, **2010**, 2, 691-702.

(73) C. Viñas, J. Pedrajas, J. Bertran, F. Teixidor, R. Kivekäs and R. Sillanpää, Synthesis of Cobaltabis (dicarbollyl) Complexes Incorporating Exocluster SR Substituents and the Improved Synthesis of [3,3‘-Co(1-R-2-R‘-1,2-$C_2B_9H_9$)$_2$]$^-$Derivatives, *Inorg. Chem.*, **1997**, 36, 2482-2486.

(74) R. N. Grimes, *Metal interactions with boron clusters*, Springer Science & Business Media, **2013**.

(75) I. Rojo, F. Teixidor, C. Viñas, R. Kivekäs and R. Sillanpää, Relevance of the Electronegativity of Boron in η 5-Coordinating Ligands: Regioselective Monoalkylation and Monoarylation in Cobaltabisdicarbollide [3,3′-Co(1,2-$C_2B_9H_{11}$)$_2$]$^-$ Clusters, *Chem. Eur. J.*, **2003**, 9, 4311-4323.

(76) M. Lupu, A. Zaulet, F. Teixidor, E. Ruiz and C. Viñas, Negatively Charged Metallacarborane Redox Couples with Both Members Stable to Air, *Chem. Eur. J.*, **2015**, 21, 6888-6897.

(77) D. A. Rudakov, V. L. Shirokii, V. A. Knizhnikov, A. V. Bazhanov, E. I. Vecher, N. A. Maier, V. I. Potkin, A. N. Ryabtsev, P. V. Petrovskii, I. B. Sivaev, V. I. Bregadze and I. L.

Eremenko, Electrochemical synthesis of halogen derivatives of bis(1,2-dicarbollyl)cobalt(III), *Russ. Chem. Bull.*, **2004**, 53, 2554-2557.

(78) I. Fuentes, J. Pujols, C. Viñas, S. Ventura and F. Teixidor, Dual Binding Mode of Metallacarborane Produces a Robust Shield on Proteins, *Chem. Eur. J.*, **2019**, 25, 12820-12829.

(79) A. K. Singh, A. Sadrzadeh and B. I. Yakobson, Metallacarboranes: Toward Promising Hydrogen Storage Metal Organic Frameworks, *J. Am. Chem. Soc.*, **2010**, 132, 14126-14129.

(80) I. Fuentes, A. Andrio, F. Teixidor, C. Viñas and V. Compañ, Enhanced conductivity of sodium versus lithium salts measured by impedance spectroscopy. Sodium cobaltacarboranes as electrolytes of choice, *Phys. Chem. Chem. Phys.*, **2017**, 19, 15177-15186.

(81) I. Fuentes, A. Andrio, A. García-Bernabé, J. Escorihuela, C. Viñas, F. Teixidor and V. Compañ, Structural and dielectric properties of cobaltacarborane composite polybenzimidazole membranes as solid polymer electrolytes at high temperature, *Phys. Chem. Chem. Phys.*, **2018**, 20, 10173-10184.

(82) I. Fuentes, M. J. Mostazo-López, Z. Kelemen, V. Compañ, A. Andrio, E. Morallón, D. Cazorla-Amorós, C. Viñas and F. Teixidor, Are the Accompanying Cations of Doping Anions Influential in Conducting Organic Polymers? The Case of the Popular PEDOT, *Chem. Eur. J.*, **2019**, 25, 14308-14319.

(83) R. Ruiz-Rosas, I. Fuentes, C. Viñas, F. Teixidor, E. Morallón and D. Cazorla-Amorós, Tailored metallacarboranes as mediators for boosting the stability of carbon-based aqueous supercapacitors, *Sustainable Energy & Fuels*, **2018**, 2, 345-352.

(84) T. C. Li, A. M. Spokoyny, C. She, O. K. Farha, C. A. Mirkin, T. J. Marks and J. T. Hupp, Ni(III)/(IV) Bis(dicarbollide) as a Fast, Noncorrosive Redox Shuttle for Dye-Sensitized Solar Cells, *J. Am. Chem. Soc.*, **2010**, 132, 4580-4582.

(85) A. M. Spokoyny, T. C. Li, O. K. Farha, C. W. Machan, C. She, C. L. Stern, T. J. Marks, J. T. Hupp and C. A. Mirkin, Electronic Tuning of Nickel-Based Bis (dicarbollide) Redox Shuttles in Dye-Sensitized Solar Cells, *Angew Chem.*, **2010**, 122, 5467-5471.

(86) E. J. Juárez-Pérez, P. H. Mutin, M. Granier, F. Teixidor and R. Núñez, Anchoring of Phosphorus-Containing Cobaltabisdicarbollide Derivatives to Titania Surface, *Langmuir*, **2010**, 26, 12185-12189.

CHAPTER 2

Fast and Simple B-C Bond Formation in COSAN

CHAPTER TWO

Fast and Simple B-C Bond Formation in COSAN

Due to the importance have a general synthetic route for the formation of B-C bonds in metallacarboranes, this chapter will explore from an experimental and theoretical point of view the formation of B-C bonds in COSAN. The work will propose the use of silver salt of COSAN in presence of trityl bromide to lead in seconds the mono and disubstituted trityl derivatives of COSAN. In addition, this work will consider the possibility to use benzhydryl bromide or benzyl bromide as carbocations generated *in situ*. This study will include the characterization of the products formed which NMR will help us to understand the nature of the B-C bonds formed but, MALDI-TOF will be the star technique. MALDI-TOF will help to identify all the species formed in the reaction and to propose a reaction mechanism. Moreover, this research will present DFT calculation that will be key to demonstrate the unexpected role of the Tr^+ proposed by the experimental studies. The results will offer a useful tool for the synthesis of multiple B-C derivatives of COSAN. Finally, the chapter will include a demonstration of the quantitative character of the MALDI-TOF technique for this type of compounds.

2.1 B-C Bond: Synthesis of new derivatives of COSAN

Metallacarborane derivatives with organic molecules normally present interesting chemical and physical properties associated with the new fragment. Much effort has been done over the last decades to develop new synthetic routes for this class of compounds that give a twist to the common application of metallacarboranes.

The possibility of derivatization of metallacarboranes, including the number, type and position of the substituents, is higher than in their common organic counterparts with similar molecular weight. This behaviour is mainly due to the straightforward formation of $C_{cluster}$-C_{org} or $B_{cluster}$-C_{org} bond. The latter bond dominates most of the reactions in this field and is indeed the most studied. However, for the sake of completeness, the formation of $C_{Carborane}$-C, B-N, B-S and B-P has been also widely studied and sometimes determinant in the final products yield.[1-8]

The major part of the research, which is based on the B-C bond formation, relies on methods borrowed from classical organic chemistry because both COSAN and benzene are aromatic systems. However, the Y-C organic coupling reactions in carbon chemistry commonly works differently in boron chemistry.[9-12]

The first reaction of B-C formation bond in COSAN ([**1**]$^-$) was developed by Hawthorne in 1972 and consisted on the addition of bridging aryl group position between the B(8) and B(8'). The reaction occurs by radical intermediates resulting in decomposition of diazonium salts.[13] Despite the novelty of the Hawthorne method, the process cannot be used with a wide range of substituents. Conversely, the Friedel-Crafts reaction had been commonly applied in metallacarborane derivatives synthesis. Concretely, the synthesis of [3,3'-Co(8-μ-(*o*-C_6H_4)-1,2-$C_2B_9H_{10})_2]^-$ from pristine COSAN in benzene as a solvent and in presence of the Lewis acid $AlCl_3$ produced a yield of 86%.[14] An equivalent reaction with naphthalene led to a bridge derivative, but in this case, the naphthalene undergoes to a rare carbon extrusion, reducing one of its 6 C aromatic cycles to five carbons (**Scheme 2.1**).[15]

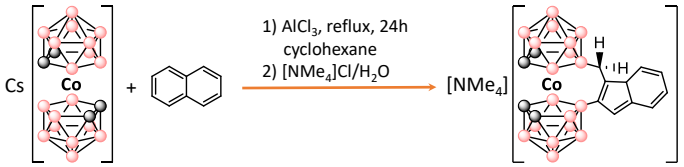

Scheme 2.1. Reaction condition of Cs[**1**] with naphthalene in presence of Lewis acid, $AlCl_3$.[16]

Another example is described by Electrophilic-Induced Nucleophilic Substitution (EINS) that works well for halogens, OH, OR and other nucleophiles[17-20] but is less efficient to produce B-C bonds. This reaction mechanism may involve the attack of an electrophilic agent resulting in the elimination of the hydride hydrogen atom to form a pseudoelectrophilic centre on the boron atom, which is then subjected to the attack of a nucleophilic species.[21]

With this in mind, the next strategy to generate B-C bonds was based on the use of halo-derivatives of COSAN and a Palladium catalyst as starting material (**Scheme 2.2**). These halogenated vertices have been identified as the site of maximum electron density in the dicarbollide ligand, and hence the preferred position to react with electrophiles.[22] The synthesis of $[MePPh_3][3,3'\text{-}Co(8,9,12\text{-}(CH_3)_3\text{-}1,2\text{-}C_2B_9H_8)_2]$ from the hexa-iodo derivative and methyl magnesium bromide as methylating agent in presence of $[Pd(PPh_3)_2Cl_2]$ and CuI was the first of a large queue of Palladium-catalysed cross-coupling reactions,[23] some examples such as Kumada (purple),[24] Negishi (blue and orange), [25] Sonogashira [9,26] and Heck (yellow)[10] reactions are represented in **Scheme 2.2**.

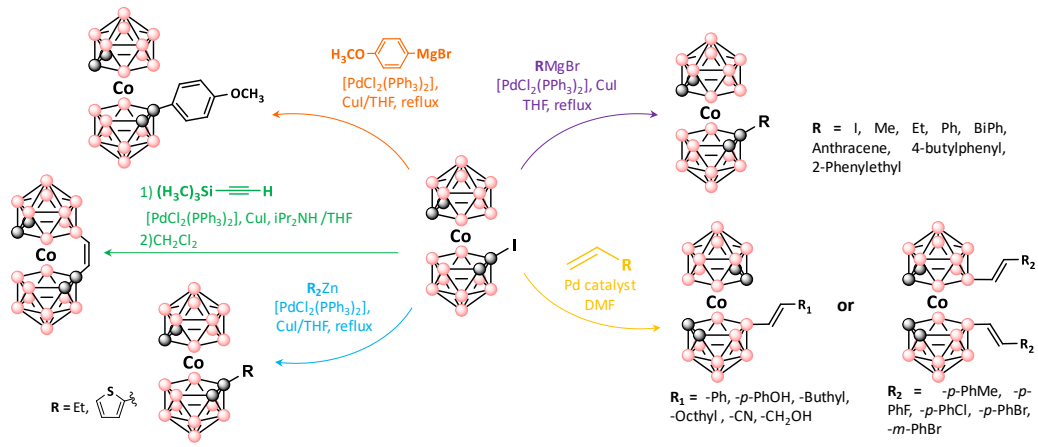

Scheme 2.2. Palladium catalyst cross-coupling reactions with COSAN founded in the bibliography.

However, many efforts have been made to avoid the use of expensive and toxic Palladium catalysts.[27] The most significant alternative to synthesized arene derivatives of COSAN was the use of an iodonium-bridge derivative, [3,3'-Co(8-μ-I-1,2-$C_2B_9H_{10}$)$_2$]$^-$, in combination with a Lewis acid as starting reagent.[28,29]

In this direction, we demonstrate for the first time the formation of a B-C bond in the absence of both any metal catalyst and iodo substituent containing cluster. We discovered this mechanism during a preliminary study where the reaction of the naphtalenyl derivative of COSAN, Cs[3,3'-Co(8-$C_{10}H_7$-1,2-$C_2B_9H_{10}$) (1',2'-$C_2B_9H_{11}$)] (Cs[**3**]), with triphenylcarbenium tetrafluoroborate ($TrBF_4$) in dimetoxyethane (DME) was designed to add a naphthalene bridge molecule by the formation of two B-Csp^2 bonds on a COSAN but it led to an unexpected but most wanted product: a tritylnaphthalenyl derivative of COSAN.

2.2 Synthesis and characterization of the tritylnaphthalenyl derivatives

The triphenylcarbenium tetrafluoroborate is an *in situ* cation generator (Tr^+) which act as a starter for cationic polymerization, as well as weak cation or hydride scavenger.[30-34] Moreover, the study of the crystal structures has shown that even though aryl metallacarboranes tend to possess *trans* configuration,[16,24] in solution a further degree of freedom of the pristine *ortho*-metallacarboranes lead to the stabilization of the *cis* configuration.[35,36] Therefore it was reasonable that the formation of a B-C_{sp2} could occur in solution due to the mobility of the clusters through a hydride removal by Tr^+ and B^+ formation.

The reaction of the cesium salt of naphtalenyl COSAN Cs[**3**] in DME with $TrBF_4$ under nitrogen and stirring overnight was analysed by MALDI-TOF-MS. The target product was not the desired compound; conversely, upon reaction with TrBr, an electrophilic substitution occurred, leading to tritylnaphthalenyl derivative of COSAN ([**4**]$^-$, see **Figure 2.1** and **Appendix B**). The mass of the base peak on the MALDI-TOF-MS is the sum of the molecular peak of the initial metallacarborane (450 m/z) plus a triphenylmethyl moiety (243 m/z) resulting in a new and unexpected molecule with 692.68 m/z ([**4**]$^-$). Despite this behaviour

was previously observed for the $[CB_{11}H_{12}]^-$ boron cluster, [37] Reed and co-workers research in a very similar reaction[34] did not report any B-C formation.

MALDI-TOF-MS gives us important information, but it is not complete. The molecular peak at 450m/z (**Figure 2.1**), could correspond to the formation of 1-methyleneinden-2-yl-bridged derivative $[3,3'\text{-}Co(8\text{-}\mu\text{-}C_9H_6CH_2\text{-}1,2\text{-}C_2B_9H_{10})_2]^-$ like in the already discussed reaction of pristine COSAN with naphthalene in the presence of $AlCl_3$.[16] However, the unique peak at 11.05 ppm in the ^{11}B-NMR spectrum confirm the absence of this product (see **Appendix B**). Thus we ascribe the MALDI-TOF peak at 450 m/z to the unreacted product.[38]

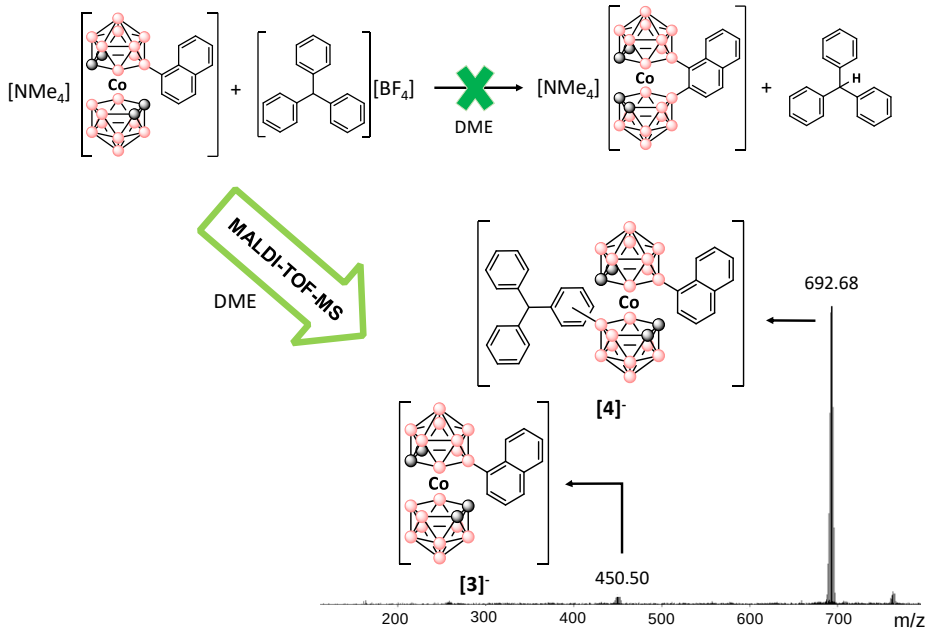

Figure 2.1. Reaction initially proposed, and MALDI-TOF-MS of the crude of the reaction, leading the formation of a B-C_{sp2} bond.

Based on these results we realized that with this method we could have been able to create a B-C bond simply and straightforwardly, so we tried to widen the substitution possibilities by changing the reagents and exploring the formation of new derivatives.

2.3 Synthesis of triphenylmethane derivatives of COSAN

2.3.1 Synthesis with triphenylcarbenium salts

To confirm the formation of the B-C bond, we carried out the same reaction discussed in the previous section and depicted in **Figure 2.1**, but this time using [**1**]$^-$ and $TrBF_4$ with 1:1 ratio in DME (**Scheme 2.3**). The result was again the formation of the B-C bond with a yield of 60%, corresponding to the triphenyl derivative ([**5**]$^-$).

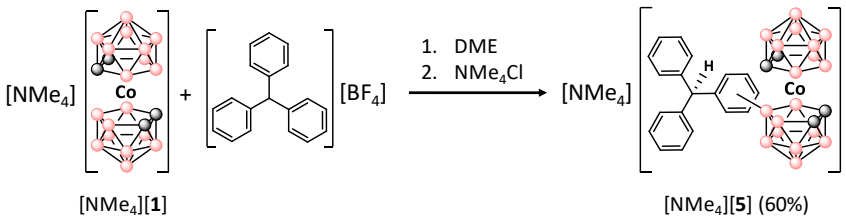

Scheme 2.3. Reaction conditions for the synthesis of $[NMe_4][5]$.

The reaction was also performed with 2 equivalents of $TrBF_4$ (**Scheme 2.4**). The MALDI-TOF-MS of the crude of the reaction displayed the base peak at 808.74 m/z that corresponds to a COSAN disubstituted with two triphenylmethyl moieties ([**6**]$^-$).[38] Thus, depending on the stoichiometry of the reaction, one or two units of the triphenylmethyl group can be joined to COSAN. A further increase of the $TrBF_4$ to 3 equivalents led to [**6**]$^-$, implying that the next B-H entities to be replaced are not nucleophilic enough to initiate the substitution. This reaction led to B(8) or B(8,8') substitution.

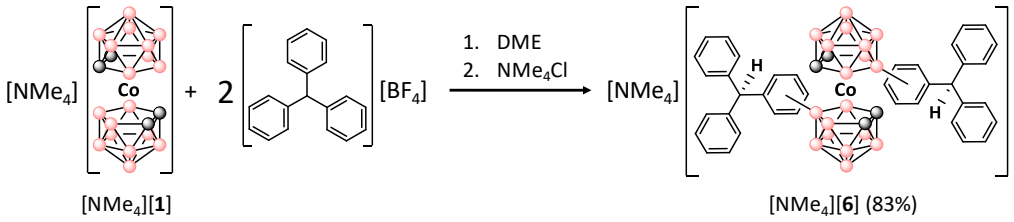

Scheme 2.4. Reaction conditions for the synthesis of $[NMe_4][6]$.

2.3.2 Synthesis with carbocations generated *in situ*

The list of stable electrophiles available is not very extensive hence we suggest producing the carbocations *in situ* aiming at increasing the total number of

substituents. One way of producing carbocations is by mixing halogenated reagents (RX) with soluble silver salts, the AgX salt precipitates, and the carbocation is formed.[39] In our case, we have taken advantage of the anionic nature of the COSAN so that we have prepared its silver salt, with the expectation that Ag^+ will precipitate with the halogen and the *in situ* formed carbocation will react directly with [**1**]$^-$. The silver salt of COSAN is soluble in DME or THF.

The selected reagents were the bromomethane derivatives with three, two or one phenyl group. We expect that the purity of the reaction product increases with the stability of the carbocations and hence with the number of benzene rings. Therefore, our research started with bromotriphenylmethane (TrBr), benzhydryl bromide (BzhBr) and benzyl bromide (BnBr) to study the influence of the number of aromatic rings in the carbocation behaviour.

A solution of bromomethane derivative in THF was added drop by drop to Ag[**1**] in THF in a molar ratio 1:1 (**Scheme 2.5** and **Scheme 2.6**). Immediately, denoting the speed of the reaction, a precipitate of AgBr appears while the colour of the solution remains orange, the typical colour of COSAN. The solution was immediately filtered to avoid oxidation processes generated by Ag^+ and a saturated solution of sodium chloride was added to the reaction mixture to produce two phases. The organic phase was dried and analysed by MALDI-TOF-MS. The reactions of TrBr and BzhBr with Ag[**1**] proved the formation of mono and disubstituted products, leaving behind unreacted reagent [**1**]$^-$. Both mixtures were purified by chromatography obtaining an isolated yield of 75% and 76% for [**5**]$^-$ and [**7**]$^-$ respectively. In addition, around 8% of the product in each reaction corresponds to the disubstituted compounds [**6**]$^-$ and [**8**]-, along with 8% of unreacted reagent [**1**]$^-$, respectively.

The high rate of reaction and perhaps the enhanced nucleophilic character of the B(8)'-H moiety after the first B-Tr formation could explain the tendency to form the disubstituted species. The same reactions were carried out with 2 equivalents of TrBr or BzhBr and the main products were [**6**]$^-$ and [**8**]$^-$ with yields of 83 and 87% respectively.

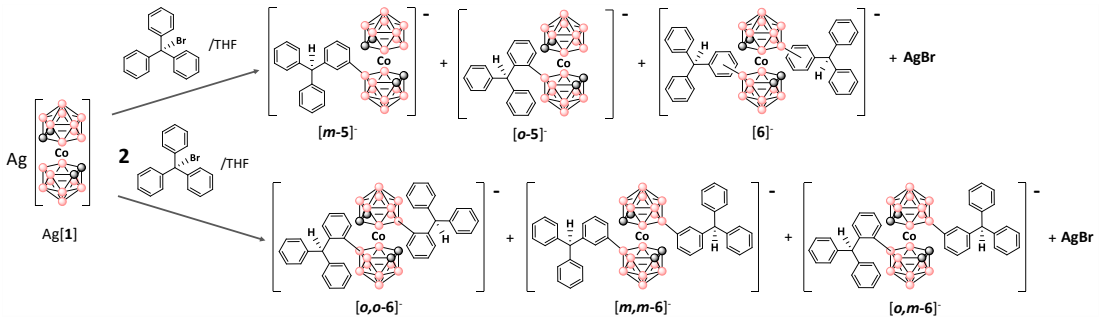

Scheme 2.5. Synthesis of [**5**]⁻ (above) and [**6**]⁻ (below) *via* carbocation generation *in situ.*

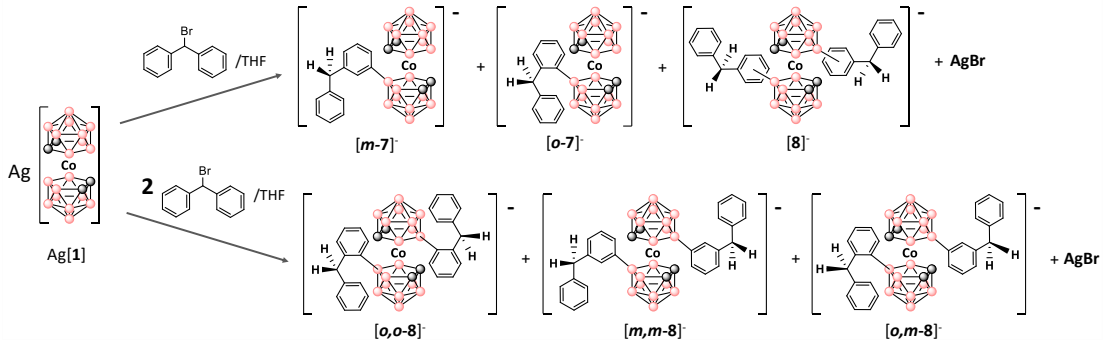

Scheme 2.6. Synthesis of [**7**]⁻ (above) and [**8**]⁻ (below) *via* carbocation generation *in situ.*

The reaction of BnBr with Ag[**1**] lead as the major product the unreacted [**1**]⁻ and some no quantitative fractions of the products [**Bn-1**]⁻ ([**9**]⁻), [**HO-1**]⁻ and [**Br-1**]⁻. This result was not as successful as the others in THF and as a consequence, we performed the same reaction in DME as an alternative solvent. The main product was again the unreacted [**1**]⁻, but the yield of the sought product [**9**]⁻ increased significantly (**Scheme 2.7**).

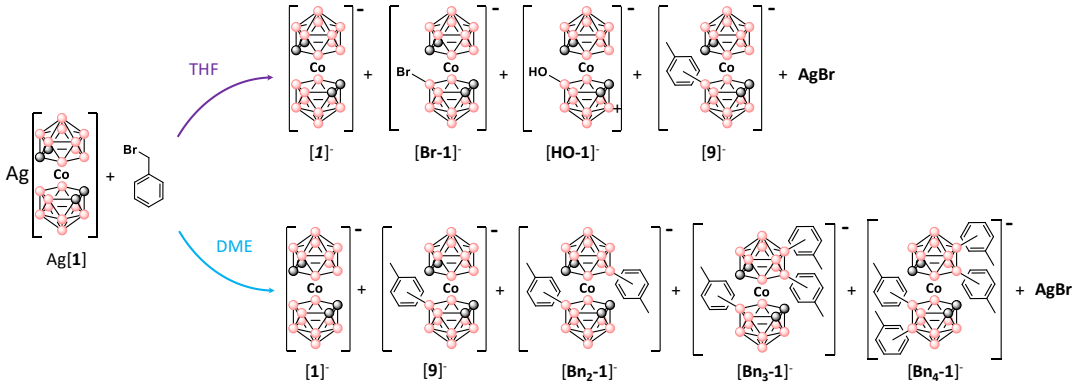

Scheme 2.7. Reaction of [**1**]⁻ with BnBr in THF (above) or DME (below) *via* carbocation generation *in situ.*

2.4 Characterization

The characterization of the products [**5**]$^-$ and [**6**]$^-$ synthesized by the two different methodologies present equal characteristics hence we will comment only once for every product.

MALDI-TOF-MS was the preferred technique used as a preliminary test to know if the reaction worked out. It gives us clear and straightforward information about the mass of the compounds present in the crude mixture of the reaction. The mass spectra of the products from reaction with TrBr and BzhBr with 1 or 2 equivalents corresponds to the sought products [**5**]$^-$, [**6**]$^-$, [**7**]$^-$ and [**8**]$^-$ display peaks at 566.59, 808.74, 490.24 and 655.37 m/z respectively.In some cases, especially to confirm the kind of bonds and the presence of specific substituents standard NMR techniques have been used probing boron nucleus so the resulting spectra give us information on the proximity configuration of boron atoms

2.4.1 Monosubtituted compounds [5]$^-$ and [7]$^-$ and isomeric mixtures

The NMR spectra were fundamental to demonstrate the formation of the B-C bond and identify the atoms involved in it. Once the reaction finished a preparative TLC on silica was fabricated, by which the layer corresponding to [**5**]$^-$ was analyzed. The COSAN B(8)-C_{sp2} resonance appears at 12.3 ppm in the ^{11}B-NMR,[11,24,36] consistent with the resonance at 5.5 ppm in ^{1}H-NMR corresponding to the H-C_{sp3} of triphenylmethane. Thus the B-C bond shall be between an aromatic carbon of Tr and the B(8). Moreover, the 4 signals corresponding to the H-$C_{cluster}$, 2+2 signals in the ^{1}H-NMR spectrum and 2 C_{sp3} signals in the ^{13}C-NMR spectrum reveal the presence of two isomeric products (**Figure 2.2**).

The benzhydryl derivative ([**7**]$^-$) presents an equivalent characterization, with a resonance at 12.5 ppm in the ^{11}B-NMR and double H_2-C_{sp3} proton signal at 3.90 and 3.87 ppm that indicates the presence of different isomers in the mixture (**Figure 2.2**). Unfortunately, the isomers in these mixtures had so similar physical properties that required many sequential TLC steps to separate them. Also, as we intended to demonstrate the feasibility of the B-C formation, we decided to characterize and work with the isomeric mixture.

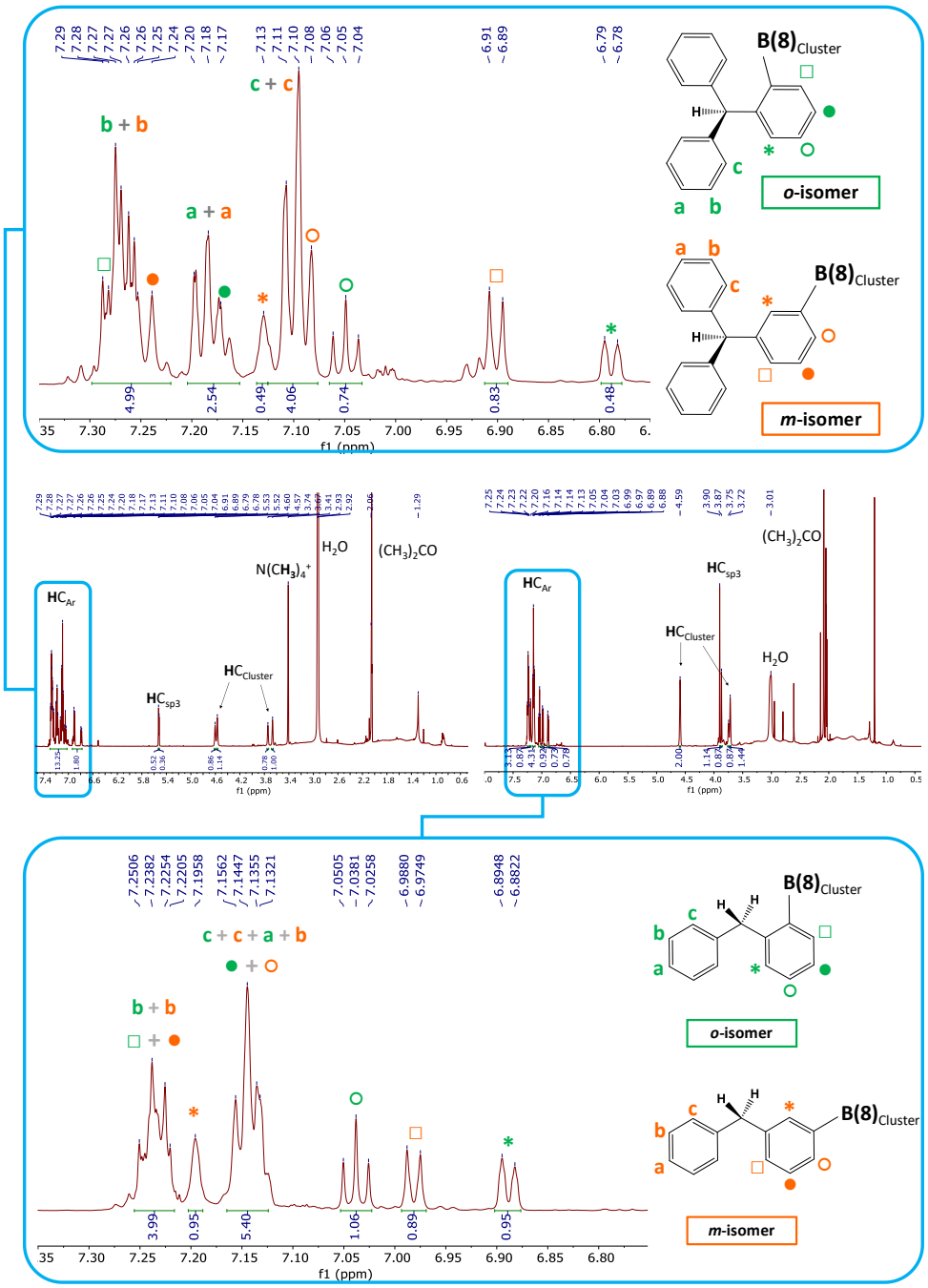

Figure 2.2. ^{1}H-NMR of [**5**]$^{-}$ (left) and [**7**]$^{-}$ and their ^{1}H-NMR amplified spectra (above and below respectively) with the complete characterization of the aromatic signals and identification of the different isomers.

The 1D and 2D-NMR spectroscopy provided sufficient clues to permit a consistent but not unambiguous isomeric assignation of compound $[NMe_4][\mathbf{5}]$ and Cs[**7**] (see **Appendix B**). The ^{1}H-NMR spectrum of the mixture of NMe_4[**5**] shows a singlet at 7.13 ppm indicating the presence of the *meta-* isomer and the two triplets at 7.05 and 7.16 ppm that can only be explained by the existence of the *ortho-* isomer in the mixture. Meanwhile, the compound Cs[**7**] present an equivalent ^{1}H-NMR spectrum with the singlet and triplets assigned to *meta-* and *ortho-* isomers at 7.19, 7.04 and 7.15 ppm respectively. Moreover, the ^{1}H COSY NMR spectra indicate which aromatic proton signals belong to every isomer as is described in the **Figure 2.2**.[38] Finally, it was possible to obtain the *ortho*:*meta* (2:3) and (1:1) ratio from the integration of H-$C_{cluster}$ protons in ^{1}H-NMR spectrum for $[NMe_4][\mathbf{5}]$ and Cs[**7**] respectively.

2.4.2 Disubstituted compounds [6]$^-$ and [8]$^-$

The NMR spectra of the disubstituted products $[NMe_4][\mathbf{6}]$ and Cs[**8**] are roughly similar to the monosubstituted derivatives $[NMe_4][\mathbf{5}]$ and Cs[**7**].

First, the ^{11}B-NMR of disubstituted compounds $[NMe_4][\mathbf{6}]$ and Cs[**8**] present more symmetric spectra with fewer signals respect to the ^{11}B-NMR of monosubstituted ones and the integration of the peaks confirm the double substitution (**Figure 2.3**). The ^{1}H-NMR spectra of $[NMe_4][\mathbf{6}]$ and Cs[**8**] display three peaks around 3.8 ppm (due to the H-$C_{Cluster}$) probably, explained by the existence of three isomers in the mixture (**Figure 2.4**). Even though the overlap of the proton signals did not permit us to identify with precision the isomeric mixture, we assumed based on the ^{1}H-NMR interpretation of the monosubstituted species, that the disubstituted species [**6**]$^-$ and [**8**]$^-$ are mixtures of their [*o,m-*], [*o-,o-*] and [*m,m-*] isomers. Unfortunately, the signal overlap did not allow proposing an isomer ratio too.

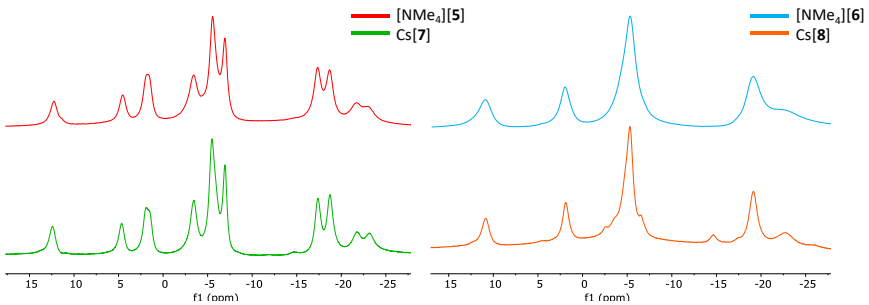

Figure 2.3. Comparative $^{11}B\{^{1}H\}$-NMR spectra of $[NMe_4][\mathbf{5}]$ (red), $[NMe_4][\mathbf{6}]$ (blue), Cs[**7**] (green) and Cs[**8**] (orange).

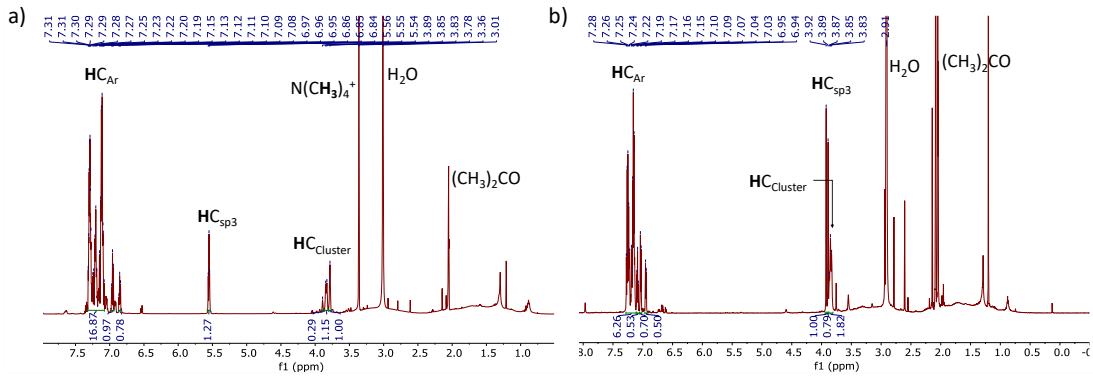

Figure 2.4. ^{1}H-NMR spectra of $[NMe_4][\mathbf{6}]$ (left) and Cs[**8**] [40].

2.4.3 Reactions with benzyl bromide

The mass spectra of the crude from the reaction of $[\mathbf{1}]^-$ with 1 equivalent of BnBr displays 4 major peaks that have been assigned as follows: unreacted COSAN at 324 m/z, that is the more intense and to [3,3'-Co(8-OH-1,2-$C_2B_9H_{10}$)(1',2'-$C_2B_9H_{11}$)]$^-$ ([**HO-1**]$^-$) at 340 m/z; [3,3'-Co(8-Br-1,2-$C_2B_9H_{10}$)(1',2'-$C_2B_9H_{11}$)]$^-$ ([**Br-1**]$^-$) at 403 m/z; at [**9**]$^-$ at 414 m/z corresponding to the formation of the targeted compound. We suggest substitution at the position B(8), as it is the most plausible, and the one given by the computational study, but have not done an experimental exhaustive study leading to unambiguously know where the substitution did occur.

As an alternative, we run the reaction of $[\mathbf{1}]^-$ with BnBr in DME. The result was significantly different, the MALDI-TOF-MS shows five peaks separated by 90 m/z corresponding to the sequential addition of up to four benzyl group units, the

base peak being for [**1**]$^-$. The reaction presumably is so fast that the substitution is multiple. To target for one major product the experiment was done at different conditions as well as modifying the ratios of benzyl bromide (to two, three and ten), decreasing the reaction temperature to -20°C and replacing the benzyl bromide by the chloride to slow the reaction speed. However, the results show that the largest component in the mixture is always [**1**]$^-$ (**Appendix B**).

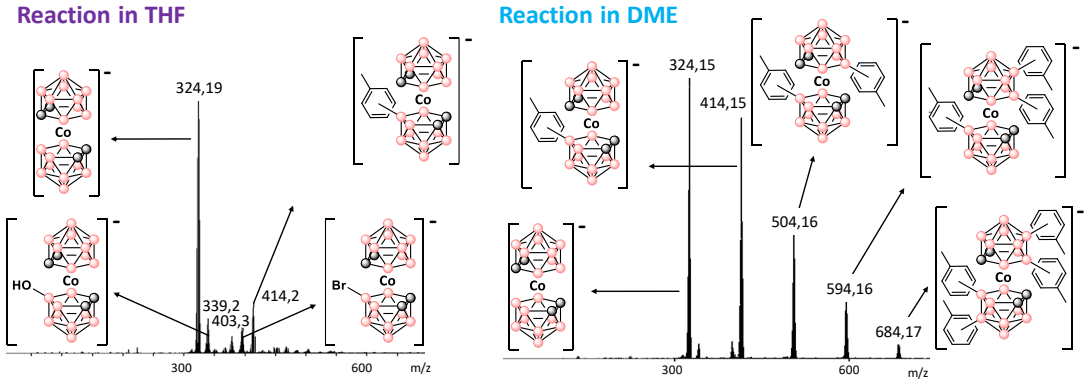

Figure 2.5. MALDI-TOF-MS of the crude of the reaction between BnBr and Ag[**1**] in THF (left) and DME [40].

* Quantitative MALDI-TOF spectra analysis

In the introduction, we indicated how important is the information drawn from the MALDI-TOF-MS concerning [**1**]$^-$ and its derivatives. Worth to notice is that these studies have permitted to demonstrate the quantitative capability of the MS. Commonly, MS has been seen as a tool for qualitative chemical analysis, although much progress is being done to convert it also in a quantitative tool for metallacarborane derivatives. We noticed in 2009 that the MS-height of related COSAN derivatives was proportional to the concentration.[41,42] This represented a great advance in COSAN research. However, we had not found a distinct type of experiment to the one described to test the validity of the approach. As seen in **Figure 2.5** on the right for an equimolar ratio of Ag[1] and BnBr five peaks are formed, the more intense being unreacted [**1**]$^-$. This was done on the crude of the reaction, so all reagents were there. The addition of the heights of the five peaks corresponds to the total amount of [**1**]$^-$ [A] (**Figure 2.6**), whereas the addition of the peaks weighted by the number of benzyl units each one carries lead to the total amount of benzyl [B]. If the reactant ratio was 1:1 and the reaction went to

completion, the two numbers A and B should be identical, given that the MS was quantitative. The calculation exhibited in **Appendix B** shows a discrepancy of less than 1,3 %. Moreover, these results are supported by the NMR data found in the literature.[38]

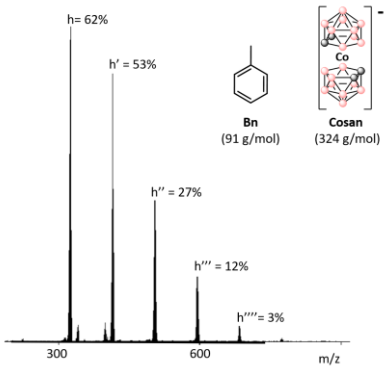

Figure 2.6. Representation of the height percentage of every peak in MALDI-TOF-MS of the reaction of BnBr with [**1**]$^-$ in DME.

2.5 Reaction mechanism study

2.5.1 Defining the reaction mechanism: DFT Calculation

Bregadze et al. interpret the halogenations and mercuriation of metallacarboranes as an electrophilic aromatic substitution. Lavallo considers that the borate performs a nucleophilic aromatic substitution.[43] In our case, this is not that obvious as can be deduced from this section. The next reading will unveil the behaviour of the Tr^+.

We formally consider that Tr^+ loses its positive charge upon extraction of the H^- in B(8)-H. [21,44-48] In its simplest explanation, two formal processes occur in this reaction: i) the Tr^+ removes the B(8)-H and generates a B^+, and ii) the B^+ is an electrophile that attacks the aromatic system, probably following an A_EAr mechanism. As in any electrophilic aromatic substitution, a regioselective issue appears. If we focus our attention on the electrophilic aromatic substitution on Ph_3CH, there is a common shared CH that by itself is weakly activating, thus directing the substitution to *ortho-* and *para-* positions. Therefore it would be reasonable to assume that *ortho-* and *para-* isomers are generated by the electrophilic attack of $[3,3'Co(1,2\text{-}C_2B_9H_{10})(1',2'\text{-}C_2B_9H_{11})]^0$. However, our

interpretation of the experimental data unveil counterintuitive results where the isomers *ortho*- and *meta*-dominate the product yield [49]

To get more insight into the reaction mechanism, DFT calculations, at ωB97XD/6-31+G* level of theory, were performed and three main steps can be identified.

i) The initial step (which is the rate-limiting step with 6-8 kcal/mol barriers) is the hydride transfer which results in the formation of the adduct of the formal B^+ intermediate (B^+) and triphenylmethane. As seen in **Figure 2.7**, the transition state (TS) shows a boronium ion and a carbocation sharing a hydride.

ii) The latter stage is followed by the nucleophilic attack of triphenylmethane to the boronium, which seems to be almost barrierless. Unfortunately, all attempts to localize this transition state failed in our hands, but scan calculations (decreasing stepwise the B-C distance by 0.1 Å) showed that the energy of the system decreases continuously, indicating no significant barrier of this process. In agreement with the proposed very small barrier, starting the geometry optimization of the slightly modified geometry of the complex of Ph_3CH and B^+ gives the protonated *ortho*-[4]$^-$, *meta*-[4]$^-$ and *para*-[4]$^-$ which are more stable by 14.5, 10.0 and 11.9 kcal/mol, respectively.

iii) The last step is the proton abstraction, which results in the final products. The small barriers were in agreement with the observed fast reaction; the initially formed triphenylmethane immediately attacks the electrophilic center. Indeed some works propose an ion pair complex,[43,] e.g. indicated as **3**$[CPh_3]^+$; although structurally not informative, which is not so far from the transition state in our proposed mechanism, in which the H is shared by the $[CPh_3]^+$ and the borinium in [3,3'-Co(1,2-$C_2B_9H_{10}$)(1',2'-$C_2B_9H_{11}$)]^0.

The difference is that in the mechanism proposed by Lavallo the anionic boron cluster performs as a nucleophile on the Ph on Tr^+ whereas in our computationally described mechanism there is an electrophilic attack to the Ph on Tr^+. Our suggested mechanism was also supported by the experimental reaction of Tr^+ and

[**1**]$^-$ in the presence of 10 eq. of benzene. The initial idea was to introduce in the reaction benzene as a possible competitor of Tr^+ in order to have a possible competing reaction between the two arenes PhH and Ph_3CH. However, according to MALDI-TOF-MS, the derivatives of Ph_3CH were dominant in relation to the ones of PhH in a ratio of 11:2. This behaviour suggests a rapid reaction than once the boronium is formed it reacts immediately with the closest molecule, which in this case is the Ph_3CH. This experiment supports our hypothesis where the Tr^+ works as hydride scavenger.[38]

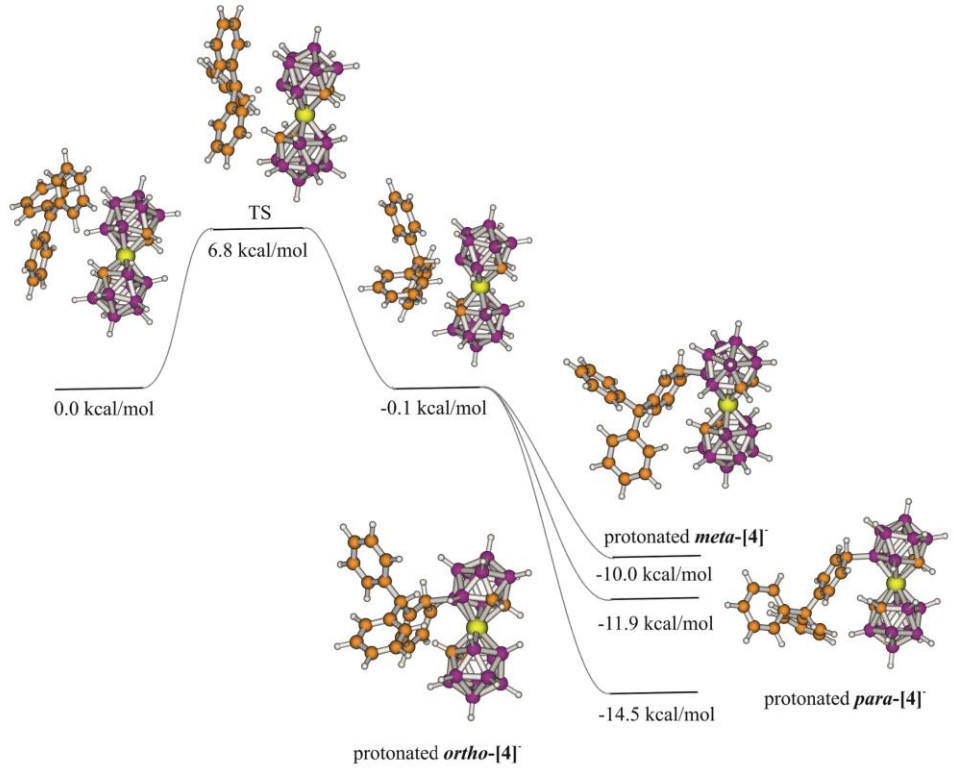

Figure 2.7. Calculated reaction mechanism of the hydride abstraction and the nucleophilic attack of Ph_3CH.

2.5.2 Defining the reaction mechanism: experimental part

The synthesis leading to [**5**]$^-$ with TrBr and [**1**]$^-$ was carried out in different solvents to these already discussed to assess the role of Tr^+ in the reaction. We selected benzene, toluene and dichloromethane (DCM) as solvents while the reactions were either carried out at reflux or at room temperature. Firstly, 30 mg of Ag[**1**]

(0.07 mmols) was dissolved in 2 mL of solvent and the reaction was set up at one of the above mentioned conditions. Subsequently, 1 equivalent of TrBr, dissolved in 1 mL of the same solvent, was added drop by drop to the mixture. The precipitation of AgBr was instantaneous but, the mixture was left stirring for 5 minutes at the same conditions. The AgBr was filtered and the solvents removed under vacuum, finally, the products were analysed by MALDI-TOF-MS (**Figure 2.8**).

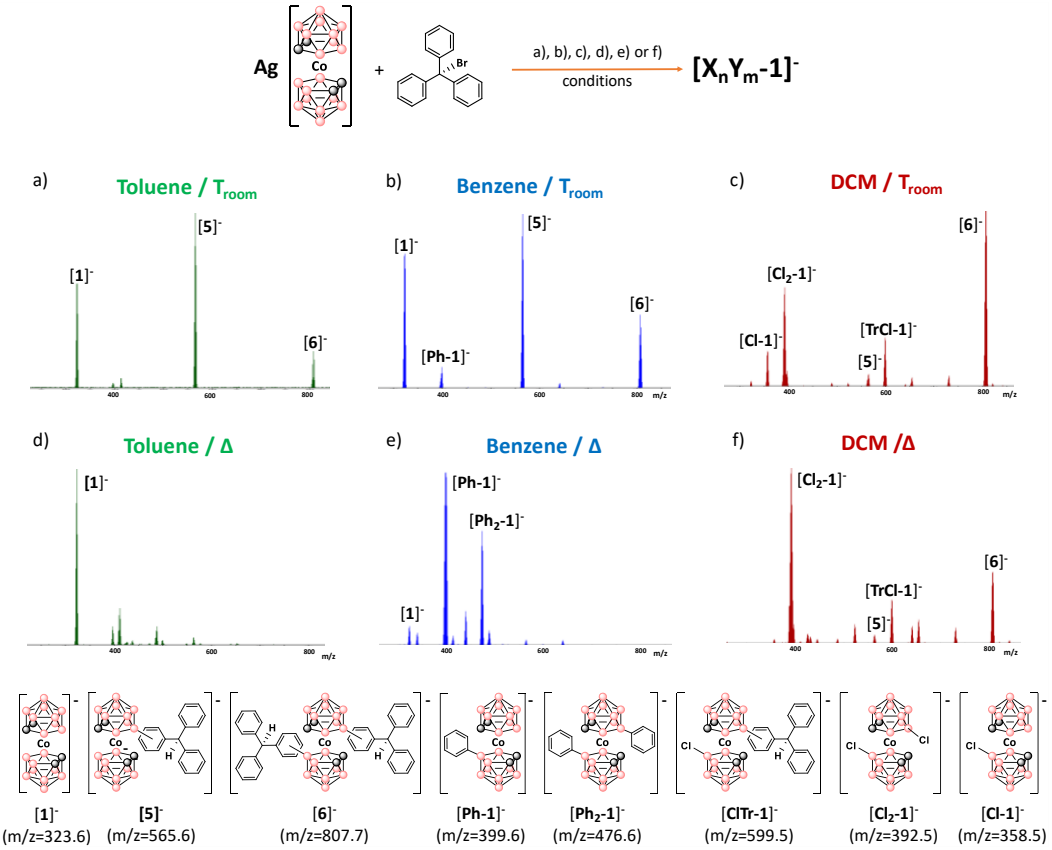

Figure 2.8. MALDI-TOF-MS spectra of the synthesis conditions to lead [**4**]$^-$ but in different solvents and at different temperatures: a) in toluene at room temperature; b) in benzene at room temperature; c) in DCM at room temperature; d) in toluene at reflux temperature; e) in benzene at reflux temperature; c) in DCM at reflux temperature. All the compounds formed are represented by the formula $X_nY_{m,}$, were X= Tr, Ph or Cl , Y = Tr, Ph or Cl, n and m are the numbers 1 or 0. The chemical structures proposed for the different peaks of the MALDI-TOFs.

- *Room temperature outcomes.* The outcome of the reactions at room temperature with benzene and toluene do not show differences with the results obtained in THF, but in the case of DCM we clearly see a rise of new peaks. Actually,

while for the first two trials the main product is always [**5**]$^-$, when the solvent is DCM the MALDI-TOF-MS shows some minor peaks corresponding to mono ([**Cl$_1$-1**]$^-$), dichloro ([**Cl$_2$-1**]$^-$), chlorotrityl COSAN ([**TrCl-1**]$^-$) and [**6**]$^-$, dominants over the [**5**]$^-$.

- *Reflux outcomes.*_Conversely, the results are different in refluxing conditions. When using toluene the reaction does not take place, as corroborated by MALDI-TOF-MS that presents [**1**]$^-$ as the dominant compounds and some very small additional peaks. If benzene is used as a solvent the reaction leads to only benzene derivatives of COSAN, which once again demonstrates the hydride scavenger behaviour of Tr^+. The MALDI-TOF-MS displays two major peaks at 399 and 476 m/z corresponding to [**Ph-1**]$^-$ and [**Ph$_2$-1**]$^-$ respectively (**Figure 2.8**). The reaction in refluxing DCM shows the same three major peaks in the MALDI-TOF spectra as at room temperature, but now the major peak is due to [**Cl$_2$-1**]$^-$.

To confirm our hypothesis that Tr^+ works as hydride scavenger, the same conditions were used in benzene or DCM but in the absence of TrBr (**Figure 2.9**). The MALDI-TOF-MS show the same results for both solvents at room temperature or refluxing conditions. As seen, no reaction occurred as only the peak corresponding to [**1**]$^-$ is found. These results are quite conclusive to understand the role of TrBr in these B-C coupling processes. The reaction in PhH explains that TrBr indeed acts as a hydride scavenger, but the electrophilic attack by the boronium is so fast that it attacks the closer aryl groups in Ph_3C-H. However, under refluxing conditions, molecules move much quicker than at room T and in these conditions, the attack occurs to the more available arenes, which in this case is the benzene solvent.

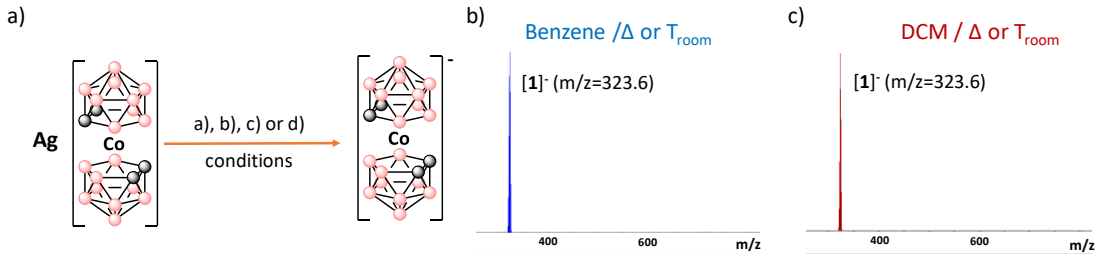

Figure 2.9. General reaction scheme for the synthesis conditions to lead [**4**]$^-$ but in different solvents and at different temperatures and in the absence of TrBr (above) and the MALDI-TOF-MS of the reactions.

2.6 Conclusions

It is important to highlight that this work is the first report of a fast procedure to form B-C bonds in metallacarboranes without the use of any catalyst (Lewis acid or Pd) or iodometallacarboranes. The synthesis has been studied with different benzyl stabilized carbocations demonstrating that three or two aryl groups stabilize more the carbocation than one. In these cases, the reactions with Tr^+ or Bzh^+ are successful with very high yields although a mixture of isomers (*ortho-* and *meta-*) have been detected. It is worth noting that they are predominately *ortho-* and *meta-*, and not *ortho-* and *para-* as we could expect to form taking into account the classical electrophilic aromatic substitution. This anomalous isomeric mix can be attributed to the very high rate of the reaction that occurs in less than half a minute. In addition, DFT calculation and experimental studies have been able to demonstrate the reaction mechanism which corroborates the hydride scavenger behaviour of the TrBr.

Finally, less stable carbocations such as allyl or alkyl that do not have a "built-in" nucleophile do not lead to the targeted B-C bond formation. The high speed of the reaction permits to get distinct products either acting on the solvent on the temperature as well as on the presence of one arene reagent. Although this study is very preliminary, this B-C bond coupling reaction opens the way to rich derivatization of the COSAN and probably other sandwich metallacarboranes in a simple and fast reaction. It is a step ahead to the Kumada and Heck reaction, as the need of [Pd] catalysts, Grignard reagents and metallacarborane's iodo derivatives can be avoided. Furthermore, the fact that this reaction works with as-generated carbocations in-situ is a great advantage, as the range of available reagents is way higher than all the synthesis already developed. Direct implications of the wide tunability of the organic substituent will be the easy functionalization of metallacarborane for heterogeneous catalysis, energy harvesting and molecular electronics.

2.7 References

(1) R. N. Grimes, *Carboranes*, US, 3rd edn., **2016**.

(2) D. Olid, R. Nuñez, C. Viñas and F. Teixidor, Methods to produce B-C, B-P, B-N and B-S bonds in boron clusters, *Chem. Soc. Rev*, **2013**, 42, 3318-3336.

(3) B. Grüner, V. Šícha, D. Hnyk, M. G. S. Londesborough and I. Císařová, The Synthesis and Structural Characterization of Polycyclic Derivatives of Cobalt Bis(dicarbollide)(1−), *Inorg. Chem.*, **2015**, 54, 3148-3158.

(4) A. B. Buades, V. Sanchez Arderiu, D. Olid-Britos, C. Viñas, R. Sillanpää, M. Haukka, X. Fontrodona, M. Paradinas, C. Ocal and F. Teixidor, Electron Accumulative Molecules, *J. Am. Chem. Soc.*, **2018**, 140, 2957-2970.

(5) I. B. Sivaev, M. Y. Stogniy, S. A. Anufriev, M. V. Zakharova and V. I. Bregadze, New sulfur derivatives of carboranes and metallacarboranes, *Phosphorus, Sulfur Silicon Relat. Elem.*, **2017**, 192, 192-196.

(6) S. A. Anufriev, S. A. Erokhina, K. Y. Suponitsky, I. A. Godovikov, O. A. Filippov, F. Fabrizi de Biani, M. Corsini, A. O. Chizhov and I. B. Sivaev, Methylsulfanyl-Stabilized Rotamers of Cobalt Bis(dicarbollide), *Eur. J. Inorg. Chem*, **2017**, 4444-4451.

(7) A. V. Shmal'ko, S. A. Anufriev, A. A. Anisimov, M. Y. Stogniy, I. B. Sivaev and V. I. Bregadze, Synthesis of cobalt and nickel 6,6′-diphenylbis(dicarbollides), *Russ. Chem. Bull.*, **2019**, 68, 1239-1247.

(8) X. Zhang and H. Yan, Transition metal-induced B–H functionalization of o-carborane, *Coord. Chem. Rev.*, **2019**, 378, 466-482.

(9) I. Rojo, F. Teixidor, R. Kivekäs, R. Sillanpää and C. Viñas, Formation of Bridging Alkene and Conjugated Dialkenes Exclusively Generated from Alkynes on the [3,3'-Co(1,2-$C_2B_9H_{11})_2]^-$ Platform. The Unique Hydroboration Role of [3,3'-Co(1,2-$C_2B_9H_{11})_2$], *J. Am. Chem. Soc.*, **2003**, 125, 14720-14721.

(10) P. Farràs, D. Olid-Britos, C. Viñas and F. Teixidor, Unprecedented B–H Activation Through Pd-Catalysed B–Cvinyl Bond Coupling on Borane Systems, *Eur. J. Inorg. Chem*, **2011**, 2525-2532.

(11) V. S. Arderiu, C. Viñas and F. Teixidor, Skipping the one C–X one C–C bond rule in Kumada cross coupling reaction. Diarylation from an only B–I in metallacarboranes, *J. Organomet. Chem.*, **2015**, 798, 160-164.

(12) D. Olid, C. Viñas and F. Teixidor, Li^+-Mediated B-C Cross-Coupling, *Chem. Eur. J.*, **2012**, 18, 12936-12940.

(13) J. Francis, C. Jones and M. Hawthorne, Chemistry of bis (. pi.-7, 8-dicarballyl) metalates. Reaction between [(. pi.-7,8-$B_9C_2H_{11})_2$Co]-and aryl diazonium salts, *J. Am. Chem. Soc.*, **1972**, 94, 4878-4881.

(14) J. Plešek and S. Heřmánek, Introduction of an HS-group into electron donor positions in icosahedral heteroboranes. A new method for the preparation of metallocarborane

sandwich compounds with o-phenylene bridges, *Collect. Czech. Chem. Commun.*, **1978**, 43, 1325-1331.

(15) A. Franken, J. Plešek and C. Nachtigal, Unusual Rearrangement of Naphthalene in the Synthesis of a Novel B8-B8-Bridged Derivative in the [(1, 2-$C_2B_9H_{11}$)$_2$-3-Co]$^-$ Series. X-Ray Structure and ^{11}B NMR Spectra of [8, 8'-μ-(CH_2-C_9H_6)-(1, 2-$C_2B_9H_{10}$)$_2$-3-Co]-(CH_3)$_4N^+$, *Collect. Czech. Chem. Commun.*, **1997**, 62, 746-751.

(16) J. Plešek, S. Heřmánek, A. Franken, I. Císařová and C. Nachtigal, Dimethyl Sulfate Induced Nucleophilic Substitution of the [Bis (1, 2-dicarbollido)-3-cobalt (1-)] ate Ion. Syntheses, Properties and Structures of Its 8, 8'-μ-Sulfato, 8-Phenyland 8-Dioxane Derivatives, *Collect. Czech. Chem. Commun.*, **1997**, 62, 47-56.

(17) T. Peymann, C. B. Knobler and M. F. Hawthorne, A Study of the Sequential Acid-Catalyzed Hydroxylation of Dodecahydro-closo-dodecaborate(2−), *Inorg. Chem.*, **2000**, 39, 1163-1170.

(18) M. F. Hawthorne, D. C. Young, T. D. Andrews, D. V. Howe, R. L. Pilling, A. D. Pitts, M. Reintjes, L. F. Warren Jr and P. A. Wegner, . pi.-Dicarbollyl derivatives of the transition metals. Metallocene analogs, *J. Am. Chem. Soc.*, **1968**, 90, 879-896.

(19) B. Grüner, J. Plešek, J. Báča, I. Císařová, J. F. Dozol, H. Rouquette, C. Viñas, P. Selucký and J. Rais, Cobalt bis(dicarbollide) ions with covalently bonded CMPO groups as selective extraction agents for lanthanide and actinide cations from highly acidic nuclear waste solutions, *New J. Chem.*, **2002**, 26, 1519-1527.

(20) I. Rojo, F. Teixidor, R. Kivekäs, R. Sillanpää and C. Viñas, Methylation and demethylation in cobaltabis (dicarbollide) derivatives, *Organometallics*, **2003**, 22, 4642-4646.

(21) V. I. Bregadze, S. V. Timofeev, I. B. Sivaev and I. A. Lobanova, Substitution reactions at boron atoms in metallacarboranes, *Russ. Chem. Rev.*, **2004**, 73, 433.

(22) A. Goursot, E. Pénigault, H. Chermette and J. G. Fripiat, Structure électronique des dianions $B_{12}H_{12}^{2-}$ et $B_9C_2H_n^{2-}$, *Canadian journal of chemistry*, **1986**, 64, 1752-1757.

(23) M. D. Mortimer, C. B. Knobler and M. F. Hawthorne, Methylation of boron vertices of the cobalt dicarbollide anion, *Inorg. Chem.*, **1996**, 35, 5750-5751.

(24) I. Rojo, F. Teixidor, C. Viñas, R. Kivekäs and R. Sillanpää, Relevance of the Electronegativity of Boron in η 5-Coordinating Ligands: Regioselective Monoalkylation and Monoarylation in Cobaltabisdicarbollide [3,3′-Co(1,2-$C_2B_9H_{11}$)$_2$]$^-$ Clusters, *Chem. Eur. J.*, **2003**, 9, 4311-4323.

(25) I. P. Beletskaya, V. I. Bregadze, V. A. Ivushkin, P. V. Petrovskii, I. B. Sivaev, S. Sjöberg and G. G. Zhigareva, New B-substituted derivatives of m-carborane, p-carborane, and cobalt bis (1, 2-dicarbollide) anion, *J. Organomet. Chem.*, **2004**, 689, 2920-2929.

(26) N. N. Greenwood and A. Earnshaw, *Chemistry of the Elements*, Elsevier, **2012**.

(27) J. Emsley, *Nature's building blocks: an AZ guide to the elements*, Oxford University Press, **2011**.

(28) V. I. Bregadze, I. D. Kosenko, I. A. Lobanova, Z. A. Starikova, I. A. Godovikov and I. B. Sivaev, C−H Bond Activation of Arenes by [8,8′-μ-I-3,3′-Co(1,2-$C_2B_9H_{10})_2$] in the Presence of Sterically Hindered Lewis Bases, *Organometallics*, **2010**, 29, 5366-5372.

(29) I. D. Kosenko, I. A. Lobanova, I. A. Godovikov, Z. A. Starikova, I. B. Sivaev and V. I. Bregadze, Mild C–H activation of activated aromatics with [8, 8′-μ-I-3, 3′-Co (1, 2-$C_2B_9H_{10})_2$]: Just mix them, *J. Organomet. Chem.*, **2012**, 721, 70-77.

(30) C. Schade and H. Mayr, Tritylium ions as initiators and co-initiators in cationic polymerizations, *Makromol. Chem., Rapid Commun.*, **1988**, 9, 477-482.

(31) Y. N. Smirnov, V. Volkov, E. Oleinik, B. Komarov, B. Rozenberg and N. Yenikolopyan, The mechanism of initiation of polymerization of trioxan in the presence of tritylium salts, *Polym. Sci. USSR*, **1974**, 16, 846-854.

(32) Y. Xiong, T. Szilvási, S. Yao, G. Tan and M. Driess, Synthesis and Unexpected Reactivity of Germyliumylidene Hydride [: GeH]+ Stabilized by a Bis (N-heterocyclic carbene) borate Ligand, *J. Am. Chem. Soc.*, **2014**, 136, 11300-11303.

(33) N. J. Patmore, M. J. Ingleson, M. F. Mahon and A. S. Weller, Investigation of the synthesis of $\{Mo(\eta 5\text{-}C_5H_5)(CO)_3\}^+$ fragments partnered with the monoanionic carboranes [closo-$CB_{11}H_{11}Br]^-$, [closo-$CB_{11}H_6Br_6]^-$ and [closo-$HCB_{11}Me_{11}]^-$ by silver salt metathesis and hydride abstraction, *Dalton Trans.*, **2003**, 14, 2894-2904.

(34) Z. Xie, T. Jelinek, R. Bau and C. A. Reed, New Weakly Coordinating Anions. III. Useful Silver and Trityl Salt Reagents of Carborane Anions, *J. Am. Chem. Soc.*, **1994**, 116, 1907-1913.

(35) E. J. Juárez-Pérez, R. Núñez, C. Viñas, R. Sillanpää and F. Teixidor, The Role of C–H···H–B Interactions in Establishing Rotamer Configurations in Metallabis(dicarbollide) Systems, *Eur. J. Inorg. Chem*, **2010**, 2385-2392.

(36) P. Farràs, A. D. Musteti, I. Rojo, C. Viñas, F. Teixidor and M. E. Light, Widely applicable metallacarborane reagents for π-conjugated systems, *Inorg. Chem.*, **2014**, 53, 5803-5809.

(37) J. F. Kleinsasser, S. P. Fisher, F. S. Tham and V. Lavallo, On the Reactivity of the Carba-closo-dodecaborate Anion with the Trityl Cation, *Eur. J. Inorg. Chem*, **2017**, 4417-4419.

(38) A. B. Buades, Z. Kelemen, V. S. Arderiu, A. Zaulet, C. Viñas and F. Teixidor, A fast and simple B–C bond formation in metallacarboranes avoiding halometallacarboranes and transition metal catalysts, *Dalton Trans.*, **2020**, 49, 3525-3531.

(39) D. Sharp and N. Sheppard, 135. Complex fluorides. Part VIII. The preparation and properties of salts of the triphenylmethyl cation: the infrared spectrum and configuration of the ion, *J. Chem. Soc*, **1957**, 674-682.

(40) S. H. J. Plesek, L. J. Todd and W.F. Wright, *Collect. Czech. Chem. Commun.*, **1976**, 3509-3515.

(41) P. González-Cardoso, A.-I. Stoica, P. Farràs, A. Pepiol, C. Viñas and F. Teixidor, Additive Tuning of Redox Potential in Metallacarboranes by Sequential Halogen Substitution, *Chem. Eur. J.*, **2010**, 16, 6660-6665.

(42) L. Urban Pawel, Quantitative mass spectrometry: an overview, *Philosophical Transactions of the Royal Society A: Mathematical, Physical and Engineering Sciences*, **2016**, 374, 20150382.

(43) S. P. Fisher, S. G. McArthur, V. Tej, S. E. Lee, A. L. Chan, I. Banda, A. Gregory, K. Berkley, C. Tsay, A. L. Rheingold, G. Guisado-Barrios and V. Lavallo, Strongly Coordinating Ligands To Form Weakly Coordinating Yet Functional Organometallic Anions, *J. Am. Chem. Soc.*, **2020**, 142, 251-256.

(44) D. Astruc, *Organometallic Chemistry and Catalysis*, Springer, Berlin, **2007**.

(45) H. Mayr, J. Ammer, M. Baidya, B. Maji, T. A. Nigst, A. R. Ofial and T. Singer, Scales of Lewis Basicities toward C-Centered Lewis Acids (Carbocations), *J. Am. Chem. Soc.*, **2015**, 137, 2580-2599.

(46) L. Cabrera, G. C. Welch, J. D. Masuda, P. Wei and D. W. Stephan, Pyridine and phosphine reactions with [CPh3][B(C6F5)4], *Inorg. Chim. Acta*, **2006**, 359, 3066-3071.

(47) V. Šícha, J. Plešek, M. Kvíčalová, I. Císařová and B. Grüner, Boron(8) substituted nitrilium and ammonium derivatives, versatile cobalt bis(1,2-dicarbollide) building blocks for synthetic purposes, *Dalton Trans.*, **2009**, 5, 851-860.

(48) V. M. Retivov, E. Y. Matveev, M. V. Lisovskiy, G. A. Razgonyaeva, L. I. Ochertyanova, K. Y. Zhizhin and N. T. Kuznetsov, Nucleophilic substitution in closo-decaborate [B10H10]2− in the presence of carbocations, *Russ. Chem. Bull.*, **2010**, 59, 550-555.

(49) G. Olah and S. Kobayashi, Aromatic substitution. XXIX. Friedel-Crafts acylation of benzene and toluene with substituted acyl halides. Effect of substituents and positional selectivity, *J. Am. Chem. Soc.*, **1971**, 93, 6964-6967.

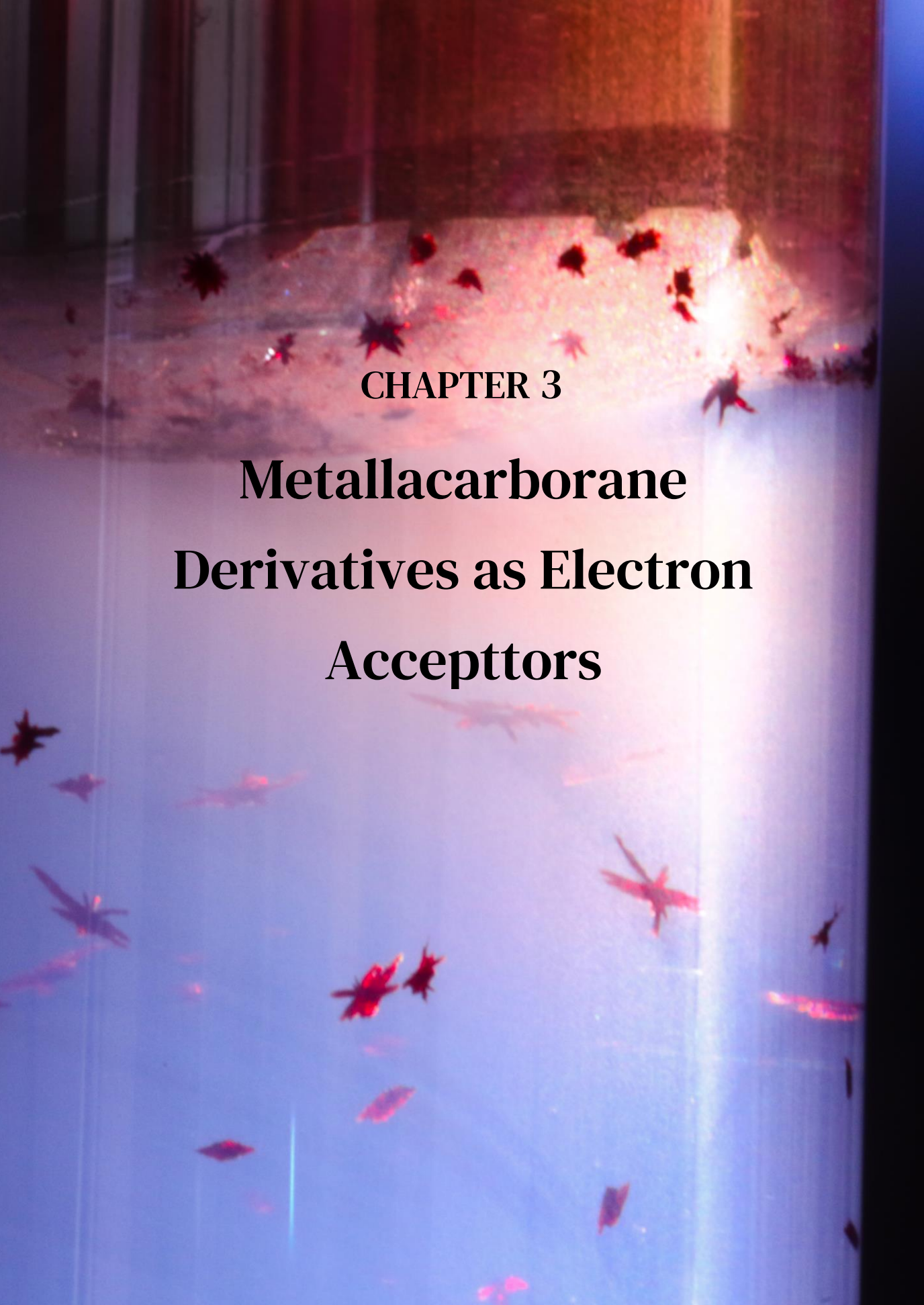

CHAPTER 3

Metallacarborane Derivatives as Electron Accepttors

CHAPTER THREE

Metallacarborane Derivatives as Electron Acceptors

The develop of molecules able to accept a lot of electrons is a hot topic were the C60 and PCBM seem to be the starts of the material's science field. However, the low processability of these compounds as a result of their low solubility push us to continue with the research of new molecules with the same electron-acceptor properties but, with higher processability. This work selects the metallacarboranes COSAN and FESAN and adds them a derivative of methyl viologen, molecule able to accept up to 4 electrons, with the idea to increase the number of electrons the COSAN and FESAN structures could be able to accept. As a result, this chapter will focus on the synthesis of pyridine or bipyridine derivatives of COSAN and FESAN. In addition, the work will display the complete NMR characterization for all the compounds and the crystal structure for the bipyridine derivatives. Moreover, the electrochemical characterization will unveil products able to accept up to 5 electrons in a reversible way. Finally, the electrochemical communication between the metallic centers for the products with two metallacaboranes will be confirmed by crystal characterization together with the NMR, cyclic voltammetry and UV-vis-NIR.

3.1 Electron acceptor

Molecules with dimensions of few nanometers that can store a high number of electrons find important applications in material's science as molecular switches,[1] receptors,[2] photoconductors and photoactive dyads.[3] These applications are generally based on their excellent electron-accepting properties along with low reorganization energy.[4] Despite the outstanding capabilities of these so called electron acceptor molecules, their synthesis, processing and integration for the real application it is still the Achilles' heel of these compounds.

The most successful molecules for this purpose up till now are C_{60} and PCBM. These molecules have a capability of accepting up to six electrons according to Cyclic Voltammetry (CV), four or three of them in reversible way for C_{60} or PCBM respectively (**Figure 3.1**).[5-7] Other molecules that present very good results as electron acceptors are polyoxometallates (POMs).[8,9] In this context, one of the most significant properties of POMs is the ability of many of them to accept and release a big amount of electrons without decomposing or change in their structural arrangements.[10] Each of the overmentioned example molecules, fullerenes and polyoxometallates, have nanometer dimensions, excellent electron-accepting properties and low reorganization energy upon the capture or release of one electron. Thus, they are currently exploited in a wide range of applications in molecular electronics.[11,12] However, functionalization and integration of these structures require so much effort that sometimes simply is not convenient to implement real application despite the outstanding electronic properties. This is the main drawback and the one we want to tackle with this study.

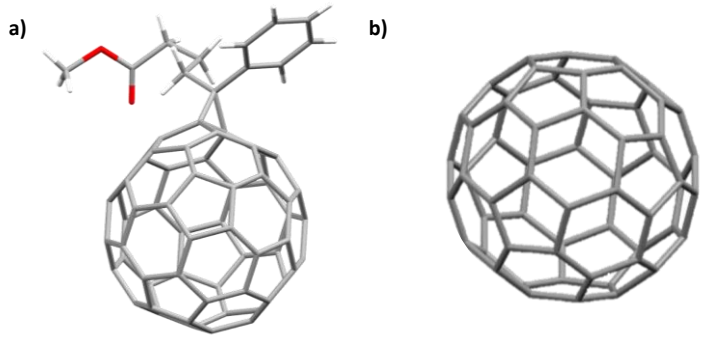

Figure 3.1. a) crystal structure of PCBM.[13] b) Crystal structure of C_{60}.[14]

As we mentioned in the introduction, metallacarboranes as COSAN ([**1**]$^-$) and FESAN ([**2**]$^-$)[15-17] present a non-localized negative charge spread over the whole molecule[18] and high solubility either in water or in organic solvents depending on the cation.[19,20] Moreover, the addition of specific electroactive derivatives to the metallacarborane backbone permits to control and tune the number of the redox events, their potential as well as the possibility to prompt electronic communication between metallacarboranes *via* unsaturated bridges between them tailoring their properties for specific purposes.[21,22] These unique features of metallacarboranes led us to consider the possibility to produce good electron-acceptors[23] that show electronic communication and easy processability.

Methylviologen, MV, is a well-known electron acceptor able to accept up to two electrons and can change colour reversibly upon reduction/oxidation processes.[24,25] As a consequence we proposed the structure 4,4'-bipyridine as a substituent for increasing the electron acceptor behaviour of the metallacarboranes and also to serve as a linker between two metallacarboranes.

Metallacarboranes have two distinct binding sites, namely C and B. Despite the few reports existing in the literature on the formation of B-N bonds,[26-32] our recent studies have demonstrated that boron substitution leads to an appealing large range of distinct E½ values, that change accordingly with the number of boron substitutions.[33,34] This latter property, motivated us toward the optimization of B-N bond synthesis.

In this work, we present the synthetic route optimized for the creation of B-N bonds, controlling the position and number of substituents. Further electrochemical studies will show the electronic properties unveiling the potential of these molecules as an electron acceptor on par with and under some point of view better than, the classical fullerene and polyoxometallates molecules.

3.2 Synthesis of metallacarborane derivatives

Pyridine was chosen as a substituent to develop the first derivative of this work. The initial idea was to find a way to produce B-N bonds from pristine Cs[3,3'-Co(1,2-$C_2B_9H_{11}$)$_2$], Cs[**1**]. However, we were not able to find the optimal

conditions to obtain the desired products therefore it was considered to explore a new procedure starting with Cs[3,3'-Co(8-I-1,2-$C_2B_9H_{10}$)(1,2-$C_2B_9H_{11}$)], Cs[**I-1**].[35]

- *Solid-state.* The procedure consists on mixing the Cesium salt of $[I\text{-}1]^-$ with pyridine as reagent and solvent. The reaction is carried out in a Pyrex sealed tube in an oven at 200º C for 16h. The procedure was successful and after workup, led to the sought pyridinium derivative 10 in 70% yield. The reaction mechanism that we suggest for this reaction is based on the formation and precipitation of the CsI salt that acts as a driving force leading to a B^+electrophile position that reacts with pyridine and generates the B-N bond (**Scheme 3.1**). Finally, the purification process of all the compounds of this work requires extraction with an organic solvent and chromatographic separation by preparative TLC on silica.

- *Solution.* Unfortunately, the solid-state procedure was inapplicable to achieve compound 11. The synthesis requires a less harsh method which consists in mixing Cs[I-2], excess pyridine in dry toluene as solvent, refluxing conditions and N_2 atmosphere for 4 days (**Scheme 3.1**b). The purification process is the same as the solid-state process.

3.2.1 The synthesis of 12, 13, [14]I and [15]I

Once optimized the more suitable conditions for a simple B-N bond we start to complicate the system replacing the pyridine with 4,4'- bipyridine, the future unsaturated bridge. The synthesis of compounds **12** and **13** follow the same synthetic strategy used for **10** and **11** (**Scheme 3.1**).

Compound **12** requires the mix of a 4-fold excess of 4,4'-bipyridine with Cs[**I-1**] in a sealed pyrex tube introduced in an oven at 200ºC for 16h (**Scheme 3.1**c). As for **11**, this solid-state procedure could not be used to synthesize the iron analogue compound **13** because the conditions are too harsh, and the cluster suffers degradation. For this reason, the alternative solution procedure in dry toluene used for **11** was applied to **13** but using a 3-fold excess of 4,4'-bipyridine (**Scheme 3.1**d).

Both **12** and **13** could be adequate starting wildcard reagents to generate challenging compounds that will be the object of future research. The simplest one is the N'-methyl derivative of **12** and **13** ([**14**]I and [**15**]I) showed in **Scheme 3.1** that, as methylviologen $[MV]^{2+}$, is a dicationic salt.

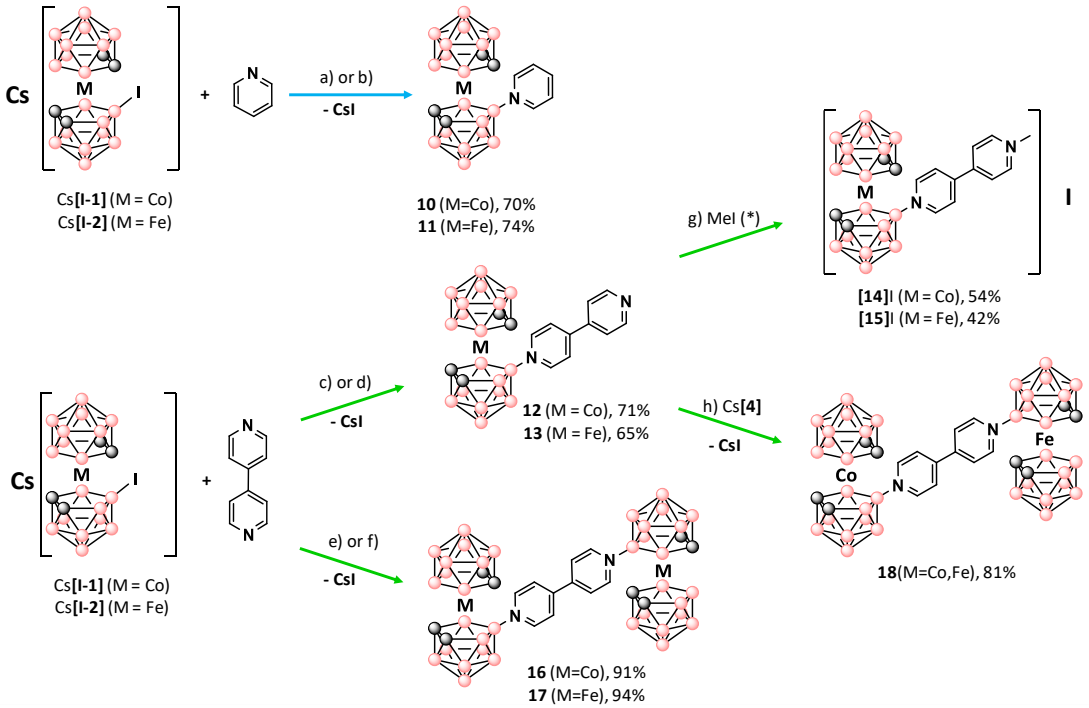

Scheme 3.1. Reaction condition for the synthesis of compounds **10**, **11**, **12**, **13**, [**14**]I, [**15**]I, **16**, **17** and **18**.

3.2.2 The synthesis of 16, 17 and 18

The synthesis of bipyridine disubstituted with COSAN (**16**) follow the sealed tube method, starting from the bare reagents, Cs[**I-1**] and 4,4'-bipyridine in 2:1 ratios, at 200°C in the oven, but utilizing naphthalene as a solvent due to the low quantity of 4,4'-bipyridine of the reaction (**Scheme 3.1**e). Conversely, the solution protocol, is the one utilized to produce bipyridine disubstituted with FESAN (**17**) (**Scheme 3.1**f). Finally, the synthesis of COSAN, FESAN-bipyridine (**18**) was made from compound **11** mixed with a 2-fold excess of Cs[**I-2**] in dry toluene at reflux for four days.

3.3 Structural characterization of derivatives

All the molecules (**10-18**) have been characterized by ^{1}H-, ^{1}H{^{11}B}-, ^{13}C{^{1}H}-, ^{11}B-, ^{11}B-{^{1}H}-NMR and for the cases of **10, 11, 12, 13, 16, 17** by X-ray diffraction.[36]

3.3.1 NMR Characterization

* COSAN derivatives

The ^{1}H-, ^{1}H{^{11}B}-, ^{11}B and ^{11}B{^{1}H}- NMR spectra were key in determining the Cobalt derivatives structure. The ^{11}B{^{1}H}-NMR spectra of **10**, **12**, [**14**]I and **16** present a characteristic signal corresponding to the B-N bond around 16.5 ppm (**Figure 3.2**).[37] Moreover, the ^{1}H-NMR spectra describe clearly the aromatic system added to the COSAN. The spectra of **10** show three signals in the aromatic region with integration 2:1:2 corresponding to the hydrogens on the pyridine ring. In addition, compounds **12** and [**14**]I present four aromatic signals with integrations 2:2:2:2 corresponding to the four different protons of bipyridine and 4-methylbipyridine but, [**14**]I shows one signal more at 4.7 ppm assigned to the methyl group of the bipyridine. Finally, compound **16** presents a more symmetric spectrum due to the symmetry of the aromatic protons that results in a double signal with integration 4:4 (**Figure 3.3**).

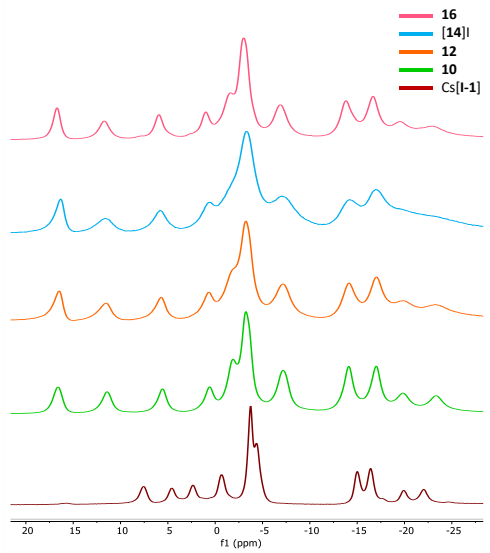

Figure 3.2. ^{11}B-{^{1}H}-NMR comparison spectra of products Cs[I-1](red), **10** (green), **12** (orange), [**14**]I (blue) and **16** (pink).

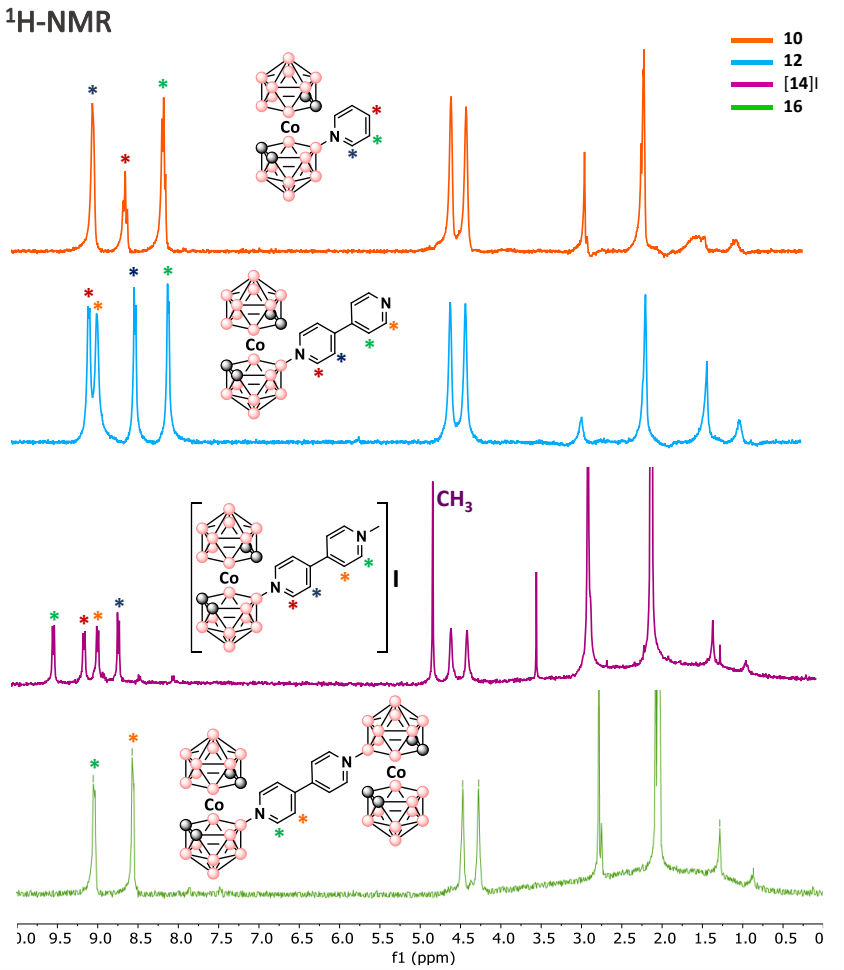

Figure 3.3. ^{1}H-NMR comparison and proton assignment of compounds **10** (orange), **12** (blue), [**14**]I (purple) and **16** (green).

- FESAN derivatives

The NMR characterization of the FESAN (Fe^{3+}) derivatives present a dependent behaviour on the electronic structure on the metal that completely redistributes the signal along the NMR spectra. For this reason, will not make a comparative study between COSAN and FESAN derivatives.

FESAN (Fe^{3+}) is paramagnetic, where the unpaired electron makes the NMR characterization slightly more complicated than before. The unpair electron, in the iron atoms affect significantly both the relaxation time of the nucleus and the

chemical shifts. FESAN derivatives peaks between 120 and -30 ppm or 120 and -600 ppm for the ^{1}H- and ^{11}B- NMR spectra respectively (**Figure 3.4**). The signals corresponding to the atoms close to the metal would have a higher shift than the ones placed farther, resulting in a poor resolution of the substituent's signals. On one hand, the signals from ^{1}H-NMR are hard to interpret especially the resonances of the bipyridine unit. On the other hand, in the ^{11}B-NMR we can better appreciate valuable information which helps to follow the progress of the reaction. Actually, the peak at -520 ppm, characteristic of the B-I vertex, is shifted upfield near -586 ppm upon the formation of the B-N bond. However, the ^{11}B-NMR does not prove whether we obtained the **13** or the **17**. This information was retrieved after the cyclic voltammetry experiments (**Section 3.4**).

Compound **18**, leads to the most complex ^{11}B-NMR spectra due to the presence of both para and diamagnetic metals in the molecule (**Figure 3.4**).[38-40] The ^{11}B-NMR signals falls at -586 for **16** and 15 ppm for **17** indicating the formation of the B-N bond between the bipyridine and FESAN or COSAN respectively. Interestingly, all the common peaks in both compounds appear in the compound **18** at the same chemical shift demonstrating the correct formation of the heterometallic structures.

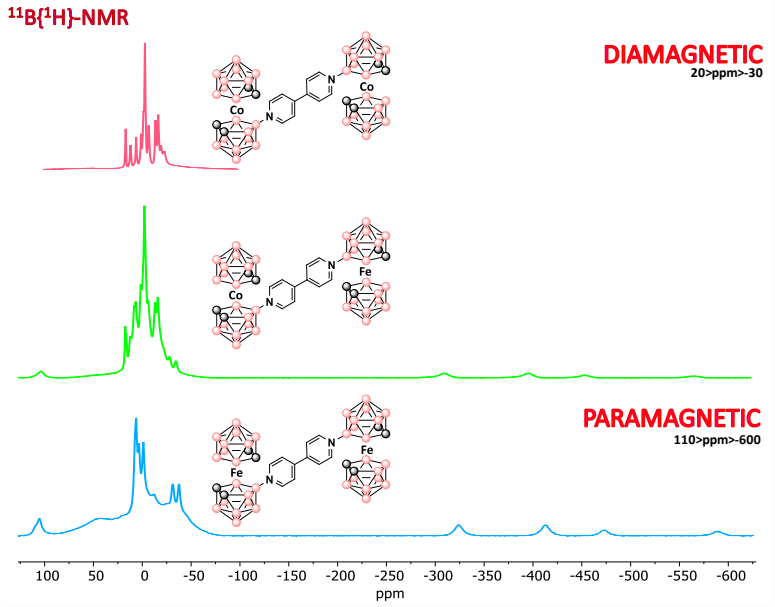

Figure 3.4. ^{11}B{^{1}H}-NMR spectra of the diamagnetic compound **16**, the paramagnetic **17** (blue) and the mix of both **18**.

3.3.2 Crystal Structures

The crystalline structure is always key information in the characterization of inorganic compounds. It gives us clues on how our molecule is distributed in the space and let us understand a series of macroscopic properties like luminescence, conductivity, mechanical and chemical resistance, among others. Obtaining a suitable single crystal is the main, but sometimes impossible, step that becomes more difficult as the size and branches of the molecule increase. In our case COSAN derivatives (**10**, **12** and **16**) single crystals were obtained by slow evaporation of the solvent from solutions of acetonitrile, acetone and tetrahydrofuran, respectively. The FESAN derivatives (**11**, **13** and **17**) instead, were quite more complicated to crystallize hence we had to use the crystallization gel technique which is not really common for those who does not strictly work in the field of crystallography.[41]

The technique consists in preparing a silica gel in a tube inducing the crystallization the product inside the gel. The first step requires to prepare a water glassy solution of a density of 1.06 g/mL from a mother solution commercially obtained with a density of 1.39 g/mL. The quantities were calculated following **Equation 1**.

$$V_i = V_T \frac{(\rho_f - \rho_{H_2O})}{(\rho_i - \rho_{H_2O})} \quad (1)$$

Where, V_i and V_T are the mother solution and total volumes, respectively and ρ_f, ρ_{H2O} and ρ_i are the density of the final solution, water and initial, respectively. The solution of 1.06 g/mL is left under vigorous agitation during a minimum of 4 hours to obtain the water-glassy solution. The next step is the meticulous preparation of the gel. 15 mL of water-glassy solution is added drop by drop to 15 mL of 1M HCl solution with vigorous agitation and controlling constantly the pH of the reaction; once added all the volume the pH should be at 5, if the pH is higher, some more drops have to be added to adjust it as needed. Then we rapidly poured the solution into different test tubes, filling them halfway and left the gel closed two days. For the crystallization step, we add three different solutions of **11**, **13** and **17** in ACN. Our compounds slowly diffuse through the gel which helps the creation of small seeds that after 4 days of progressive slow growth produce a visible monocrystal that is left growing for 2-3 more days.(**Figure 3.5**).

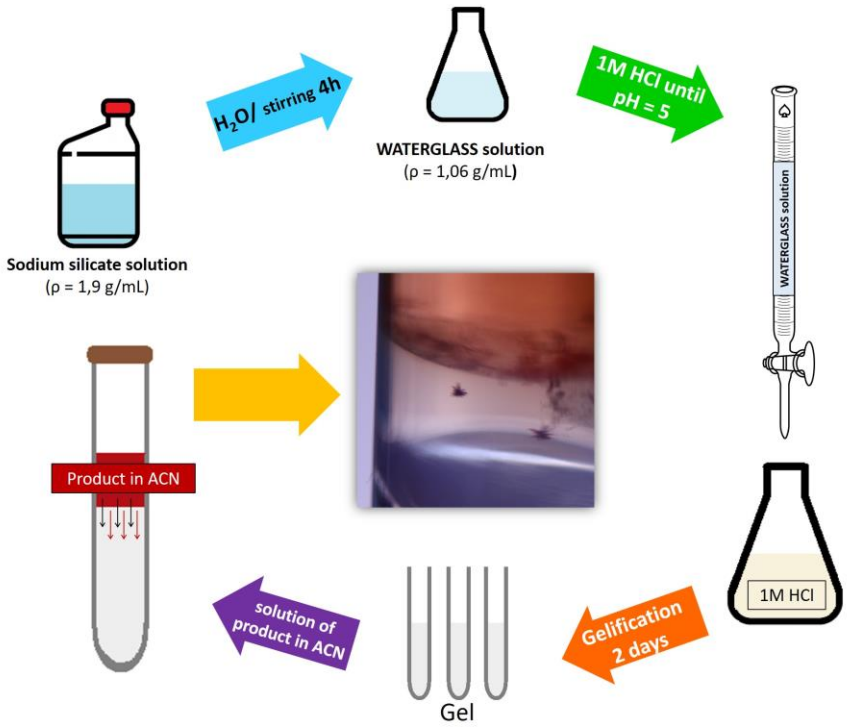

Figure 3.5. Fabrication scheme of silica gel and crystallization of products 11, 13 and 17 inside the gel. Photo of the crystal of **17** growing in a silica gel.

In this work, we were able to obtain high-quality single crystals of compounds **10**, **11**, **12**, **13**, **16** and **17** (**Appendix B**). Each of them has been analysed with X-ray diffraction and at first glance they show the common basic paraments found in other known metallacarborane derivatives with substituents at the B(8) position (see **Appendix B**).[39,42,43] Accordingly to the Cambridge Structural Database[44] only eight compounds are registered (seven for cobaltabisdicarboranes[45] and one for ferrabisdicarboranes[46]) with direct boron nitrogen bonds. All the metallacarboranes crystalized within this work present *cis* configuration even though the *trans* is the most stable. This counterintuitive behaviour can be due to the fact that in the solid-state of the *cis* rotamer the C_C-H···H-B interactions are maximized.

* Structures 10 and 11

Structures **10** and **11** present equivalent crystal structures with very similar atom distances. Both are closely packed with no available voids for solvent molecules.

The neighbouring molecules are held together mainly by the weak van der Waals type interactions (**Figure 3.6**).

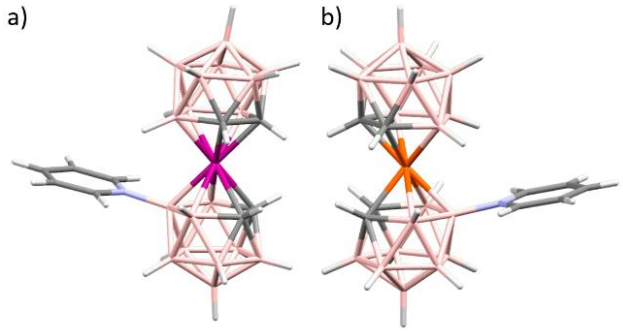

Figure 3.6. Crystal structures of compounds a) **11** and b) **10** (B in pink, C in grey, H in white, N in blue, Co^{3+} in orange and Fe^{3+} in purple).

* Structures 12 and 13

Structures **12** and **13** exhibit similar molecular structures. However, the dihedral angles of 20.3º and 32.09º respectively, and the crystallization solvents (acetone and acetonitrile respectively) lead to a different crystal packing.[37] It is also worth noting that the configuration of the bipyridine in the COSAN **Figure 3.7** presents a structure that will facilitate the electronic communication between the benzene rings so we think it will work better for our aim where we seek an unsaturated molecular bridge, able to interconnect electronically the metallacarboranes in the final structure.

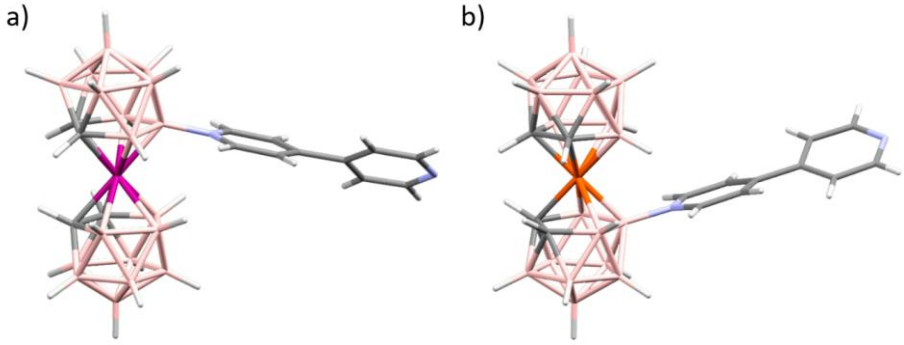

Figure 3.7. Crystal structure of compounds a) **13** and b) **12** (B in pink, C in grey, H in white, N in blue, Co^{3+} in orange and Fe^{3+} in purple).

* Structures 16 and 17

Compounds **16** and **17** are not so similar as the previous pairs of compounds and the differences can be clearly appreciated on the reconstructed structures shown in **Figure 3.8**. The 4,4'-bipyridine of **16** makes a nearly flat bridge between the two COSAN moieties, where the central C-C bond creates a dihedral angle between the two pyridines of about -0.1° and an almost perfect center of inversion of the whole molecule. The co-planarity induced by the center of symmetry raises the hopes of good electronic communication between the two COSANs. Conversely, in **17**, the 4,4'-bipyridine that bridges the two FESANs moieties present a dihedral angle between the pyridines of 24° that reduces the overall symmetry and decrease the effectiveness of the electronic delocalization between the two molecular moieties anticipating a worst electronic communication between the two FESANs. In the following paragraph, we will explore the electrochemical properties of those structures determining the effective electronic delocalization of the charge all over the whole molecule.

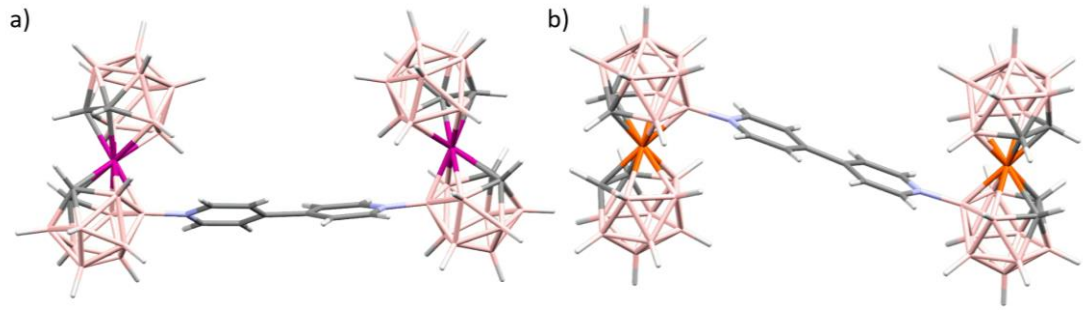

Figure 3.8. Crystal structure of compounds a) **17** and b) **16** (B in pink, C in grey, H in white, N in blue, Co^{3+} in orange and Fe^{3+} in purple).

3.4 Electrochemical characterization

We performed a thorough study of the redox process of our compounds to understand the electronic behaviour and assess the potential of these new structures as electron acceptor molecules. The electrochemical characterization involves mainly cyclic voltammetry. It allows us to study the number and the types of redox processes that take place in our structures besides the redox potential value. Through this technique, we were also able to assign every electrochemical wave to each molecular moiety and that was relevant to demonstrate and understand the electronic communication between the two clusters in the case of

16, **17** and **18**. The amount of electrons accepted or released by the structures is given by the relative area of each peak in the CV. **Table 3** presents the values of $E_{1/2}$ of the molecules [MV]Cl_2, **10**, **11**, **12**, **13**, **14**, **15**, **16**, **17** and **18** divided into three columns that indicate the value of every molecular moiety.

Table 3. $E_{1/2}$ values and assignments of the CV waves (vs. Fc^+/Fc) for all synthesized compounds and free methylviologen (MV).

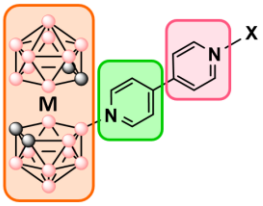

Compound	Cluster-Pyr(+)-Pyr/Pyr(+)-X	Cluster-Pyr(+)-Pyr/Pyr(+)-X	Cluster-Pyr(+)-Pyr/Pyr(+)-X
[**MV**]Cl_2			-0.86/-1.23
10	-1.35		
11	-0.39		
12	-1.34	-1.75	-2.25
13	-0.37	-1.74	-2.24
[**14**]I	-1.35	-0.92	-1.67
[**15**]I	-0.34	-1.07	-1.52
16	-1.40 / -1.53	-0.99	-1.79
17	-0.28	-1.36	-1.79
18	-0.34 / -1.47	-1.15	-1.78

* Compounds 10 and 11

The CV analysis of the zwitterion pyridine derivatives **10** and **11**[3] provide information about $E_{1/2}$ when moving from one anion ([**1**]$^-$ or [**2**]$^-$) to the very similar but neutral compound (**10** or **11**) that causes a shift in the redox potential that is near to +0.40 V (**Table 3**).

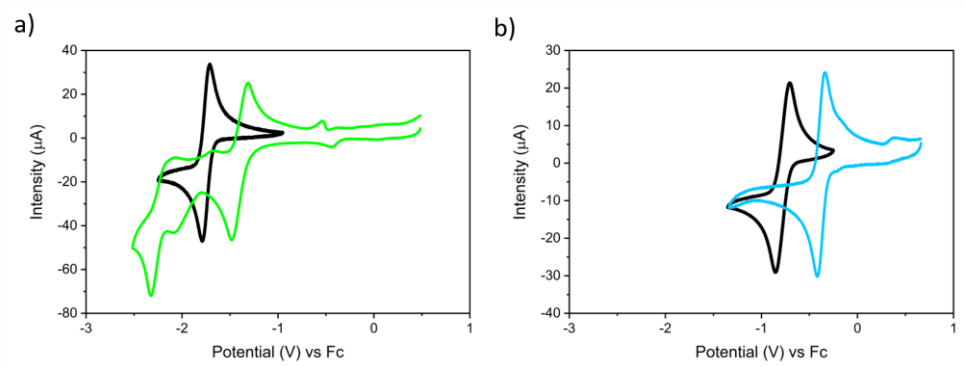

Figure 3.9. a) CV of [**1**]$^{-}$ in black and **10** in green. b) CV of [**2**]$^{-}$ in black and **11** in blue.

* Compounds 12 and 13

This information enables to assign the peaks of **12** and **13** considering that these are also zwitterions, and the $E_{1/2}$ of the central metal ion (Co or Fe) is expected to be very similar to those of **10** and **11**. The CVs of **12** and **13** present two additional peaks, one for each nitrogen of the bipyridine (**Table 3** and **Figure 3.10**). The first one has a positive charge and is represented as Pyr(+) (green column). The second one, which is neutral, it's shown under the column Pyr in **Table 3** highlighted in pink. At first glance, we deduce that the easiest position in being reduced is the first positive one ($E_{1/2}$ -1.75 V) while the reduction of the neutral nitrogen appears to require more energy to happen ($E_{1/2}$ -2.25 V).

* Compounds [14]I and [15]I

The similar compound [**14**]I which presents a structure like **12** but with just one additional methyl group, gives an unexpected CV profile. Actually, we can distinguish three main peaks (**Figure 3.10**) one less compared with the CV of **12**. While the peaks bipy^{+}/bipy and Co^{+3}/Co^{+2} retain their position, the peak at -2.25 V that corresponds to the Co^{+2}/Co^{+1} couple present in **12** does not appear in for [**14**]I. This unusual behaviour can be explained by the formation of a double zwitterionic compound with both nitrogen atoms positively charged. Otherwise, [**14**]I display a peak at -0.92 V in agreement with the peak at -0.86 V of [**MV**]Cl_2 (**Figure 3.10** and **Table 3**). An equivalent interpretation can be given when comparing the CVs of [**15**]I and **13**, in which the new peak that appears at -1.07 is

assigned to the methylated pyridine reduction while the other two peaks remain almost at the same position.

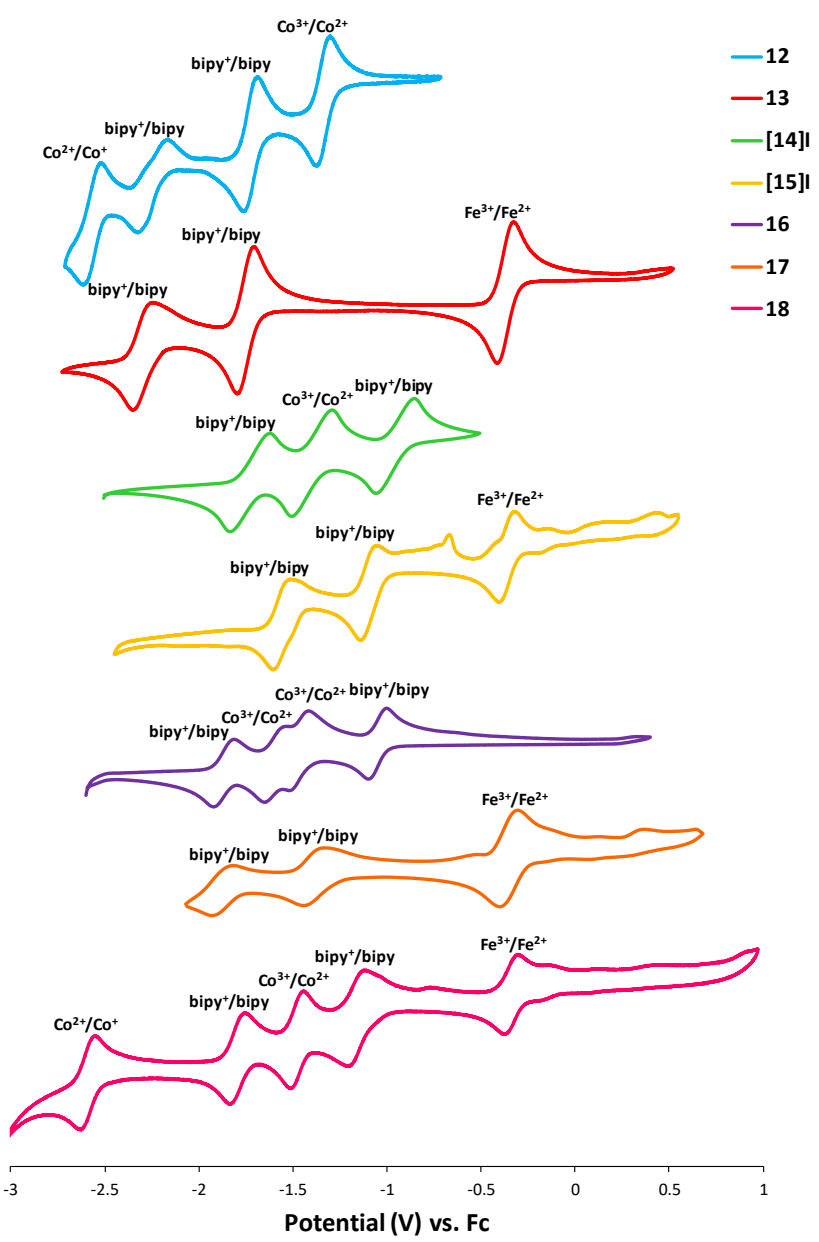

Figure 3.10. Comparative CVs and peak assignation of 12, 13, [14]I, [15]I, 16 ,17 and 18.

* Compounds 16 and 17: the potentially new electron acceptor molecules

Compound **17** was easily assigned thanks to the $E_{1/2}$ of the $Fe^{3+/2+}$ that is twice more intense than the other two redox processes. It indicates that both FESAN units are reduced at the same time (**Figure 3.10**). On the contrary, the assignment of the redox processes for **16** was not as straightforward. In this case, we started to assign the easiest one, noticing that the two peaks have a very similar potential to the ones recorded in **14**. We, therefore, consider those signals as a consequence of the reduction of both positive pyridine units. The other two peaks are assigned to a stepwise reduction of the two COSAN units with a $\Delta E_{½}$ of 130 mV (**Table 3**).

- *Electron acceptor state of art. C_{60} and PCBM.*

Following the characterized of the electronic processes involved in these molecules, if we focus our attention to the redox potentials of **16** and **17** we can observe that their values and number of waves resemble the ones relative to C_{60} or PCBM suggesting very similar electrochemical properties. In this sense, it has been reported that the redox processes for C_{60} are -1.10, -1.49 and -1.94 and for PCBM -1.18, -1.55 and -2.05 V *vs* Fc.[47] Other values given for C_{60} are -0.89, -1.37, -1.87, -2.35, -2.85 and -3.26 (all values are reported *vs* external Ferrocene) (**Figure 3.11**).[48] These values are in the same region of redox potentials of our compounds corroborating the feasibility of our compound to work as electron acceptor molecules. Least but not less important property that is worth for comparison is indeed the number of accepting electrons that for C_{60} reach 3 electrons reversibly exchanged while for our innovative molecules **16** or **17** we reach up to 4 electrons exchanged reversibly.

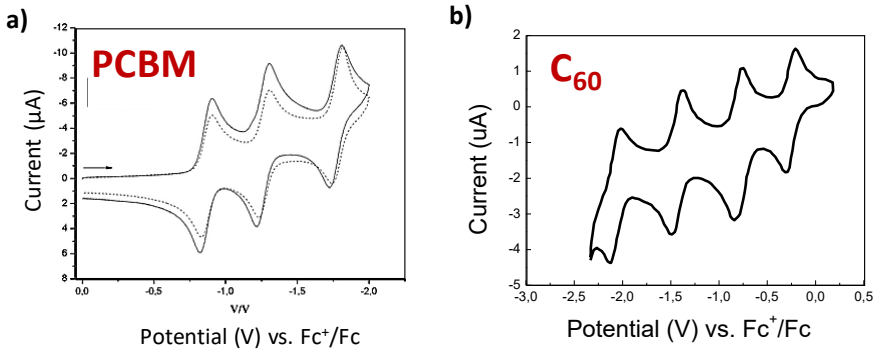

Figure 3.11. a) CV of PCBM from reference [49]. b) CV of C_{60} from reference [50]

* Compound 18: The candidate for intercluster electronic communication

Finally, the assignment of the CV peaks for **18**, was easily done on the basis of the former assignments. The more anodic peak at -0.34 V corresponds to the $Fe^{3+/2+}$ redox process, followed by the reduction of one of the pyridinium units at -1.15 V, that in turn, is followed by the $Co^{3+/2+}$ reduction at -1.47 V and finally by the second pyridinium unit at -1.78 V as it was expected (**Table 3**). These values slightly differ from the redox signals of compounds **16** and **17** suggesting that some degree of electronic communication may exist between the two metallacarboranes. Unfortunately, we have not succeeded in getting good crystals that could unambiguously prove the co-planarity of the bipyridine bridge.

3.5 Electronic communication

The efficient electronic communication between two equivalent redox centers favours the electron delocalization and it is not only important from a fundamental point of view but also relevant for the design of compounds with potential applications in molecular electronics. [51-53]

The crystal structure of **16 (Figure 3.8)** exhibits two pyridine units on the bipyridine bridge in a coplanar position suggesting, as previously introduced, that the lack of structural hindering will enhance the Co-Co electronic communication (**Figure 3.8**). This idea is corroborated by the CV of **16** that presents two distinct $1e^-$ curves for two chemically equivalent Co atoms. In other words, the first redox process affects the energy of the second one increasing the redox potential by 130 mV. This latter result confirmed once again the electronic communication between the two COSAN units. We suggested and confirmed that there is a mixed-valence compound (**Figure 3.10**). Conversely, the loss of the symmetry centre due to the dihedral angle of 24º between the pyridine rings in the crystal structure of **17** and also the two-fold peak at -0.28V in the CV should hinder the electronic communication between the two Fe-Fe units (**Figure 3.8**).[54]

To solve this riddle, the following experiment was performed. A fresh solution of sodium naphthalenide was prepared mixing a solution of naphthalene in THF with metallic sodium under nitrogen. After a few minutes, with vigorous stirring, the solution became dark green. After all sodium had reacted, the solution was

titrated in water, with HCl 0.1 N standard solution. Then, an NMR tube with a known concentration of **17** in THF and 1 eq of sodium naphthalenide was prepared to perform a monoreduction of one of the two iron centers. The tube was sealed under nitrogen and the ^{11}B-NMR was run at different temperatures (**Figure 3.12**). From the NMR, the following two conclusions can be drawn: first, there is a shifting of the outer peaks towards the center of the spectrum due to the monoreduction and second, there is not a dependence of the peak position with the temperature for the compound [**17**]$^{-}$ (**Figure 3.12**).

The first conclusion drawn from **Figure 3.12**, in which the peripheral peaks shift towards the centre of the unperturbed ^{11}B-NMR spectrum, is that the singly reduced [Fe-Fe]$^{-}$ molecule cannot be interpreted as a fix charge site complex of the type [Fe^{2+}-Fe^{3+}]- but by a rapidly exchanging [Fe^{2+}-Fe^{3+}]$^{-}$ ↔ [Fe^{3+}-Fe^{2+}]$^{-}$ system in which the oxidation states of the Fe are constantly interconverting due to a fast inner electron transfer (Intervalence Charge Transfer). This fast interconversion leads to an intermediate species in which formally there are two $Fe^{2.5+}$. This implies that the resulting NMR would be an intermediate between the paramagnetic NMR (two Fe^{3+}) and the diamagnetic NMR (two Fe^{2+}). If there was no electronic communication between both FESAN units, the ^{11}B-NMR peaks would be the sum of the paramagnetic NMR and the diamagnetic NMR in similarity with the ^{11}B-NMR of **18** [Fe-Co] that has one diamagnetic center (the Co) and one paramagnetic one (the Fe). The second conclusion is the observed non-dependence of the ^{11}B-NMR with the temperature indicating that the rate of the intervalence charge transfer is fast between the NMR at 290 K and the NMR at 213 K.

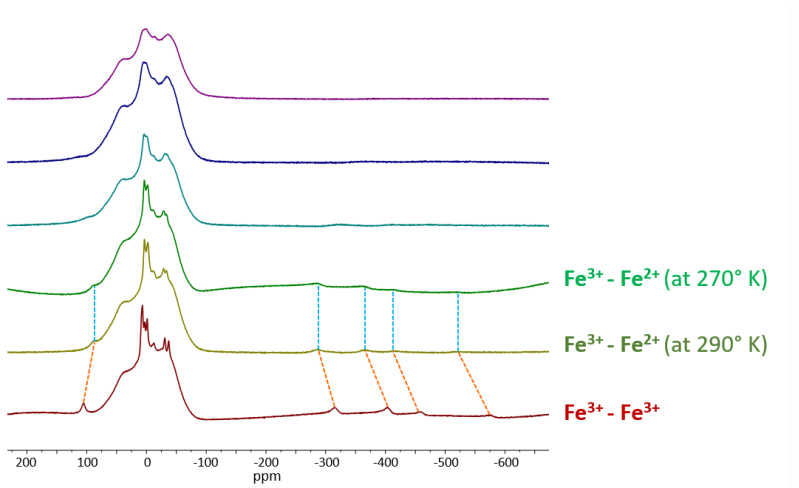

Figure 3.12. In red, the $^{11}B\{^{1}H\}$-NMR of **17**. In olive, the $^{11}B\{^{1}H\}$-NMR of [**17**]$^{-}$ at 290 K, and subsequently the $^{11}B\{^{1}H\}$-NMR of [**17**]$^{-}$ decreasing the temperature 20 K between each NMR. Orange dotted lines indicate the shift of $^{11}B\{^{1}H\}$-NMR between compound **17** an [**17**]$^{-}$. The blue dotted lines show how the peaks are independent of the temperature. The large bump between +75 and -75 is due to the $^{11}B\{^{1}H\}$-NMR signals inherent to the NMR tube, which contains boron oxides. The fine signals on the bump are due to the boron atoms on the cluster.

To demonstrate this intervalence charge transfer, we run the UV-Vis-NIR spectroscopy for compounds 17, [17]$^{-}$ and [17]$^{2-}$. For comparison, we have also run the UV-Vis-NIR of compounds 11 and [11]$^{-}$. As it is shown in **Figure 3.13**, the broadband with a maximum wavelength at 708 nm and expanding to the NIR region until 1250 nm is associated with an Intervalence Charge Transfer (IVCT) or also known as a metal to metal charge transfer, demonstrating again the electronic communication between the two metal centers of the molecule through the bipyridine moiety.

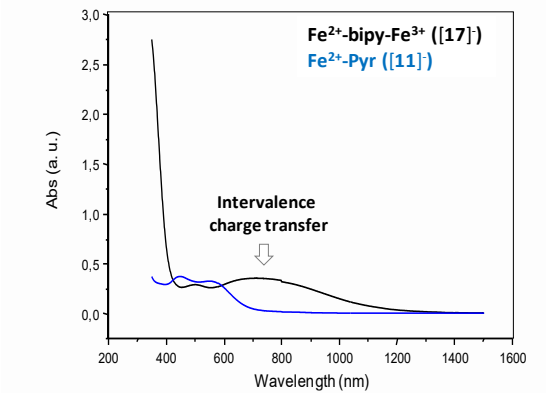

Figure 3.13. UV-vis-NIR of compounds [11]$^{-}$ (in blue) and [17]$^{-}$ (in black).

3.6 Solubility and processability

The fabrication of any electronic device not only requires some specific electrochemical properties but also compounds easy to be manipulated and among other requirements a high solubility in different solvents is one of the properties that permits the easy processability of compounds.

Table 4 summarizes the results of solubility in mg/mL for compound **16** in some of the more common organic solvents and compares the results with the solubility of compounds C_{60} and PCBM in the same solvents. [37,55,56] The values indicate that the metallacarborane derivatives are much more soluble and possess a wider solvent range than C_{60} and its derivatives hence could be good candidates for molecular electronics and molecular materials in general.

Table 4. Comparison between the solubility measurements for compound **16** and the ones from the literature for C_{60}[55] and PCBM.[56]

Solvent/Compound	16 (mg/mL)	C_{60} (mg/mL)	PCBM (mg/mL)
Acetonitrile	22.6	0.000	
CH_2Cl_2	46.7	0.26	
Ethanol	25.4	0.001	< 0.1
Tetrahydrofuran	155.3	0.000	1.8
Toluene	17.8	2.8	15.6
N-N'-dimethylformamide	387.3	0.03	

3.7 Conclusions

For the first time, a generation of metallacarborane derivatives with aromatic N bonded to the cluster have been synthesized and completely characterized. The synthetic strategy of using Cs[**I-1**] or Cs[**I-2**] to generate CsI salt and activate the B(8) of the cluster has been so successful that has led to nine electron cumulative metallacarborane derivatives with Fe, Co or a mix of both.

These molecules are able to accept up to five electrons and to donate one in single electron steps at accessible potentials and in a reversible way. By targeted synthesis and corresponding electrochemical tests each electron transfer (ET) step has been

assigned to specific fragments of the molecules. The molecules have been carefully characterized and the electronic communication between both metal centers (when this situation applies) has been definitely observed through the co-planarity of both pyridine fragments. The structural characteristics of these molecules imply low reorganization energy that is a requirement for low energy ET processes. This makes them electronically comparable to fullerenes, but with a wide range of possible solvents. We consider that these molecules thanks to their easy synthesis, ET, self-organizing capacity, wide range of solubility and easy processability can find important applications in any area where ET is paramount.

3.8 References

(1) J. L. Zhang, J. Q. Zhong, J. D. Lin, W. P. Hu, K. Wu, G. Q. Xu, A. T. S. Wee and W. Chen, Towards single molecule switches, *Chem. Soc. Rev*, **2015**, 44, 2998-3022.

(2) R. Nuñez, I. Romero, F. Teixidor and C. Vinas, Icosahedral boron clusters: a perfect tool for the enhancement of polymer features, *Chem. Soc. Rev*, **2016**, 45, 5147-5173.

(3) R. Núñez, M. Tarrés, A. Ferrer-Ugalde, F. F. de Biani and F. Teixidor, Electrochemistry and Photoluminescence of Icosahedral Carboranes, Boranes, Metallacarboranes, and Their Derivatives, *Chem. Rev.*, **2016**, 116, 14307-14378.

(4) D. M. Guldi, Fullerenes: three dimensional electron acceptor materials, *Chem. Comm.*, **2000**, 321-327.

(5) M. S. Dresselhaus, G. Dresselhaus and P. C. Eklund, in *Science of Fullerenes and Carbon Nanotubes*, Academic Press, San Diego, **1996**, pp. 870-917.

(6) P. W. Stephens, L. Mihaly, P. L. Lee, R. L. Whetten, S.-M. Huang, R. Kaner, F. Deiderich and K. Holczer, Structure of single-phase superconducting K3C60, *Nature*, **1991**, 351, 632-634.

(7) H. Tanaka and K. Takeuchi, Diameter determination of C60 and C70 monomers in the gas phase using a differential mobility analyzer, *Appl. Phys. A.*, **2005**, 80, 759-761.

(8) M. Ammam, Polyoxometalates: formation, structures, principal properties, main deposition methods and application in sensing, *J. Mater. Chem*, **2013**, 1, 6291-6312.

(9) D.-L. Long, E. Burkholder and L. Cronin, Polyoxometalate clusters, nanostructures and materials: From self assembly to designer materials and devices, *Chem. Soc. Rev*, **2007**, 36, 105-121.

(10) C. Busche, L. Vila-Nadal, J. Yan, H. N. Miras, D.-L. Long, V. P. Georgiev, A. Asenov, R. H. Pedersen, N. Gadegaard, M. M. Mirza, D. J. Paul, J. M. Poblet and L. Cronin, Design and fabrication of memory devices based on nanoscale polyoxometalate clusters, *Nature*, **2014**, 515, 545-549.

(11) R. Ganesamoorthy, G. Sathiyan and P. Sakthivel, Review: Fullerene based acceptors for efficient bulk heterojunction organic solar cell applications, *Sol. Energy Mater Sol. Cells*, **2017**, 161, 102-148.

(12) E. M. Speller, The significance of fullerene electron acceptors in organic solar cell photo-oxidation, *Mater. Sci. Tech.*, **2017**, 33, 924-933.

(13) M. Casalegno, S. Zanardi, F. Frigerio, R. Po, C. Carbonera, G. Marra, T. Nicolini, G. Raos and S. V. Meille, Solvent-free phenyl-C61-butyric acid methyl ester (PCBM) from clathrates: insights for organic photovoltaics from crystal structures and molecular dynamics, *Chem. Comm.*, **2013**, 49, 4525-4527.

(14) P. Dahlke and M. J. Rosseinsky, Molecular Structure, Orientational Order, and Jahn−Teller Distortion of the C604- Anion in Cs4C60, *Chem. Mater.*, **2002**, 14, 1285-1291.

(15) M. F. Hawthorne and T. D. Andrews, Carborane analogues of cobalticinium ion, *Chem. Commun, (London)*, **1965**, 443-444.

(16) M. F. Hawthorne, D. C. Young, T. D. Andrews, D. V. Howe, R. L. Pilling, A. D. Pitts, M. Reintjes, L. F. Warren and P. A. Wegner, .pi.-Dicarbollyl derivatives of the transition metals. Metallocene analogs, *J. Am. Chem. Soc.*, **1968**, 90, 879-896.

(17) I. B. Sivaev and V. V. Bregadze, Polyhedral Boranes for Medical Applications: Current Status and Perspectives, *Eur. J. Inorg. Chem*, **2009**, 2009, 1433-1450.

(18) C. Masalles, J. Llop, C. Viñas and F. Teixidor, Extraordinary Overoxidation Resistance Increase in Self-Doped Polypyrroles by Using Non-conventional Low Charge-Density Anions, *Adv. Mater.*, **2002**, 14, 826-829.

(19) J. C. Fanning, L. A. Huff, W. A. Smith, A. S. Terrell, L. Yasinsac, L. J. Todd, S. A. Jasper and D. J. McCabe, Caesium cobalt dicarbollide—solubility, precipitation and reactivity in basic aqueous solution, *Polyhedron*, **1995**, 14, 2893-2900.

(20) M. Tarrés, C. Viñas, P. González-Cardoso, M. M. Hänninen, R. Sillanpää, V. Ďorďovič, M. Uchman, F. Teixidor and P. Matějíček, Aqueous Self-Assembly and Cation Selectivity of Cobaltabisdicarbollide Dianionic Dumbbells, *Chem. Eur. J.*, **2014**, 20, 6786-6794.

(21) P. González-Cardoso, A.-I. Stoica, P. Farràs, A. Pepiol, C. Viñas and F. Teixidor, Additive Tuning of Redox Potential in Metallacarboranes by Sequential Halogen Substitution, *Chem. Eur. J.*, **2010**, 16, 6660-6665.

(22) A. Pepiol, F. Teixidor, R. Sillanpää, M. Lupu and C. Viñas, Stepwise Sequential Redox Potential Modulation Possible on a Single Platform, *Angew. Chem. Int. Ed.*, **2011**, 50, 12491-12495.

(23) M. Tarres, V. S. Arderiu, A. Zaulet, C. Viñas, F. Fabrizi de Biani and F. Teixidor, How to get the desired reduction voltage in a single framework! Metallacarborane as an optimal probe for sequential voltage tuning, *Dalton Trans.*, **2015**, 44, 11690-11695.

(24) R. J. Mortimer, Organic electrochromic materials, *Electrochim.Acta*, **1999**, 44, 2971-2981.

(25) M. Suzuki, N. D. Morris and T. E. Mallouk, Photosensitized production of doubly reduced methylviologen followed by highly efficient methylviologen radical formation using self-assembling ruthenium(ii) complexes, *Chem. Comm.*, **2002**, 1534-1535.

(26) B. Grüner, M. Kvíčalová, J. Plešek, V. Šícha, I. Císařová, M. Lučaníková and P. Selucký, Cobalt bis(dicarbollide) ions functionalized by CMPO-like groups attached to boron by short bonds; efficient extraction agents for separation of trivalent f-block elements from highly acidic nuclear waste, *J. Organomet. Chem.*, **2009**, 694, 1678-1689.

(27) F. H. R. J. Plesek, V. Vangani and J. Fuse, *Collect. Czech. Chem. Commun.*, **1994**, 1326-1336.

(28) B. S. J. Plesek, S. Hermanek, *Collect. Czech. Chem. Commun.*, **1984**, 1492-1496.

(29) S. H. J. Plesek, L. J. Todd and W.F. Wright, *Collect. Czech. Chem. Commun.*, **1976**, 3509-3515.

(30) D. Olid, R. Nuñez, C. Viñas and F. Teixidor, Methods to produce B-C, B-P, B-N and B-S bonds in boron clusters, *Chem. Soc. Rev*, **2013**, 42, 3318-3336.

(31) J. P. V. Sícha, M. Kvícalova, I. Cisarova, B. Grüner, *Dalton Trans.*, **2009**, 851-860.

(32) L. I. Zakharkin, V. N. Kalinin and V. V. Gedymin, Synthesis and some reactions of 3-amino-o-carboranes, *J. Organomet. Chem.*, **1969**, 16, 371-379.

(33) M. Lupu, A. Zaulet, F. Teixidor, E. Ruiz and C. Viñas, Negatively Charged Metallacarborane Redox Couples with Both Members Stable to Air, *Chem. Eur. J.*, **2015**, 21, 6888-6897.

(34) C. Douvris and J. Michl, Update 1 of: Chemistry of the Carba-closo-dodecaborate(−) Anion, $CB_{11}H_{12}^-$, *Chem. Rev*, **2013**, 113, PR179-PR233.

(35) Ľ. Mátel, F. Macášek, P. Rajec, S. Heřmánek and J. Plešek, B-Halogen derivatives of the bis(1,2-dicarbollyl)cobalt(III) anion, *Polyhedron*, **1982**, 1, 511-519.

(36) Crystal structure determination of complex **12**: $C_{17}H_{35}B_{18}CoN_2O$, M = 536.98, Orthorhombic, a = 12.2131(2) b= 12.3627(2), c = 37.7627(7) Å, V = 5701.67(19) Å^3, T = 120 K, space group $P2_12_12_1$ (no.19), Z = 8, 28104 reflections measured, 13955 unique (Rint = 0.0552), which were used in all calculations. The final wR(F2) was 0.0994 (all data).

Crystal structure determination of complex **13**: $C_{30}H_{63}B_{36}Fe_2N_5O$, M = 1010.71, Monoclinic, a = 12.295(6) Å, b = 11.814(6) Å, c = 18.592(12) Å, β = 99.332(10) deg, V = 2665(3) Å^3, T = 100(2) K, space group Pc (no.7), Z = 2, 32964 reflections measured, 12527 unique (Rint = 0.0435), which were used in all calculations. The final wR(F2) was 0.1118 (all data).

Crystal structure determination of complex **16**: $C_{26}H_{66}B_{36}Co_2N_2O_2$, M = 945.82, monoclinic, a = 12.2514(4), b= 17.1579(5), c = 13.0272(4) Å, β = 114.8840(10) deg, V = 2484.19(13) Å^3, T = 170 K, space group P21/n (no.14), Z = 2, 25212 reflections measured, 6672 unique (Rint = 0.0687), which were used in all calculations. The final wR(F2) was 0.1880 (all data).

Crystal structure determination of complex **17**: $C_{20}H_{53}B_{36}Fe_2N_3$, M = 836.51, Orthorhombic, a = 13.293(9) Å, b = 24.939(17) Å, c = 25.915(17) Å , V = 8592(10) Å^3, T = 100(2) K, space group Pbca (no.61), Z = 8, 49719 reflections measured, 9361 unique (Rint = 0.4326), which were used in all calculations. The final wR(F2) was 0.2798 (all data).

(37) A. B. Buades, V. Sanchez Arderiu, D. Olid-Britos, C. Viñas, R. Sillanpää, M. Haukka, X. Fontrodona, M. Paradinas, C. Ocal and F. Teixidor, Electron Accumulative Molecules, *J. Am. Chem. Soc.,* **2018,** 140, 2957-2970.

(38) P. Farràs, A. M. Cioran, V. Šícha, F. Teixidor, B. Štíbr, B. Grüner and C. Viñas, Toward the Synthesis of High Boron Content Polyanionic Multicluster Macromolecules, *Inorg. Chem.,* **2009,** 48, 8210-8219.

(39) P. Farràs, F. Teixidor, R. Kivekäs, R. Sillanpää, C. Viñas, B. Grüner and I. Cisarova, Metallacarboranes as Building Blocks for Polyanionic Polyarmed Aryl-Ether Materials, *Inorg. Chem.,* **2008,** 47, 9497-9508.

(40) A. M. Cioran, F. Teixidor and C. Vinas, The effect of a paramagnetic metal ion within a molecule: comparison of the structurally identical paramagnetic $[3,3\text{-Fe}(1,2\text{-}C_2B_9H_{11})_2]^-$ with the diamagnetic $[3,3\text{-Co}(1,2\text{-}C_2B_9H_{11})_2]^-$ sandwich complexes, *Dalton Trans.,* **2015,** 44, 2809-2818.

(41) H. K. Henisch, Cry*stals in Gels and Liesegang Rings, C*ambridge University Press, New York, **1988.**

(42) I. Rojo, F. Teixidor, C. Viñas, R. Kivekäs and R. Sillanpää, Relevance of the Electronegativity of Boron in η 5-Coordinating Ligands: Regioselective Monoalkylation and Monoarylation in Cobaltabisdicarbollide [3,3′-Co(1,2-$C_2B_9H_{11})_2]^-$ Clusters, *Chem. Eur. J.,* **2003,** 9, 4311-4323.

(43) J. Llop, C. Masalles, C. Vinas, F. Teixidor, R. Sillanpaa and R. Kivekas, The [3,3[prime or minute]-Co(1,2-$C_2B_9H_{11})_2]^-$ anion as a platform for new materials: synthesis of its functionalized monosubstituted derivatives incorporating synthons for conducting organic polymers, *Dalton Trans.,* **2003,** 556-561.

(44) I. J. Bruno, J. C. Cole, P. R. Edgington, M. Kessler, C. F. Macrae, P. McCabe, J. Pearson and R. Taylor, New software for searching the Cambridge Structural Database and visualizing crystal structures, *Acta Crystallogr., Sect. B,* **2002,** 58, 389-397.

(45) For Co: DOSJAX, DOSJIF, DOSJOL, DOSJUR in V. Sıcha, J. Plesek, M. Kvıcalov, I. Cısarova and B. Gruner. *Dalton Trans.*, **2009**, 851–860; HATRID in I. Císarová, K. Malý and L. Hummel. *Acta Cryst*. (**1994**). C50, 198-200; IMEKOB in V. I. Bregadze, I. D. Kosenko, I. A. Lobanova, Z. A. Starikova, I. A. Godovikov, and I. B. Sivaev. *Organometallics* **2010**, 29, 5366–5372; UNACIX in I. Kosenko, I. Lobanova, I. Ananyev, J. Laskova, A. Semioshkin, V. Bregadze. *Journal of Organometallic Chemistry* 818 **(2016)** 58-67.

(46) For Fe, KIWJIJ in H. C. Kang, S. S. Lee, C. B. Knobler, and M. F. Hawthorne, *Inorg. Chem.* **1991**, 30, 2024-2031.

(47) K. Komatsu, N. Takimoto, Y. Murata, T. S. M. Wan and T. Wong, Synthesis and properties of dialkyl derivatives of di[60]fullerenylbutadiyne and di[60]fullerenylacetylene: the buckydumbbells, *Tetrahedron Lett.,* **1996,** 37, 6153-6156.

(48) C. Boudon, J.-P. Gisselbrecht, M. Gross, A. Herrmann, M. Rüttimann, J. Crassous, F. Cardullo, L. Echegoyen and F. Diederich, Redox Characteristics of Covalent Derivatives of the Higher Fullerenes C70, C76, and C78, *J. Am. Chem. Soc,* **1998,** 120, 7860-7868.

(49) H. J. Bolink, E. Coronado, A. Forment-Aliaga, M. Lenes, A. La Rosa, S. Filippone and N. Martín, Polymer solar cells based on diphenylmethanofullerenes with reduced sidechain length, *J. Mater. Chem.,* **2011,** 21, 1382-1386.

(50) B. P. Rand, D. P. Burk and S. R. Forrest, Offset energies at organic semiconductor heterojunctions and their influence on the open-circuit voltage of thin-film solar cells, *Phys Rev. B,* **2007,** 75, 115327.

(51) A. E. Kaifer and M. Gómez-Kaifer, *Supramolecular electrochemistry, J*ohn Wiley & Sons, **2008.**

(52) H. Sun, J. Steeb and A. E. Kaifer, Efficient electronic communication between two identical ferrocene centers in a hydrogen-bonded dimer, *J. Am. Chem. Soc.,* **2006,** 128, 2820-2821.

(53) N. Robertson and C. A. McGowan, A comparison of potential molecular wires as components for molecular electronics, *Chem. Soc. Rev,* **2003,** 32, 96-103.

(54) A. C. Benniston and A. Harriman, Charge on the move: how electron-transfer dynamics depend on molecular conformation, *Chem. Soc. Rev,* **2006,** 35, 169-179.

(55) K. N. Semenov, N. A. Charykov, V. A. Keskinov, A. K. Piartman, A. A. Blokhin and A. A. Kopyrin, Solubility of light fullerenes in organic solvents, *J. Chem Eng. Data,* **2010,** 55, 13-36.

(56) F. Machui, S. Langner, X. Zhu, S. Abbott and C. J. Brabec, Determination of the P3HT: PCBM solubility parameters via a binary solvent gradient method: Impact of solubility on the photovoltaic performance*, Sol. Energy Mater Sol. Cells,* **2012,** 100, 138-146.

CHAPTER 4

Highly Chlorinated Derivatives of COSAN

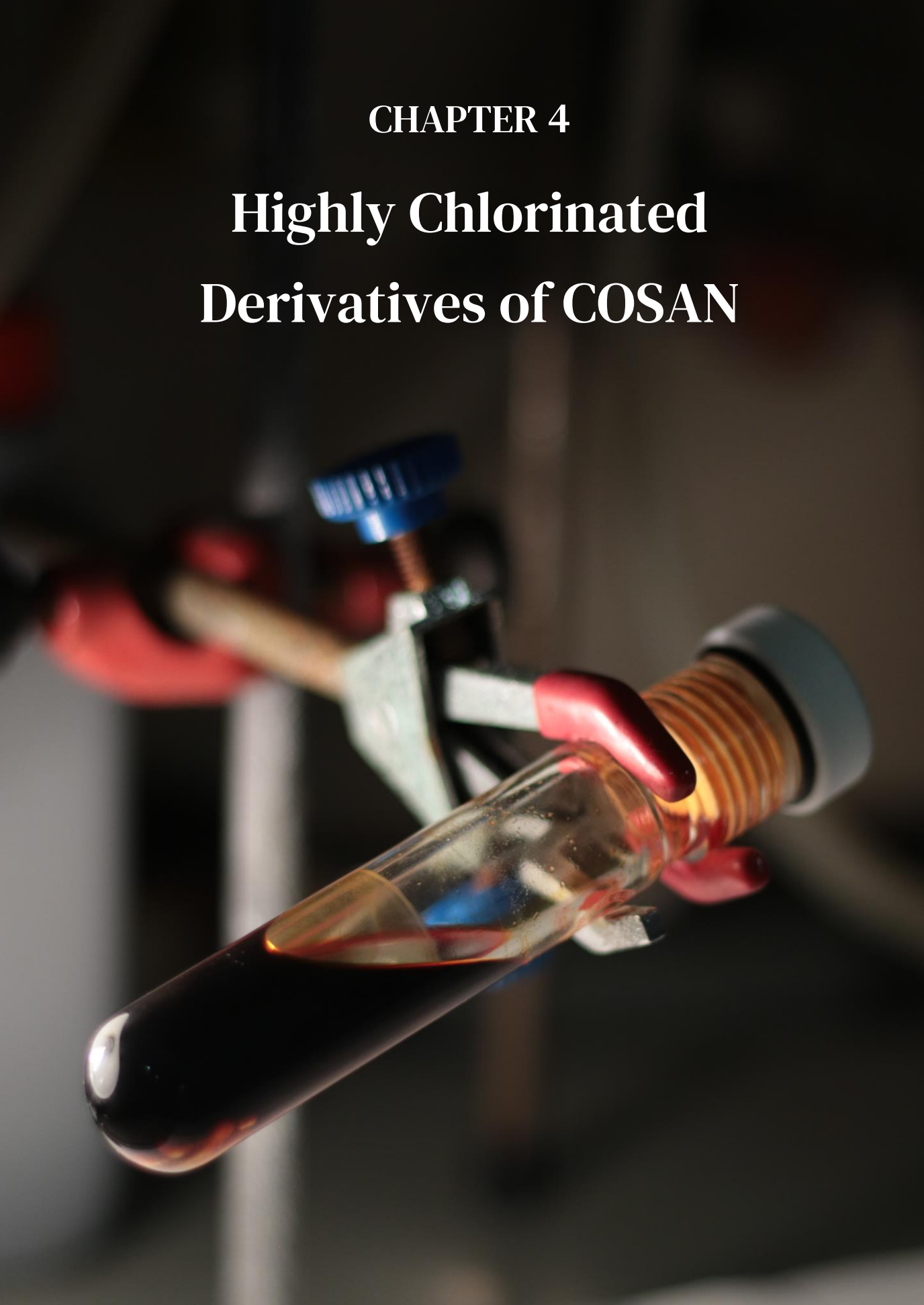

CHAPTER FOUR

Highly Chlorinated Derivatives of COSAN

Synthesis of chlorinated derivatives of COSAN was very prompt by their possible applications. However, since the synthesis of the pure hexachloro COSAN in 1982 not many attempts to increase the chlorination order appear in the bibliography

Now, 38 years later, this research will present the synthesis of the chloro derivatives of COSAN with eight, ten and twelve chloron atoms. The synthesis will be based on the use of a protonated salt of COSAN for use a friendly chlorinated agent in one or two steps and with a very easily purification process. The work will display the characterization of the products by MALDI-TOF, NMR, and IR technics demonstrating their purity. In addition, the crystal characterization will unveil the existence of two isomers in the same crystal of the octaderivative as a result of two equivalent chlorination positions in the COSAN and a different chlorination order than the established by the theoretical studies. Finally, the electrochemical characterization will provide the redox potential values of the all the compounds and the comparison with the values of other chloroderivatives of the literature, will reveal how not only the substituent but also its position affects the redox potential value of the molecule.

This research will put on the table again these highly chlorinated derivatives as electroactive molecules with high stability and processability for real electrochemical applications.

4.1 History of halo derivatives of COSAN

The development of halo derivatives of COSAN started with the synthesis of [3,3'-Co(8,9,12-Br_3-1,2-$C_2B_9H_8)_2$]$^-$ ([**Br_6-1**]$^-$) in 1968[1] and since then, many strategies have been devised to develop more halo derivatives for different applications such as radiolysis[2] or weakly coordinating anions.[3]

- *Bromo derivatives*. The synthesis of bromo derivatives such as [3,3'-Co(8-Br-1,2-$C_2B_9H_{10}$)(1',2'-$C_2B_9H_{11}$)]$^-$ ([**Br-1**]$^-$) or [3,3'-Co(8-Br-1,2-$C_2B_9H_{10})_2$]$^-$ ([**Br_2-1**]$^-$) from COSAN generally demands bromine and iron powder in methanol or THF, giving yields of 75-85%.[2,4] Conversely, the tetrabromo derivative requires building up the molecule starting from the synthesis of [*nido*-9,11-Br_2-7,8-$C_2B_9H_{10}$]$^-$ to continue with the synthesis of the metallacarborane. As a consequence, the bromo positions in [3,3'-Co(4,7-Br_2-1,2-$C_2B_9H_9)_2$]$^-$ ([**Br_4-1**]$^-$) built from the components are different from the product synthesized by dehydrobromination from COSAN due to the synthetic strategy utilized.[5]

- *Iodo derivatives*. Iodinated derivatives of metallacarboranes have attracted interest because of their potential as precursors in boron substitution reactions.[6] The typical process involved the use of iodine as iodinating agent that makes possible to obtain [3,3'-Co(8-I-1,2-$C_2B_9H_{10}$)(1',2'-$C_2B_9H_{11}$)]$^-$ ([**I-1**]$^-$), [3,3'-Co(8-I-1,2-$C_2B_9H_{10})_2$]$^-$ ([**I_2-1**]$^-$) and [3,3'-Co(8,9,12-I_3-1,2-$C_2B_9H_8)_2$)]$^-$([**I_6-1**]$^-$).[2] However, compounds [**I_2-1**]$^-$ and [**I_6-1**]$^-$ were synthesized using iodine monochloride instead of iodine, hence improving the yield to 98% and 92% respectively.[7,8] Nevertheless, the synthesis of [**I_4-1**]$^-$ and [**I_8-1**]$^-$ require to build-up the molecule from its single components hence we should first synthesize either [*nido*-9,11-I_2-7,8-$C_2B_9H_{10}$]$^-$ or [*nido*-1,5,6,10-I_4-7,8-$C_2B_9H_{10}$]$^-$, and only then prompt their complexation with $CoCl_2$ giving the corresponding [3,3'-Co(8,9-I_2-1,2-$C_2B_9H_9)_2$)]$^-$ and [3,3'-Co(8,9,12,10-I_4-1,2-$C_2B_9H_7)_2$)]$^-$ (**Figure 4.1**). This latter product is the halo derivative of COSAN with the highest number of halo substituents produced until now.[5,9]

- *Fluoro derivatives*. Fluorinated compounds have also been studied, and despite fewer advances in this area, the successful mono substitution with a fluoro group has been reported using a mild fluorinating agent such as F-TEDA.[10]

- *Chloro derivatives*. Abundant literature exists on chlorination reactions of COSAN that involve chlorine gas as the chlorinating agent. This methodology leads to several chloroderivatives such as [3,3'-Co(8-Cl-1,2-$C_2B_9H_{10}$)(1',2'-$C_2B_9H_{11}$)]$^-$ ([**Cl-1**]$^-$), [3,3'-Co(8-Cl-1,2-$C_2B_9H_{10}$)$_2$]$^-$ ([**Cl$_2$-1**]$^-$), [3,3'-Co(8,9-Cl$_2$-1,2-$C_2B_9H_9$)(8'-Cl-1',2'-$C_2B_9H_{10}$)]$^-$ ([**Cl$_3$-1**]$^-$), [3,3'-Co(8,9-Cl$_2$-1,2-$C_2B_9H_9$)$_2$]$^-$ ([**Cl$_4$-1**]$^-$) and [3,3'-Co(8,9,12-Cl$_3$-1,2-$C_2B_9H_8$)$_2$]$^-$ ([**Cl$_6$-1**]$^-$) with yields around 75%.[2,4] [**Cl$_6$-1**]$^-$ is the highest *seemingly* pure chlorinated COSAN since 1982.[2] An alternative method which avoids the use of chlorine gas involves the reaction with N-Chlorosuccinimide (NCS). The reaction could undergo in solution to obtain the [**Cl$_2$-1**]$^-$ or in solid-state yielding a mixture from mono to octachlorinated derivatives but their similar physical properties hinder their isolation and post-processing.[2,4,11] Finally, the strategy to synthesize the chloroderivative of the *nido*-carborane in a first step to generate the metallacarborane in a second one requires a lot of purifying procedures, implies long synthesis times, yield losses and not improving the chlorination degree.[5]

In this work we propose the chlorination of COSAN using sulfuryl chloride to go a step beyond the current halogenated derivatives of COSAN. The novelty is in the selected reagent that could act both as a source of chlorine and solvent. Furthermore, it is less hazardous, cheaper, easier to handle than chlorine gas and has been successfully applied as a chlorinating agent in organic chemistry. This methodology was used first in 1980 in boron cluster chemistry to obtain $[B_9Cl_9]^{2-}$ giving a yield of 30-60%.[12] However, the low solubility of the cesium and tetramethylammonium (the most common) salts of the different boron clusters in sulphuryl chloride reduced the success of the dehydrochlorination reactions. This changed a bit in 2010 when the addition of acetonitrile to the sulfuryl chloride was found to increase the solubility allowing the synthesis of pure[13] $[B_{12}Cl_{12}]^{2-}$ as well as the hexachloroderivative of FESAN,[14] and the chloroderivatives of COSAN [**Cl$_4$-1**]$^-$ [15] and [**Cl$_6$-1**]$^-$.[16]

Finally, the highest chlorinated COSAN derivative ([**Cl$_8$-1**]), in a mixt of different chlorinated derivatives, was obtained in the ove,n in a sealed tube with NCS. Thus we already anticipated that both long reaction times and high temperatures are required to achieve the highest degree of substitution in COSAN.[11]

The seek of efficient and wide range electrochemically active compounds was the driving force that prompted the research toward further addition of different chloro units on the COSAN skeleton. Moreover, based in our knowledge about how the redox potential value can be tailored changing the number of chloro units it is possible to predict that the resulting pool of chloro derivatives can find nowadays application in many energy fields.[15,16] Until now the [**Cl$_8$-1**]$^-$ was the highest chloro derivative obtained but was impossible to purify from the other less substituted derivatives that grow in the same reaction.[11] To tackle this issue, in this work we develop the synthesis of highly chlorinated derivatives of COSAN, synthetically pure, obtained with only one step and with the minimum purification process (**Figure 4.1**). Namely, [**Cl$_8$-1**]$^-$, [**Cl$_{10}$-1**]$^-$ and [**Cl$_{12}$-1**]$^-$ are produced, the latter is the highest halo derivative of COSAN ever synthesized since the date.

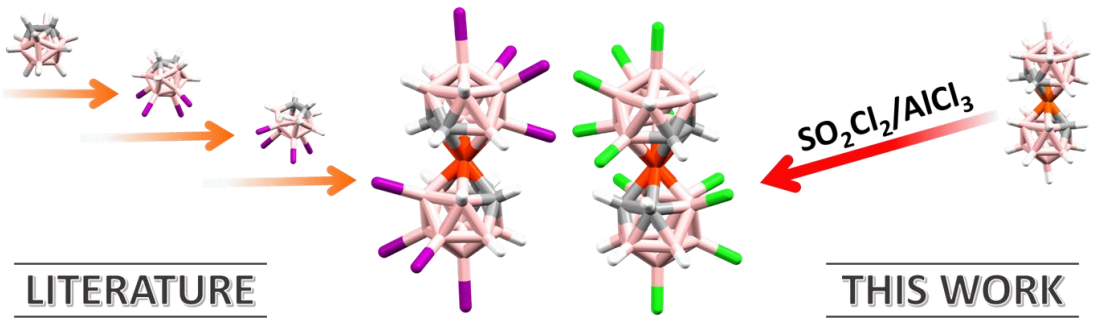

Figure 4.1 Left, synthesis of [3,3'-Co(8,9,10,12-I$_4$-1,2-C$_2$B$_9$H$_7$)$_2$]$^-$ from [*nido*-1,5,6,10-I$_4$-7,8-C$_2$B$_9$H$_8$]$^-$ found in the literature.[9] At right, the method proposed in this research for the synthesis of [3,3'-Co(4,7,8,9,10,12-Cl$_6$-1,2-C$_2$B$_9$H$_5$)$_2$]$^-$. The colours represent the different atoms cobalt (orange), boron [5], hydrogen (white), carbon (grey), iodo (purple) and chloro [17].[17]

4.2 Synthesis

Once we selected sulphuryl chloride as the chlorinated agent, we aimed at optimizing the reaction mix. In this way, we bet on using the protonated salt of COSAN synthesized following the standard procedure,[18] instead of the cesium or tetramethylammonium salt because they are soluble in neat sulfuryl chloride. Keeping in mind the low boiling point of sulfuryl chloride, 69 °C, we also aimed at increasing the reaction pressure to lower the reaction times. For this purpose, we used a thick-walled glass pressure tube as a reaction recipient.

4.2.1 [NMe$_4$][Cl$_8$-1]

The reaction of 50 mg of H[3,3'-Co(1,2-$C_2B_9H_{11}$)$_2$][18] with 8 mL of SO_2Cl_2 in a thick-walled glass pressure tube immersed in an oil bath at 70 °C for 4 days is a convenient route to prepare [**Cl$_8$-1**]$^-$. The purification process consists on removing the solvent under reduced pressure, extract the product with diethyl ether and 0.1 M aqueous HCl solution three times and dry the organic layer. Finally, the residue was redissolved in water and a saturated solution of NMe_4Cl was added promoting the precipitation of the orange product [NMe_4][**Cl$_8$-1**] with a yield of 70%. The characterization unveil the existence of two isomers of [NMe_4][**Cl$_8$-1**], in particular, the [NMe_4][3,3'-Co(8,9,12-Cl_3-1,2-$C_2B_9H_8$)(4',7',8',9',12'-Cl_5-1,2-$C_2B_9H_6$)]$^-$ ([NMe_4][**Cl$_{8\alpha}$-1**]) and [NMe_4][3,3'-Co(7,8,9,12-Cl_4-1,2-$C_2B_9H_7$)$_2$]$^-$ ([NMe_4][**Cl$_{8\beta}$-1**]), two compounds with eight chloro substituents but in different positions. This turned out to be the maximum chlorination degree achievable by this method. (**Scheme 4.1**).

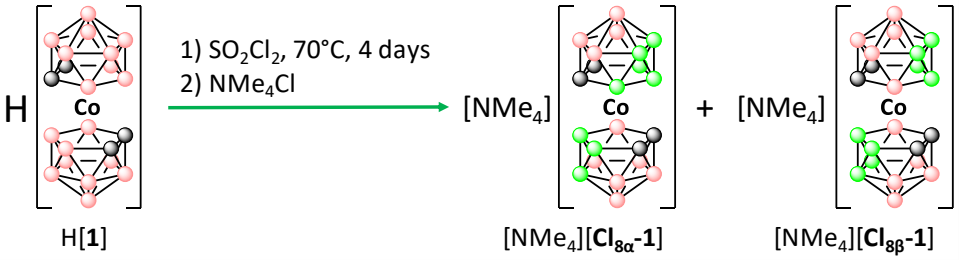

Scheme 4.1. Reaction conditions for the synthesis of the isomeric mixture [NMe_4][**Cl$_{8\alpha}$-1**] [NMe_4][**Cl$_{8\beta}$-1**].

Attempts to increase the chlorination degree by increasing the reaction time to few weeks or use of higher temperatures did not lead to notable amounts of [**Cl$_9$-1**]$^-$ or [**Cl$_{10}$-1**]$^-$) derivatives. We had then proven that a convenient and easy method leading to constitutionally although not isomerically pure [**Cl$_8$-1**]$^-$ was available. To go further and increase the number of chloro groups in the molecule, $AlCl_3$ Lewis acid was added to the reaction mixture and this turned to be determinant to get a higher chlorination degree leading to [3,3'-Co(4,7,8,9,12-Cl_5-1,2-$C_2B_9H_6$)$_2$]$^-$ ([**Cl$_{10}$-1**]$^-$), and [3,3'-Co(4,7,8,9,10,12-Cl_6-1,2-$C_2B_9H_5$)$_2$]$^-$ ([**C$_{12}$-1**]$^-$), the highest chlorinated derivative of COSAN to date (**Scheme 4.2**).

4.2.2 Cs[Cl_{10}-1]

The synthesis of [**Cl_{10}-1**]$^-$ was carried out in two steps because the chlorination degree of the reaction is controlled by the amount of SO_2Cl_2. Thus 1 equivalent of H[**1**][18] and 0.1 equivalent of $AlCl_3$ were dissolved with 65 equivalents of SO_2Cl_2 in a thick-walled glass pressure tube at 70°C during 2 days. Once the reactionarrived at room temperature, the system is opened and the solvent was removed under reduced pressure. Then 0.1 and 65 equivalents of $AlCl_3$ and SO_2Cl_2 respectively, were added again and the reaction was carried out for 2 more days at 70ºC. Finally, the same purification process used for the synthesis of [NMe_4][**Cl_8-1**] but using CsCl as a precipitant agent instead of NMe_4Cl led to a red solid corresponding to Cs[**Cl_{10}-1**] with a yield of 90 % (**Scheme 4.2**).

4.2.3 Cs[Cl_{12}-1]

The synthesis of [**Cl_{12}-1**]$^-$ demands a huge excess of reagents. 650 equivalents of SO_2Cl_2 and 1 of $AlCl_3$ for every equivalent of H[**1**][18] in an ace tube during 4 days at 70ºC is required to achieve the twelve chloro substitution. After the same purification process used for the synthesis of Cs[**Cl_{10}-1**], the reaction leads to Cs[**Cl_{12}-1**] with a yield of 95 % (**Scheme 4.2**). An increment of the reagent excess, temperature or reaction time led always to the same product [**Cl_{12}-1**]$^-$, hence twelve is the maximum substitution degree achieved by this methodology. In addition, these results are consistent with the Viñas's study found in the literature[19] about the preferential chlorination vertices in COSAN. The work presents the kinetic plus thermodynamic component values required to substitute every B-H of the COSAN structure by a B-Cl concluding that the B(5, 11 and 6) positions would be very difficult to substitute.

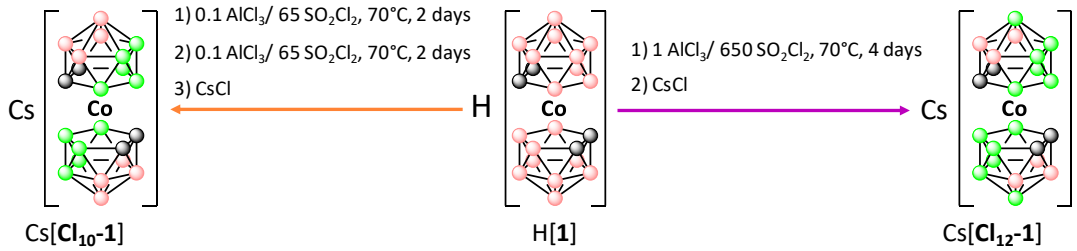

Scheme 4.2. Reaction conditions for the synthesis of [NMe_4][**Cl_{10}-1**] (orange arrow) and [NMe_4][**Cl_{10}-1**] (purple arrow).

4.3 Characterization

[NMe_4][Cl_8-1], Cs[Cl_{10}-1] and Cs[Cl_{12}-1] were characterized by ^{1}H-, ^{1}H{^{11}B}-, ^{13}C{^{1}H}-, ^{11}B-, ^{11}B{^{1}H}-NMR, MALDI-TOF, Elemental Analysis (EA), Infrared (IR) spectroscopy and X-ray diffraction (**Appendix B**).

IR spectra give us a qualitative analysis of the reaction through the monitoring of the characteristic B-H band around 2600 cm^{-1}. The comparison of the FT-IR spectra of the Na[**1**] with the spectra of the products [NMe_4][**Cl_8-1**], [NMe_4][**Cl_{10}-1**] and [NMe_4][**Cl_{12}-1**] unveil a band at 992 cm^{-1} corresponding to B-Cl that increase with the chlorination degree.[20] On the other hand, MALDI-TOF was fundamental to develop this work. The technique provides faster and secure information about the exact number of chloro substituents directly from the reaction mixture (**Figure 4.2**). Finally, the study of NMR spectra together with x-ray diffraction, led us to unveil the exact position of the substituents in these chlorinated boron clusters.

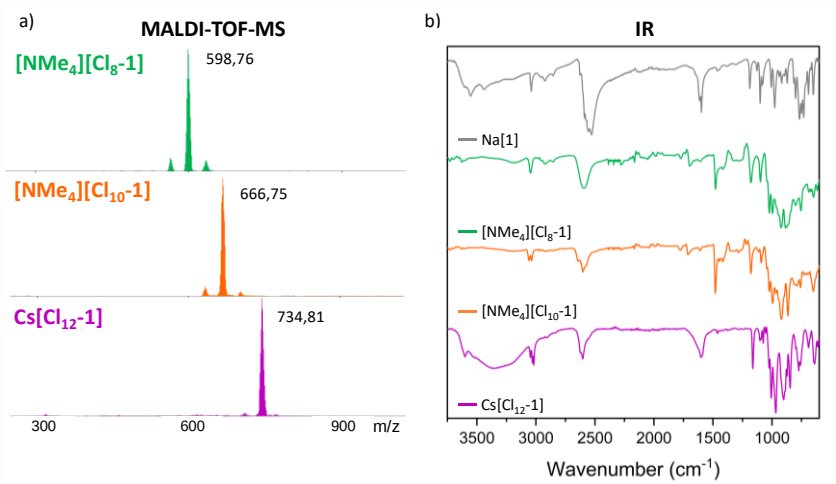

Figure 4.2. a) MALDI-TOF-MS and b) IR spectra of compounds Na[**1**] (grey), [NMe_4][**Cl_8-1**], [NMe_4][**Cl_{10}-1**] (orange) and Cs[**Cl_{12}-1**] (purple).

4.3.1 Crystallographic Characterization

Suitable single crystals of [NMe_4][**Cl_8-1**] and [NMe_4][**Cl_{10}-1**] were obtained by slow evaporation in acetone; the Cs[**Cl_{12}-1**] crystal was obtained in CH_2Cl_2. To the best of our knowledge, these are the highest halo metallacarborane derivatives ever crystallized (**Figure 4.3**).

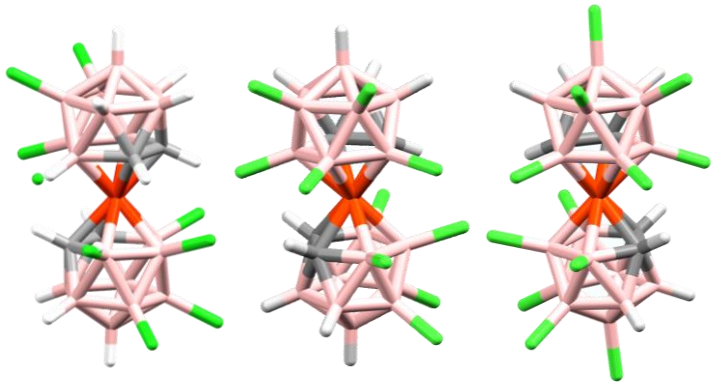

Figure 4.3. Crystal structures of [NMe_4][**Cl_8-1**],[NMe_4][**Cl_{10}-1**] and Cs[**Cl_{12}-1**] (from left to right). The representation of a chloro and a hydrogen atom in B(4,4') positions of [NMe_4][**Cl_8-1**] indicates the isomers present in the crystal (B in pink, C in grey, H in white, Cl in green and Co^{3+} in orange).

The X-ray analysis of [NMe_4][**Cl_8-1**] revealed the solid solution nature of the crystal due to the existence of two isomers in the same monocrystal. Namely, 80% of [NMe_4][**$Cl_{8\alpha}$-1**] isomer and 20% of the [NMe_4][**$Cl_{8\beta}$-1**] **(Figure 4.3)**.

Intramolecular interactions play an important role in defining the physicochemical properties, especially in our compounds [NMe_4][**Cl_8-1**] and [NMe_4][**Cl_{10}-1**] show different types of intermolecular interactions. The dihydrogen bond C_{Me}-H···H-B between tetramethylammonium and COSAN is the most abundant interaction in the crystal structure of [NMe_4][**1**].[21] In addition, this interaction is the most abundant for [NMe_4][**Cl_8-1**] structure too in spite of the *trans* conformation supposed to be incapable of produce such interactions.[22] Finally, the moderated hydrogen bonds C_{Me}-H···Cl-B dominate the intermolecular interaction in [NMe_4][**Cl_{10}-1**] because of its higher chlorination degree. Moreover, the double contact between Cl-B_B(4) of the metallacarborane (B) and the C_{CA}-H of the near metallacarborane (A) is the most important intermolecular interaction in the crystal structure of [NMe_4][**Cl_{10}-1**] as it forces the gauche conformation. Actually, **Figure 4.4** display the C_{CA}(1) -H···Cl-B_B(4) and B_B(4) -Cl···H-C_{CA}(1') with distances of 2.877 and 2.657Å respectively and an angle of 51.4° (**Figure 4.4**).[23]

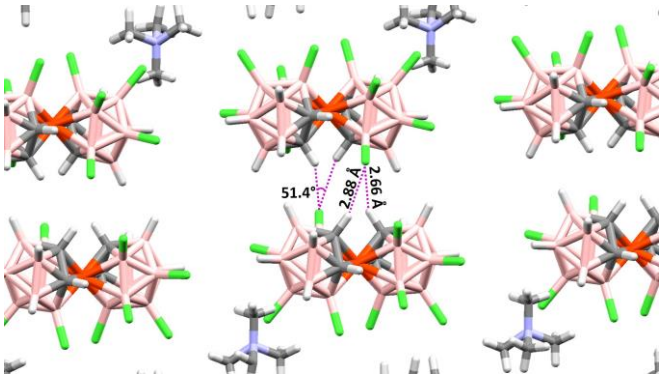

Figure 4.4. $C_{CA}(1)$-H···**Cl**[-$B_B(4)$] ···H-$C_{CA}(1')$ double interaction between two close [**Cl_{10}-1**]$^-$ in the crystal packing (B in pink, C in grey, H in white, Cl in green, Co^{3+} in orange and N in blue).

The study of the Cs[**Cl_{12}-1**] crystal structure reveals three types of intermolecular interactions. The double contact of two molecules of [**Cl_{12}-1**]$^-$ (A and B) with cesium cation, actually, the interactions $B_A(9')$-Cl···Cs···Cl-$B_B(9)$ with distances of 3.597 and 3.671 Å respectively (**Figure 4.5**a). The second type involves three [**Cl_{12}-1**]$^-$ molecules and the interactions of $B_A(7)$–Cl···H-$B_B(11)$ and $B_A(8')$-Cl···H-$B_C(5)$ with distances of 3.118 and 2.999 Å respectively (**Figure 4.5**a and b). Third interaction type involves [**Cl_{12}-1**]$^-$ and CH_2Cl_2, the solvent molecule interacts with the B(5)-H and B(9)-Cl positions of two [**Cl_{12}-1**]$^-$ with distances of 2.251 and 2.902 Å (**Figure 4.5**c). Surprisingly, the H-C_C position of Cs[**Cl_{12}-1**] does not show any contact in the structure.

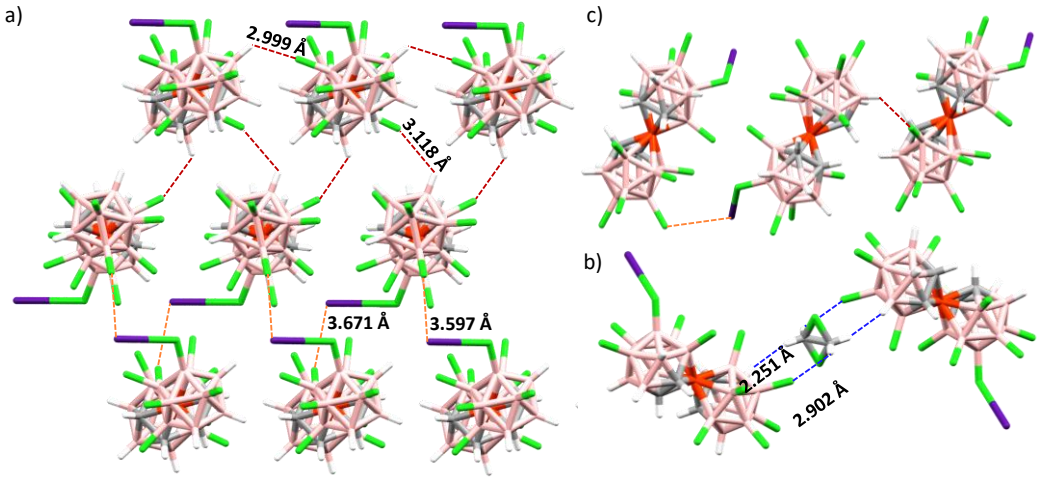

Figure 4.5. a) Double contact scheme of $B_A(9')$-Cl···Cs···Cl-$B_B(9)$ (in orange) between two close [**Cl_{12}-1**]$^-$ and $B_A(7)$–Cl···H-$B_B(11)$ and $B_A(8')$-Cl···H-$B_C(5)$ (in red) between three [**Cl_{12}-1**]$^-$ units, in

the crystal packing. b) View of a) at 90º. c) Representation of the double interaction B(5)-H···CH_2Cl_2···B(9)-Cl (in blue), between two [**Cl_{12}-1**]$^-$ and one molecule of solvent (B in pink, C in grey, H in white, Cl in green, Co^{3+} in orange and Cs in purple).

As a result of all these contacts, the three structures revealed the less common conformations in COSAN derivatives.[21] The crystal structure of [NMe_4][**Cl_8-1**] shows a *transoid* rotamer in solid-state, even though this conformation should be the less energetic, the enthalpic component is not the decisive factor in these cases. Normally, the intermolecular interaction and the crystal packaging used to be decisive on the rotamer present in the crystal, see **Figure 4.3** and **Figure 4.6**. However, in this structure we have a solid solution hence the packaging should permit the exchange of Cl by H and *vice versa* in the B(4) and B(7') positions, and the more advantageous conformation to allow it, is the *trans*. In addition, the structures [NMe_4][**Cl_{10}-1**] and Cs[**Cl_{12}-1**] surprisingly present *gauche 1* and *gauche 2* rotamers, the second less common rotamer for COSAN derivatives with centroid distances between η^5-C_2B_3 and Co^{III} of 1.514 and 1.539 Å respectively (**Figure 4.3**),[21] probably as a result of the addition of chloron atoms redistribution in the COSAN skeleton and the intermolecular interactions with the near molecules.

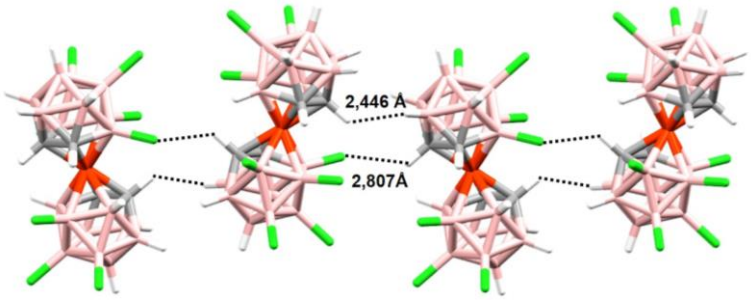

Figure 4.6. interactions C_{2A}-H···H-B_{6B} and $B_{7'A}$-Cl···H-C_{1B} between near [**Cl_8-1**]- molecules forming a chain in the crystal packing (B in pink, C in grey, H in white, Cl in green and Co^{3+} in orange).

4.3.2 NMR Characterization

* Cs[Cl_{10}-1] and Cs[Cl_{12}-1]

Gauche rotamers present in the crystal structures of [NMe][**Cl_{10}-1**] and Cs[**Cl_{12}-1**] are so stable that they are retained even in solution that accounts for the extra peaks that appear in the NMR spectra of both compounds. The *gauche*

conformation breaks the symmetry of the structure and consequently, ^{1}H-NMR spectrum shows two C_C-H because of the presence of two spectroscopically different C_C-H protons (**Figure 4.7**).

Boron NMR spectroscopy, as thoroughly explained in the introduction, is a fundamental technique to study these compounds because allows to know the number and position of chloro substituents in the COSAN structure. ^{11}B{^{1}H}-NMR presents as many signals as the number of spectroscopically non-equivalent boron atoms because the experiment avoids the B-H signals coupling. However, this coupling does not occur between the B and Cl nucleus hence the ^{11}B-NMR spectrum displays BH signals as doublets and BCl signals as singlets. Consequently, ^{11}B{^{1}H}-NMR and ^{11}B-NMR spectra together with the ^{11}B-NMR information found in the literature made it possible to determine the precise chlorinated positions of the COSAN skeleton.[4,15,16]

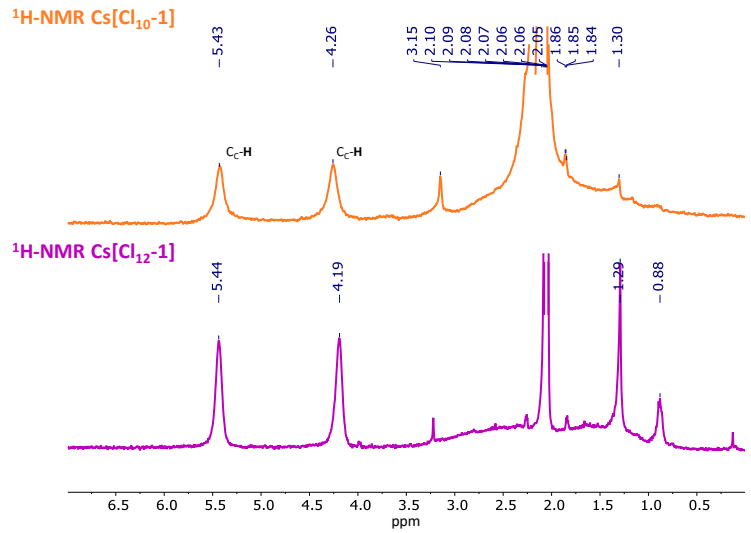

Figure 4.7. ^{1}H-NMR spectra of Cs[Cl_{10}-1] and Cs[Cl_{12}-1] in $(CD_3)_2CO$.

^{11}B-NMR spectra of Cs[**Cl_{10}-1**] displays three singlets at 12.4, 6.4 and 1.6 ppm corresponding to ten B-Cl units at B(8,8'), B(4,4',9,9',12,12') and B(7,7') positions respectively. The four doublets that appear in **Figure 4.8** at 0.2, -14.3, -17.1 and -27.7 ppm correspond to the B-H units of the boron atoms B(10,10'), B(5,5', 11, 11') (we are not able to differentiate between the position 5 and 11 in the ^{11}B-NMR spectra) and B(6,6') respectively. Moreover, ^{11}B-NMR spectrum of Cs[**Cl_{10}-1**]

presents a B(4)-Cl signal shifted from the supposed equivalent B(7)-Cl (Δppm=-4.81) as a result of the interaction between B(4)-Cl and C_C-H of the two close [**Cl_{10}-1**]$^-$ and demonstrates again that the compound in solution retains some intermolecular interactions, see **Figure 4.8**. Finally, ^{11}B-NMR spectrum of Cs[**Cl_{12}-1**] displays another three singlets with integration twelve corresponding to the positions B(8,8'), B(4,4',7,7',9,9',12,12') and B(10,10') at 11.5, 5.6 and 0.7 ppm respectively confirming the substitution degree (**Figure 4.8**). In addition, ^{11}B-NMR presents too three doublets at -14.2, -17.0 and -27.9 ppm corresponding to the positions B(5,5',11,11') and B(6,6') respectively.

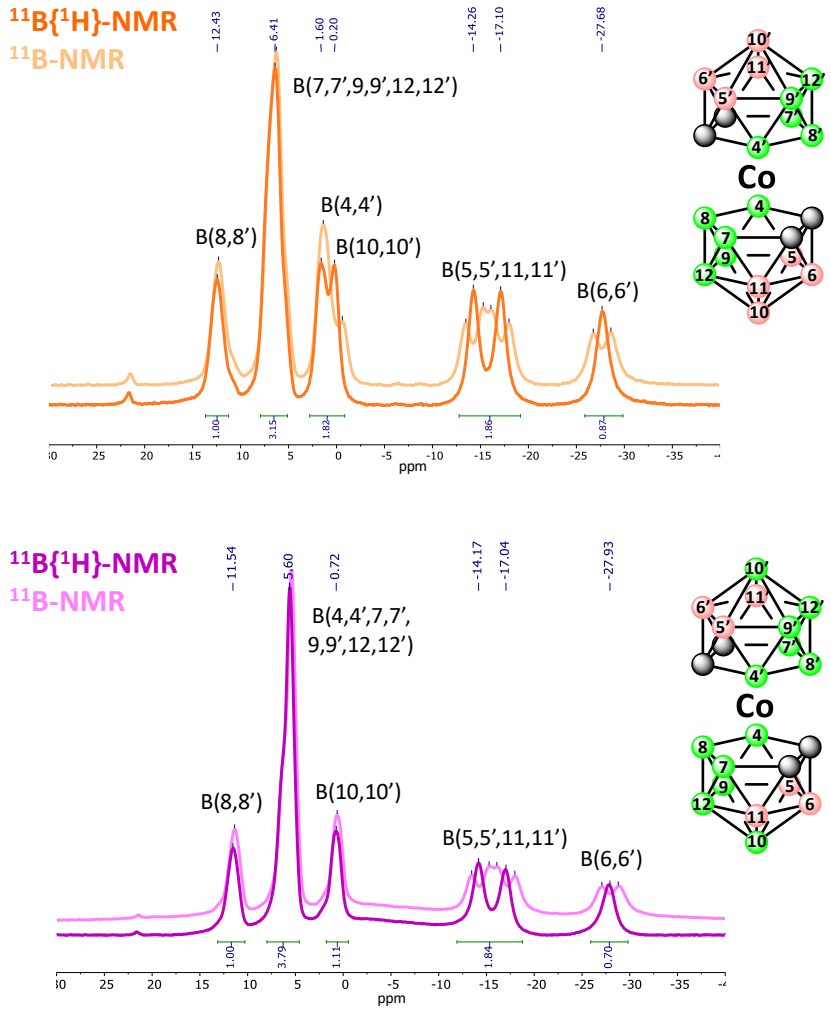

Figure 4.8. ^{11}B{^{1}H}-NMR and ^{11}B-NMR of Cs[Cl_{10}-1] (in orange) and Cs[Cl_{12}-1] (in purple).

* $[NMe_4][Cl_{8\alpha}\text{-}1]$ and $[NMe_4][Cl_{8\beta}\text{-}1]$

NMR characterization of $[NMe_4][\mathbf{Cl_8\text{-}1}]$ presents a different situation respect the characterization of $Cs[\mathbf{Cl_{10}\text{-}1}]$ and $Cs[\mathbf{Cl_{12}\text{-}1}]$. Even though the EA confirm the purity of the product, the ^{11}B-NMR is more complex and difficult to interpret than the previous cases because the spectra show many more signals due to the presence of two different structural isomers $[\mathbf{Cl_{8\alpha}\text{-}1}]^-$ and $[\mathbf{Cl_{8\beta}\text{-}1}]^-$. The ^{1}H-NMR show two signals at 4.92 and 4.87 ppm and one broad peak at 4.07 ppm indicating that the main product is an isomeric mixture (**Figure 4.9**). Moreover, the integration of the proton peaks corresponding to the C_C-H signals in the ^{1}H-NMR spectrum leads to a rough ratio α:β isomers of 55:45. Fortunately, the separation of the mixture was possible thanks to the different polarity of the isomers. Actually, the isomer $[\mathbf{Cl_{8\alpha}\text{-}1}]^-$ was more insoluble in chloroform than $[\mathbf{Cl_{8\beta}\text{-}1}]^-$, leading to isomeric pure products that were analyzed by ^{1}H- ^{11}B- and ^{13}C-NMR (**Figure 4.9** and **Figure 4.10**).

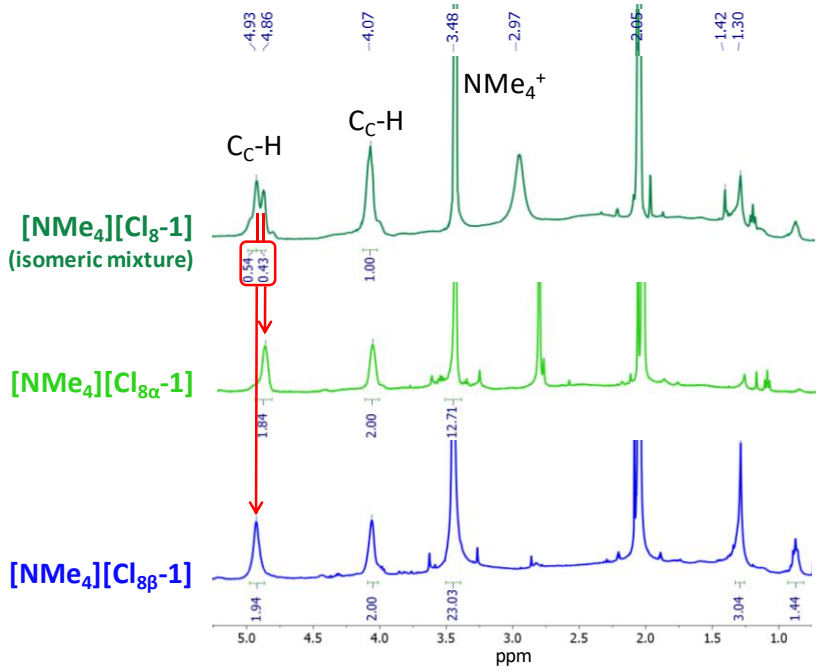

Figure 4.9. ^{1}H-NMR of the mixture $[NMe_4][\mathbf{Cl_8\text{-}1}]$ (in dark green), isolated $[NMe_4][\mathbf{Cl_{8\alpha}\text{-}1}]$ (in light green) and isolated $[NMe_4][\mathbf{Cl_{8\beta}\text{-}1}]$ (in blue).

The ^{11}B-NMR spectra analysis helped us to characterize and identify both isomers of $[NMe_4][\mathbf{Cl_8\text{-}1}]$. Two signals corresponding to B(6,6') is not common in the

COSAN. Viñas's theoretical studies on the sequential addition of substituents in the COSAN scaffold tends to substitute the less substituted carboranyl moiety so that the substitution is alternated.[19] In other words, the substitution occurs in the cluster where there is a minor number of substituents. If the first substitution occurs at the B(8) position the second will be at the B(8'), if the third occurs in B(9), the fourth one will be in B(9') and so on. Consequently, two different signals for B(6) and B(6') are quite rare for what one would consider normal in a typical ^{11}B-NMR spectrum of a COSAN with even number of substituents; the explanation is the existence of the different number of substituents in one moiety with regard to the second one in the same COSAN.

The reason why the COSAN does not follow the alternate rule could have a kinetic origin, with two positions B(4) and B(7) energetically equivalent and due to the high velocity of substitution the system is not able to differentiate between both providing the two α and β isomers.

Moreover, despite the chlorination order proposed starts by B(8) position, continues on the B(9,12) without preference between them and finally ends with B(10), the ^{11}B-NMR suggests (**Figure 4.10**), and the crystal structure confirms (**Figure 4.3**), that for both isomers the B(4,7) positions are chlorinated before B(10). Due to the equivalence between the B(4,7) positions, the synthesis of COSAN with eight chloro derivatives provides two isomers as a result of the non-preference between B(4) and B(7).

Figure 4.10 shows the assignment of all signals for both isomers. The number of singlets that appear in the ^{11}B{^{1}H}-NMR spectrum defines the number of chloro units of the molecule. Furthermore, the assignment of the peaks was possible thanks to the contrast of other chloroderivative spectroscopic details found in the literature. [4,15,16]

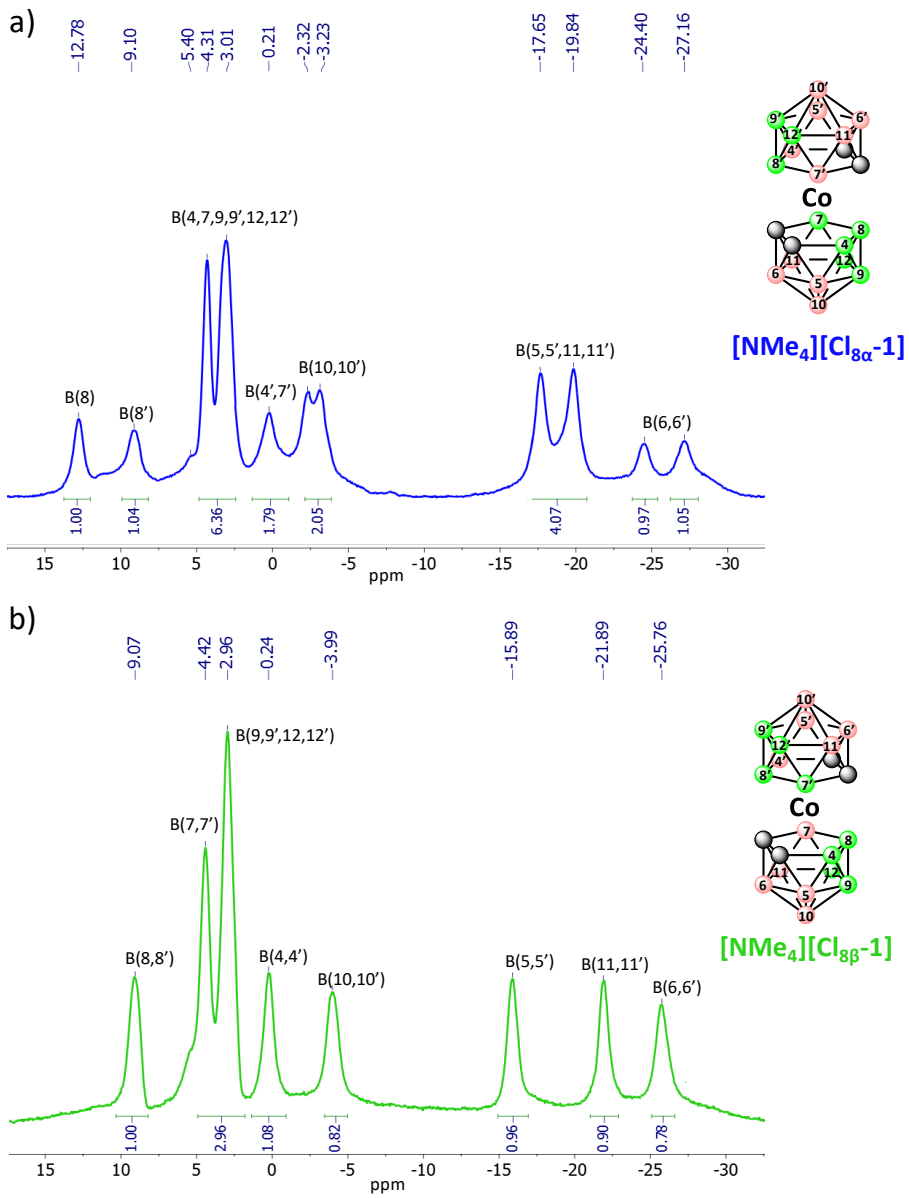

Figure 4.10. ^{11}B-NMR of a) isolated [NMe_4][**$Cl_{8\alpha}$-1**] (blue) and b) isolated [NMe_4][**$Cl_{8\beta}$-1**] [17].

4.3.3 Electrochemical characterization

The study of the electrochemical properties of these chlorinated COSAN derivatives is fundamental to open up the way toward possible applications of these metallacarboranes as redox catalysts or electroactive electrolytes for energy

harvesting and storage. The analysis of the redox potential value and the reversibility of the redox process provides the basics about the working range of these compounds and their electrochemical stability.

The $E_{1/2}(Co^{III}/Co^{II})$ values for [**Cl_8-1**]$^-$, [**Cl_{10}-1**]$^-$ and [**Cl_{12}-1**]$^-$ were experimentally determined by cyclic voltammetry and compared with the most promising chlorinated derivatives found in the literature, see **Figure 4.11**, **Figure 4.12** and **Table 4.1**. These results not only provide the redox potential of $Co^{(III)}/Co^{(II)}$ but also give us evidence of reversibility of the system. A reversible system is able to repeat the redox process theoretically infinite times because the structure is not irreversibly affected by the redox reaction. Systems with differences between the anodic and cathodic peak of the cyclic voltammetry (ΔmV) smaller than 100 mV are considered reversible hence Cs[**Cl_{10}-1**] and Cs[**Cl_{12}-1**] are electrochemically reversible systems with ΔmV values of 99.8 and 62 mV respectively. Even though, [NMe_4][**Cl_8-1**] show a broader signal, with a ΔmV of 183, see **Figure 4.11** and **Table 4.1**, we propose the system [NMe_4][**Cl_8-1**] as electrochemically reversible and the isomeric mixture as responsible of the wide ΔmV value. Our hypothesis is based on that every isomer possesses a different redox potential but, the isomer signals are so close that the device is not able to resolve them leading to a single broad signal.

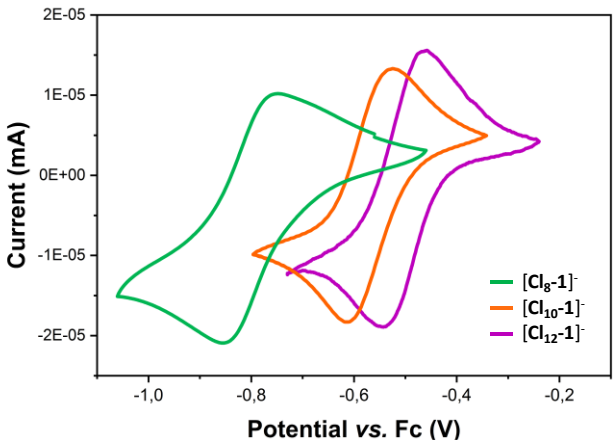

Figure 4.11. Cyclic voltammetry of [**Cl_8-1**]$^-$ (in green), [**Cl_{10}-1**]$^-$ (in orange) and [**Cl_{12}-1**]$^-$ (in purple) was carried out in dry acetonitrile as solvent and $TBAPF_6$ (0.1 M) as supporting electrolyte. For the electrodes, Glassy Carbon [24] as working electrode, Ag wire as pseudo-reference electrode and Pt wire as the counter electrode. Measurements were referenced to internal Fc^+/Fc couple.

Table 4.1. $E_{1/2}$ of (Co^{III}/Co^{II}) data for $[Cl_n\text{-}1]^-$,(n= 0, 1, 2, 4, 6, 8, 10 and 12). The superindex indicate the reference. Besides, [ΔmV] indicate the potential difference between the reduction and oxidation potential. Finally, $\Delta E_{1/2}$ is the redox potential difference between $[Cl_n\text{-}1]^-$ and $[Cl_{(n-2)}\text{-}1]^-$.

Compound	$E_{1/2}$ *vs.* Fc (V) [ΔmV]$^{ref.}$	$\Delta E_{1/2}$ (V)
$[\mathbf{1}]^-$	-1.75[25]	
$[\mathbf{Cl_2\text{-}1}]^-$	-1.39[26,27]	0.36
$[\mathbf{Cl_4\text{-}1}]^-$	-1.20[15]	0.19
$[\mathbf{Cl_6\text{-}1}]^-$	-1.01[16]	0.19
$[\mathbf{Cl_8\text{-}1}]^-$	-0.79 [183]	0.22
$[\mathbf{Cl_{10}\text{-}1}]^-$	-0.56 [99.8]	0.23
$[\mathbf{Cl_{12}\text{-}1}]^-$	-0.49 [63]	0.07

As a rule of thumb, it was considered that every added chloro contributes in +0.12V to the $E_{1/2}(Co^{III}/Co^{II})$ of the initial scaffold.[11] This is seen from $[\mathbf{1}]^-$ to $[\mathbf{Cl_{10}\text{-}1}]^-$ with an average+0.12V. However, **Figure 4.12** shows how the increment of the value of $E_{1/2}(Co^{III}/Co^{II})$ ($\Delta E_{1/2}$) to be quasi linear, but for the edges of the series, the first and last points $[\mathbf{1}]^-$ and $[\mathbf{Cl_{12}\text{-}1}]^-$. The explanation of this phenomenon previously observed in the iodinated derivatives,[28] takes into consideration the importance of the chlorinated position. The COSAN is a 3D aromatic system with an unpaired electron delocalized along the whole structure. Considering that the chloro is an electron-withdrawing group, every substituent polarizes the anion electron density making the redox potential of Co^{III}/Co^{II} more positive. In addition, the strength of this effect depends on the distance and position of the Cl from the Co atom. The substituents that are in the plane (η^5-C_2B_3) closer to Co affect more the redox potential of the Co^{III}/Co^{II} compared to the ones in the next plane (η^5-B_5) or in the B(10) position. Crystal structures of $[NMe_4][\mathbf{Cl_8\text{-}1}]$, $[NMe_4][\mathbf{Cl_{10}\text{-}1}]$ and $Cs[\mathbf{Cl_{12}\text{-}1}]$ suggest that the preferred chlorination order for COSAN is first B(8) followed by B(9,12) (equivalent positions), B(4,7), B(10), B(5,11) and finally B(6). Therefore, the largest potential gaps are found for $[\mathbf{Cl_2\text{-}1}]^-$, $[\mathbf{Cl_8\text{-}1}]^-$ and $[\mathbf{Cl_{10}\text{-}1}]^-$, whose chlorinated positions are the ones on the η^5-C_2B_3 plane. Furthermore, the potential gap of $[\mathbf{Cl_{12}\text{-}1}]^-$, corresponding to the chlorination of the B(10), the furthest position, is the lower experimentally determine gap with a value of 0.07V.

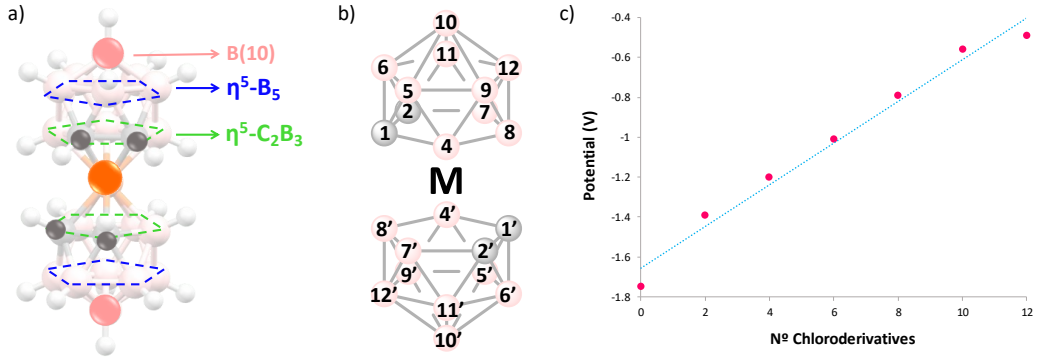

Figure 4.12. a) Representation of the different planes of a metallacarborane. b) Metallacarborane scheme representing the vertex numbering. c) Graphical representation of the redox potential varying by each newly added chloro substituent. The blue line corresponds to the trend line.

* Synthesis and characterization of [NMe_4][Cl_4-1]

To unveil the role of the substituent position on the metallacarborane redox potential, we synthesized NMe_4][3,3'-Co(4,7-Cl_2-1,2-$C_2B_9H_9$)$_2$], studied its electrochemistry and compared it with the one of [NMe_4][3,3'-Co(8,9-Cl_2-1,2-$C_2B_9H_9$)$_2$].[15] The synthesis was carried out following the methodology depicted in the **Scheme 4.3** with no further modification to what we found in the literature.[5]

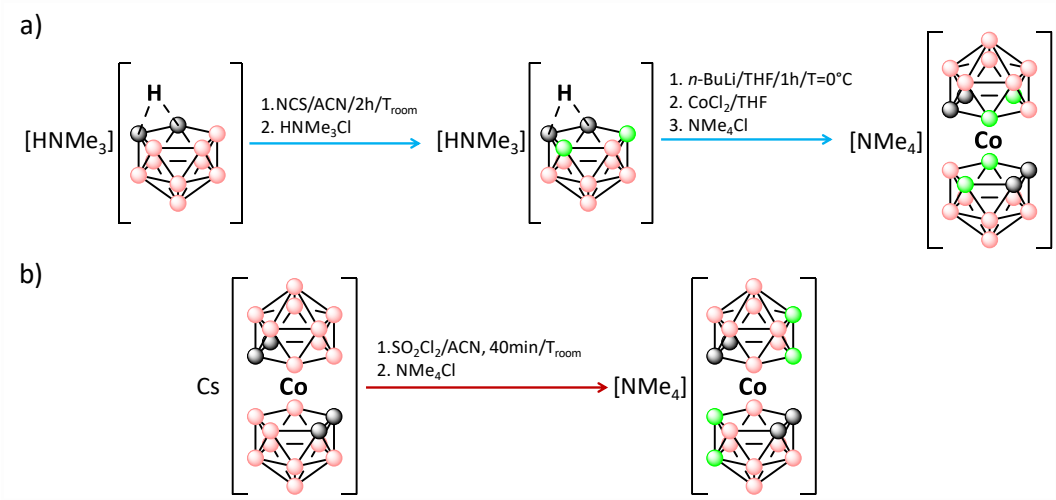

Scheme 4.3. a) Reaction conditions for the synthesis of [NMe_4][3,3'-Co(4,7-Cl_2-1,2-$C_2B_9H_9$)$_2$] based on the literature.[5] b) Reaction conditions for the synthesis of [NMe_4][3,3'-Co(8,9-Cl_2-1,2-$C_2B_9H_9$)$_2$] found in the literature.[15]

The procedure consists in taking 200mg of [NMe_4][*nido*-9,11-Cl_2-7,8-$C_2B_9H_{10}$] (0.73 mmol) dissolved in 5 mL of dry THF under nitrogen and cool it at 5ºC with an ice-water bath for 30 min. 1.12 mL of *n*-BuLi (2.2 mmol, 2 M) was added dropwise. In the meanwhile, a suspension of 303 mg (2.2 mmol) of anhydrous $CoCl_2$ in dry THF (5 mL) was prepared in another flask. The transparent solution of ligand was transferred to the suspension of $CoCl_2$ and the reaction was stirred under reflux at inert atmosphere overnight. Then, the system was opened and left under reflux condition during 2h. This step allows the oxidation of the Co(II) complex to Co(III) in presence of air. Once the reaction is finished, the solvent was removed in vacuum, and the product was extracted with diethyl ether and HCl (0.1 M) solution three times. The organic phase was evaporated; the brown solid was dissolved in water and precipitated using an aqueous solution of CsCl. The brown precipitate was filtrated and washed with water obtaining 70 mg (36 %) of [NMe_4][3,3'-Co-(4,7-Cl_2-1,2- $C_2B_9H_9)_2$]. MALDI-TOF demonstrated the formation of the desired product with a peak at 461.36 m/z (**Figure 4.13**) and the ^{11}B-NMR spectra confirm the homogeneity of the sample displaying the signals at (multiplicity, intensity): 9.0 (s, 2B), 6.0 (d,2B), 4.2 (s,2B), -0.4 (d,4B), -3.0 (d,2B), -5.5 (d,2B), -14.5 (d, 2B), -21 ppm (d, 2B).

The cyclic voltammetry of [NMe_4][3,3'-Co-(4,7-Cl_2-1,2- $C_2B_9H_9)_2$ (**Figure 4.13**) displays a redox potential of 1.13 V *vs*. Fc, a value of $E_{1/2}(Co^{III}/Co^{II})$ 0.07 V higher than the redox potential of [NMe_4][3,3'-Co(8,9-Cl_2-1,2-$C_2B_9H_9)_2$ with the same number of chloro substituents but in other positions. This result confirms not only that the number but also the position of the chloro substituents affects the redox potential of the structure. Moreover, the small difference between the redox potential of the two isomers of [**Cl_4-1**]$^-$ (0.07 V) support also the fact that the wide redox signal of [NMe_4][**Cl_8-1**] in the CV is the sum of two signals corresponding to the [NMe_4][**$Cl_{8\alpha}$-1**] and [NMe_4][**$Cl_{8\beta}$-1**] isomers while both are reversible systems.

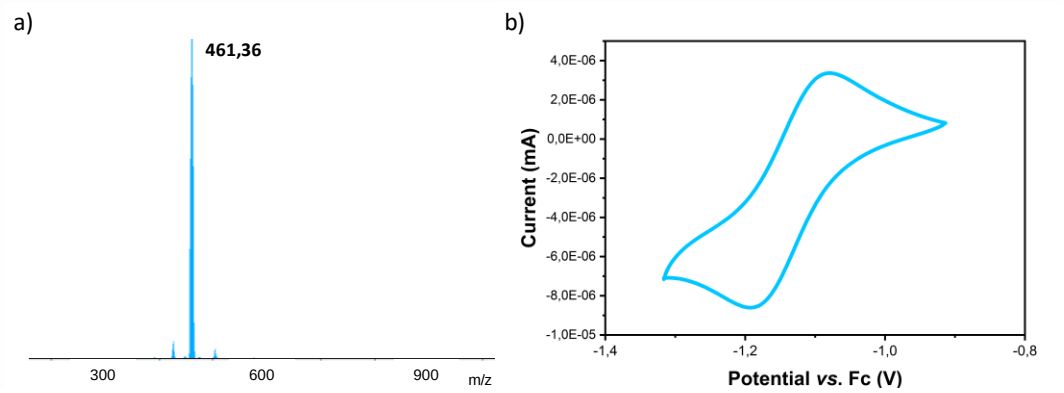

Figure 4.13. a) MALDI-TOF-MS of $[NMe_4][3,3'\text{-}Co(4,7\text{-}Cl_2\text{-}1,2\text{-}C_2B_9H_9)_2]$; b) Cyclic voltammetry of $[NMe_4][3,3'\text{-}Co(4,7\text{-}Cl_2\text{-}1,2\text{-}C_2B_9H_9)_2]$ in dry acetonitrile as solvent and $TBAPF_6$ (0.1 M) as supporting electrolyte. For the electrodes, Glassy Carbon as working electrode, Ag wire as pseudo-reference electrode and Pt wire as the counter electrode. Measurements were referenced to internal Fc^+/Fc couple.

4.4 Thermostability study

All the reported compounds show good stability upon the several redox processes. In addition, the thermal stability of salts of NMe_4^+ and Cs^+ of $[\mathbf{1}]^-$ is well established.[29] However, we were interested in demonstrating that these compounds can resist high temperatures for possible applications. Thus we made a thermogravimetric analysis (TGA) of $[NMe_4][\mathbf{Cl_8\text{-}1}]$, $[NMe_4][\mathbf{Cl_{10}\text{-}1}]$ and $Cs[\mathbf{Cl_{12}\text{-}1}]$. TGA of $[NMe_4][\mathbf{Cl_{10}\text{-}1}]$ and $Cs[\mathbf{Cl_{12}\text{-}1}]$ display a step near to 350°C corresponds to the loss of chloro substituents hence to the decomposition of the molecule, on contrast, TGA of $[NMe_4][\mathbf{Cl_8\text{-}1}]$ start to decompose at 200°C. In addition, Differential Scanning Calorimetry (DSC) of $[NMe_4][\mathbf{Cl_{10}\text{-}1}]$ presents a peak at 100°C correspondings with the step of -2.6% of the mass in the TGA indicating the loss of a water molecule. Finally, TGA comparison of the three products presents the $Cs[\mathbf{Cl_{12}\text{-}1}]$ as the most stable compound followed by $[NMe_4][\mathbf{Cl_{10}\text{-}1}]$ and $[NMe_4][\mathbf{Cl_8\text{-}1}]$ (**Figure 4.14**).

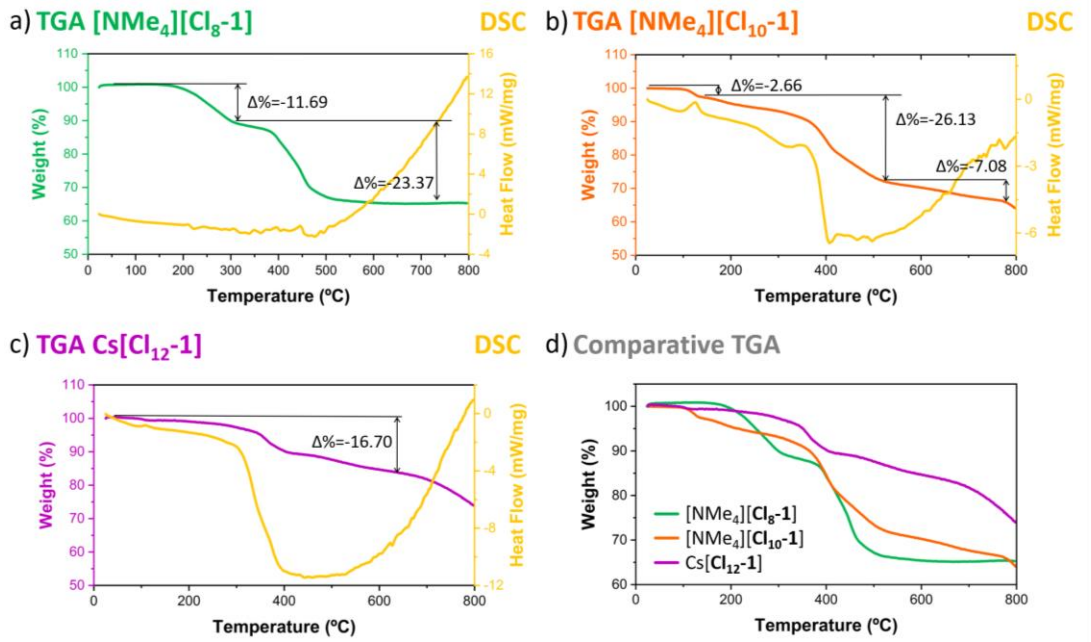

Figure 4.14. TGA and DSC (in yellow) of the compounds: a) $[NMe_4]$[**Cl_8-1**] (in green), b) $[NMe_4]$[**Cl_{10}-1**] (in orange), c) Cs[**Cl_{12}-1**] (in purple), d) Comparative TGA of the three compounds. The samples were placed in a ceramic crucible, while the tests were carried out with a flow of N_2 gas of 70 cm^3/min and a heating rate of 20ºC/10 min.

4.5 Conclusions

Up to now, [**Cl_6-1**]$^-$ was the highest chloroderivative of COSAN synthetically quasi pure. Now, after 38 years since the first synthesis of [**Cl_6-1**]$^-$, three new high chlorinated derivatives of COSAN are introduced in good yields into the group of chloro derivatives of COSAN: [**Cl_8-1**]$^-$, [**Cl_{10}-1**]$^-$ and [**Cl_{12}-1**]$^-$.

The work presents a fast, easy and synthetic friendly route based on the use of protonated salts of COSAN along with the addition of $AlCl_3$ as catalyst/reagent. The latter along with the amount of SO_2Cl_2, that performs as solvent and chlorinating agent, have been key points to increase the chlorination degree up to twelve substituents. The three chloro COSAN derivatives were fully characterized, and the crystal structure together with the NMR characterization unveil the presence of two isomers $[NMe_4]$[**$Cl_{8\alpha}$-1**] and $[NMe_4]$[**$Cl_{8\beta}$-1**] in a ratio 55:45 as a result of the no preference of the system between the position B(4') or

B(7). Moreover, the crystal structures display the rotamers *trans*, *gauche 1* and *gauche 2* for the crystals $[NMe_4][\mathbf{Cl_8\text{-}1}]$, $[NMe_4][\mathbf{Cl_{10}\text{-}1}]$, $Cs[\mathbf{Cl_{12}\text{-}1}]$, respectively, promoted by their intermolecular interactions.The crystal characterization of the three compounds displays an interesting behaviour of the COSAN skeleton related to the chloro substitution order. The crystal structure of $[NMe_4][\mathbf{Cl_8\text{-}1}]$ appears as a solid solution with a mix between the two isomers, in particular, $[NMe_4][\mathbf{Cl_{8\alpha}\text{-}1}]$ and $[NMe_4][\mathbf{Cl_{8\beta}\text{-}1}]^-$. In addition, the crystal structures of the three compounds unveil preferential chlorination vertices in the COSAN structure that differ of previous theoretical studies, which indicates that there is an important kinetic component in the substitution.[19] The order established by the crystal structure starts with the chlorination of B(8), followed by B(9,12) without preferences between them, B(4,7) and finally B(10). The theoretical studies proposed the chlorination at position B(10) before B(4,7). The products are electrochemically active and stable to redox processes. It has been demonstrated that not only the addition but also the position of the chlorosubstituent in the COSAN structure affect the redox potential of the molecules depending on the distance of the substituent from Co atom. Moreover, all the products present a thermostability beyond 350ºC.

The electroactive properties together with the redox and thermostability offer a wide range of possible applications for $[\mathbf{Cl_8\text{-}1}]^-$ $[\mathbf{Cl_{10}\text{-}1}]^-$ and $[\mathbf{Cl_{12}\text{-}1}]^-$ in the material science field. So this works opens new avenues for the development of these compounds as an electroactive electrolyte for Dye Sensitized Solar Cells (DSSCs), as redox catalyst for water oxidation or as electron transfer in bioenergetics such as artificial photosynthesis.

4.6 References

(1) M. F. Hawthorne, D. C. Young, T. D. Andrews, D. V. Howe, R. L. Pilling, A. D. Pitts, M. Reintjes, L. F. Warren Jr and P. A. Wegner, . pi.-Dicarbollyl derivatives of the transition metals. Metallocene analogs, *J. Am. Chem. Soc.*, **1968**, 90, 879-896.

(2) Ľ. Mátel, F. Macášek, P. Rajec, S. Heřmánek and J. Plešek, B-Halogen derivatives of the bis(1,2-dicarbollyl)cobalt(III) anion, *Polyhedron*, **1982**, 1, 511-519.

(3) J. Plesek, Potential applications of the boron cluster compounds, *Chem. Rev.*, **1992**, 92, 269-278.

(4) P. K. Hurlburt, R. L. Miller, K. D. Abney, T. M. Foreman, R. J. Butcher and S. A. Kinkhead, New synthetic routes to B-halogenated derivatives of cobalt dicarbollide, *Inorg. Chem.*, **1995**, 34, 5215-5219.

(5) E. C. Santos, A. B. Pinkerton, S. A. Kinkead, P. K. Hurlburt, S. A. Jasper, C. W. Sellers, J. C. Huffman and L. J. Todd, Syntheses of nido-9,11-X2-7,8-C2B9H10− anions (X=Cl, Br or I) and the synthesis and structural characterization of N(C2H5)4[commo-3,3′-Co(4,7-Br2-3,1,2-CoC2B9H9)2], *Polyhedron*, **2000**, 19, 1777-1781.

(6) I. Rojo, F. Teixidor, C. Viñas, R. Kivekäs and R. Sillanpää, Relevance of the Electronegativity of Boron in η 5-Coordinating Ligands: Regioselective Monoalkylation and Monoarylation in Cobaltabisdicarbollide [3,3′-Co(1,2-C2B9H11)2]− Clusters, *Chem. Eur. J.*, **2003**, 9, 4311-4323.

(7) I. Rojo, F. Teixidor, R. Kivekäs, R. Sillanpää and C. Viñas, Methylation and demethylation in cobaltabis (dicarbollide) derivatives, *Organometallics*, **2003**, 22, 4642-4646.

(8) M. D. Mortimer, C. B. Knobler and M. F. Hawthorne, Methylation of Boron Vertices of the Cobalt Dicarbollide Anion, *Inorg. Chem.*, **1996**, 35, 5750-5751.

(9) A. Pepiol, F. Teixidor, R. Sillanpää, M. Lupu and C. Viñas, Stepwise Sequential Redox Potential Modulation Possible on a Single Platform, *Angew. Chem. Int. Ed.*, **2011**, 50, 12491-12495.

(10) A. N. Gashti, J. C. Huffman, A. Edwards, G. Szekeley, A. R. Siedle, J. A. Karty, J. P. Reilly and L. J. Todd, Fluorination studies of the [commo-3, 3′-Co (3, 1, 2-CoC2B9H11) 2− 1] ion, *J. Organomet. Chem.*, **2000**, 614, 120-124.

(11) P. González-Cardoso, A.-I. Stoica, P. Farràs, A. Pepiol, C. Viñas and F. Teixidor, Additive Tuning of Redox Potential in Metallacarboranes by Sequential Halogen Substitution, *Chem. Eur. J.*, **2010**, 16, 6660-6665.

(12) E. H. Wong and R. M. Kabbani, Boron halide clusters and radicals: synthesis and interconversions of the three oxidation states of a nine-boron polyhedron, *Inorg. Chem.*, **1980**, 19, 451-455.

(13) W. Gu and O. V. Ozerov, Exhaustive chlorination of [B12H12] 2− without chlorine gas and the use of [B12Cl12] 2− as a supporting anion in catalytic hydrodefluorination of aliphatic C− F bonds, *Inorg. Chem.*, **2011**, 50, 2726-2728.

(14) T. García-Mendiola, V. Bayon-Pizarro, A. Zaulet, I. Fuentes, F. Pariente, F. Teixidor, C. Viñas and E. Lorenzo, Metallacarboranes as tunable redox potential electrochemical indicators for screening of gene mutation, *Chem. Sci.*, **2016**, 7, 5786-5797.

(15) R. Ruiz-Rosas, I. Fuentes, C. Viñas, F. Teixidor, E. Morallón and D. Cazorla-Amorós, Tailored metallacarboranes as mediators for boosting the stability of carbon-based aqueous supercapacitors, *Sustainable Energy & Fuels*, **2018**, 2, 345-352.

(16) I. Fuentes, J. Pujols, C. Viñas, S. Ventura and F. Teixidor, Dual Binding Mode of Metallacarborane Produces a Robust Shield on Proteins, *Chem. Eur. J.*, **2019**, 25, 12820-12829.

(17) N. N. Greenwood and A. Earnshaw, *Chemistry of the Elements*, Elsevier, **2012**.

(18) J. Plešek, K. Baše, F. Mareš, F. Hanousek, B. Štíbr and S. Heřmánek, Potential uses of metallocarborane sandwich anions for analysis, characterization and isolation of various cations and organic bases, *Collect. Czech. Chem. Commun.*, **1984**, 49, 2776-2789.

(19) P. Farràs, C. Viñas and F. Teixidor, Preferential chlorination vertices in cobaltabisdicarbollide anions. Substitution rate correlation with site charges computed by the two atoms natural population analysis method (2a-NPA), *J. Organomet. Chem.*, **2013**, 747, 119-125.

(20) W. H. Knoth, H. Miller, J. C. Sauer, J. Balthis, Y. Chia and E. Muetterties, Chemistry of boranes. IX. Halogenation of B10H10-2 and B12H12-2, *Inorg. Chem.*, **1964**, 3, 159-167.

(21) E. J. Juárez-Pérez, R. Núñez, C. Viñas, R. Sillanpää and F. Teixidor, The Role of C–H···H–B Interactions in Establishing Rotamer Configurations in Metallabis(dicarbollide) Systems, *Eur. J. Inorg. Chem*, **2010**, 2385-2392.

(22) D. C. Malaspina, C. Viñas, F. Teixidor and J. Faraudo, Atomistic Simulations of COSAN: Amphiphiles without a Head-and-Tail Design Display "Head and Tail" Surfactant Behavior, *Angew. Chem. Int. Ed.*, **2020**, 59, 3088-3092.

(23) G. A. Jeffrey, *An Introduction to Hydrogen Bonding*, Oxford University Press, **1997**.

(24) J. Xu, Z. Lian, B. Wei, Y. Li, O. Bondarchuk, N. Zhang, Z. Yu, A. Araujo, I. Amorim, Z. Wang, B. Li and L. Liu, Strong Electronic Coupling between Ultrafine Iridium–Ruthenium Nanoclusters and Conductive, Acid-Stable Tellurium Nanoparticle Support for Efficient and Durable Oxygen Evolution in Acidic and Neutral Media, *ACS Catal.*, **2020**, 10, 3571-3579.

(25) M. Tarres, V. S. Arderiu, A. Zaulet, C. Vinas, F. Fabrizi de Biani and F. Teixidor, How to get the desired reduction voltage in a single framework! Metallacarborane as an optimal probe for sequential voltage tuning, *Dalton Trans.*, **2015**, 44, 11690-11695.

(26) D. A. Rudakov, V. L. Shirokii, V. A. Knizhnikov, A. V. Bazhanov, E. I. Vecher, N. A. Maier, V. I. Potkin, A. N. Ryabtsev, P. V. Petrovskii, I. B. Sivaev, V. I. Bregadze and I. L. Eremenko, Electrochemical synthesis of halogen derivatives of bis(1,2-dicarbollyl)cobalt(III), *Russ. Chem. Bull.*, **2004**, 53, 2554-2557.

(27) R. Núñez, M. Tarrés, A. Ferrer-Ugalde, F. F. de Biani and F. Teixidor, Electrochemistry and Photoluminescence of Icosahedral Carboranes, Boranes, Metallacarboranes, and Their Derivatives, *Chem. Rev.*, **2016**, 116, 14307-14378.

(28) M. Lupu, A. Zaulet, F. Teixidor, E. Ruiz and C. Viñas, Negatively Charged Metallacarborane Redox Couples with Both Members Stable to Air, *Chem. Eur. J.*, **2015**, 21, 6888-6897.

(29) I. B. Sivaev and V. I. Bregadze, Chemistry of cobalt bis (dicarbollides). A review, *Collect. Czech. Chem. Commun.*, **1999**, 64, 783-805.

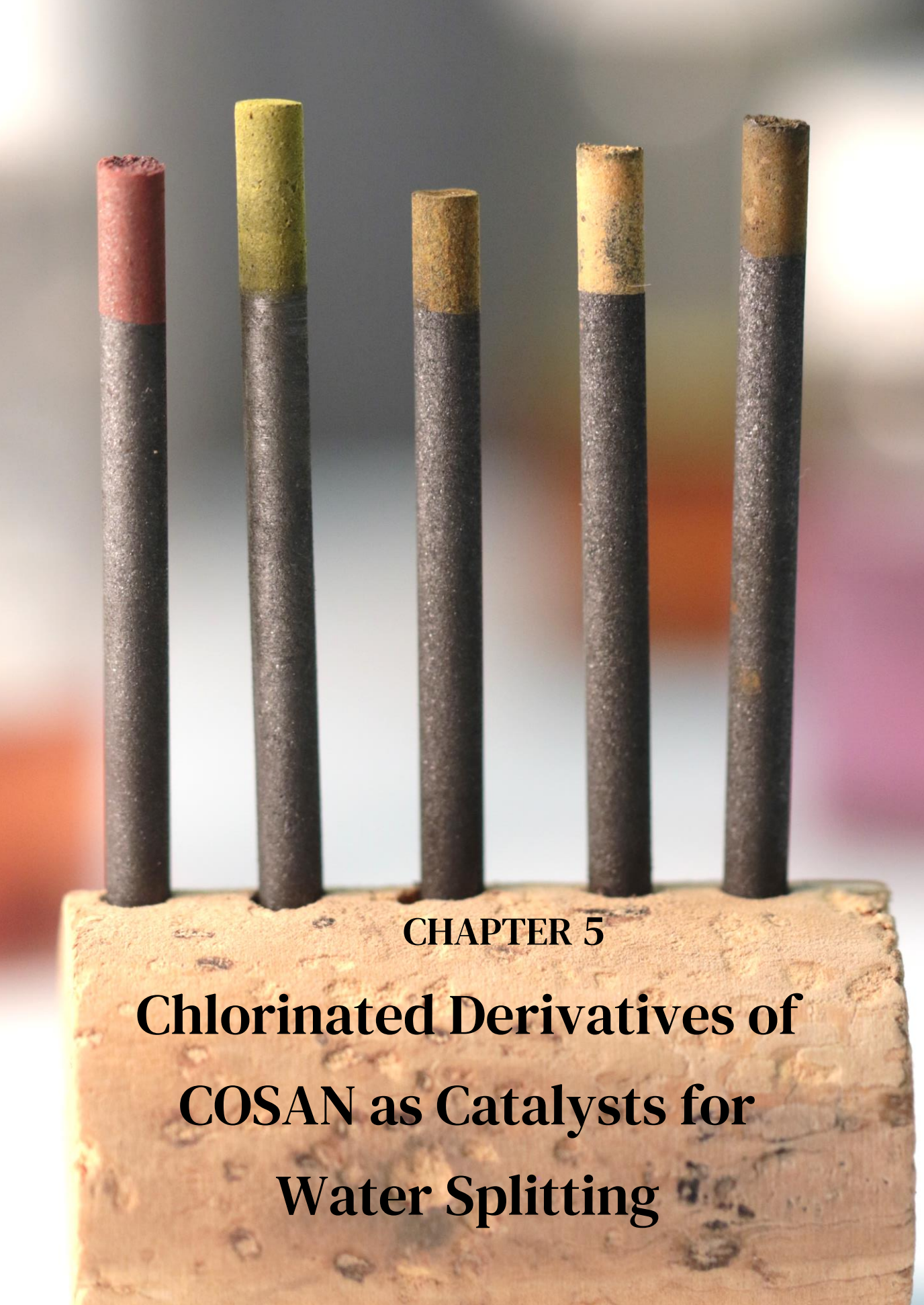

CHAPTER 5

Chlorinated Derivatives of COSAN as Catalysts for Water Splitting

CHAPTER FIVE

Chlorinated Derivatives of COSAN as catalysts for Water Splitting

Development of electrochemical systems for water splitting is one of the energetic challenges where the scientific community is putting more efforts. The develop of catalysts for oxygen evolution reaction provide the tool to develop fuel cells, water splitting and metal-air batteries systems. This work will focus on functionalized graphite surface with metallacarboranes to construct a working electrode for oxygen evolution reaction. Preliminary studies will unveil the electrocatalytic power of the chlorinated derivatives of COSAN respect to $NaSO_4$. However, these systems required huge quantities of metallacarboranes that will prompt to design a method to functionalize a graphite rod with our metallacarboranes. The research will display the study of a methodology to oxidize the most external layers of a graphite rod. In addition, a study to functionalize the surface with one amine and a comparative study between different amines to know which one favour better the electronic communication. Finally, the metallacarboranes will be added to the chemical scaffold construct with the amines in the graphite surface taking profit to the high affinity of the metallacarboranes by the amines.

Once we have the functionalized working electrodes with COSAN, octa, deca and dodeca derivatives of COSAN, this work will measure the catalyst power for oxygen evolution reaction by linear sweep voltammetry experiment. Finally, the stability of the electrodes to the electrochemical system will be measured to know if the electrodes can be used for real applications.

5.1 Electrocatalytic oxygen evolution reaction

Creating a global-scale sustainable energy system for future generations while preserving our environment is one of the most crucial challenges facing humanity today.[1] Energy conversion from renewable sources has been considered as an encouraging solution to significantly reduce the dependency on fossil fuels. Among the several energy systems based on electrochemical reactions, fuel cells, water splitting and, metal-air batteries are the simplest, most efficient, and reliable classifications.[2-4] Water oxidation reaction or oxygen evolution reaction [5] is the core reaction for all these systems to carry out their reversible process along with oxygen reduction reaction (ORR) and/or hydrogen evolution reaction (HER).

The oxygen evolution reaction involves four-electron transfer and is much more complicated than HER. The reaction is highly pH-dependent, and an external current is required to create the potential difference of 1.23 V *vs*. normal hydrogen electrode[6] to drive the OER at pH=0. Thus, a shift in reaction potential i.e. ~59 mV per unit pH, occurs theoretically according to Nernst equation.[7] However, in order to avoid the pH influence on the applied potential and keep the working voltage around 1.23 V for OER, reversible hydrogen electrode [8] is commonly used as a reference electrode. Moreover, the sluggish four-electron transfer kinetics for OER process can severely hamper its further practical applications.[2] However, the efficiency of the process is greatly limited by the slow kinetics of the anodic oxygen evolution reaction and require efficient catalysts to accelerate reaction kinetic to make the electrolyzer feasible.[9]

The equilibrium half-cell potentials (E^o) at 1 atm and 25°C for OER are shown as follows:

$4OH^- \leftrightarrow O_{2(g)} + 2H_2O_{(l)} + 4e^-$ ($E^o = 0.404$ V) alkaline solution [10]

$2H_2O_{(l)} \leftrightarrow O_{2(g)} + 4H^+ + 4e^-$ ($E^o = 1.23$ V) acid solution[11]

Where (l) and (g) refer to liquid and gas phases, respectively.

Ideally, the OER catalyst must have low overpotential and high stability as well as large earth-abundance and available at low cost to be scalable. However, ruthenium and iridium oxides are among the best electrocatalysts in this regard

due to their optimum binding with the essential intermediates, but their applicability is limited by the high cost and scarcity of the metals.[12]

5.2 Metallacarboranes as electrocatalysts

The potential of COSAN as electroactive electrolyte for electrolysis of water was previously studied by Teixidor and coworkers. This study demonstrates the surfactant behaviour of the COSAN[13] and compares its halo derivative mixtures with some common electrolytes such as HNO_3, $HClO_4$, HBF_4, *p*-toluenesulfonate (PTS) and dodecylbenzenesulfonate (DBS). Experiments were carried out with a variable DC power supply, recording the current *vs.* voltage (*I/V*) with two graphite bars as electrodes. These experiments demonstrated that COSAN did not perform better than the common electrolytes used for water electrolysis.[13] We repeated the experiments with several chloro derivatives of COSAN (Chapter 4) and the results were completely different.

We carried out the analysis of the *I/V* curve of the protonated salts of the different electrolytes, among them, compounds [**1**]$^-$, [**Cl$_6$-1**]$^-$, and [**Cl$_{12}$-1**]$^-$. The experiment consists of a system with two graphite rods as electrodes equally immersed in a solution 0.072 M of electrolyte in water. Finally, the electrodes are connected to a variable DC power supply, see **Figure 5.1**a.

The electrolytes used were HBF_4, $HClO_4$, H_2SO_4, HNO_3, HPTS (*p*-toluenesulfonate), HDBS (dodecylbenzenesulfonate), H[**1**], H[**Cl$_6$-1**] and H[**Cl$_{12}$-1**] and the intensity of 40 mA was used as a threshold to compare the different compounds. The representation of the data shows H[**Cl$_{12}$-1**] to be the best electrolyte of all of them with a potential of 2.5 V at 40 mA, 0.5 V less than the next ones that would be H[**Cl$_6$-1**] and $HClO_4$ (**Figure 5.1**a).

With these results, we decided to do the same experiments with the other highly chlorinated derivatives of COSAN already discussed in chapter 4. The hypothesis was to demonstrate how the chlorination degree could improve the properties of the COSAN platform as an electrolyte. The result displays a gradual improvement of the electrolyte character of COSAN with an increasing number of chloro substituents (**Figure 5.1**b).

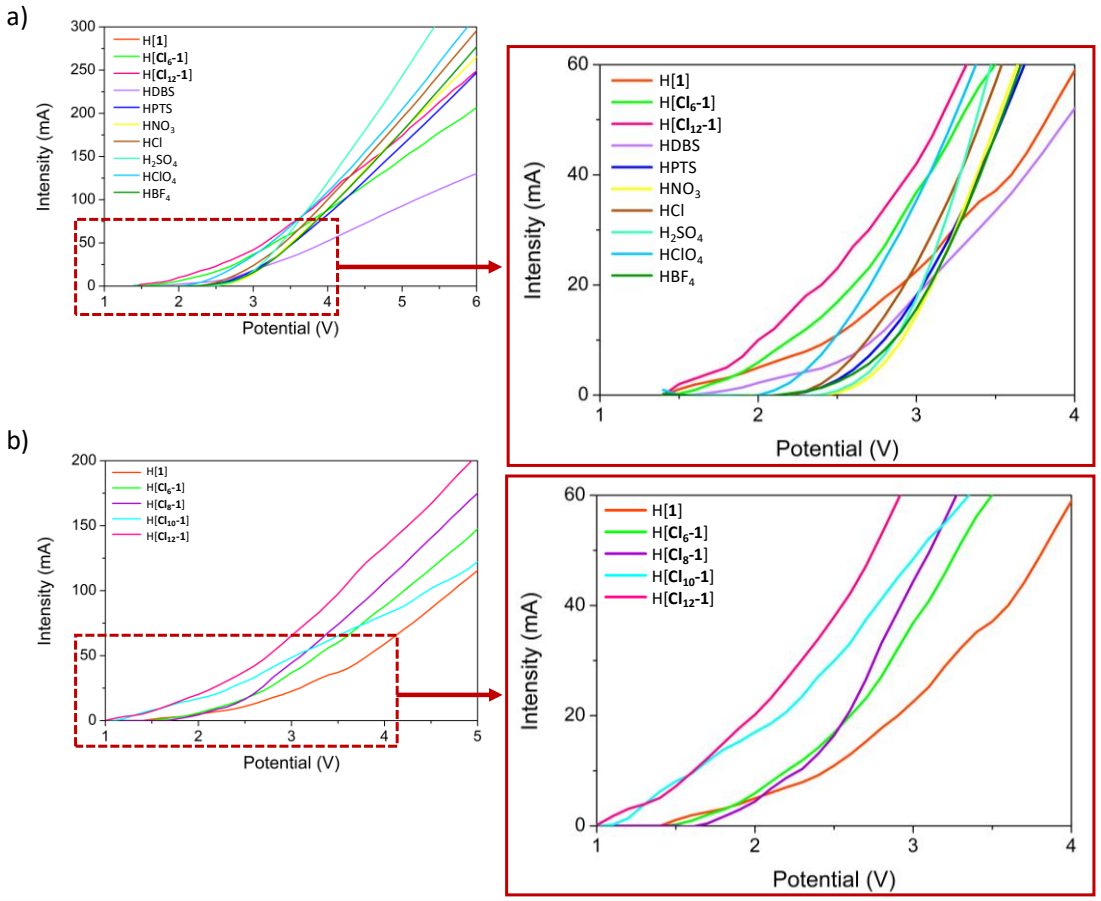

Figure 5.1. a) *I/V* curve of protonated salts, b) *I/V* curve of the protonated salts of the chlorinated derivatives of COSAN. Both present their amplify graph at right.

5.2.1 Study of the coordinating properties of the of COSAN derivatives

These electrochemical experiments revealed whether foam was generated while they were being conducted, and also showed what electrolytes were causing it. HDBS was expected to generate foam because it is a classic surfactant. Conversely, HNO_3 was not expected to foam because it is not a surfactant. This is what is observed in **Figure 5.2**. Photos for the other experiments with H[**1**], H[**Cl$_6$-1**], H[**Cl$_{10}$-1**] and H[**Cl$_{12}$-1**] present a gradual increase of the foam, picking with H[**Cl$_{12}$-1**] which prevents from continuing with the experiment after 3 V, actually, **Figure 5.1.**a shows how the slope of the curve of H[**Cl$_{12}$-1**] starts to decrease at 3.5 V because the foam affect to the electrochemical system, see **Figure 5.2**.

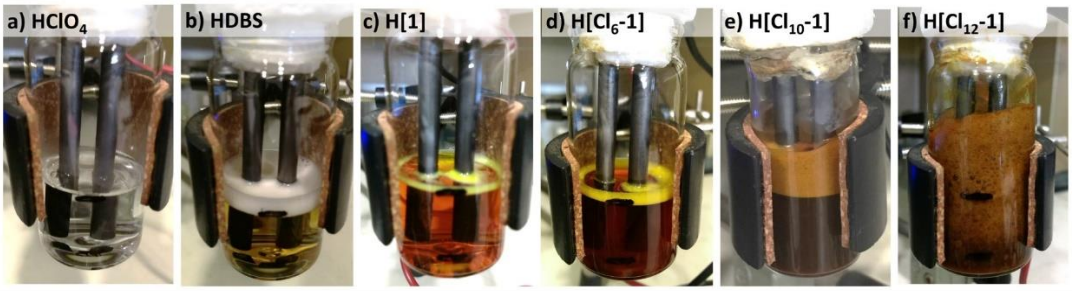

Figure 5.2. Images of the foam generated during the electrochemical process for the solutions of a) $HClO_4$, b) HDBS, c) H[**1**], d) H[**Cl$_6$-1**], e) H[**Cl$_{10}$-1**] and d) H[**Cl$_{12}$-1**].

Summarizing, comparison of the images of the different electrolyte solutions following the electrochemical process support the previous study by Teixidor *et al.* demonstrating that the addition of chloro substituents increase the surfactant character of the molecule while weakening their non-covalent bonding character. The possible explanation of this performance is the number of B-H···H-C_C dihydrogen bonds present in the structure. The H[**1**] is the worst electrolyte of the COSAN set of compounds but at the same time is the framework with more dihydrogen bonds. The formation of these molecular interaction promotes the molecular self-assembling that prompts the formation of aggregates and reduces the overall conductivity which in turn explain the poor electrolyte behaviour.[13,14]

The larger production of foam by the chloro-COSAN derivatives in parallel with a higher degree of chlorination would be consistent with a higher capacity to lower the surface tension, and also with a higher capacity to aggregate, but this would imply a worst electrolyte performance. Contrarily, H[**Cl$_6$-1**]< H[**Cl$_{10}$-1**]<H[**Cl$_{12}$-1**] improve the current to voltage value in this order that suggests that these species may perform better as electrocatalysts for water oxidation than as electrolytes. However, the experiments present an important drawback that limits their large-scale application in the future. 10 mL of solution 0.072 M of H[**Cl$_{12}$-1**] requires near 530 mg of H[**Cl$_{12}$-1**] **(*this is a lot!*)**, and the high price of the metallacarboranes hinders the industrial scale-up of the proposed system.

To solve this problem, we followed a different approach. Instead of using highly concentrated solutions, we covered the electrode surface with the metallacarborane to maximize the concentration there while minimizing the amount of electrocatalyst. One possibility is the functionalization of the graphite

bars. There are several options for this purpose. In the next section, we explain how we achieve stable functionalization that resists several cycles without losing the active material and the oxidating power.

5.3 Physical functionalization: Chitosan gel graphite coating

The first attempt to functionalize graphite rods aimed at embedding the graphite rod in chitosan, gellifying it and adding the metallacarborane. Chitosan is a structure similar to cellulose made of several hundred to more than thousands β-(1-4) linked D-glucose units in which the hydroxyl position C-2 of cellulose has been replaced by a primary amino group.[15] The procedure is based in preparing a solution of chitosan 1 % in 0.1M HCl with stirring overnight, immerse a graphite rod in the chitosan solution for 1h, take it out and immerse them in a 1M solution of NaOH. The gellification process occurs immediately. Then the rods are immersed in a 30.7 mM solution of H[**1**] for 5 days. COSAN is added to the surface of the chitosan due to the strong interaction that [**1**]$^-$ has to the amine groups (**Figure 5.3**a).[16]

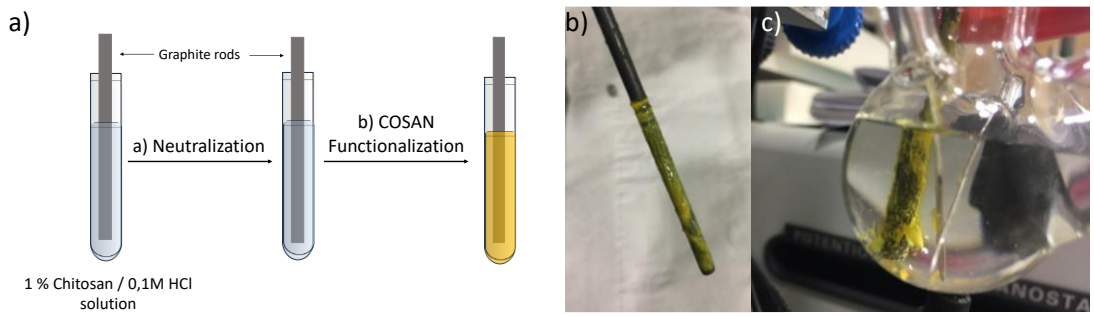

Figure 5.3. a) Procedure to coating a graphite rod with chitosan, followed by the functionalization with COSAN, b) Image of the functionalized rod and c) Image of the electrochemical process where it is possible to observe the layer cracking due to O_2 formation.

The incorporation of COSAN to the gel is easily visualized by the acquired yellow/orange color, see **Figure 5.3**b. It was also evidenced by cyclic voltammetry (CV). Unfortunately, the functionalized chitosan is not able to resist the electrochemical process because the formation of bubbles breaks and detaches the gel from the rod (**Figure 5.3**c). Thus, the strategy of adsorbing chitosan in the graphite surface does not lead to satisfactory results. Thus if bubbles were considered responsible of the layer detachment we sought for an alternative way

that prevented this. So, we decided to build a molecular scaffold of COSAN units chemically bonded to the graphite surface able to resist the electrochemical process in water and incorporate our chlorinated derivatives as electrocatalysts.

5.4 Chemical functionalization

The most accessible way to functionalize graphite is oxidizing it and generating functional groups in the surface able to interact with our metallacarboranes. Three major methods exist for solution-based synthesis of graphite oxide (GO), these of Staudenmaier,[17] Brodie[18] and Hummers[19] (**Figure 5.4a**). Among them, the former two involve toxic reactions due to the generation of noxious gases and highly reactive species.[20] In contrast, Hummers method is widely used for preparing GO due to its nontoxicity.[21]

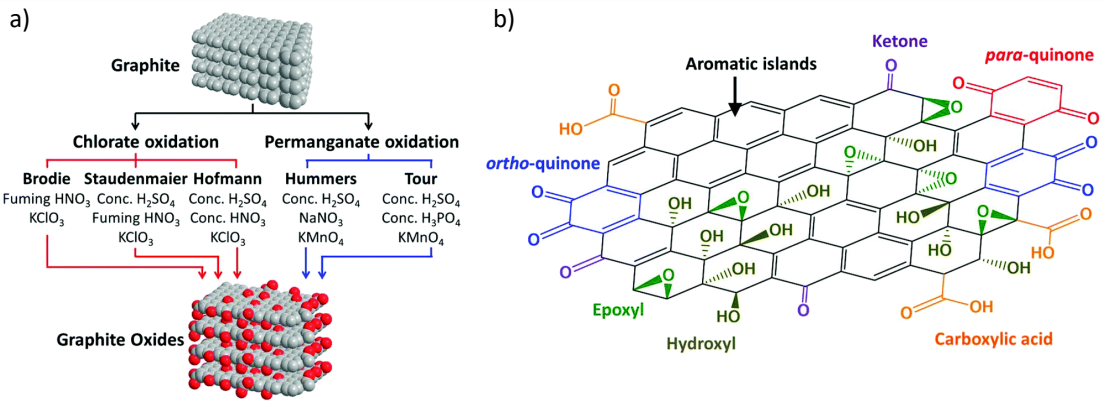

Figure 5.4. a) Schematic illustration of the most famous graphite oxidation methods based either on chlorate or permanganate oxidation routes, b) General model of graphite oxide indicating various oxygen functional groups. Figures adapted from reference 23.

The functional groups generated depend on the oxidation methods[22,23] but, generally, following the approaches previously mentioned, the graphite end-up with hydroxyl, epoxide, diol, ketone and carboxyl functional groups, this last one is less abundant because it is generated in the borders of the sheets, see **Figure 5.4**b.[21,24]

It is very difficult to find in the literature methods perfectly tailored to oxidize only the most external layers of a graphite rod because the major part of the research uses strong oxidizing agents to obtain graphene sheets as the final product.

Therefore, we proposed new different oxidation processes represented in **Scheme 5.1**. Our method is based on the well-established ones but focusing on affecting only the most outer layers of our graphite rod.

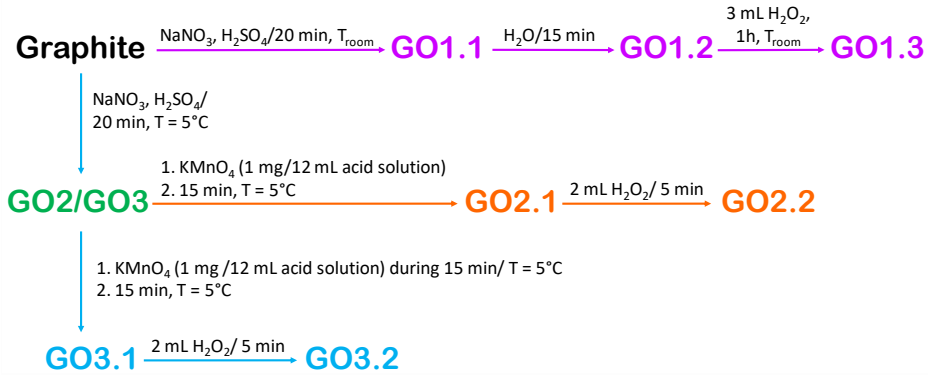

Scheme 5.1. Tested routes for oxidizing the graphite rod surface.

All methods described in **Scheme 5.1** are modifications of the Hummers's one. The use of $KMnO_4$ as the oxidating agent was removed or the quantity was drastically reduced in these tests because it works as intercalating agent producing the expansion of graphitic material and leads to the final exfoliation of the material.[25] Moreover, the temperature and the reaction time was adjusted to get the best oxidation degree.

The experiment consists in applying different conditions to nine G rods to analyse all the steps of the different reactions. Three G rods immersed in a solution of 0.5 g of $NaNO_3$ in 25 mL of H_2SO_4 at room temperature during 15 min. Then, GO1.1was put apart, 15 mL of the acid solution was removed and 15 mL of H_2O were added slowly all at room temperature for 15 min, then GO1.2 is ready to be analysed. Finally, the GO1.2 was immersed in an H_2O_2 solution for 1 h at room temperature to yield GO1.3.

Other five rods were immersed in an equal solution of $NaNO_3/H_2SO_4$ but at 5°C for 15 min and GO2/GO3 were put apart. The acid solution was divided in two vials with two rods in each, 1 mg of $KMnO_4$ was added at once to one and the reaction was kept at 5°C for 15 min. to produce GO2.1. Then, 2 mL of H_2O_2 was added slowly to the acid solution at 5°C for 15 min leading to GO2.2. In addition, 1 mg of $KMNO_4$ was slowly added to the second acid solution over a period of 15

min and GO3.1 was separated. This was followed by 2 mL of H_2O_2 added slowly to the acid solution at 5ºC for 15 min producing GO3.2.

5.4.1 Characterization of the GO rods

The physico-chemical characterization of graphite rods permits to study the oxidation process. SEM images analysis indicates a different composition of the surface comparing with the inner part of the rod. In addition, FTIR analysis provides information about the oxygenated functional groups formed in the graphite during the oxidation process, hence the comparison of the FT-IR of the surface comparing with the internal part of the rod could confirm the outer functionalization.

* SEM-EDX

All rods were analysis by Scanning Electron Microscopy (SEM). The technique provides excellent surface topography images with high resolution that permitted to observe and compare the effect of the oxidation process on the rod surface.

SEM images of **Figure 5.5**a, d and g display the surface of the rods damaged as a consequence of the mild but still aggressive oxidation process. Magnification of these images show an irregular surface with some deposits of material that we interpret as graphite oxidation products (**Figure 5.5** b, e and h). The study of the internal part of the rods was important to demonstrate only the outer layer of the rod was oxidized hence. The analysis consisted on cut the road and take images from the internal part. The images present a very irregular surface because the rods are fabricated from compact graphite but do not seem to be the same material as in the surface (**Figure 5.5** c, f and i).

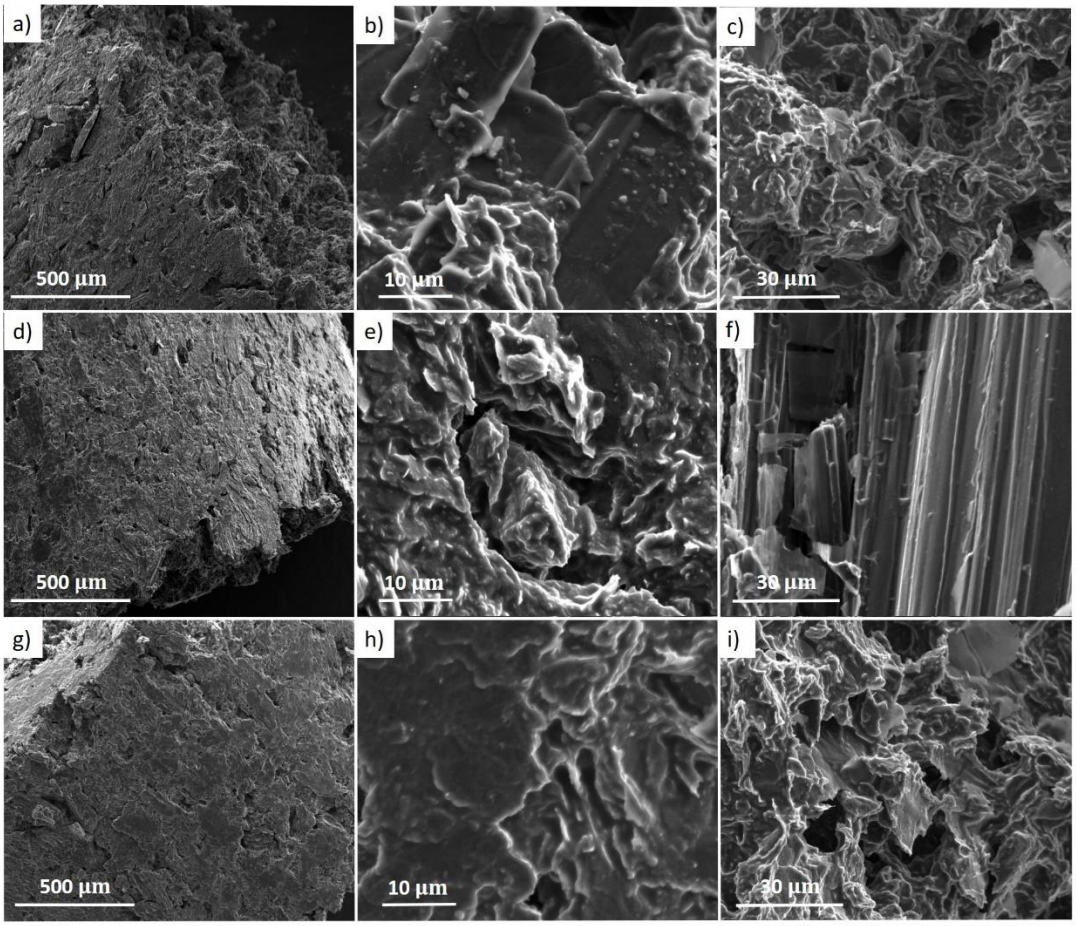

Figure 5.5. SEM images of the surface of the oxidized graphites a) GO1.1, d) GO2.1 and g) GO3.1. SEM images of the amplified zone of b) GO1.1, e) GO2.1 and h) GO3.1. SEM images of the radial cut of c) GO1.1, f) GO2.1 and i) GO3.1.

* FT-IR

The technique provides qualitative information about the functional groups of the GO. The characteristic bands of GO are observed at 1725 cm^{-1} (C=O stretching in carboxylic acid), 1628 cm^{-1} (C=C stretching in aromatic ring), 1230 cm^{-1} (C-O stretching in C-OH) and 1050 cm^{-1} (C-O stretching in epoxy).[25] However, these values are illustrative because some authors present similar but not exact values[26-28]

Figure 5.6 displays the FT-IR of our GO rods, graphite and the typical FT-IR of GO extract from the literature.[29] The samples have been obtained scratching the GO surface and measuring the powder by FT-IR. The analysis confirms the oxidation of all the rods and unveils similar oxidation degrees. All spectra display similar bands at 1006.7 cm^{-1} and1146.7 cm^{-1} corresponding to the ether and epoxy stretching mode located over the basal plane of graphite oxide. Bands between 1635 and 1732 cm^{-1} corresponding to aromatic rings and carboxyl functional groups located on the edge of the graphite oxide, a signal at ~2300 cm^{-1} correspond to the absorbed CO_2 molecules and a big band around 3350 cm^{-1} corresponds to the hydroxyl groups, demonstrating the superficial oxidation of all graphite rods.[30] In addition, the FT-IR of the internal part of the graphite, obtained by a radial cut of the rod and scratching the internal part, do not show any functional group, demonstrating the external functionalization of the rod.

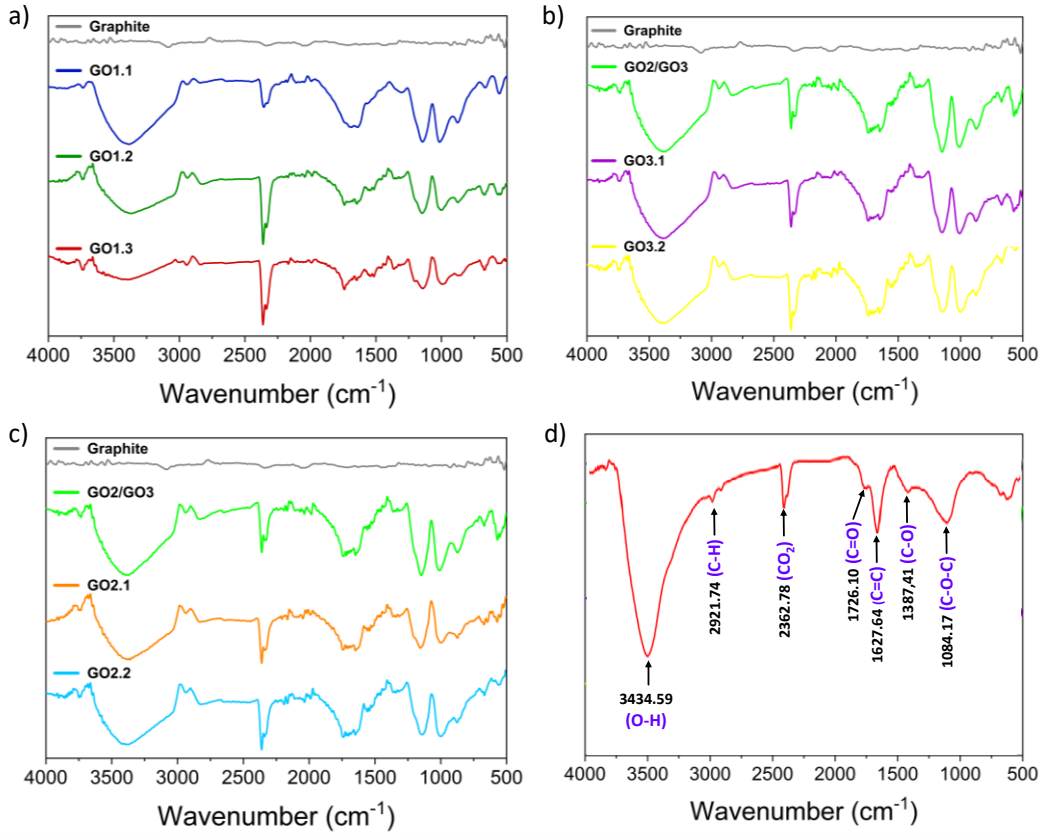

Figure 5.6. FT-IR comparative spectra of the different oxidation routes: a) Graphite, GO1.1, GO1.2 and GO1.3, b) Graphite, GO2/GO3, GO3.1 and GO3.2, c) Graphite, GO2/GO3, GO2.1 and GO2.2. d) FT-IR of GO standard extract from reference 28.

In conclusion, SEM images together with FT-IR analysis demonstrates the new non-aggressive oxidation method able to oxidize only the outer layers of a graphite rod.

* Study of conductivity losses

Despite graphite is not the best electrode (~$3 \cdot 10^5$ S/m) in terms of conductivity as compared with other common electrodes as platinum ($9.43 \cdot 10^6$ S/m), it is excellent due to its availability and the possibility that it offers to be decorated with functional groups. The oxidation process breaks some of the aromatic rings to add oxygenated functional groups hence reduce the conductivity of the material (see **Figure 5.4**). To minimize this effect we focused on functionalizing only the surface of the electrode but this functionalization affects the conductivity too. Therefore, we control the conductivity of the material depending on the oxidation time.

The first conductivity study consisted on using GO1.1 as working electrode and measuring the cyclic voltammetry of H[**2**] (FESAN) in ACN (4.65 mM) and $TBAPF_6$ (0.01M) because its curve appears in the middle of the electrochemical window (**Figure 5.7**a). This result was compared with the same experiment using graphite as the working electrode. The ΔmV between the anodic and cathodic peak of the CV indicates the reversibility, that is dependent among others, on the conductivity of the electrode. Instead of the concentration of electrolyte ($TBAPF_6$) should be 100 times the concentration of the analyte (FESAN), we decide to use a 0.01M solution in order to increase the separation of the anodic and cathodic curve. At this concentration, it is possible to observe more clearly the differences between the working electrodes. **Figure 5.7**a displays the cyclic voltammetry of H[**2**] using GO (in blue) and graphite (in red) with ΔmV of 640 and 400 mV respectively indicating a clear decrease of the material's conductivity.

The second study consisted on analysing the conductivity of graphite rods oxidized following the GO1.1 method varying the reaction time to 10, 20 and 40 min. Moreover, the addition of a fourth GO rod fabricated by the method of GO3.1 but, increasing the $KMnO_4$ quantity to 50 mg, allowed us to assess the effect on the conductivity of the over oxidized electrodes. The CVs of protonated salt of FESAN (7.76 mM) and $TBAPF_6$ (0.01M) in water, using the graphites

oxidized by GO1.1 method for 10, 20 and 40 min present ΔVm values of 370, 340 and 480 mV, respectively. These values indicate similar conductivity losses for 10 and 20 min oxidation time and a drastic decrease in conductivity when reaching 40 min (**Figure 5.7**b).

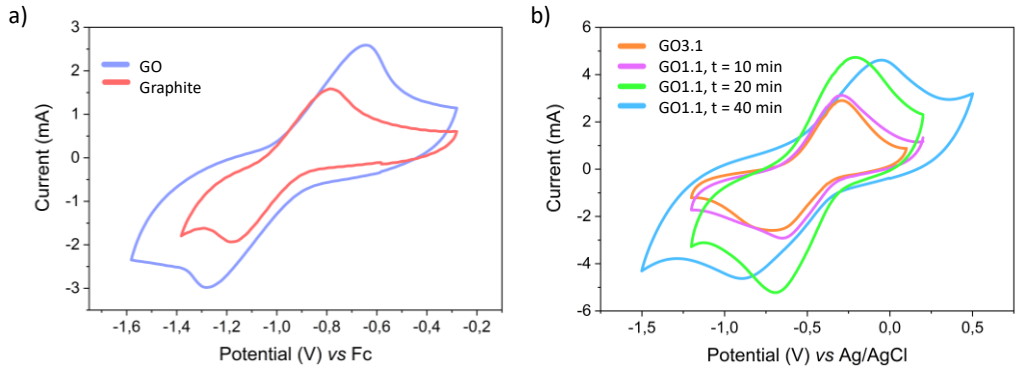

Figure 5.7. a) CV of FESAN (4.65 mmM) carried out in dry acetonitrile as solvent and $TBAPF_6$ (0.01M), Ag as pseudo-reference electrode, Pt as counter electrode and GO1.1 (in blue) or graphite (in red) as working electrode, the measurements were referenced to internal Fc^+/Fc couple. b) CV of protonated salt of FESAN (7.76 mM) in water as a solvent and $TBAPF_6$ (0.01M), Ag/AgCl reference electrode, Pt as counter electrode and GO3.1 (in orange), graphite oxide by method GO1.1 changing the reaction time 10 (in purple), 20 (in green) or 40 minutes (in blue) as working electrode.

Moreover, the addition of $KMnO_4$ increases the oxidizing power but it changes the volume of the rod due to the capacity of manganese to intercalate between the graphite sheets. This effect increases the distance between the layers and causes the loss of conductivity. Coherently, the GO3.1 present the higher ΔmV value with 846 mV demonstrating our hypothesis (**Figure 5.7**).

As a result, the methodology used in this work to oxidize the graphite surface consists in preparing a solution of fuming nitric acid after dissolving 0.5 g of $NaNO_3$ in 25 mL of H_2SO_4 by slow addition of the acid in the salt. Once the salt is completely solubilized in the acid, the graphite bar was immersed for 15 min. Then, the graphite bars were immersed in deionized water for 5 min x three to clean from acid the graphite oxide surface. At first glance, the surface of the graphite looks smooth and clean as if no process had occurred during the oxidation. However, the FTIR and the SEM-EDX confirm the oxidation of the surface with minimum conductivity losses confirmed by CV.

5.4.2 Functionalization of GO with metallacarboranes by amines

The oxygen functional groups on the graphite surface offer the opportunity to interact and react with different molecules. Even though metallacarboranes do not interact strongly with the oxygen functional groups, it is possible to substitute some of these by amino groups, which facilitates a strong non-covalent interaction with the metallacarboranes.

The main reactive sites generated during the oxidation are the epoxy groups of GO. In our approach, we decided to substitute the epoxy group with an amine group. This approach has been considered to be a promising method for the large-scale production of functionalized graphene. There exists a huge number of possible amino groups in the literature ready to functionalize the graphite surface to allow the interaction with metallacarboranes. We were looking for a rapid, easy and scalable method able to add metallacarboranes to the graphite surface as a catalyst for the electrolysis of water.[24]

* Functionalization with amines

In our study we choose triethylamine (NEt_3), ethylenediamine (NH_2EtNH_2) and *p*-phenylenediamine (NH_2PhNH_2) as linkers to functionalize graphite with metallacarboranes to construct a working electrode for oxygen evolution.

Triethylamine was the first amine tested because is one of the most used in boron cluster chemistry as a counter cation. However, we considered the possibility that the ethyl groups of the amine could hinder the interaction $N^+\cdots$Metallacarborane weakening the electronic communication between the metallacarborane and the graphite. Thus, we proposed the diamines ethylenediamine and *p*- phenylenediamine because will permit us to study the influence of the group between the amines in electronic communication. The initial idea was based on the hypothesis that the aromatic groups improve the electronic communication between the graphite and the catalyst more than non-aromatic ones.

Finally, the metallacarboranes chosen as catalysts for oxygen evolution reaction were $[\mathbf{1}]^-$, $[\mathbf{Cl_8\text{-}1}]^-$, $[\mathbf{Cl_{10}\text{-}1}]^-$ and $[\mathbf{Cl_{12}\text{-}1}]^-$, the chlorinated metallacarboranes

presented in the previous chapter and studied for the two graphite bar experiments in section 5.2.

The amination reaction consists in a nucleophilic attack of the epoxy groups of the graphite oxide surface by the amine, based on the mechanism found in the literature.[31] In comparison to other methods, this nucleophilic substitution occurs very easily, also at room temperature and in aqueous medium. The graphite rods were covered with Teflon tape allowing only 0.5 cm of bare surface to control the area to be functionalized. Then the rods were immersed in a solution of 1 mL of trimethylamine in 12 mL of water strongly stirring the reaction overnight. Afterwards, the rods were immersed with water two times and one more in a 0.1M solution of HCl. Finally, the rods were immersed in a 5 mM metallacarborane solution with continuous agitation for 2 hours. The FTIR and the SEM-EDX confirmed the functionalization of the graphite rods as shown in **Figure 5.9** and **Figure 5.10**. Furthermore, the characteristic colour of metallacarborane salts present on the rod's surface indicates the successful functionalization (**Figure 5.8**).

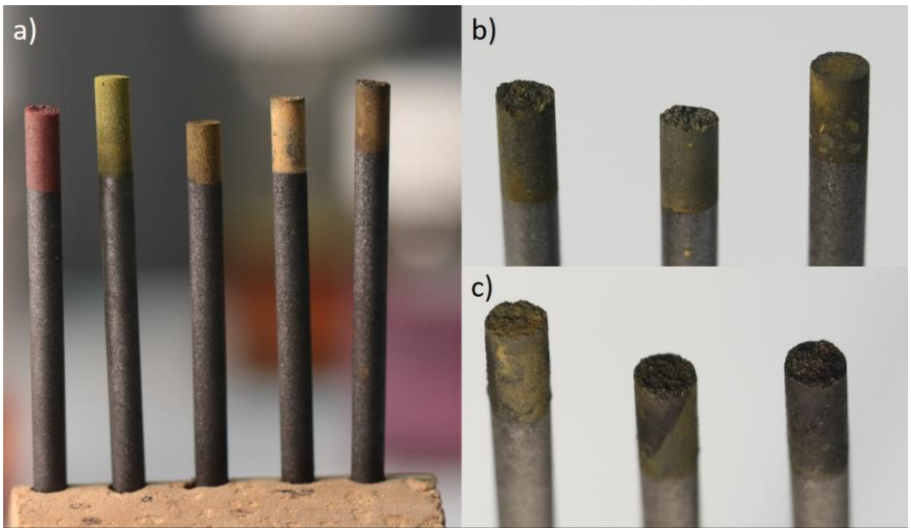

Figure 5.8. Functionalized graphite rods, a) with triethylamine as linker and with [**2**]$^-$, [**1**]$^-$, [**Cl$_8$-1**]$^-$, [**Cl$_{10}$-1**]$^-$ or [**Cl$_{12}$-1**]$^-$ as catalyst (from left to right). b) Functionalized graphite rods with ethylenediamine and [**Cl$_8$-1**]$^-$, [**Cl$_{10}$-1**]$^-$ or [**Cl$_{12}$-1**]$^-$ (from left to right). c) Functionalized graphite rods with *p*-phenylenediamine and [**Cl$_8$-1**]$^-$, [**Cl$_{10}$-1**]$^-$ or [**Cl$_{12}$-1**]$^-$ (from left to right).

5.4.3 Characterization of functionalized graphite rods

* FT-IR

The experiment consists in scratching the functionalized surface and measuring the powder by FT-IR. Instead of the FT-IR study of this research included the analysis of all the functionalized graphites of this work, **Figure 5.9** presents only the FT-IRs of the graphite rods functionalized with [**Cl$_{12}$-1**]$^-$ and the amines NEt_3, NH_2EtNH_2 or NH_2PhNH_2 for clarity.

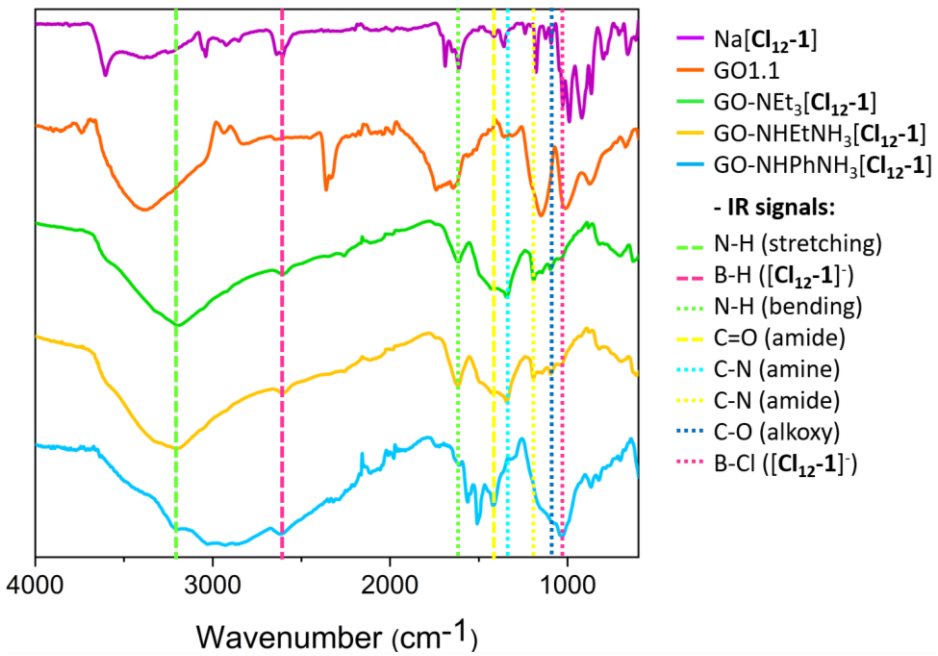

Figure 5.9. FT-IR spectra of the Na[**Cl$_{12}$-1**] (purple), GO1.1 (orange), GO-NEt_3[**Cl$_{12}$-1**] [37], GO-$NHEtNH_3$[**Cl$_{12}$-1**] (yellow) and GO-$NHPhNH_3$[**Cl$_{12}$-1**] (blue). Lines with dots indicates the common signals between different spectra.

We firstly identified two signals, the ones corresponding to the B-H and B-Cl stretching vibrational peaks at 2609 and 1032 cm^{-1}, respectively (see **Figure 5.9**).[32] However, these bands do not demonstrate surface functionalization. After the process, there is a dramatic decrease in the peak intensities corresponding to the COOH stretching vibration band between 1732 and 1635 cm^{-1}. The intensity of the epoxy and alkoxy at 1146.6 and 1006.7 cm^{-1} also decrease in the functionalized graphites.[33] On the contrary, C=O and C-N stretching vibrational peaks, that

appear at 1423 and 1192 cm^{-1} respectively, demonstrate the substitution of the carboxylic groups by the amide. In addition, the substitution of the epoxy by amine is clearly observed by the C-N and N-H stretching vibrations and N-H bending vibration peaks at 1346, 3195 and 1614 cm^{-1} respectively (**Figure 5.9**).[34-36] Finally, instead of the IR spectra of GO-NEt_3[**Cl_{12}-1**] and GO-$NHEtNH_3$[**Cl_{12}-1**] are very similar, the spectrum of GO-$NHEtNH_3$[**Cl_{12}-1**] display the peaks at 1509.6 and 1563.9 cm^{-1} corresponding to the C=C aromatic signals of the *p*-phenylenediamine demonstrating the functionalization of the graphite surface.

* SEM-EDX

The analysis of the rods by SEM consisted in taking the rod and make a cross-section cut to be able to observe the internal and external part of the bar. SEM images of rods display a homogeneous solid coating on the surface that does not exist in the interior of the rod (**Figure 5.10**).

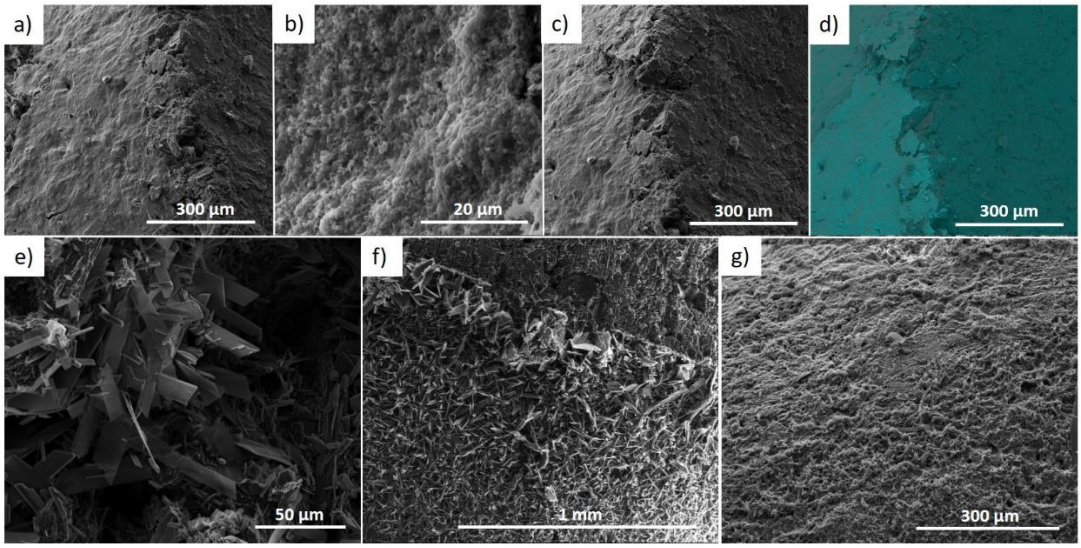

Figure 5.10. a-b) SEM images of the surface of GO-NEt_3[**Cl_{10}-1**] at different magnification. c) SEM image of the surface (left bright side) and the interior part (right dark side) of GO-NEt_3[**Cl_{12}-1**] d) Backscattered electrons image representing the different atomic composition of (c). SEM images of the surfaces of: e) GO-NEt_3[**1**], f) GO-$NHEtNH_3$[**1**] and g) GO-$NHPhNH_3$[**1**].

Finally, the comparative EDX analysis of the surface and the internal part of the rods unveil the presence of Co from the COSAN only in the surface demonstrating the external functionalization of the graphite rod.

5.5 Functionalized graphite: Catalytic power

The study of the graphite rods functionalized with metallacarboranes as working electrodes for the oxygen evolution reaction was based in computing the potential at 10 mA/cm^2 ($E_{j=10}$), because it is considered more reliable and commonly used in the literature for OER.[5] In addition, the overpotential is taken as the difference between the potentials at $E_{j=10}$ vs RHE and 1.229; this is the value that discloses the catalytic power of a compound. An electrocatalyst reduces this difference, thus the smaller is the overpotential the better is the catalyst. Generally, a catalyst that has overpotential in the range of 300-400 mV is considered to be an excellent catalyst for OER, however, there are very few catalysts that have an overpotential much less than 300 mV.[4]

The O_2 evolving activity of the metallacarborane catalysts was tested using linear sweep voltammetry (LSV) measured at 10 mV/s in 1 M KOH electrolyte with a functionalized graphite rod as working electrode, a platinum wire as counter electrode and Ag/AgCl as the reference electrode. Instead the LSV without any treatment are presented in the **Appendix B**. In this chapter, we represent the data as Current density/Potential vs. RHE because of the effect that the active area and the pH have on the catalytic power. The current density is obtained dividing the measured current by the functionalized rod area (radius = 0.15 cm and length = 0.5 cm). Moreover, the potential vs. RHE was calculated following **equation 5.1**.

$$E_{RHE} = E_0 + 0.059pH + E_{ref} \qquad \textbf{(5.1)}$$

Where, $E_{ref} = 0.209$ V.

Figure 5.11 displays LSVs for the graphite rods functionalized with the three tested amines: triethylamine (GO-NEt$_3^+$), ethylenediamine (GO-NHEtNH$_3^+$) and *p*-phenylenediamine (GO-NHPhNH$_3^+$)[38] as linkers to the metallacarboranes [**1**]$^-$, [**Cl$_8$-1**]$^-$, [**Cl$_{10}$-1**]$^-$ and [**Cl$_{12}$-1**]$^-$. The analysis of the electrochemical processes indicates that the graphites functionalized by *p*-phenylenediamine have higher catalytic power with smaller values of potential at $E_{j=10}$.

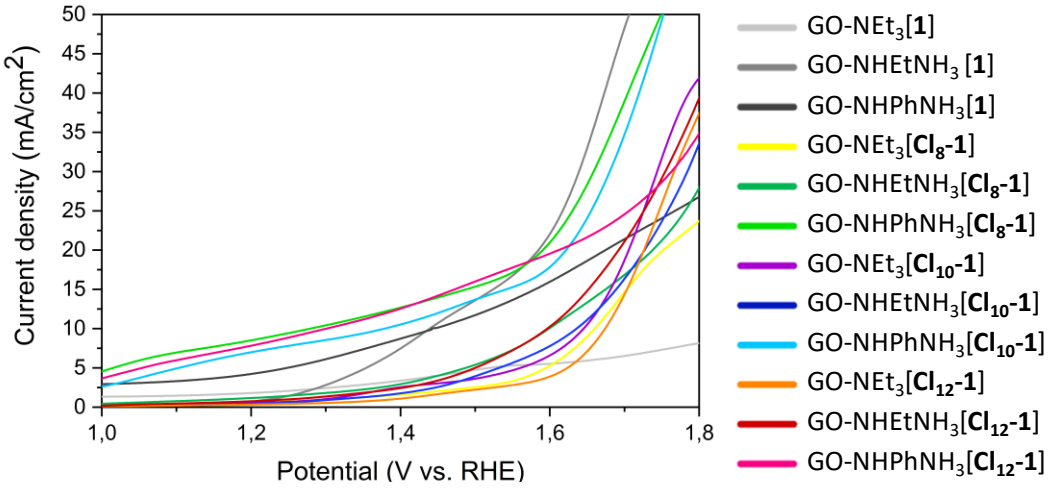

Figure 5.11. Linear sweep voltammetry carried out in a 1 M solution of KOH. Ag/AgCl as reference electrode, Pt wire as counter electrode and the functionalized graphite rods as working electrodes.

Further, the study of the potential at $E_{j=10}$ on the basis of the metallacarborane or the linker unveil the importance of the ammine linker. **Figure 5.12**a shows how the catalytic power increases with the number of chloro units in the COSAN structure, except for ethylenediamine, which presents better results with COSAN as catalyst than [**Cl_{12}-1**]. Moreover, **Figure 5.12**b display *p*-phenylenediamine to be the best linker, decreasing the overpotential down to 300 mV, probably thanks to the aromatic ring that favour the electronic communication between the catalyst and the working electrode.

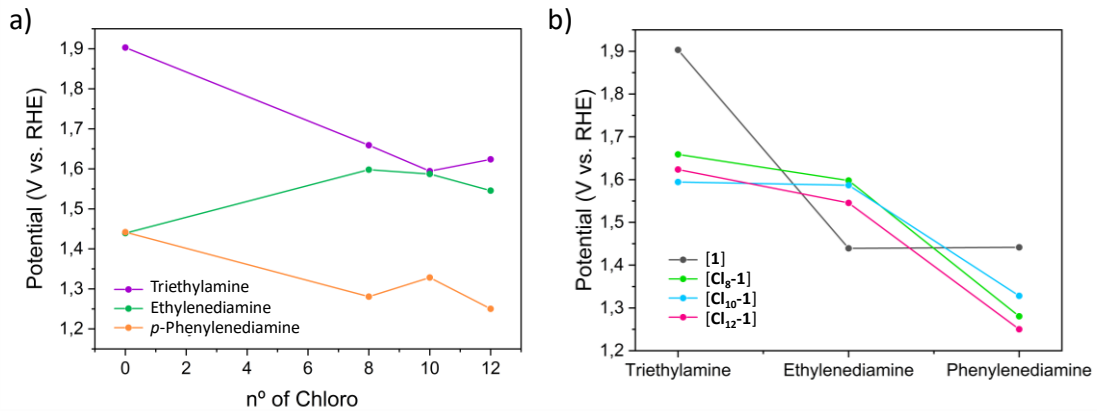

Figure 5.12. a) Representation of the potential at Ej=10 varying with a) the number of chloro substituents in the COSAN structure and b) the selected amine as a linker.

The calculation of the overpotential for the functionalized graphite gave surprising results. Chlorinated derivatives of COSAN present excellent properties as catalyst for OER. But for the GO-NEt_3[**Cl_8-1**], all graphite bars present overpotentials less than 400 mV. Indeed, the graphites functionalized by *p*-phenylenediamine present overpotentials lower than 100mV, specifically 51, 98 and 20 for [**Cl_8-1**], [**Cl_{10}-1**] and [**Cl_{12}-1**] being this last one the best performing among all the tested combinations.

In the literature, most of the overpotential results are given for basic media because the proposed catalysts are not stable in neutral or acidic conditions.[36,38-40] In our case the catalytic study in basic media gives outstanding results for OER because the presence of OH- favours the water splitting and ranks as one of the best performing systems compared to previously published catalysts. Merging all these ideas together and after these excellent results, the next step was to do the electrochemical experiments at pH 7. The overpotential data values vary from 648 for the GO-$NHEtNH_3$[**Cl_{12}-1**] to 858 mV for GO-NEt_3[**Cl_{10}-1**] except for GO-NEt_3 [**1**] with an overpotential of 1059 mV (**Figure 5.13**). The overpotential does not as excellent as much as in basic media. However, exist scarce literature that present results in neutral media due to the difficulty to find catalyst stable in those conditions, only some iridium or ruthenium compounds, elements with low availability, have been proposed.[38,40] Thus this COSAN derivatives open an avenue for metallacarboranes as catalysts in neutral media.

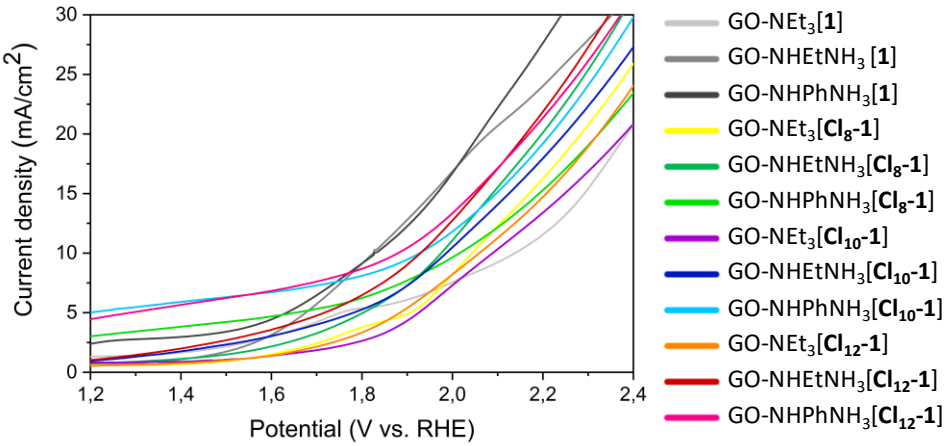

Figure 5.13. Linear sweep voltammetry carried out in a 0.1 M solution of $NaSO_4$. Ag/AgCl as reference electrode, Pt wire as counter electrode and the functionalized graphite rods as working electrodes.

Table 2. Overpotentials of the functionalized graphite electrodes in basic (1 M KOH) and neutral (0.1 M Na_2SO_4) media.

	Overpotential (mV)	
	1 M KOH	0.1 M Na_2SO_4
GO-NEt_3[**1**]	494	1059
GO-$NHEtNH_3$[**1**]	209	704
GO-$NHPhNH_3$[**1**]	623	697
GO-NEt_3[$\mathbf{Cl_8}$**-1**]	429	814
GO-$NHEtNH_3$[$\mathbf{Cl_8}$**-1**]	368	746
GO-$NHPhNH_3$ [$\mathbf{Cl_8}$**-1**]	51	785
GO-NEt_3[$\mathbf{Cl_{10}}$**-1**]	364	858
GO-$NHEtNH_3$[$\mathbf{Cl_{10}}$**-1**]	357	755
GO-$NHPhNH_3$ [$\mathbf{Cl_{10}}$**-1**]	98	697
GO-NEt_3[$\mathbf{Cl_{12}}$**-1**]	394	829
GO-$NHEtNH_3$[$\mathbf{Cl_{12}}$**-1**]	316	699
GO-$NHPhNH_3$ [$\mathbf{Cl_{12}}$**-1**]	20	648

5.6 Functionalized graphite: Electrochemical stability

The stability of the functionalized graphite is a key point to assess our system and demonstrate the possible real application. We already know that both metallacarboranes and amines are stable in basic and neutral media. However, the industrial applications require stable systems able to resist several cycles during time hence the stability of the system to the electrochemical process should be evaluated.

We carried out a chronopotentiometry at a constant potential. Actually, at the potential required to achieve 10 mA/cm^2. The measure was realized in a solution 0.1 M of Na_2SO_4 with continuous stirring because the system was constantly bubbling (**Figure 5.14**). We chose GO-$NHEtNH_3$[**1**] and GO-$NHPhNH_3$[$\mathbf{Cl_{12}}$**-1**] as representative electrodes because these were the electrodes that presented better results. **Figure 5.14** shows how GO-$NHEtNH_3$[**1**] and GO-$NHPhNH_3$[$\mathbf{Cl_{12}}$**-1**] were able to resist up to 10 h and 14 h, respectively, before the current density started to decay below 10 mA/cm^{-1}, demonstrating the high stability of the system.

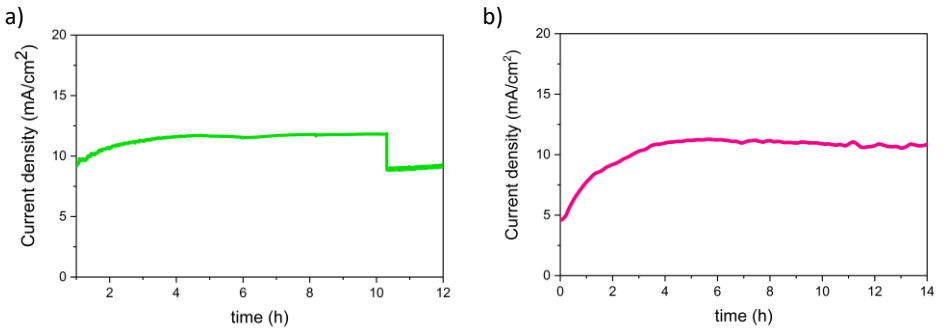

Figure 5.14. Chronoamperometry at $E_{j=10}$ for the electrodes GO-NHEtNH$_3$[**1**] and GO-NHPhNH$_3$[**Cl$_{12}$-1**].

5.7 Conclusions

First studies indicate that the chloro substitution in COSAN increases their catalytic power for water electrolysis. In addition, the appearance of foam during the electrochemical process unveil the surfactant performance of chloro derivatives of COSAN; this behaviour indicates these molecules possess highly self-assembling properties that increase with the number of chloro substituents in the COSAN skeleton. The use of electrode coating with a polymer such as chitosan incorporating COSAN to functionalize graphite electrodes for water splitting is not an option of choice because these systems are not able to resist the bubbles formed during the electrochemical process. Therefore a new soft method to oxidize the graphite surface has been developed and the best compromise between surface oxidation and conductivity losses was achieved by fine-tuning the Hummer reaction conditions. The rapid and easy interaction of amines with the epoxy and carboxylic groups of the GO surface and their high affinity by the metallacarboranes allowed us to synthesize a molecular scaffold that connects the metallacarborane with the graphite. This scaffold presents high physicochemical stability and great affinity to COSAN derivatives paving avenues for different functionalized graphites with a wide range of metallacarborane derivatives. In addition, the amines selected in this work (triethylamine, ethylenediamine and *p*-phenylenediamine) have shown influence into the stability and catalytic power of the metallacarboranes hence this work opens the possibility to continue research with other amines that improve the properties of our working electrodes.

Finally, we demonstrated the catalytic power of the chlorinated derivatives of COSAN for water electrolysis. These pioneering studies display impressive overpotential values of 20, 98 and 51 mV for the electrodes GO-NHPhNH$_3$[**Cl$_{12}$-1**], GO-NHPhNH$_3$[**Cl$_{10}$-1**] and GO-NHPhNH$_3$[**Cl$_8$-1**] respectively, becoming the smallest found in the literature for systems based on the readily available graphite.

These results altogether show promising systems based on an easy and straightforward method to fabricate performing catalysts for oxygen evolution reaction. Systems like the ones presented in this chapter can make way towards the implementation of these new materials for real application such as water splitting, metal-air batteries or fuel cells.

5.8 References

(1) Z. W. Seh, J. Kibsgaard, C. F. Dickens, I. Chorkendorff, J. K. Nørskov and T. F. Jaramillo, Combining theory and experiment in electrocatalysis: Insights into materials design, *Science*, **2017**, 355, eaad4998.

(2) L. Zhang, J. Xiao, H. Wang and M. Shao, Carbon-Based Electrocatalysts for Hydrogen and Oxygen Evolution Reactions, *ACS Catal.*, **2017**, 7, 7855-7865.

(3) L. C. Seitz, C. F. Dickens, K. Nishio, Y. Hikita, J. Montoya, A. Doyle, C. Kirk, A. Vojvodic, H. Y. Hwang, J. K. Norskov and T. F. Jaramillo, A highly active and stable $IrO_x/SrIrO_3$ catalyst for the oxygen evolution reaction, *Science*, **2016**, 353, 1011-1014.

(4) M. Tahir, L. Pan, F. Idrees, X. Zhang, L. Wang, J.-J. Zou and Z. L. Wang, Electrocatalytic oxygen evolution reaction for energy conversion and storage: A comprehensive review, *Nano Energy*, **2017**, 37, 136-157.

(5) B. G. DeBoer, A. Zalkin and D. H. Templeton, Crystal structure of a brominated carborane-metal sandwich compound, N $(CH_3)_4[(B_9C_2H_8Br_3)2Co]$, *Inorg. Chem.*, **1968**, 7, 2288-2294.

(6) B. Maertz, A. Wijnheijmer, G. Fuchs, M. Nowakowski and D. Awschalom, Vector magnetic field microscopy using nitrogen vacancy centers in diamond, *Appl. Phys. Lett.*, **2010**, 96, 092504.

(7) M. Gong and H. Dai, A mini review of NiFe-based materials as highly active oxygen evolution reaction electrocatalysts, *Nano Res.*, **2015**, 8, 23-39.

(8) S. P. Fisher, S. G. McArthur, V. Tej, S. E. Lee, A. L. Chan, I. Banda, A. Gregory, K. Berkley, C. Tsay, A. L. Rheingold, G. Guisado-Barrios and V. Lavallo, Strongly Coordinating Ligands To Form Weakly Coordinating Yet Functional Organometallic Anions, *J. Am. Chem. Soc.*, **2020**, 142, 251-256.

(9) L. Gong, X. Y. E. Chng, Y. Du, S. Xi and B. S. Yeo, Enhanced Catalysis of the Electrochemical Oxygen Evolution Reaction by Iron(III) Ions Adsorbed on Amorphous Cobalt Oxide, *ACS Catal.*, **2018**, 8, 807-814.

(10) J. Zhang, Z. Zhao, Z. Xia and L. Dai, A metal-free bifunctional electrocatalyst for oxygen reduction and oxygen evolution reactions, *Nat. Nanotechnol.*, **2015**, 10, 444-452.

(11) M. Li, L. Zhang, Q. Xu, J. Niu and Z. Xia, N-doped graphene as catalysts for oxygen reduction and oxygen evolution reactions: Theoretical considerations, *J. Catal.*, **2014**, 314, 66-72.

(12) A. Eftekhari, Tuning the electrocatalysts for oxygen evolution reaction, *Mater. Today Energ.*, **2017**, 5, 37-57.

(13) C. Viñas, M. Tarrés, P. González-Cardoso, P. Farràs, P. Bauduin and F. Teixidor, Surfactant behaviour of metallacarboranes. A study based on the electrolysis of water, *Dalton Trans*, **2014**, 43, 5062-5068.

(14) P. Bauduin, S. Prevost, P. Farràs, F. Teixidor, O. Diat and T. Zemb, A Theta-Shaped Amphiphilic Cobaltabisdicarbollide Anion: Transition From Monolayer Vesicles to Micelles, *Angew. Chem. Int. Ed.*, **2011**, 50, 5298-5300.

(15) S. Islam, M. R. Bhuiyan and M. Islam, Chitin and chitosan: structure, properties and applications in biomedical engineering, *J. Polym. Environ.*, **2017**, 25, 854-866.

(16) I. Fuentes, J. Pujols, C. Viñas, S. Ventura and F. Teixidor, Dual Binding Mode of Metallacarborane Produces a Robust Shield on Proteins, *Chem. Eur. J.*, **2019**, 25, 12820-12829.

(17) L. Staudenmaier, Verfahren zur darstellung der graphitsäure, *Berichte der deutschen chemischen Gesellschaft*, **1898**, 31, 1481-1487.

(18) B. C. Brodie, XIII. On the atomic weight of graphite, *Philosophical Transactions of the Royal Society of London*, **1859**, 249-259.

(19) W. S. Hummers Jr and R. E. Offeman, Preparation of graphitic oxide, *J. Am. Chem. Soc.*, **1958**, 80, 1339-1339.

(20) D. R. Dreyer, S. Park, C. W. Bielawski and R. S. Ruoff, The chemistry of graphene oxide, *Chem. Soc. Rev*, **2010**, 39, 228-240.

(21) L. Shen, L. Zhang, K. Wang, L. Miao, Q. Lan, K. Jiang, H. Lu, M. Li, Y. Li, B. Shen and W. Zheng, Analysis of oxidation degree of graphite oxide and chemical structure of corresponding reduced graphite oxide by selecting different-sized original graphite, *RSC Advances*, **2018**, 8, 17209-17217.

(22) C. K. Chua, Z. Sofer and M. Pumera, Graphite Oxides: Effects of Permanganate and Chlorate Oxidants on the Oxygen Composition, *Chem. Eur. J.*, **2012**, 18, 13453-13459.

(23) A. Y. S. Eng, C. K. Chua and M. Pumera, Refinements to the structure of graphite oxide: absolute quantification of functional groups via selective labelling, *Nanoscale*, **2015**, 7, 20256-20266.

(24) T. Kuila, S. Bose, A. K. Mishra, P. Khanra, N. H. Kim and J. H. Lee, Chemical functionalization of graphene and its applications, *Prog. Mater. Sci.*, **2012**, 57, 1061-1105.

(25) F. Pendolino and N. Armata, *Graphene oxide in environmental remediation process*, Springer, **2017**.

(26) A. Bagri, C. Mattevi, M. Acik, Y. J. Chabal, M. Chhowalla and V. B. Shenoy, Structural evolution during the reduction of chemically derived graphene oxide, *Nat. Chem*, **2010**, 2, 581-587.

(27) J. Guerrero-Contreras and F. Caballero-Briones, Graphene oxide powders with different oxidation degree, prepared by synthesis variations of the Hummers method, *Mater. Chem. Phys.*, **2015**, 153, 209-220.

(28) D. C. Marcano, D. V. Kosynkin, J. M. Berlin, A. Sinitskii, Z. Sun, A. Slesarev, L. B. Alemany, W. Lu and J. M. Tour, Improved Synthesis of Graphene Oxide, *ACS Nano*, **2010**, 4, 4806-4814.

(29) Sudesh, N. Kumar, S. Das, C. Bernhard and G. D. Varma, Effect of graphene oxide doping on superconducting properties of bulk MgB2, *Supercond. Sci. Tech.*, **2013**, 26, 095008.

(30) N. I. Zaaba, K. L. Foo, U. Hashim, S. J. Tan, W.-W. Liu and C. H. Voon, Synthesis of Graphene Oxide using Modified Hummers Method: Solvent Influence, *Procedia Engineering*, **2017**, 184, 469-477.

(31) A. B. Bourlinos, D. Gournis, D. Petridis, T. Szabó, A. Szeri and I. Dékány, Graphite Oxide: Chemical Reduction to Graphite and Surface Modification with Primary Aliphatic Amines and Amino Acids, *Langmuir*, **2003**, 19, 6050-6055.

(32) W. H. Knoth, H. Miller, J. C. Sauer, J. Balthis, Y. Chia and E. Muetterties, Chemistry of boranes. IX. Halogenation of B10H10-2 and B12H12-2, *Inorg. Chem.*, **1964**, 3, 159-167.

(33) N. H. Kim, T. Kuila and J. H. Lee, Simultaneous reduction, functionalization and stitching of graphene oxide with ethylenediamine for composites application, *J. Mater. Chem*, **2013**, 1, 1349-1358.

(34) B. Xue, J. Zhu, N. Liu and Y. Li, Facile functionalization of graphene oxide with ethylenediamine as a solid base catalyst for Knoevenagel condensation reaction, *Catal. Commun.*, **2015**, 64, 105-109.

(35) A. Benghnia, J. R. Ares, F. Leardini, R. B. Slama, B. Ayed and B. Chaouachi, Synthesis and functionalization of graphite oxide: structural, morphological and thermal properties for hydrogen storage, *J. Mater. Sci. Mater. El.*, **2019**, 30, 5044-5051.

(36) B. Jiang, X. Fan, Q. Dang, F. Liao, Y. Li, H. Lin, Z. Kang and M. Shao, Functionalization of metal oxides with thiocyanate groups: A general strategy for boosting oxygen evolution reaction in neutral media, *Nano Energy*, **2020**, 76, 105079.

(37) N. N. Greenwood and A. Earnshaw, *Chemistry of the Elements*, Elsevier, **2012**.

(38) J. Xu, Z. Lian, B. Wei, Y. Li, O. Bondarchuk, N. Zhang, Z. Yu, A. Araujo, I. Amorim, Z. Wang, B. Li and L. Liu, Strong Electronic Coupling between Ultrafine Iridium–Ruthenium Nanoclusters and Conductive, Acid-Stable Tellurium Nanoparticle Support for Efficient and Durable Oxygen Evolution in Acidic and Neutral Media, *ACS Catal.*, **2020**, 10, 3571-3579.

(39) L. Wang, X. Duan, X. Liu, J. Gu, R. Si, Y. Qiu, Y. Qiu, D. Shi, F. Chen, X. Sun, J. Lin and J. Sun, Atomically Dispersed Mo Supported on Metallic Co9S8 Nanoflakes as an Advanced Noble-Metal-Free Bifunctional Water Splitting Catalyst Working in Universal pH Conditions, *Adv. Energy Mater.*, **2020**, 10, 1903137.

(40) F. Luo, L. Guo, Y. Xie, J. Xu, K. Qu and Z. Yang, Iridium nanorods as a robust and stable bifunctional electrocatalyst for pH-universal water splitting, *Appl. Catal. B Environ.*, **2020**, 279, 119394.

CHAPTER 6

FESAN as Single-Molecule Magnet

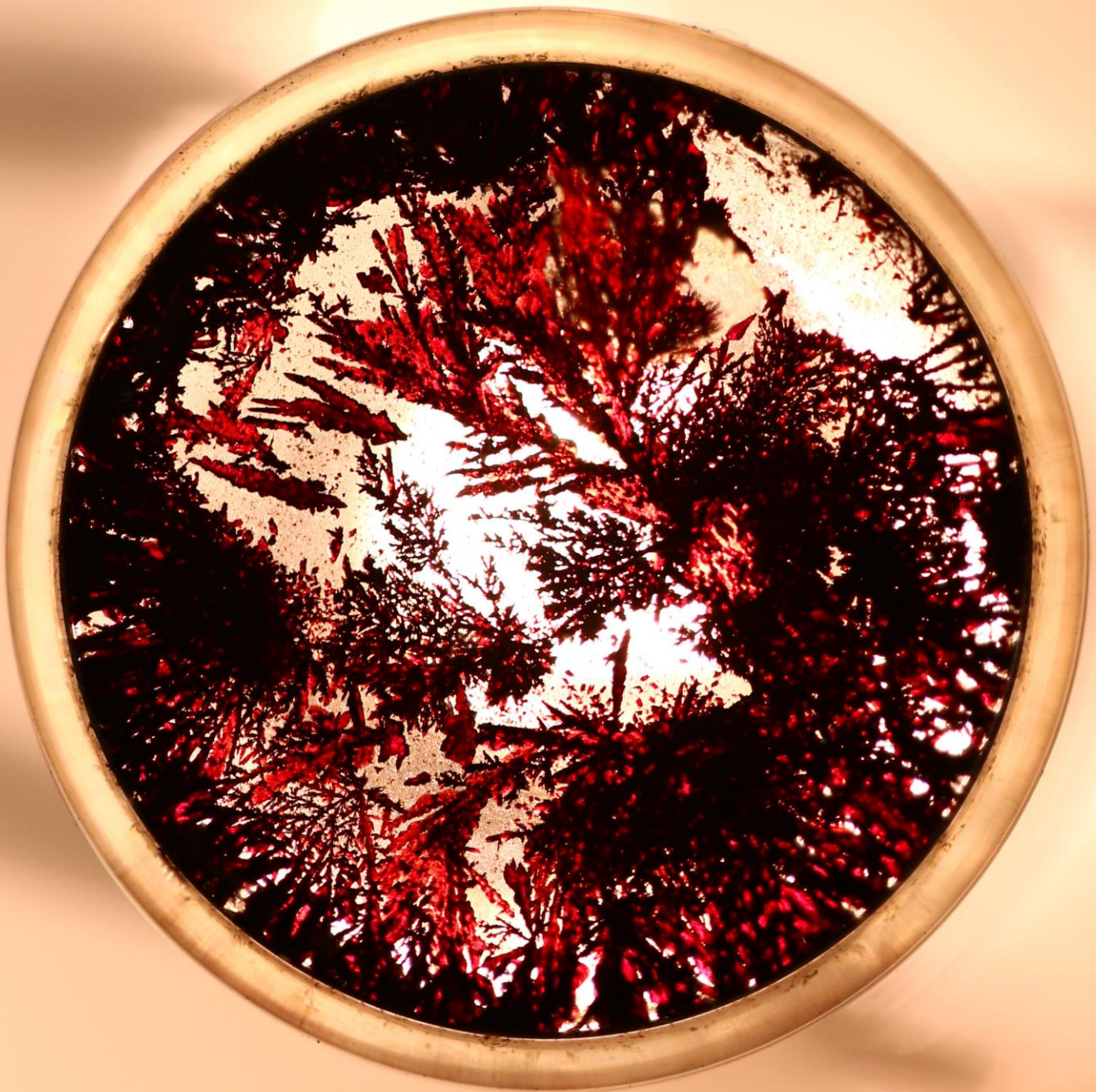

CHAPTER SIX

FESAN as Single-Molecule Magnet

The development of qubits for quantum computing requires some magnetical properties together with concrete relaxation times in order to maintain the coherence time the maximum as possible. The last researches indicate that Single-Molecule Magnet (SMM) are the best option for this application. This work will propose FESAN as SMM due to the unpair electron able to behave as a qubit for quantum computing. Actually, these studies already found it in the bibliography but, the nature of counter cation is key for the magnetical properties of FESAN. Base on previous studies did it for COSAN this study will focus on obtaining the crystal structure of the tetramethylammonium salts of FESAN. In addition, this research will explain how getting a monocrystal of FESAN will permit the theoretical study of the anisotropy of the molecule from the crystal characterization. Besides these crystals could be used for the experimental study of the relaxation time of the molecule with a Superconducting Quantum Interference Device (SQUID).

This work has been made in collaboration with the Departament de Química Inorgànica i Orgànica and Intitut de Química Teòrica i Computacional, Universitat de Barcelona (UB) in Barcelona.

6.1 Quantum tunneling in Magnetism

Quantum physics represents one of the most active research branches of modern science since their discovery at first of 20th century. The understanding and application of quantum phenomena has led to the development of new fields such as superconductivity and magnetism along others.[1]

Quantum theory made it evident some fundamental limitations of the classical models when are applied to atomic phenomena.[2] For instance, at the atomic scale, quantum tunnelling (QT) phenomenon that is represented by the famous and poor Schrödinger's cat, are not negligible and cannot be explained by classical physics. The paradox presents the hypothetical scenario where there is a cat in a box that is alive and dead simultaneously representing the quantum superposition. The system will remain in a quantum state until it interacts with the environment; in other words, until we open the box, at that moment it will produce the "decoherence" effect, the system will pass from quantum to classic state. Despite quantum effects are not observable in macroscopic systems, nowadays they are at the base of recent advanced techniques such as the Superconducting Quantum Interference[3] (SQUID) or the Scanning Tunneling Microscopy (STM)[4]

During the last decades, many researches have been focused on the search of "Schrodinger's cats" through the study of mesoscopic materials, which are more complex than an atom but small enough to present quantum effects. The observation of quantum phenomena in mesoscopic matter provides, in principle, confirmation to the so-called "Copenhagen interpretation" established by Niels Bohr and Werner Heisenberg in 1927. The theory assumes that there is a continuous transition from the field of the small objects, where quantum mechanics is required, to macroscopic objects, where classical physics operates well.[5] Magnetic materials have a very important role in this field.

Magnetism is a property of matter which is closely related to the quantum structure of the system. It is determined by the Hund's rules, the electron configuration, the Pauli Exclusion Principle and the existence of a freedom degree, the spin, without classic analogous. Quantum computing exploits magnetic materials particularly those that present the peculiar property to retain its magnetization even after a magnetic field is applied and retired. This class of

compounds are called ferromagnetic material and the retaining process is described by the magnetic hysteresis. This occurs despite ferromagnetism is a prohibited phenomenon for classic physics by the Bohr-van Leeuwen theorem,[1] it is at the base to the data storage technology and in classical computing.[6]

One of the greatest invention of 20th century was the discovery of the transistor. The transistor is a device used to amplify or switch electronic signals. This system is based on the use of bits, the basic units of information in computing. It is a binary system represented by $|0\rangle$ or $|1\rangle$ and rules all the informatics systems. Technological development has permitted us to produce smaller and even faster transistors. Nowadays, a chip of a 1mm^2 can store up to 9 million of transistors each in dimensions of less than 10 nm. However, the limitation is just around the corners as we reach a threshold were electrons can arbitrarily escape from the canals they are supposed to travel through due to quantum tunnelling effect.

This drawback pushed the research toward new challenges, and instead fighting the problem, Paul Benioff in 1980 presented his theory to take advantage of the quantum physics, opening the era of quantum computing.[7] The proposed mechanism suggested working at the level of quanta of light instead of electric voltages. This change would permit to reduce the computing time because the system could perform more operations at once so it can solve computational problems that would have been impossible to solve with classical computating.[8,9]

Quantum computers are model devices that process information encoded in quantum states. The model of a quantum computer is built in analogy to a classical computer. The system is based on the qubit as analogous to a bit in a classical digital computer. The quantum state of a single qubit,$|\psi\rangle = \alpha|0\rangle + \beta|1\rangle$ is an arbitrary normalized linear combination of the logical basis states $|0\rangle$ and $|1\rangle$. The state of N qubits is an arbitrary superposition of the 2^N basis states in which every qubit is in one of the computational basis states (**Figure 6.1**).[8,10]

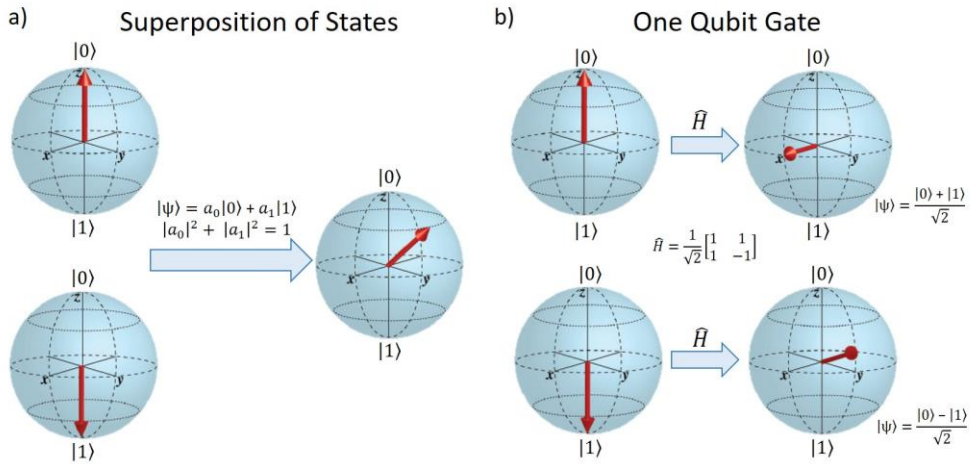

Figure 6.1. (a) The quantum version of the bit, a qubit, can be represented in the Bloch sphere with an arrow pointing north representing de |0⟩ state, while when pointing south it represents the |1⟩ state. Unlike the bit, the qubit can possess many more states; which can be viewed as an arrow pointing in any other direction of the sphere. The new states are quantum superposition of the |1⟩ and |0⟩ states, giving the computational power expected in quantum computers. (b) One qubit Hadamard gate acting on initial qubit. After each operation superposition of states are obtained, all of them containing all possible combination of states. Figure adapted from reference 11.

Quantum computing offers promising outlook, however, the fabrication of these devices is not straightforward because they need extreme cryogenic environment along other precautions to avoid the environmental noise to destroy the data stored. For this reason, in the last decades, many projects have been devoted to the study of these systems to find efficient ways to fabricate a stable quantum processor. Some results can be summarized in a list proposed by Di Vicenzo who suggest a series of important criteria that represent a must forquantum computers:

- a well-defined two-dimensional subspace that is clearly isolated and scalable, i.e. it must be easy to add an extra qubit to the computer,
- a procedure to prepare the qubits in a state, like |00 ... 0⟩,
- an implementation of one- and two-qubit quantum gates,
- coherence times long enough compared to the switching time to allow efficient error correction,
- the possibility to measure the qubits state at the end of the computation.

These criteria describe the minimal set of requirements for any quantum computing implementation and all the criteria from the list must be in a single device at the same time and in the same experiment.[10]

From 1980 and the introduction of the possibility to perform operations with qubits instead of bits, significant advances have been achieved. For example, ion traps and optical cavities have been used to encrypt qubit states[11]. Further breakthroughs come from the realization of a quantum algorithm using a bulk nuclear magnetic resonance technique,[12] in which the nuclear spins act as 'quantum bits to induce spin level transitions in organic molecules to offer promising experimental approaches. Nevertheless, noise, loss of coherence, and manufacturing problems make the construction of large-scale quantum computers difficult, so the development of strong candidates to develop these systems still remain a challange.[13,14]

In solid-state settings, the qubits based on spin typically show longer coherence times that the charge-based qubits. The paradigmatic way of producing a solid-state qubit is to isolate an island of electrons in a piece of semiconductor and contact it with metallic electrodes. This typical top-down approach gives quantum dots with different electrostatic confinement, and spins can feel such differences through spin-orbit coupling. On the other hand, the Single-Molecular-Magnets (SMM) are designed from bottom up, using synthetic chemistry and, starting from identical atoms, it is possible to guarantee that all of the qubits of the system are identical.[10] In addition, chemical synthesis offer a wide range of possible molecules with different properties useful for quantum computing applications.[10]

If the spin in a molecular magnet represents a qubit, the quantum computer can be realized as a set of qubits connected in a cluster because the intervention of the binding groups in the cluster regulates the interaction of qubits.[15] The first molecular magnet discovered was a cluster synthesised in 1980 with chemical formula $[Mn_{12}O_{12}(O_2CCH_3)16(H_2O)_4]\cdot 4H_2O\cdot 2CH_3CO_2H$ (Mn12Ac).[16] The structure possesses a magnetic core composed of four Mn^{4+} ions enclosed in a ring of eight Mn^{3+} ions and finally linked by O^{2-} ions between them (**Figure 6.2**a). The cluster has a total spin of S=10 as a result of the antiferromagnetic coupling between the ions with different oxidation state. As a consequence of its

magnetically isolated core, the cluster Mn12Ac presents the typical behaviour of small particles of magnetically ordered materials such as blocking temperature, which depends on the frequency of the experiment and the hysteresis below this temperature. In addition, its discovery represented the best example of a superparamagnet without particle size distribution and was a model system for testing theories of mesoscopic physics such as quantum tunnelling of magnetization. However, the system is not similar to a piece of a three-dimensional magnet; instead, it is better described as a paramagnet, in which the single-ion uniaxial magnetic anisotropy is responsible for the relaxation times of the order of a few seconds around 4 K and of the order of two months at 2 K.[17,18]

The structure $[Fe_8O_2(OH)_{12}(tacn)_6]Br_8$ (tacn = 1,4,7-triazacyclononane) or Fe8 (**Figure 6.2**b) was another molecule intensively investigated for its SMM behaviour. The cluster presents eight Fe^{3+} ions in its center with a low symmetry that improve the tunnelling effect, approximate D_2 symmetry and $S = 10$.[19] The spin structure of the ground is represented by arrows in the **Figure 6.2**b and provide a magnetization density map of the cluster.[20] The structure present slow relaxation times and the cluster show for the first time biaxial anisotropy that promotes tunneling effects.[21] Overall, the net result is that the relaxation of the magnetization near a resonance at 0.35 K is in the order of few hours and the effect is even more pronounced below 0.35 K where the relaxation time increases by 3-4 orders, in the pure tunnelling regime.[22]

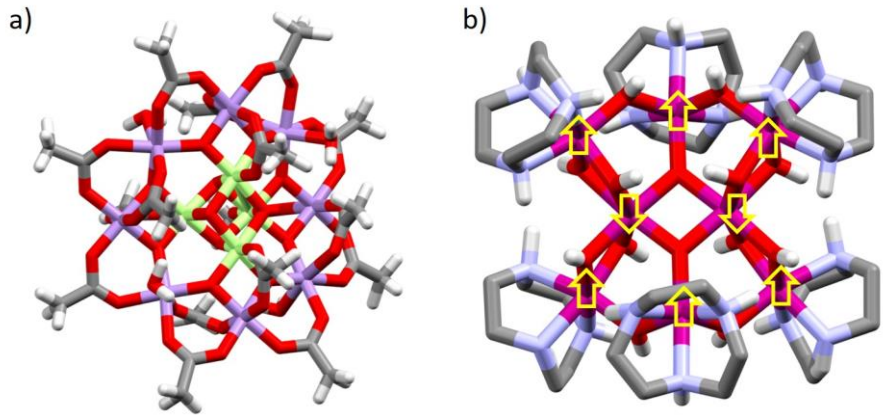

Figure 6.2. (a) Crystal structure of the cluster Mn12Ac obtained from the CCDC (Mn^{4+} in green, MN^{3+} in violet, O in red, C in grey),[17] b) Crystal structure of the cluster Fe8 from the CCDC (Fe in purple, O in red, C in grey), The spin structure is schematized by yellow arrows.[24]

During many years, the research in this direction had as a milestone the overmentioned SMM. However, the issues of difficult manufacturing and lack of tunability of magnetic properties hindered the development of this field which remained in the shadow for almost 15 years. Only recently, in the last decade scientists moved towards the synthesis of new metal complexes that could represent good candidates to implement qubit devices for quantum computing and that can overcome the known drawbacks.[23-25]

Microwave superconductor resonators have been good candidates to build up a dense 2D network of qubits in a single device.[26] Usually, magnetic S = 1 nitrogen-vacancy [27] centres in diamond have been used due to the relatively long coherence T_2 time (around 10 ms) despite their highly complicated synthesis procedure (high energy irradiation for long periods).[28,29] Another example is provided by magnetic molecules with small spin values that could be alternatives if they can reach high decoherence times, [30-33] so far, the best ones are $S = 1/5$ V^{4+} complexes presenting time coherence values of 0.01 ms.[34]

The use of these type of molecules as qubit relies on the fact that every molecule can be described as having spin S under an electric field generated by the ligands. Due to spin-orbit coupling, the crystal field energy depends on the spin orientation; this effect is known as magnetic anisotropy and represents the two states $|0\rangle$ and $|1\rangle$. Normally these two states can be filled by a microwaves energy.

The candidate proposed for the design of qubit systems in this research was the iron metallacarborane, namely the tetramethylammonium salt of FESAN ([NMe_4][**2**]) with $S = 1/2$. This structure is composed by one single magnetic nucleus inserted between two carborane clusters that isolate the metal center from the external interactions. The energy of the system depends on the unique spin orientation represented by the two states $|0\rangle$ and $|1\rangle$ that is reflected with a low magnetic anisotropy. SMMs as Mn12Ac or Fe8 present a high number of magnetic atoms that at first glance could seem a favourable point. However the complex and high global magnetic anisotropy hinder a thorough control on their properties and makes it useless for their real application [35] Conversely, our [NMe_4][**2**] structure presents a clear advantage since it only has one magnetically active nucleus, easy to study and to control. It is not the first time that a

metallacarborane is considered to act as SMM, actually, the $[Fe(C_5Me_5)_2][\mathbf{2}]$ was the first salt of FESAN considered for its magnetic properties. In the initial idea, the $[Fe(C_5Me_5)_2]^+$ was believed to have ferromagnetic coupling but, in reality, it did not show significant ferromagnetic or antiferromagnetic interactions between the unpaired spins, even at low temperatures.[36] Subsequently, $[(H_2C_2S_2C)_2][\mathbf{2}]$ was the candidate which should have shown enhanced magnetic properties due to the packing of prolate ions in a regular crystal lattice. Unluckily, the structure did not show ferromagnetic interactions either.[37] However, these studies shed light on the key role of the salt on the behaviour of the spins. In particular, the presence of one-dimensional linear chains of either cation or anions is a condition necessary for the observation of bulk ferromagnetism in a charge-transfer salt.[36]

In this work, we present the synthesis and characterization of $[NMe_4][\mathbf{2}]$ for the use of small molecular magnets. Particular attention will be devoted to the counter ion that has been demonstrated to be determinant to induce ferroelectric behaviour.

6.2 Characterization of Single Molecular Magnets

6.2.1 X-ray structure and computational details

Crystallographic characterization of our material is a necessary condition to unveil the chemical and physical properties of our SMM. This information enables theoretical calculations that helps to shed light on the nature of our material. Thus, the crystallization of a single monocrystal is the first basic, but not easy, fundamental step when we study SMMs. Namely, our crystallographic data were collected at 100K at XALOC beamline at ALBA synchrotron (λ = 0.82654 Å) and the structure was resolved following the methodology and programs described in the bibliography.[38]

The X-ray structure permitted to make thoroughful calculations and get plenty of valuable information out of our crystal. From the X-ray structure it was possible to know:

- The distances and angles between atoms and the intermolecular interactions; besides, it was possible to confirm the rotamer present in the crystal structure

- The relative energy of our structure and their possible rotamers. Further, it was possible to estimate the energy of our molecule in a solvent as THF.

- The energy splitting of the external shell orbitals, namely the d orbitals to know which are the less energetic.

- The important *g* tensors, values very important to understand the magnetic anisotropy of the molecule.

- Predict magnetic properties such as magnetization and susceptibility not only of our structure but also of the possible isomer. Furthermore it was possible to predict the EPR behaviour of our molecule in powder and in solution.

All the estimations, equations, methodologies and software packages used to calculate the different properties of the material are described in the bibliography.[38]

6.2.2 Magnetometry experiments

The superconducting quantum interference device (SQUID is one of the most sensitive experimental techniques to characterize magnetic properties with a demonstrated field resolution down to 10^{-17} T.[39,40] SQUIDs are able to detect the minimum flux variation signal by using Josephson junction. The Josephson junction is a connection between two superconductors, which are lightly separated by an insulating material so thin that electrons can travel from one electrode to the other even without an applied voltage.[41]

In this work, we used this technique to characterize our FESAN complex and unveil those properties typical of SMM. We will focus on the following measurements:

- *DC (Direct Current)* or Static magnetic measurements determine the equilibrium value of the magnetization in a sample and give us information about the magnetic nature of the sample. The sample is magnetized by a constant magnetic field, H(T), and the magnetic moment of the sample is measured, producing a DC magnetization curve M(H).

- In *AC (Alternative Current*) or Dynamic magnetic measurements, a small AC drive magnetic field is superimposed on the DC field, causing a time-dependent moment in the sample. In other words, an alternating current in a primary electric coil, give an oscillation on the magnetization of the sample that produces an intensity variation in a second electric coil that is measured by the SQUID device. By this method it is possible to measure the sensibility of the sample to the magnetization and to study the secondary magnetic processes of the sample. This sensibility is called susceptibility and it is the summary of two components. The real (χ') component reflects the sensibility of the material to the magnetic field (H) and the imaginary component (χ'') give us information about all secondary processes that are related with losses and dissipative processes.

- *Relaxation time (τ)* data are the final goal of this research. It is fundamental for quantum computing the use of SMM with long relaxation times. These values can be extracted fitting the Cole-Cole diagram (**Appendix B**): a representation of the imaginary component of susceptibility *vs.* the real one with a fixed external magnetic field. Moreover, we are then allowed to calculate the relaxation time values and assess the potential of our material as SMM for quantum computing.

Susceptibility measurements (Direct (DC) and alternating (AC) current) were carried out with a Quantum Design SQUID MPMS device. An oscillating ac field of 4 Oe was used in the AC measurements and frequencies ranging from 1 to 1500 Hz and a 0.05 T external DC field. A polycrystalline sample was mounted in a capillary tube made of polyimide.

6.3 Crystallographic Characterization of [NMe_4][2]

The metallacarborane complexes of Fe III are some of the most studied in the literature[42,43] because of their outstanding ferromagnetic properties related to their unpair electron. Important prerequisite to characterize these complexes is the possibility to obtain pure and good crystals. Unfortunately, there is not much information about its molecular structure due to the difficulties to obtain good single crystals.[44]

In this work, we present a method to obtain FESAN single crystals which consist on a very well defined synthesis .[45] The first step involved the synthesis of the trimethylammonium salt of *nido*-7,8-$C_2B_9H_{12}$ from *closo*-1,2-$C_2B_{10}H_{12}$ (*o*-carborane) as starting material, followed by the formation of the Θ shape organometallic complex of two *nido*-carboranes with an atom of iron (III) in the middle.

We explored the influence of different Fesan salts on SMM properties. The main idea, corroborated by previous work, was that the cation could influence the formation of supramolecular structures and shape the magnetic properties of the complex *via* ferromagnetic coupling. In this framework, the necessity to obtain one-dimensional linear chains of either anions or cations has been demonstrated to affect the bulk ferromagnetism.[36,37]

The choice of tetramethylammonium was based on previous studies with Cosane. Actually, the crystal structure of their tetramethylammonium salt [46] do not show intermolecular interactions between the cation-anion. So we predict that this behaviour could appear for the analogue [NMe_4][**2**] crystal structure.

In this direction the slow evaporation of acetonitrile:water (1:1) mixture lead to, after five days, excellent single crystals of tetramethylammonium salt of Fesan.

The structure represented in **Figure 3** shows different interesting properties as the two orientations of the [NMe_4][**2**] molecules, arranged in infinite zig-zag chains and generating a zig-zag plane. Each chain is held together by dihydrogen bonds formation of the protonic C_C-H atom from one of metallacarborane and one B-H vertex of the neighbouring one. Namely, between the C(2)-H and B(11)-H with a distance and angle of 2.036 Å and 133.5°, respectively (**Figure 6.3**). In contrast,

the distance of 2.466 Å was the shortest distance find for the interaction of the B(12)-H related to the complex and the hydrogen of $[NMe_4]^+$. This distance is shorter than the sum of van der Waals radii; therefore, as we predicted, there are no interaction between the complex and the cation. In conclusion, direct interactions between the anionic FESAN complexes are observed in the supramolecular structure while the $[NMe_4]^+$ cations surround the supramolecular 1D anionic chain as is shown in Figure 6.3 c.

Another important aspect is the relative position of the carbons. In the case of $[NMe_4]$[**2**] the rotamer observed in **Figure 6.3** was the *cisoid*. At first glance, it seems an unexpected rotamer because the *trans* isomer shows better stability (**Table 6.2**). However, if we compare our crystal structure with some equivalents structures (**Table 6.1**), we will observe that this conformation is not odd as we guess.

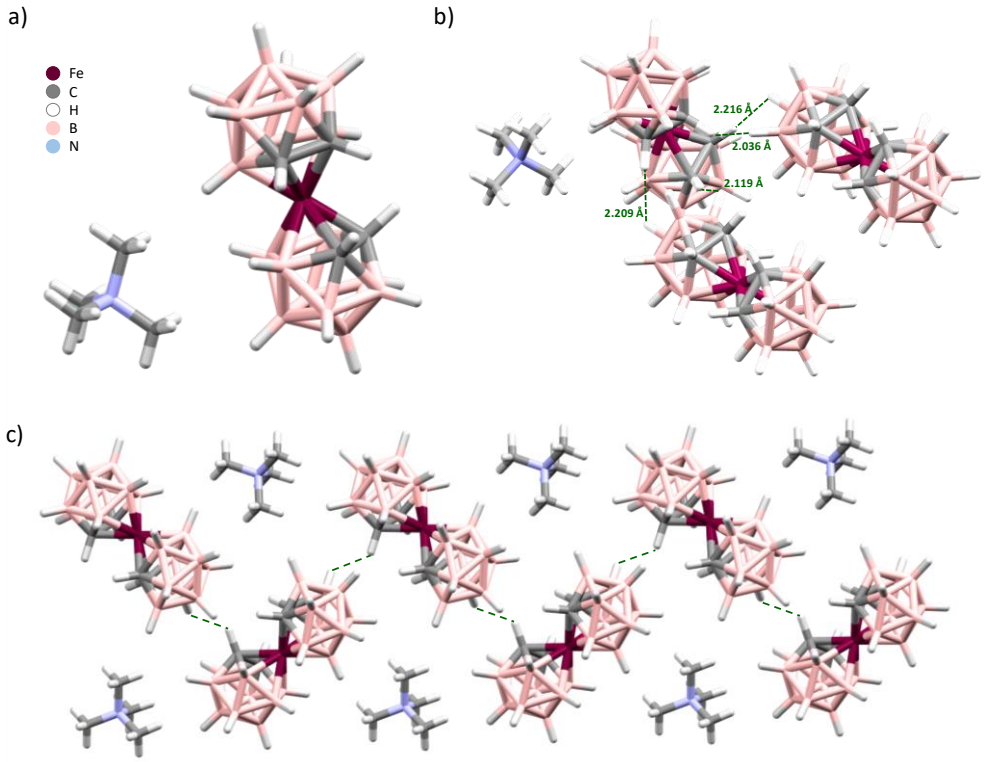

Figure 6.3. Crystal structure of $[NMe_4]$[**2**]: a) ORTEP Representation of the compound; b) Representation of the intermolecular interactions involves the C_C-H atoms of different

metallacarboranes; c) Representation of the packing displaying of one of the face of the crystal showing the supramolecular chains of tetramethylammonium and the planes form by FESAN.

The study of the different crystal structures of cobalt, iron and nickel metallacarboranes give us information on the factors that rule the formation of one isomer in respect to the other such as the metal-carborane distance, the electronic structure of the metal and finally the intermolecular interactions.

- *(η^5-C_2B_3)-Metal distance.* Previous studies by Teixidor *et al*. proposed that distance between η^5-C_2B_3 and the metal is one of the structural parameters that define the isomer in the crystal structure. [46] Unfortunately, Fesan do not show the same behaviour. The crystal structures of the different salts of FESAN present centroid distances Fe···η^5-C_2B_3 equivalents but different rotamer. For example, the $[Fe(C_5Me_5)_2]$[**2**] present a distance of 1.530 and 1.533 Å and a *gauche* rotamer. Finally, the $[NMe_4]$[**2**] salt present equivalent distances (1.525 and 1.527 Å) but *cisoid* rotamer. Therefore, we cannot establish a distance range for the structural isomers of FESAN derivatives.

- *Electronic structure of metal*. The number of outer shell electrons is another key factor proposed. Namely d orbital electrons, Fe^{3+} and Co^{3+} complexes normally show *cis* conformation in their crystal structures. However, there are some exceptions such as $[Fe(C_5Me_5)_2]$[**2**] and CsCosan that present *gauche* and *trans* conformation respectively.

- *Intermolecular interacctions*. The last factor that could to determine the conformation of the compound is represented by the intermolecular interactions. Namely the ones between C_C-H atoms are supposed to be responsible in defining the final complex conformation. We further propose that the double-interactions B(10B)-H···H-C(2A)-C(1A)-H···H-B(11C) with distances of 2.209 and 2.036 Å and the B(11B)-H···H-C(1'A)-C(2'A)-H···H-B(10C) with distances of 2.119 and 2.216 Å promote the *cis* conformation (**Figure 6.3**). Overall these data unveil the decisive influence of intramolecular interaction in defining the isomer structure and explain the reason why we obtained an apparently less stable isomer.

Table 6.1. Conformation comparison of the different structures base on de metal complex. Green for iron, orange for cobalt and blue for nickel.

Refcode in CCDC	Anion	Cation	Number e^-	Oxidation state of metal	Conformation
VOGQEQ	$[3,3'\text{-}Fe(1,2\text{-}C_2B_9H_{11})_2]^-$	NMe_4^+	d^5	Fe^{3+}	*cisoid*
WEKJEB	$[3,3'\text{-}Fe(1,2\text{-}C_2B_9H_{11})_2]^-$	$FeCp^{*+}$	d^5	Fe^{3+}	*gauche*
YEDVUY	$[3,3'\text{-}Fe(1,2\text{-}C_2B_9H_{11})_2]^-$	Ttf^+	d^5	Fe^{3+}	*cisoid*
KIWJOP	$[3,3'\text{-}Fe(1,2\text{-}C_2B_9H_{11})_2]^{2-}$	$2NMe_4^+$	d^6	Fe^{2+}	*transoid*
CABZIQ	$[3,3'\text{-}Co(1,2\text{-}C_2B_9H_{11})_2]^-$	NMe_4^+	d^6	Co^{3+}	*cisoid*
BEVBUZ	$[3,3'\text{-}Co(1,2\text{-}C_2B_9H_{11})_2]^-$	$HNEt_3^+$	d^6	Co^{3+}	*cisoid*
FQBHUQ	$[3,3'\text{-}Co(1,2\text{-}C_2B_9H_{11})_2]^-$	NH_4^+	d^6	Co^{3+}	*cisoid*
CSCBCO	$[3,3'\text{-}Co(1,2\text{-}C_2B_9H_{11})_2]^-$	Cs^+	d^6	Co^{3+}	*transoid*
RINMIK	$[3,3'\text{-}Co(1,2\text{-}C_2B_9H_{11})_2]^{2-}$	$2Cs^+$	d^7	Co^{2+}	*transoid*
UCNBOR01	$[3,3'\text{-}Ni(1,2\text{-}C_2B_9H_{11})_2]^{2-}$	NMe_4^+	d^7	Ni^{3+}	*transoid*

6.4 Magnetic anisotropy

Our complex exhibited the possibility of conversion between the isomers (*cis-gauche-trans*), changing the relative position of the C_2 units between the two ligands. In order to understand and assess the relative stabilities of the isomers, we performed DFT simulations to optimize all the possible geometries and assess the magnetic anysotropy.

Magnetic anisotropy refers to the difference of the magnetic properties of material depending on the direction of the incident magnetic field and is a necessary condition for the hysteresis effect in ferromagnets. Landé or g- factor is the value related to magnetic anisotropy, it is a multiplicative term appearing in the expression for the splitting energy levels of an atom in presence of a weak magnetic field. However, the g-factor value could not be the same for all the space directions and in that case need to be treated as g-tensors. These tensors give us information about the homogeneity of the magnetic properties with the axis space and hence about the magnetic anisotropy. For example, if the three values are equal means that the magnetization is homogenous in all the material and the material is

magnetically isotropic, if exist two values equal or the three are different both have magnetic anisotropy but they have a uniaxial or biaxial anisotropy, respectively.

The results listed in, show that the *cis* isomer present in the crystal structure is less stable compared to the *trans* isomer. Furthermore, there was an important change in the calculated *g* tensor for such isomers (**Table 6.2**).

We also performed EPR measurements in powder and THF solution to check if there was a considerable variation in the *g* values caused by isomerization when the sample was dissolved in THF. Table 6.2 shows the experimental and simulated EPR experiments revealing that there was an important reduction of the anisotropic character when the sample was dissolved. This is consistent with the conversion of the *cis* isomer to the more stable ones.

Table 6.2. Calculated relative energies (in kcal/mol) between the three isomers for the isolated molecules or in a CPCM model using THF as solvent. Calculated *g* components and excited states (D doublet or Q quartet states, in cm^{-1}) for the three DFT optimized isomers simulating the THF solvent.

isomer	isolated	THF	g_{xx}	g_{yy}	g_{zz}	energies
cis	4.0	0.6	0.68	0.69	5.60	0 (D), 877 (D), 19857 (Q)
trans	1.3	0.3	1.71	1.72	3.91	0 (D), 1660 (D), 19417 (D,Q)
gauche	0	0	1.74	1.75	3.80	0 (D), 1757 (D), 18784 (Q)

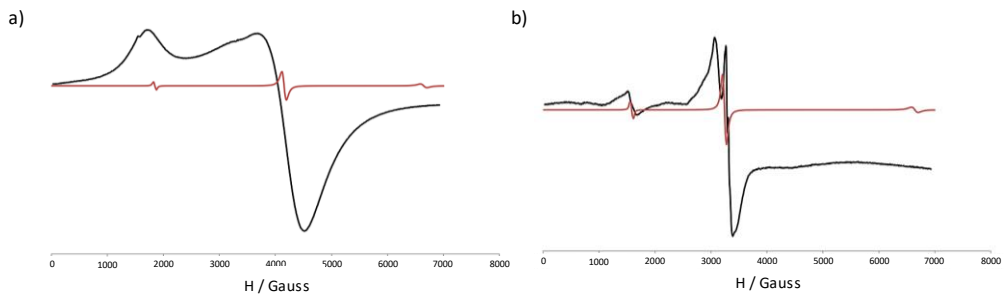

Figure 6.4. EPR (X-band) (a) powder sample (9.31635 GHz and (b) THF solution (9.302873 GHz) of the [NMe_4][**2**] complex. Experimental (in black) and simulated (in red).

The values obtained from the DFT calculations for the *g*- tensors prove the clear existence of magnetic uniaxial anisotropy around the *z*- axis in the crystal due to the g_{xx}, g_{yy} and g_{zz} tensors were 1.35, 1.36 and 4.79 respectively.

In order to understand the relatively large magnetic axial anisotropy around z- axis found for the FESAN complex, we analysed the orbital splitting. The analysis of the nature of the ground and first exited states revealed a transition between d_{xy} and $d_{x^2-y^2}$ orbitals (**Figure 6.5**, *ab initio* Ligand Field Theory orbitals (AILFT) and

Table 6.3 for the orbital energies).[47,48]

Table 6.3. Calculated energy splitting of the 5 d orbitals using the method using the experimental X-ray structure.

	E (cm^{-1})
d_{xy}	0
$d_{x^2-y^2}$	412
d_{z^2}	1590
d_{xz}	29446
d_{yz}	30951

Remarkably, the analysis of the ground state wave function reveals that the orbital occupancy was influenced by the different electronic repulsion of the orbitals instead of their energy (**Figure 6.5**). Thus, the d_{z^2} orbital remains doubly occupied while the ground and first excited states correspond to the alteration of the single and double occupancies in the $d_{x^2-y^2}$and d_{xy} orbitals, in that order. This anomalous orbital occupancy for de d^5 metallocene systems has already been reported[49] could explain the axial magnetic anisotropy around the *z*- axis.

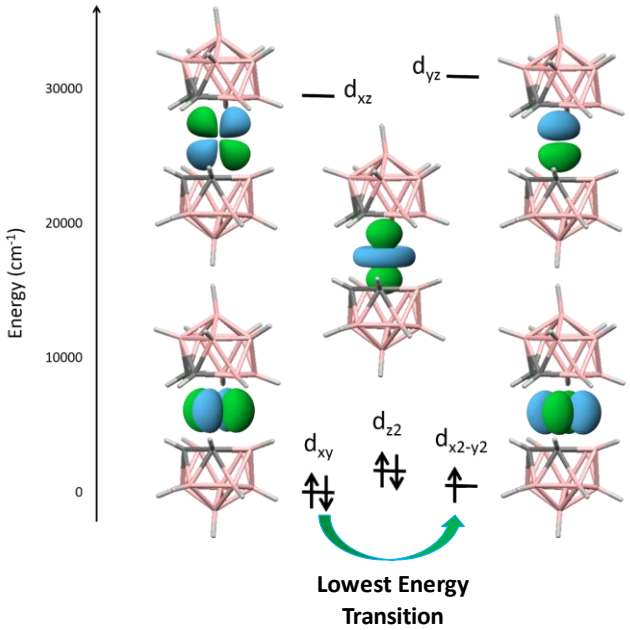

Figure 6.5. Orbital splitting of the FESAN complex obtained *via* the AILFT using the NEVPT2 wave function.

As a conclusion, our study unveiled that magnetic anisotropy together with structural parameters of the crystal are key factors over the energy of the system that determines the isomeric conformation of the molecule.

6.5 Magnetic measurements

As a preliminary study, we carried out magnetometry measurement both in solid and in solution to find the better environment to run our experiment. In this regard, the powder sample of $[NMe_4]$[**2**] did not show spin-relaxation while when the complex where dissolved in THF it does (**Figure 6.6**). However, for the sake of completeness, every experiment from now on were performed both in solid and in solution. Furthermore, the imaginary susceptibility of the powder sample depending on the frequency (Hz) at constant magnetic field was negligible.

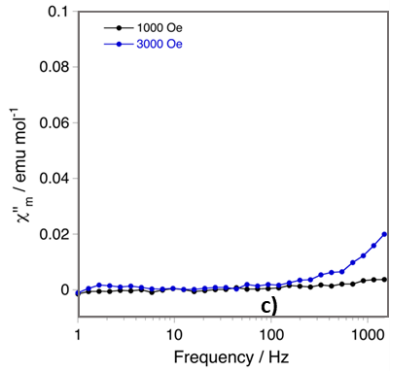

Figure 6.6. Imaginary susceptibility of powder sample *vs.* frequency at 4 K and under magnetic field of 1000 Oe (in black) or 3000 OE (in blue).

Solution sample (55.7 mM) was prepared by first dissolving 11 mg of solid sample in 0.5 ml THF in an Eppendorf; afterwards, it was transferred to one side sealed tube of polyimide and immediately after introduced in liquid nitrogen; then the second side of the tube was sealed.

* Static Magnetic properties

We want to study magnetization, susceptibility and the influence of isomers on static magnetic properties. Typical ferromagnetic materials present positive, very high magnetization values and susceptibilities higher than 10^{-3}. The magnetization indicates how much a sample is "magnetized" by an external magnetic field and the susceptibility indicates the sensibility of the sample to the magnetic field hence the by these techniques it is possible to confirm the ferromagnetic nature of the sample. In addition, it is very interesting to study the influence of the different sample state (powder or solution) as well the isomeric form in order to assess the magnetic properties of the final product.

In the first instance we run experiments aim at studying the magnetization of the powder and solution in THF sample.

The plots represented **Figure 6.7** show the magnetization values in function of the applied magnetic field. Both theoretical and experimental curves follow the classical trend for ferromagnetic materials. However, while the powder sample curve (in black) accurately fit with the theoretical calculations, the curve

corresponding to the sample in solution (in blue), differs from its theoretical counterpart. We attribute this behavior to the influence of the solvent (**Figure 6.7**a).

The experimental values of susceptibility are represented in **Figure 6.7**b as susceptibility per temperature ($\chi \cdot T$), that is the Curie constant (C). Experimental data show good accordance with theory prediction for both solid and liquid samples and a ferromagnetic behavior with susceptibility values inversely proportional to temperature. Furthermore, it is worth noting that in the case of powder at low temperature the susceptibility shows a slight increment contrary to what observed in solution. This effect can be attributed at the intermolecular interactions that are too weak and so negligible in solution (**Figure 6.7**b).

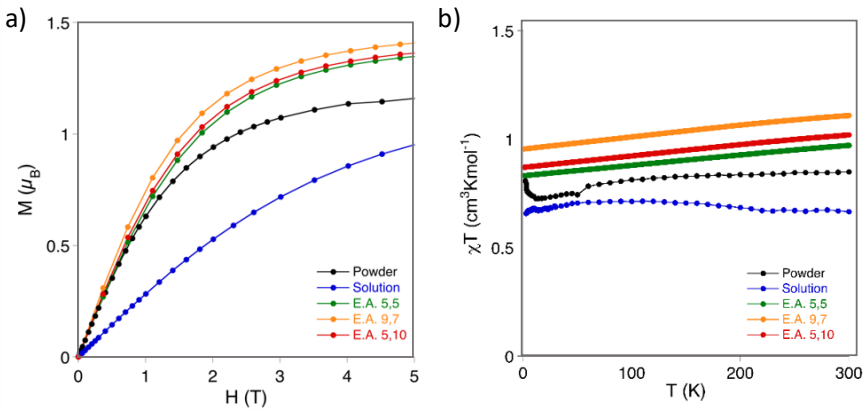

Figure 6.7. Static susceptibility (a) and magnetization (b) measured for a powder sample of the [NMe_4][**2**] compound at 2 K (black colour) and in THF solution (blue colour, magnetization at 4 K) and the same calculated magnitudes at the NEVPT2+spin orbit level (red, green and orange colours for different active spaces).

We could not perform experimental measures for each isomer, so the problem was approached theoretically and in order to assess how the spatial configuration of the complex affects the magnetic properties. we simulated the susceptibility for each 3 isomers using optimized geometries described in the literature.[38] **Figure 6.8** shows the result for the three isomers *cis*, *gauche*, *trans* compared with the experimental data of the powder and solution samples (mixed isomers). The isomer *cis* possess a higher magnetization and susceptibility than the other *gauche* and *trans* isomers. These results further corroborate the unexpected stability of cis rotamer found from crystallographic analysis.

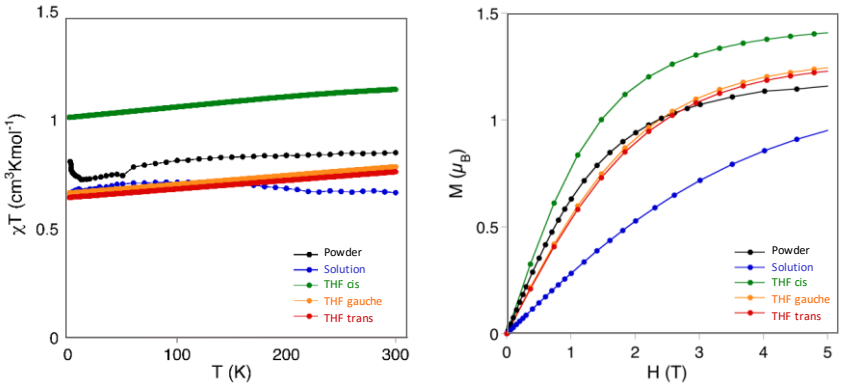

Figure 6.8. Static susceptibility (a) and magnetization (b) at 2 K measured for a powder sample of the $[NMe_4][\mathbf{2}]$ compound (black) and in THF solution (blue, magnetization at 4 K) and the same calculated magnitudes of the solutions in THF the three isomers *cis* [50], *gauche* (orange) and *trans* (red). The calculated curves at 2 K and 4 K are practically identical.

* Dynamic Magnetic properties

The study of the relaxation processes of the sample was run in AC magnetometry. Firstly we measured the real (χ') and the imaginary (χ'') susceptibility at different temperatures varying the frequency with an external field of 0.05 T (**Figure 6.9**). The representation of the χ' vs. frequency shows how an increase of temperature is reflected on the vibration of spins and how is more difficult for the system to maintain the cooperative magnetic coupling. Thus, the sensibility to the external magnetic field of the material is minor. On the other hand, the imaginary susceptibility representation shows a peak that indicates a relaxation process that decrease with the increment of the temperature indicating that the relaxation processes become faster at higher temperatures. This behaviour can be ascribed to a higher rate of phonon production in respect to phonon absorption by the lattice.

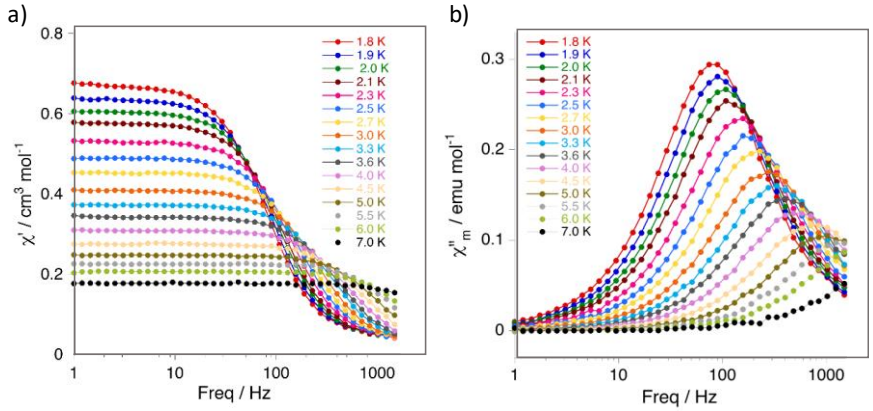

Figure 6.9. Real (left) and Imaginary [51] susceptibility measured at different frequencies (above) dependence with temperature with an external field of 0.05 T

Secondly, we always measured the real and imaginary susceptibility but, in this case, the temperature is maintaining constant to 4 K scanning the frequency at different external magnetic field (from 0 to 10 kOe). **Figure 6.10** shows the results where the maximum value for both the real and imaginary value of susceptibility do not present a significant change at different external magnetic field and the imaginary susceptibility do not present additional relaxation processes. This behaviour suggests the existence of a unique relaxation process that depends on magnetic field.

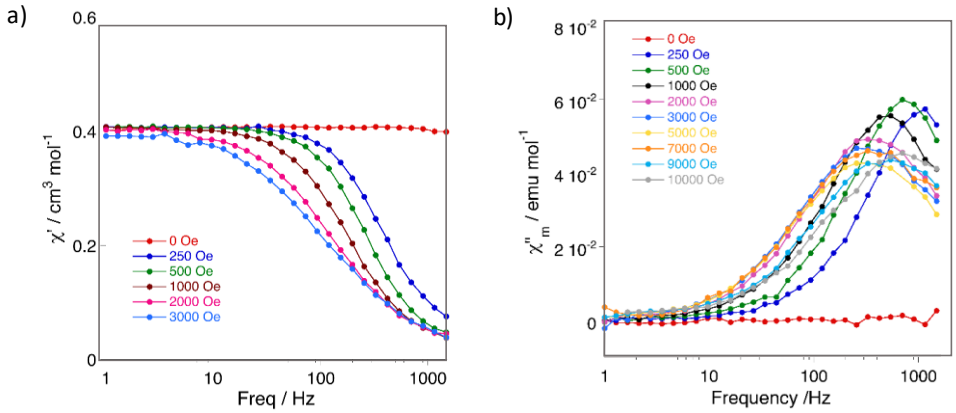

Figure 6.10. (a) Real (left) and Imaginary [51] susceptibility measured at different frequencies (above) dependence with external field with a temperature of 4 K.

* Relaxation time calculations

The relaxation time gives us information and hints on the nature and number of relaxation processes. The latter value can be directly extracted from the Cole-Cole diagram which represents the imaginary part of the susceptibility as function of the real part (**Figure 6.11**). As we expected the curve show only one maximum which confirm our previous prediction of only exist one relaxation process.

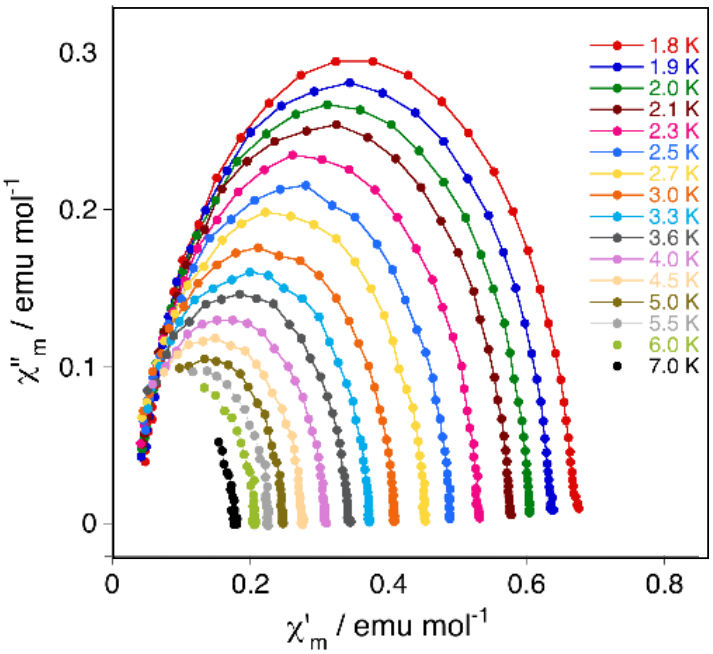

Figure 6.11. Cole-Cole diagram for a saturated THF solution of $[NMe_4][\mathbf{2}]$ under an external field of 0.05 T. (b) Sin relaxation values Spin relaxation values (τ^{-1} in s^{-1}) extracted from the Cole-Cole diagram for different temperatures using CC-fit code for saturated solution of $[NMe_4][\mathbf{2}]$ with an external field of 0.05T.

On the one hand, Cole-Cole diagram (**Figure 6.11**) together with the equations of **Appendix B** provide the required data to study the relaxation times with the temperature (**Figure 6.12a**). On the other hand, graphics of the susceptibilities *vs.* Freq at constant temperature (Figure 6.10) provide the representation of spin relaxation time *vs.* magnetic field (**Figure 6.12b**).

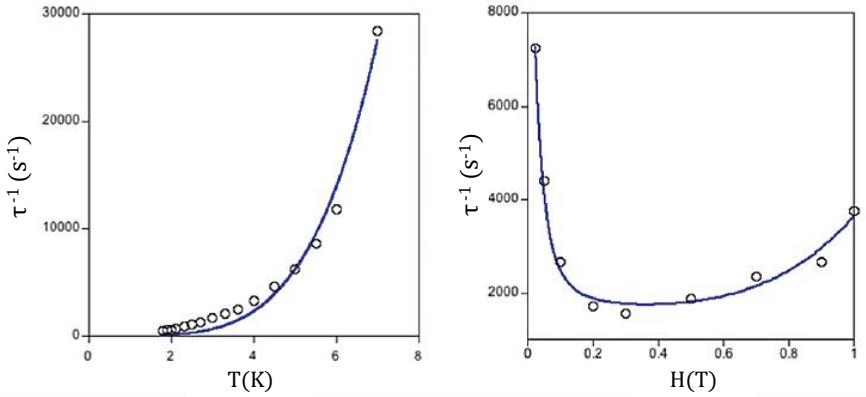

Figure 6.12. Dependence of the inverse spin-relaxation times, τ^{-1} *vs.* temperature for a saturated solution of [NMe_4][**2**] under an external field (*H*) of 0.05T (left) and with an external field at 4 K [51]. The blue lines show the fitted values using equation (5) (left) and (6) [51], respectively.

We further used a Debye generalized model to fit the relaxation times data (CC-FIT program for analytical expressions) and finally extract the spin relaxation times at each given temperature and magnetic field. Using the τ values, the spin relaxation mechanism was studied by analysing the dependence of τ on the temperature by means of the following equation assuming a constant external magnetic field *H:*

$$\tau^{-1} = AH^4 + \frac{B_2}{1 + B_1H^2} + d\frac{1 + eH^2}{1 + fH^2}T^n \qquad (4)$$

The terms of the equation refer to direct relaxation, quantum tunnelling and Raman, respectively, while Orbach phenomena related to the paired electrons was neglected because the system under study has S = ½. The Raman term which refers to the rotational contribution of spin-phonon interaction, corresponds to the field-dependent term using the Brons-van Vleck equation and the typical power-law dependence on the temperature.

Figure 6.12a shows a clear relationship with the Raman term. However, the quantum tunnelling term, which is responsible for the spin relaxation when using low external fields, appears almost negligible in this case.[51] Thus, both curves can be analysed based on the Raman contribution and including only the direct term at high external fields. Finally, the quantum tunnelling mechanism (that depends

on the intermolecular magnetic dipolar interactions) does not play an important role due to the application of an external field and the use of a solution sample with longer intermolecular distances than powder samples. As a result, in order to avoid over-parameterization in the fitting, we only used the Raman term reducing **Equation 4** as follow:

$$\tau^{-1} = CT^{n} \qquad (5)$$

where C is the Curie constant and n a factor both specifics from the material.

According to **Equation 5** the fitting of the experimental data return values of C =4.74 $s^{-1}K^{-4.45}$ and n = 4.45. The Raman term has usually n values between 4 and 9, depending on the vibrational states of the system, which is in expected range.[52]. Once we have the fitting data for the relaxation times with temperature we adjusted the field-dependent data (see **Equation 6**) with the field-dependent Raman term and with the inclusion of the direct term, which becomes predominant above 0.3 T [51].

$$\tau^{-1} = d\frac{1+eH^{2}}{1+fH^{2}}T^{4.45} + A \cdot 4 \cdot H^{4} \qquad (6)$$

The spin relaxation dependence on the external field using **Equation 6** gave rise to d = 11.75 s^{-1} (this value is constrained in the fit to be consistent with the already fitted C value), e = 150.9 T^{-2}, f = 966.0 T^{-2} and A = 490.4 $s^{-1}T^{-4}K^{-1}$ values. The $AH^{4}T$ direct term at H = 0.05 T is negligible justifying the fact that we disregarded such values in equation 6.

The fitting of relaxation time representation *vs.* temperature or magnetic field indicate values of ms for $[NMe_4]$[**2**] demonstrating its potential as SMM.

6.6 Conclusions

This work presented the synthesis, of S = 1/2 metallacarborane compound, $[NMe_4]$[**2**], as well as its complete crystallographic and magnetic characterization. With the target to identify our compound as SMM we firstly analysed the structures of the complex unveiling that despite the calculations of the energy of

all the possible isomers suggested the most stable isomer is the *trans,* the isomer present in the crystal structure is the *cis* rotamer due to:

- *Its intermolecular interactions.* our structure was compared with equivalent ones such as $[NMe_4]_2$[**2**], other salts of FESAN or the metallacarboranes of Co and Ni. As a result, we identified that the intermolecular interactions, which involve the C_C-H bond of the metallacarborane in the crystal structure, represent a significant factor that stabilizes the *cis* isomer structure.

- *Magnetic anisotropy.* The supramolecular packing which forms zig-zag chains of Fesan with the $[NMe_4]^+$ in the holes, generates an axial magnetic anisotropy around *z*-axis confirmed by theoretical calculations which enhance the magnetization and the susceptibility.

Finally, despite the crystal powder did not show spin relaxation, the magnetic characterization of the solution sample in THF presents slow relaxation of magnetization (about ms) based on one relaxation process.

In conclusion, we demonstrated that the $[NMe_4]$[**2**] presents enhanced axial anisotropy and slow relaxation times so can efficiently behave as a SMM. This work opens new and exciting ways for the use of metallocarboranes in quantum computing that also show high stability due to the extended supramolecular packing. We stress the importance to obtain a single crystal for the characterization of these compounds hence, much of the effort shall be directed to solve this issue with innovative and creative approaches. Moreover, the possibility to explore more FESAN salts pave the way toward the development of SMM with equal or even better and tunable magnetic properties.

6.7 References

(1) F. Luis, El efecto túnel en magnetismo, *REAL ACADEMIA DE CIENCIAS*, 35.

(2) N. Bohr, The quantum postulate and the recent development of atomic theory, *Nature*, **1928**.

(3) J. Gallop, SQUIDs: some limits to measurement, *Supercond. Sci. Tech.*, **2003**, 16, 1575-1582.

(4) G. Binnig, H. Rohrer, C. Gerber and E. Weibel, Surface studies by scanning tunneling microscopy, *Phys Rev. Lett.*, **1982**, 49, 57.

(5) D. Gatteschi and R. Sessoli, Quantum tunneling of magnetization and related phenomena in molecular materials, *Angew. Chem. Int. Ed.*, **2003**, 42, 268-297.

(6) J. H. Van Vleck, *The theory of electric and magnetic susceptibilities*, Clarendon Press, **1932**.

(7) P. Benioff, The computer as a physical system: A microscopic quantum mechanical Hamiltonian model of computers as represented by Turing machines, *J. Stat. Phys.*, **1980**, 22, 563-591.

(8) D. Deutsch, Quantum theory, the Church–Turing principle and the universal quantum computer, *P. R. Soc. Lond. A Mat.*, **1985**, 400, 97-117.

(9) P. A. Benioff, Decision Procedures in Quantum Mechanics, *J. Math. Phys.*, **1972**, 13, 908-915.

(10) D. Stepanenko, M. Trif and D. Loss, Quantum computing with molecular magnets, *Inorg. Chim. Acta*, **2008**, 361, 3740-3745.

(11) R. Blatt and D. Wineland, Entangled states of trapped atomic ions, *Nature*, **2008**, 453, 1008-1015.

(12) D. G. Cory, A. F. Fahmy and T. F. Havel, Ensemble quantum computing by NMR spectroscopy, *P. Natl. A. Sci.*, **1997**, 94, 1634-1639.

(13) I. L. Chuang, L. M. K. Vandersypen, X. Zhou, D. W. Leung and S. Lloyd, Experimental realization of a quantum algorithm, *Nature*, **1998**, 393, 143-146.

(14) R. Landauer, Dissipation and noise immunity in computation and communication, *Nature*, **1988**, 335, 779-784.

(15) F. Meier, J. Levy and D. Loss, Quantum computing with antiferromagnetic spin clusters, *Phys Rev. B*, **2003**, 68, 134417.

(16) T. Lis, Preparation, structure, and magnetic properties of a dodecanuclear mixed-valence manganese carboxylate, *Acta Crystallogr. B*, **1980**, 36, 2042-2046.

(17) R. Sessoli, D. Gatteschi, A. Caneschi and M. A. Novak, Magnetic bistability in a metal-ion cluster, *Nature*, **1993**, 365, 141-143.

(18) B. Barbara, L. Thomas, F. Lionti, I. Chiorescu and A. Sulpice, Macroscopic quantum tunneling in molecular magnets, *J. Magn. Magn. Mater.*, **1999**, 200, 167-181.

(19) C. Delfs, D. Gatteschi, L. Pardi and R. Sessoli, Wieghardt and KD Hanke, *Inorg. Chem*, **1993**, 32, 3099.

(20) Y. Pontillon, A. Caneschi, D. Gatteschi, R. Sessoli, E. Ressouche, J. Schweizer and E. Lelievre-Berna, Magnetization density in an iron (III) magnetic cluster. a polarized neutron investigation, *J. Am. Chem. Soc.*, **1999**, 121, 5342-5343.

(21) C. Sangregorio, T. Ohm, C. Paulsen, R. Sessoli and D. Gatteschi, Quantum Tunneling of the Magnetization in an Iron Cluster Nanomagnet, *Phys Rev. Lett.*, **1997**, 78, 4645-4648.

(22) A. Caneschi, D. Gatteschi, C. Sangregorio, R. Sessoli, L. Sorace, A. Cornia, M. Novak, C. Paulsen and W. Wernsdorfer, The molecular approach to nanoscale magnetism, *J. Magn. Magn. Mater.*, **1999**, 200, 182-201.

(23) J. M. Zadrozny, J. Niklas, O. G. Poluektov and D. E. Freedman, Millisecond coherence time in a tunable molecular electronic spin qubit, *ACS central science*, **2015**, 1, 488-492.

(24) G. Aromí, D. Aguila, P. Gamez, F. Luis and O. Roubeau, Design of magnetic coordination complexes for quantum computing, *Chem. Soc. Rev*, **2012**, 41, 537-546.

(25) E. Moreno-Pineda, C. Godfrin, F. Balestro, W. Wernsdorfer and M. Ruben, Molecular spin qudits for quantum algorithms, *Chem. Soc. Rev*, **2018**, 47, 501-513.

(26) C. Bonizzoni, A. Ghirri, K. Bader, J. Van Slageren, M. Perfetti, L. Sorace, Y. Lan, O. Fuhr, M. Ruben and M. Affronte, Coupling molecular spin centers to microwave planar resonators: towards integration of molecular qubits in quantum circuits, *Dalton Trans.*, **2016**, 45, 16596-16603.

(27) E. Jemmis and P. Pavankumar, Stability of Polyhedral borane anions and carboranes, *Proceedings of the Indian Academy of Science- Chemical Science,* Springer India, **1984**.

(28) B. Buckley, G. Fuchs, L. Bassett and D. Awschalom, Spin-light coherence for single-spin measurement and control in diamond, *Science*, **2010**, 330, 1212-1215.

(29) B. Maertz, A. Wijnheijmer, G. Fuchs, M. Nowakowski and D. Awschalom, Vector magnetic field microscopy using nitrogen vacancy centers in diamond, *Appl. Phys. Lett.*, **2010**, 96, 092504.

(30) M. S. Fataftah, J. M. Zadrozny, S. C. Coste, M. J. Graham, D. M. Rogers and D. E. Freedman, Employing forbidden transitions as qubits in a nuclear spin-free chromium complex, *J. Am. Chem. Soc.*, **2016**, 138, 1344-1348.

(31) J. M. Zadrozny and D. E. Freedman, Qubit Control Limited by Spin–Lattice Relaxation in a Nuclear Spin-Free Iron (III) Complex, *Inorg. Chem.*, **2015**, 54, 12027-12031.

(32) M. Atzori, L. Tesi, S. Benci, A. Lunghi, R. Righini, A. Taschin, R. Torre, L. Sorace and R. Sessoli, Spin dynamics and low energy vibrations: Insights from vanadyl-based potential molecular qubits, *J. Am. Chem. Soc.*, **2017**, 139, 4338-4341.

(33) M. Atzori, L. Tesi, E. Morra, M. Chiesa, L. Sorace and R. Sessoli, Room-temperature quantum coherence and rabi oscillations in vanadyl phthalocyanine: toward multifunctional molecular spin qubits, *J. Am. Chem. Soc.*, **2016**, 138, 2154-2157.

(34) M. Atzori, E. Morra, L. Tesi, A. Albino, M. Chiesa, L. Sorace and R. Sessoli, Quantum coherence times enhancement in vanadium (iv)-based potential molecular qubits: the key role of the vanadyl moiety, *J. Am. Chem. Soc.*, **2016**, 138, 11234-11244.

(35) G. Aromí Bedmar, A. Gaita-Ariņo and F. Luis Vitalla, Computación cuántica con moléculas magnéticas, *Revista Espaņola de Física, 2016, vol. 30, num. 3, p. 21-24*, **2016**.

(36) J. M. Forward, D. M. P. Mingos and A. V. Powell, Synthesis and magnetic studies of the metallocarborane sandwich salts [Fe $(C_5Me_5)_2$][$M(C_2B_9H_{12})_2$)](Me= Cr, Fe, Ni, *J. Organomet. Chem.*, **1994**, 465, 251-258.

(37) J. M. Forward, D. Michael, P. Mingos, T. E. Müller, D. J. Williams and Y.-K. Yan, Synthesis and structural characterization of metallacarborane sandwich salts with tetrathiafulvalene (ttf)[$M(C_2B_9H_{11})_2$][ttf](M= Cr, Fe, Ni), *J. Organomet. Chem.*, **1994**, 467, 207-216.

(38) A. B. Buades, V. S. Arderiu, L. Maxwell, M. Amoza, D. Choquesillo-Lazarte, N. Aliaga-Alcalde, C. Viñas, F. Teixidor and E. Ruiz, Slow-spin relaxation of a low-spin S= 1/2 Fe III carborane complex, *Chem. Comm.*, **2019**, 55, 3825-3828.

(39) M. Sawicki, W. Stefanowicz and A. Ney, Sensitive SQUID magnetometry for studying nanomagnetism, *Semicond. Sci. Tech,* **2011**, 26.

(40) R. Fagaly, Superconducting quantum interference device instruments and applications, *Rev. Sci. Instrum.*, **2006**, 77, 101101.

(41) B. Josephson, Possible new effect in superconducting tunneling, *Phys. Lett.*, **1962**, 1, 251-253.

(42) M. F. Hawthorne and T. D. Andrews, Carborane analogues of cobalticinium ion, *Chem. Commun, (London)*, **1965**, 443-444.

(43) R. N. Grimes, *Carboranes*, US, 3rd edn., **2016**.

(44) CCDC refcodes: WEKJEB ($[FeCp2^*]^+[FESAN]^-$) and YEDVUY ($[Ttf]^+[FESAN]^-$)

(45) M. F. Hawthorne, D. C. Young, T. D. Andrews, D. V. Howe, R. L. Pilling, A. D. Pitts, M. Reintjes, L. F. Warren and P. A. Wegner, .pi.-Dicarbollyl derivatives of the transition metals. Metallocene analogs, *J. Am. Chem. Soc.*, **1968**, 90, 879-896.

(46) E. J. Juárez-Pérez, R. Núñez, C. Viñas, R. Sillanpää and F. Teixidor, The Role of C–H···H–B Interactions in Establishing Rotamer Configurations in Metallabis(dicarbollide) Systems, *Eur. J. Inorg. Chem*, **2010**, 2385-2392.

(47) A. Schäfer, H. Horn and R. Ahlrichs, Fully optimized contracted Gaussian basis sets for atoms Li to Kr, *J. Chem. Phys.*, **1992**, 97, 2571-2577.

(48) F. Weigend and R. Ahlrichs, Balanced basis sets of split valence, triple zeta valence and quadruple zeta valence quality for H to Rn: Design and assessment of accuracy, *Phys. Chem. Chem. Phys.*, **2005**, 7, 3297-3305.

(49) K. D. Warren, in *Bonding forces*, Springer, **1976**, pp. 45-159.

(50) N. N. Greenwood and A. Earnshaw, *Chemistry of the Elements*, Elsevier, **2012**.

(51) S. H. J. Plesek, L. J. Todd and W.F. Wright, *Collect. Czech. Chem. Commun.*, **1976**, 3509-3515.

(52) K. Shrivastava, Theory of spin–lattice relaxation, *physica status solidi (b)*, **1983**, 117, 437-458.

(53) Y.-N. Guo, G.-F. Xu, Y. Guo and J. Tang, Relaxation dynamics of dysprosium (III) single molecule magnets, *Dalton Trans.*, **2011**, 40, 9953-9963.

(54) K. S. Cole and R. H. Cole, Dispersion and absorption in dielectrics I. Alternating current characteristics, *J. Chem. Phys.*, **1941**, 9, 341-351.

(55) C. Dekker, A. Arts, H. De Wijn, A. Van Duyneveldt and J. Mydosh, Activated dynamics in a two-dimensional Ising spin glass: Rb 2 Cu 1− x Co x F 4, *Phys Rev. B*, **1989**, 40, 11243.

(56) C. Benelli and D. Gatteschi, *Introduction to molecular magnetism: From transition metals to lanthanides*, John Wiley & Sons, **2015**.

(57) N. F. Chilton, R. P. Anderson, L. D. Turner, A. Soncini and K. S. Murray, PHI: A powerful new program for the analysis of anisotropic monomeric and exchange-coupled polynuclear d-and f-block complexes, *J. Comput. Chem.*, **2013**, 34, 1164-1175

General Conclusions

This thesis has been devoted to the synthesis and application of COSAN and FESAN derivatives.

Fast and Simple B-C Bond Formation in COSAN

- On contrary it was established, the use of trityl bromide generate a B-C bond in COSAN, in a few minutes and without any iodo derivative or palladium catalyst.

- The use of theoretical calculations was key to demonstrate our hypothesis that the precipitation of silver bromide generates a trytil stabilized carbocation that takes a hydrogen from COSAN structure and this B^+ reacts with the nearest molecule it has, included solvent molecules.

Synthesis of Metallacarborane Derivatives as Electron Acceptors

- A new generation of metallacarborane derivatives with aromatic N bonded to the cluster have been synthesized and completely characterized for the first time.

- The electrochemical characterization of these molecules unveils the possibility to accept up to five electrons in a reversible way. In addition, this characterization permitted us to assign every electron transfer step to the specific fragments of the molecules.

- Crystal characterization together with NMR, CV and UV-vis-NIR techniques have confirmed the electronic communication between the metallic centers for the products with two metallacarboranes per bipyridine.

- Finally, the high processability of the products provided from their high solubility makes these molecules comparable to fullerenes for electron transfer processes.

Highly Chlorinated Derivatives of COSAN

- The work presents the highest chloro derivatives of COSAN synthesized up to now by an easy and fast methodology. The trick point is use of protonated salt of COSAN due to its high solubility in a friendly chlorination agent SO_2Cl_2 and the use of $AlCl_3$ as the catalyst for the synthesis of [**Cl_8-1**]$^-$, [**Cl_{10}-1**]$^-$ and [**Cl_{12}-1**]$^-$ products.

- The complete NMR characterization of all the products permitted us to detect the existence of two isomers for the product [**Cl_8-1**]$^-$ and established a new chlorination order that goes against the previous theoretical studies.

- Crystal structure as well as to confirm the information provides by the NMR characterization, unveils the rotamers *trans*, *gauche1* and *gauche 2*, for the crystals [NMe_4][**Cl_8-1**], [NMe_4][**Cl_{10}-1**] and Cs[**Cl_{12}-1**], respectively less common rotamers for COSAN derivatives that appear in the literature.

- The electrochemical characterization reveals molecules with redox potential values very interesting for electrochemical application and confirms the reversibility of these electrochemical systems. In addition, the comparison of our compounds with some other chloro derivatives of COSAN found in the literature permitted us to understand how not only the number of chloro atoms in the COSAN structure but also the position of them affect the redox potential of the molecule.

- Finally, the electrochemical and thermal stability of the products unveil a wide range of possible applications for [**Cl_8-1**]$^-$, [**Cl_{10}-1**]$^-$ and [**Cl_{12}-1**]$^-$.

Chlorinated Derivative of COSAN as Catalysts for Water Splitting

- Preliminary studies unveil the potential of the highly chlorinated derivatives of COSAN as electrocatalysts for oxygen evolution reactions.

- The seek of an oxidation process able to oxide the most external layers of graphite surface permitted us to construct a chemical scaffold on it. In addition, the high affinity of the metallacarboranes for the amines lead the final functionalization of graphite with chlorinated derivatives of COSAN.

- The study of the linear sweep voltammetry of these functionalized working electrodes unveils the high catalytic power of these compounds. In addition, the stability of these functionalized graphites to the electrochemical processes put on the table the real possibility to use of these electrodes for real electrochemical applications such as water splitting.

FESAN as Single-Molecule Magnet.

- The work presents the synthesis and one of the few (three) crystal characterizations that exist for FESAN. The crystal characterization of $[NMe_4][\mathbf{2}]$ permits us to study the magnetic anisotropy of the molecules and the experimental study of the relaxation time of the molecule. The work unveils a Single-molecule magnet with axial anisotropy and ms order of relaxation times

Appendix A

A.1.List of Publications

- Ana B. Buades, I. Fuentes, Clara Viñas and Francesc Teixidor. "Metallacarboranes as catalysts for oxygen evolution reactions" *In preparation*

- Ana B. Buades, Clara Viñas and Francesc Teixidor. "Highly chlorinated derivatives of COSAN" *Submitted*

- Ana B. Buades, Zsolt Kelemen, Victor S. Arderiu, Adnana Zaulet, Clara Viñas and Francesc Teixidor. "A fast and simple B-C bond-forming in metallacarboranes avoiding halometallacarboranes and transition metal catalysts" *Dalton Trans.* **2020**, 49, 3525-3531 (DOI: 10.1039/C9DT04695J).

- Ana B.Buades, Victor S. Arderiu, Lindley Maxwell, Martín Amoza, Duane Choquesillo-Lazarte, Núria Aliaga-Alcalde, Clara Viñas Francesc Teixidor and Eliseo Ruiz. "Slow-spin relaxation of a low-spin S = ½ Fe^{III} carborane complex" *Chem. Commun.,* **2019**, 55, 3825 (DOI:10.1039/c9cc01123d)

- Ana B. Buades, Victor S. Arderiu, David Olid-Britos, Clara Viñas, Reijo Sillanpää, Matti Haukka, Xavier Fontrodona, Marcos Paradinas, Carmen Ocal and Francesc Teixidor "Electron Accumulative Molecules". *J. Am. Chem. Soc.* **2018**, 140, 8, 2957-2970 (DOI: 10.1021/jacs.7b12815)

A.2. Contributions to Scientific Events

- "Multielectron-acceptors in boron chemistry" Oral Presentation at international Conference on Phosphorous, Boron and Silicon (PBSi2018). 10-12 December **2018**

- "Metallacarboranes, new non-fullerene acceptors" Flash presentation at Severo Ochoa Summer School on Material for Energy (MATENER). 17-20 September **2018**, ICMAB, Barcelona, Spain.

- "Metallacarboranes, a new electron acceptor generation" Oral and Poster Presentation.at Jornadas Doctorales del Departamento de Química. 30 May-1 Juny **2018**, Barcelona):

- "Metal·lacarborans com transferidors d'electrons (Metallacarboranes as electron-transfers)" Oral Presentation at Desena trobada de joves investigadors dels Països Catalans. 29-30 January **2018**, Sitges, Barcelona, Spain.

- "Boron compounds for electrochemical applications" Flash presentation at XXXVI Reunión Bienal de la Real Sociedad Española de Química. 25-29 Juny **2017**, Sitges, Barcelona, Spain.

- "Luz, difracción, cristales y muchas cosas bonitas (Light, difraction, crystals and many fancy stuff)" Oral presentation at Festa de la Ciència. 27-28 May **2017** at Parc de la Ciutadella, Barcelona, Spain.

- "New series of electroactive electrolytes for molecular electronics" Poster and Flash presentation at 7th European Conference on Boron Chemistry (Euroboron7). Best flash presentation. 4August- 8September **2016**, Suzdal, Moscow.

- "Chlorinated derivatives of COSAN with electrochemical applications" Poster presentation at 5th International School of Crystallization of Granada. 29May-3Juny **2016**, Granada, Spain.

- "Dye Sensitized Solar Cells" Presentation at Organic Electronics Meeting at ICMAB (ORGI). 23-24 November **2015**, ICMAB, Spain.

Appendix B

. Chapter 2

NMR characterization of NMe_4[4].

^{1}H-NMR spectrum of [NMe_4][**4**].

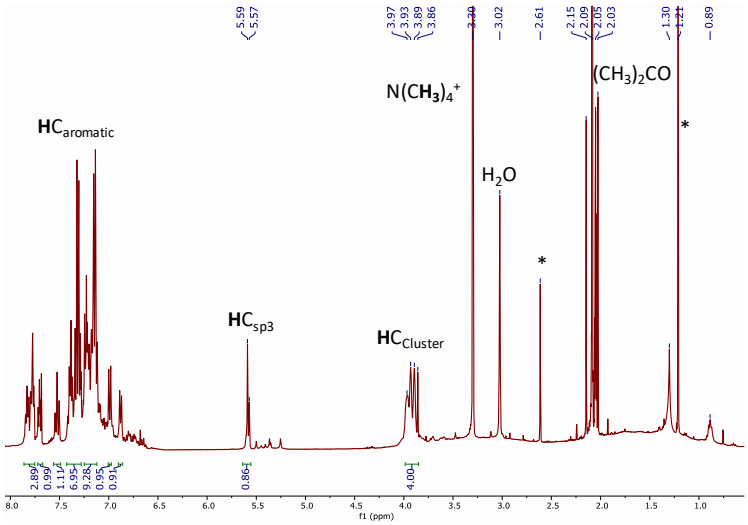

^{1}H-NMR amplified spectrum of [NMe_4][**4**]$^-$.

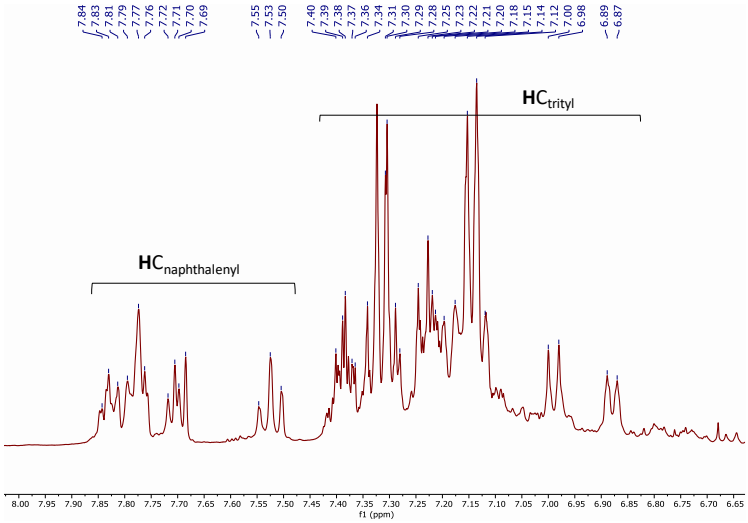

^{11}B-{^{1}H}-NMR spectrum of [NMe$_4$][**4**]$^-$.

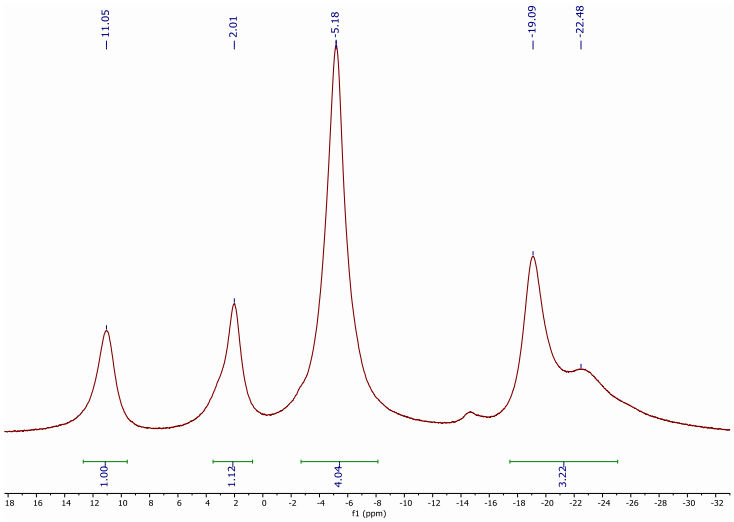

NMR characterization of NMe$_4$[**5**].

^{13}C{^{1}H}-NMR of compound [NMe$_4$][**5**]$^-$.

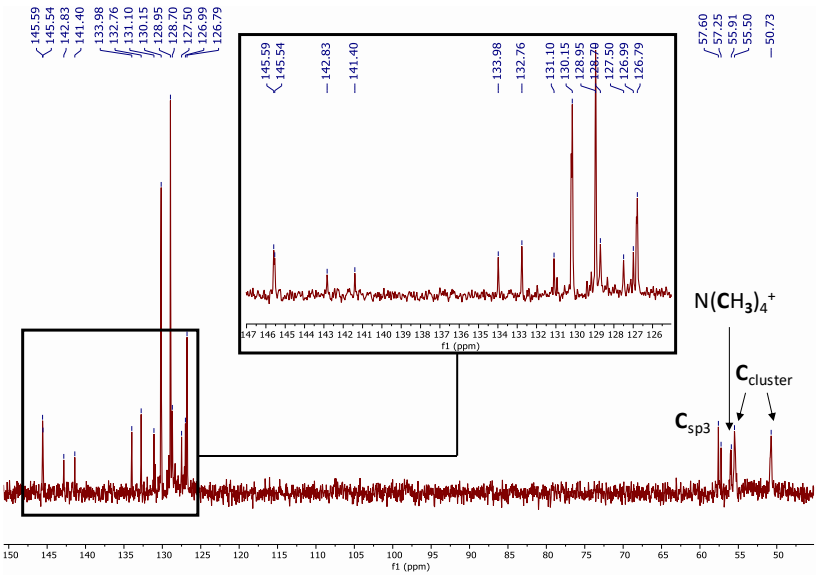

$^{13}C\{^{1}H\}$-NMR amplified spectrum of compound $[NMe_4][\mathbf{5}]^-$ with the complete characterization of the isomers *ortho* and *meta*.

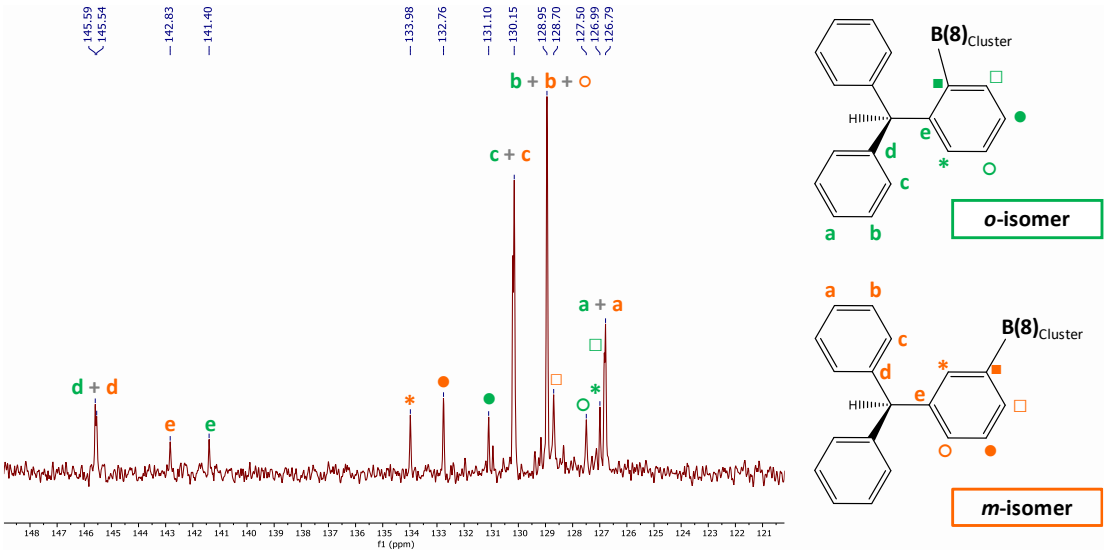

^{1}H COSY spectrum of $[NMe_4][\mathbf{5}]^-$.

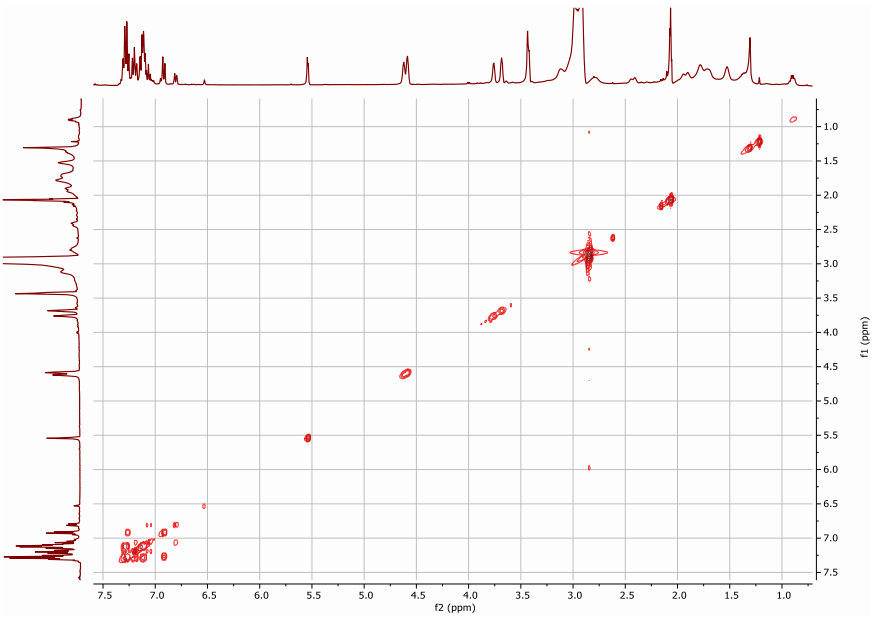

^{1}H COSY amplified spectrum of [NMe_4][**5**]$^{-}$.

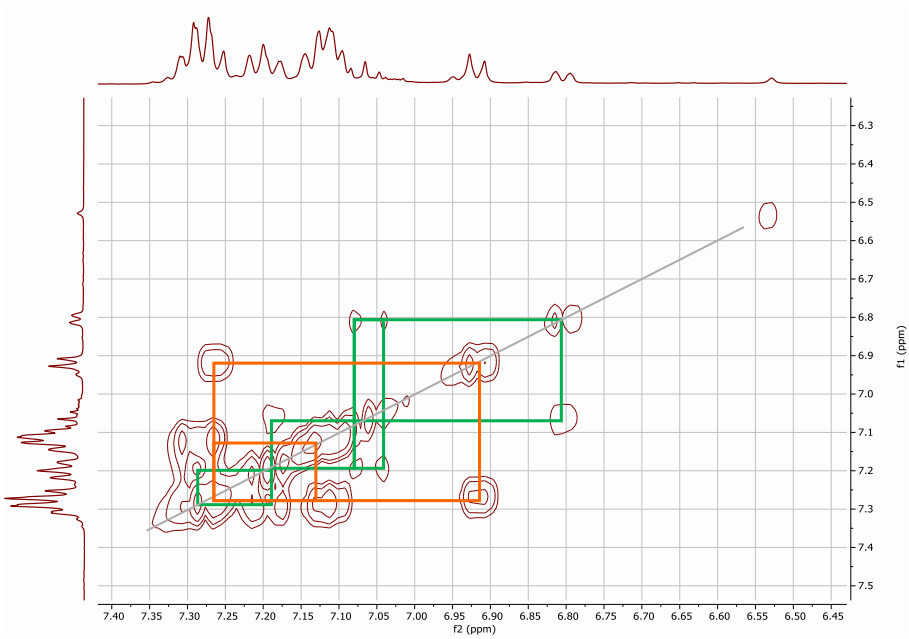

^{1}H-^{13}C HSQC spectrum of [NMe_4][**5**]$^{-}$.

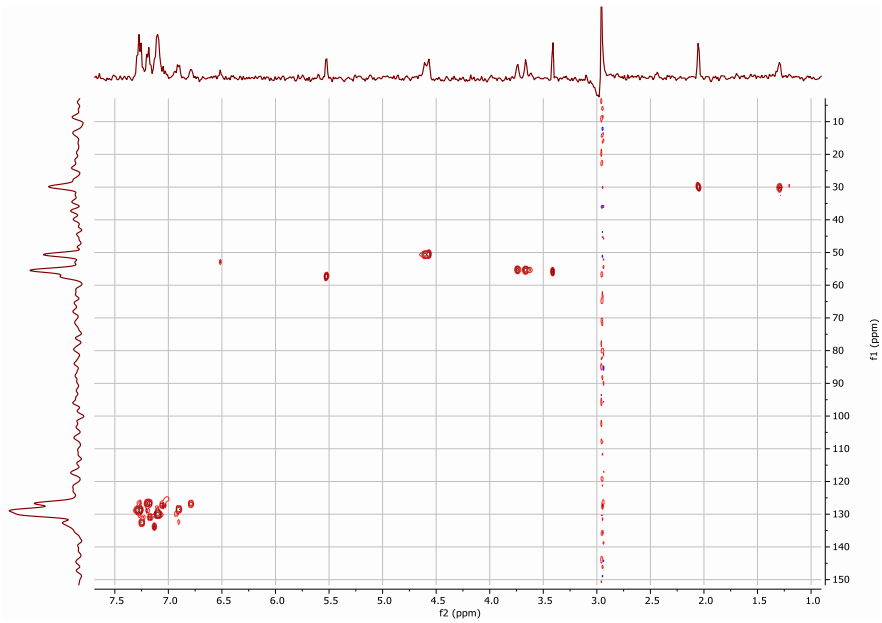

^{1}H-^{13}C HSQC amplified spectrum of [NMe_4][**5**]$^{-}$.

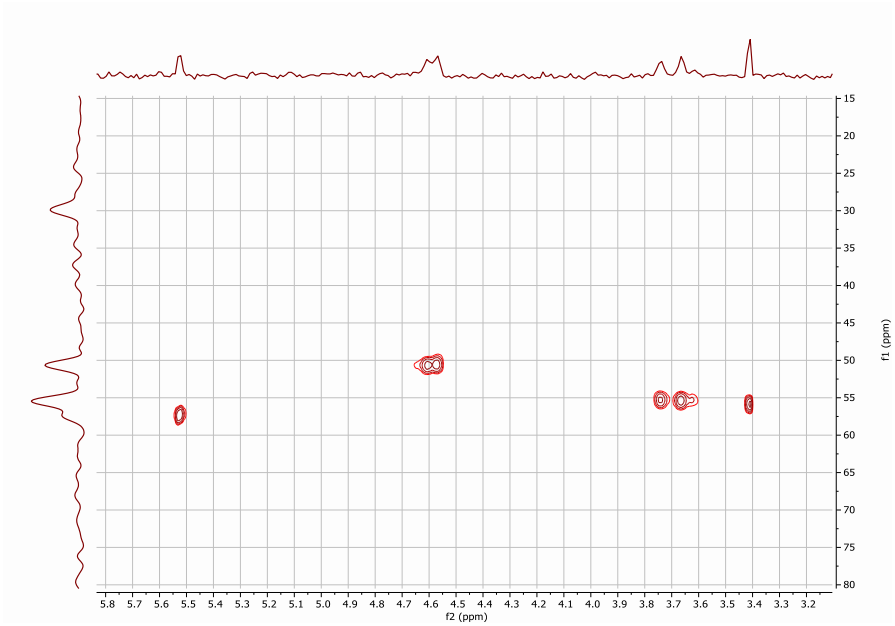

^{1}H-^{13}C HSQC amplified spectrum of [NMe_4][**5**]$^{-}$.

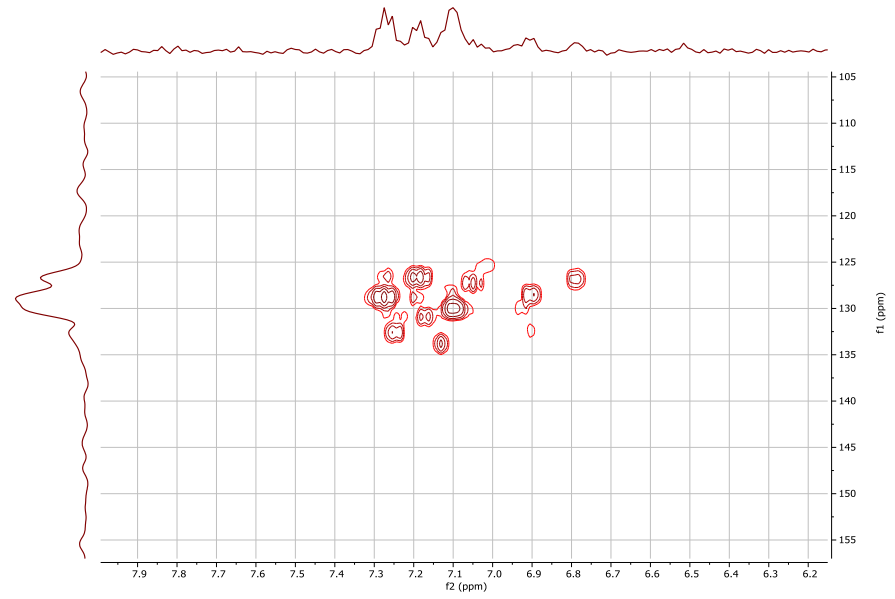

NMR characterization of Cs[7].

$^{3}C\{^{1}H\}$-NMR of compound Cs[**7**].

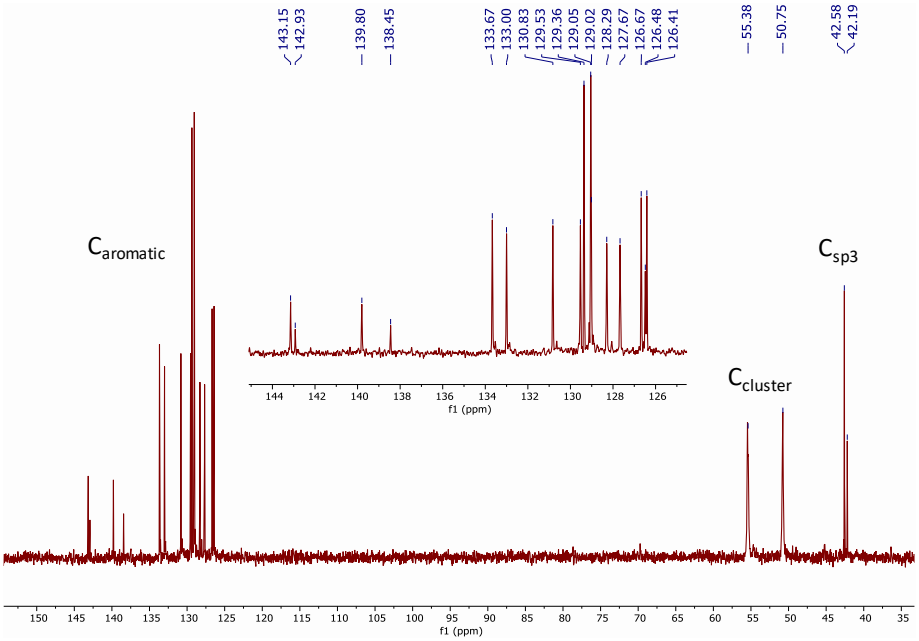

^{1}H-COSY spectrum of compound Cs[**7**].

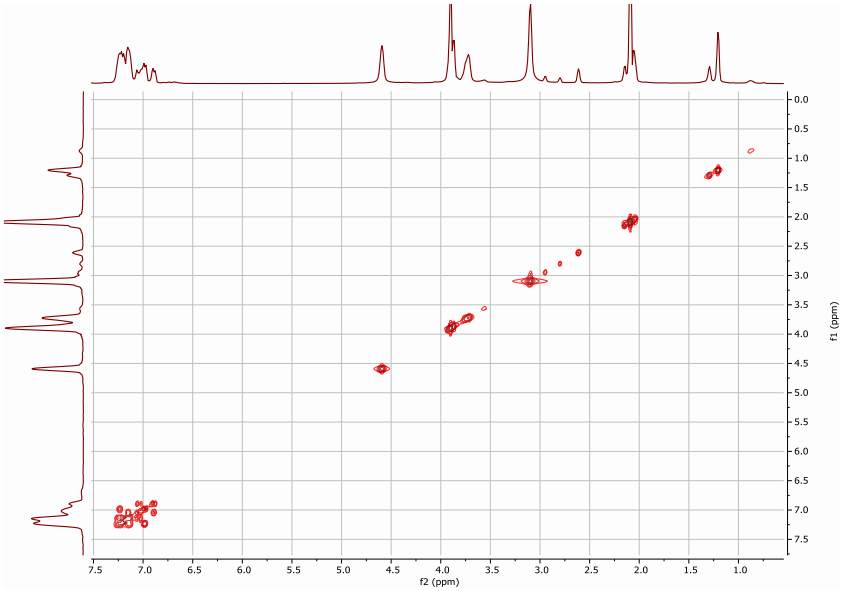

^{1}H-COSY amplified spectrum of compound Cs[**7**].

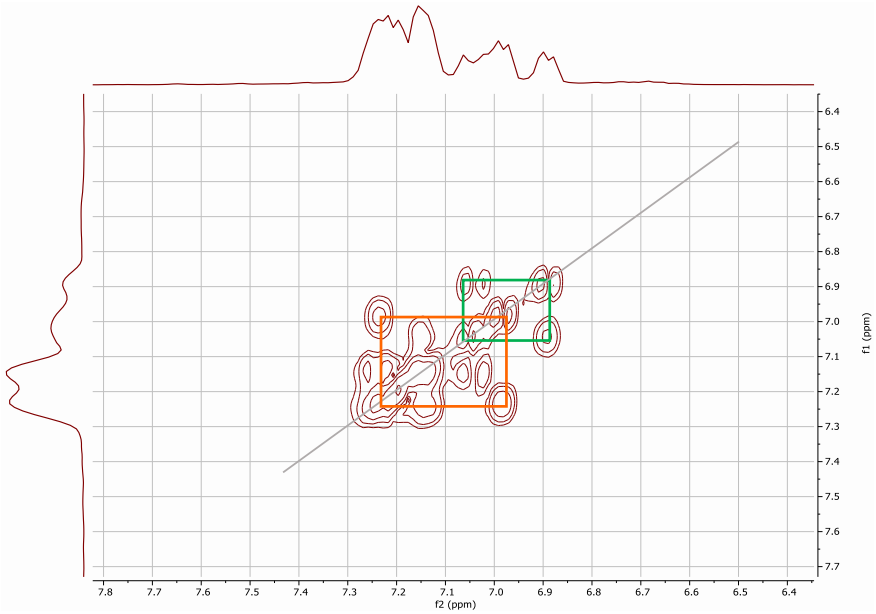

^{1}H-^{13}HSQC spectrum of compound Cs[**7**].

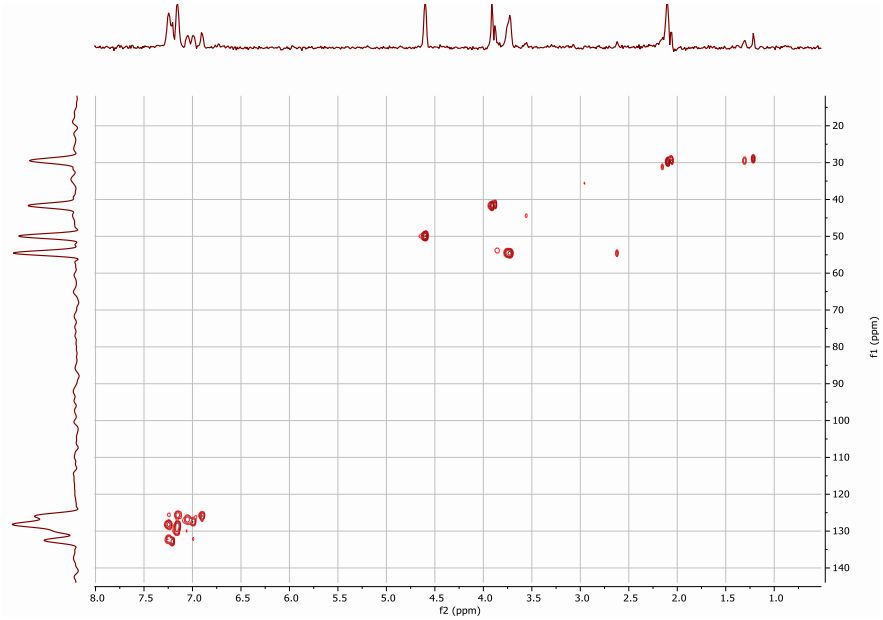

Very preliminary reaction studies of Ag[1] with different electrophiles.

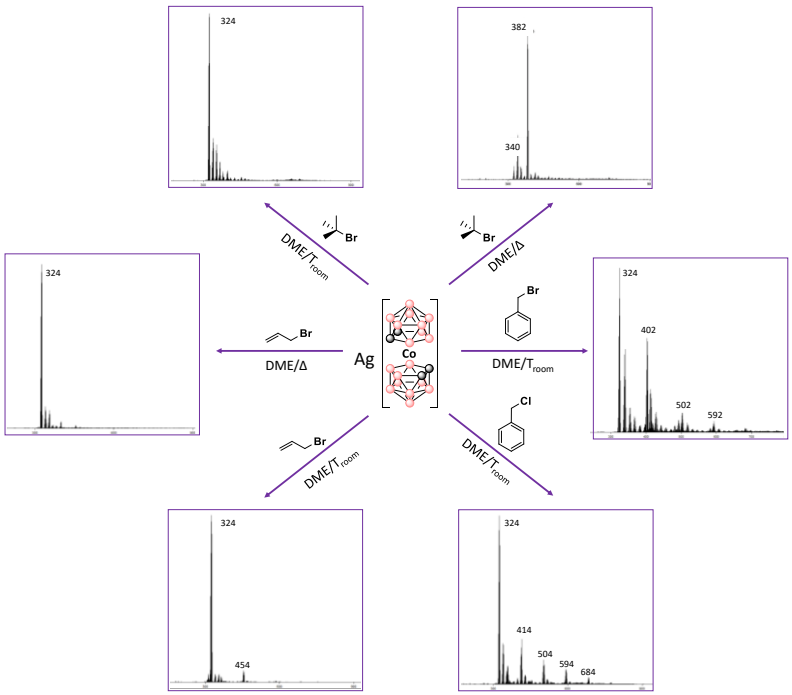

Calculation to demonstrate the quantitative behaviour of MALDI-TOF analysis in COSAN derivatives.

$$h' + h'' + h''' + h'''' = x$$

$$x \rightarrow 100$$

The result of the addition of different peaks heights is:

$$62 + 53 + 27 + 12 + 3 = 157$$

$$157 \rightarrow 100\%$$

Relation Cosane:Bn (1:1)→ $[Cosan] = [Bn]$

$$[Cosan] + [Bn] = 0{,}62[Cosan] + 0{,}53[CosanBn] + 0{,}27[CosanBn_2] + 0{,}12[CosanBn_3] + 0{,}03[CosanBn_4]$$

$$[Cosan] + [Bn] = [Cosan] \cdot (0{,}62 + 0{,}53 + 0{,}27 + 0{,}12 + 0{,}03) + [Bn] \cdot (0{,}53 + 0{,}54 + 0{,}36 + 0{,}12)$$

$$[Cosan] + [Bn] = 1{,}57[Cosan] + 1{,}55[Bn]$$

$$[Cosan] - 1{,}57[Cosan] = 1{,}55[Bn] - [Bn]$$

$$[Bn] = -\frac{0{,}57[Cosan]}{0{,}55} \rightarrow = [Bn] = -1{,}03[Cosan]$$

Chapter 3 and

Crystallographic details of compounds 10, 11, 12, 13, 16 and 17.

	10	**11**	**12**	**13**	**16**	**17**
empirical formula	$C_9H_{26}B_{18}CoN$	$C_9H_{26}B_{18}FeN$	$C_{17}H_{35}B_{18}CoN_2O$	$C_{30}H_{63}B_{36}Fe_2N_5O$	$C_{26}H_{66}B_{36}Co_2N_2O_2$	$C_{20}H_{53}B_{36}Fe_2N_3$
fw	401.82	398.74	536.98	1010.71	945.82	836.51
temp (K)	123(2)	100	120(2)	100	170(2)	100
λ(Å)	0.71073	0.71073	0.71073	0.71073	0.71073	0.71073
cryst syst	Monoclinic	Monoclinic	Orthorhombic	Monoclinic	Monoclinic	Orthorhombic
space group	$P2_1/n$	$P2_1/n$	$P2_12_12_1$	Pc	$P2_1/n$	Pbca
***a* (Å)**	6.9140(2)	6.8607(17)	12.2131(2)	12.295(6)	12.2514(4)	13.293(9)
***b* (Å)**	25.9050(5)	52.326(12)	12.3627(2)	11.814(6)	17.1579(5)	24.939(17)
***c* (Å)**	11.1660(4)	11.328(3)	37.7627(7)	18.592(12)	13.0272(4)	25.915(17)
β (dreg)	90.356(2)	90.658(5)	90	99.332(10)	114.8840(10)	90
***V* (Å^3)**	1999.87(10)	4066.5(17)	5701.67(19)	2665(3)	2484.19(13)	8592(10)
Z	4	8	8	2	2	8
ρ_{calc} (Mg/m^3)	1.335	1.303	1.251	1.260	1.264	1.293
μ(Kα) (mm^{-1})	0.854	0.737	0.620	0.580	0.701	0.702
No. reflns.	10785	28073	28104	32964	25212	49719
Unique reflns.	3515	9333	13955	12527	6672	9361
GOOF (F^2)	1.046	1.099	1.016	1.024	1.061	0.985
R_{int}	0.0528	0.0821	0.0552	0.0435	0.0687	0.4326
R1[a] ($I \geq 2\sigma$)	0.052	0.0717	0.0384	0.0470	0.0736	0.0837
wR2[b] ($I \geq 2\sigma$)	0.1119	0.1543	0.0925	0.1057	0.1579	0.1730

Crystallographic details of compounds $[NMe_4][Cl_8\text{-}1]$, $[NMe_4][Cl_{10}\text{-}1]$ and $Cs[Cl_{12}\text{-}1]$.

	$[NMe_4][Cl_8\text{-}1]$	$[NMe_4][Cl_{10}\text{-}1]$	$Cs[Cl_{12}\text{-}1]$
Identification code	BB025	BB20	BB022_2on
Chemical formula	$C_8H_{26}B_{18}Cl_8CoN$	$C_8H_{24}B_{18}Cl_{10}CoN$	$C_9H_{22}B_{36}Cl_{26}Co_2Cs_2$
Formula weight	673.41 g/mol	742.29 g/mol	1824.80 g/mol
Temperature	280(2) K	293(2) K	274(2) K
Wavelength	0.71076 Å	0.71076 Å	0.71076 Å
Crystal size	0.020 x 0.020 x 0.270 mm	0.080 x 0.080 x 0.370 mm	0.020 x 0.040 x 0.200 mm
Crystal habit	orange prism	red-orange needle	orange needle
Crystal system	orthorhombic	triclinic	monoclinic
Space group	P 21 21 21	P -1	P 1 21/n 1
Unit cell dimensions	a = 12.791(7) Å α = 90° b = 14.768(8) Å β = 90° c = 15.060(8) Å γ = 90°	a = 7.627(12) Å α = 104.93(7)° b = 13.17(3) Å β = 95.44(5)° c = 16.30(2) Å γ = 94.64(8)°	a = 16.57(2) Å α = 90° b = 7.911(10) Å β = 98.39(6) c = 24.35(3) Å γ = 90°
Volume	2845.(3) $Å^3$	1565.(5) $Å^3$	3158.(7) $Å^3$
Z	4	2	2
Density (calculated)	1.572 g/cm^3	1.574 g/cm^3	1.919 g/cm^3
Absorption coefficient	1.361 mm^{-1}	1.409 mm^{-1}	2.784 mm^{-1}
F(000)	1336	732	1724

Chapter 5

Linear Sweep Voltametry (LSV) of functionalized graphites without any treatment on the data.

LSV using with Ag/AgCl as reference electrode, Pt wire as counter electrode and the functionalized graphite rods with NEt_3 and metallacarboranes as working electrodes. The experiment was carried out in a) 0.1M Na_2SO_4 and b) 1M KOH.

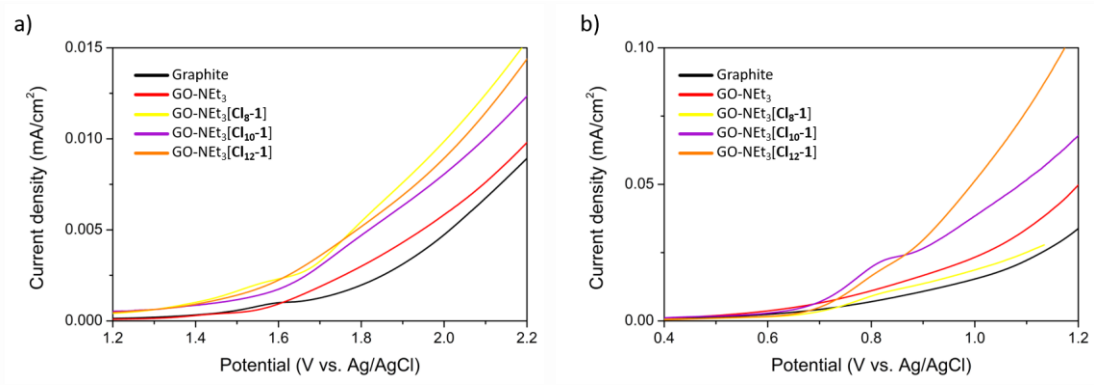

LSV using with Ag/AgCl as reference electrode, Pt wire as counter electrode and the functionalized graphite rods with NH_2EtNH_2 and metallacarboranes as working electrodes. The experiment was carried out in a) 0.1M Na_2SO_4 and b) 1M KOH.

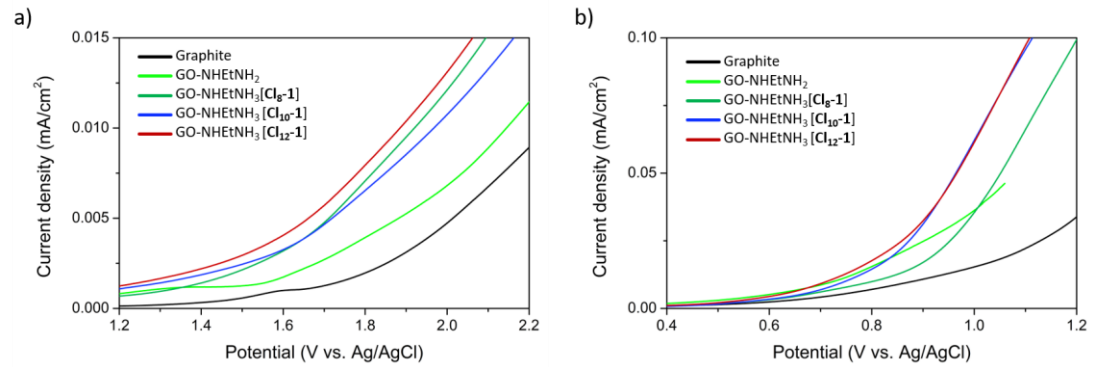

LSV using with Ag/AgCl as reference electrode, Pt wire as counter electrode and the functionalized graphite rods with NH_2PhNH_2 and metallacarboranes as working electrodes. The experiment was carried out in a) 0.1M Na_2SO_4 and b) 1M KOH.

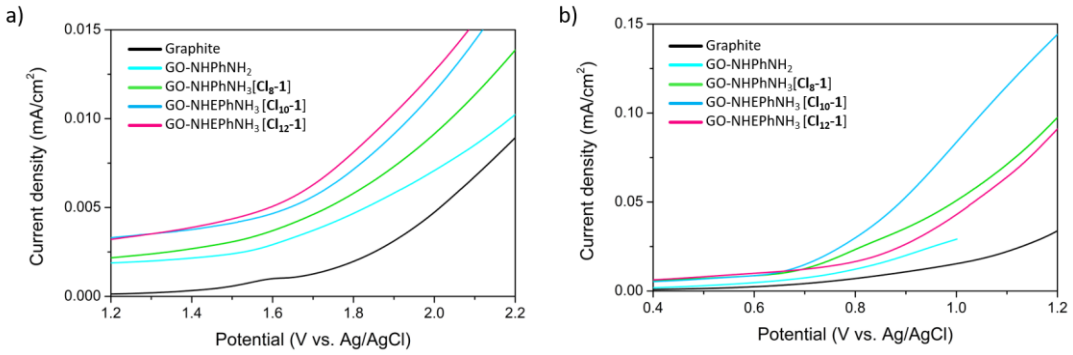

Chapter 6

The AC susceptibility data were analyzed within the extended Debye model using the CC-fit code[53] in which a maximum in the out-of-phase component χ_M'' of the complex susceptibility is observed when the relaxation time τ equals $(2\pi\nu)^{-1}$.[54,55] The Cole-Cole expression is introduced to describe distorted Argand plots,

$$\chi_{ac}(w) = \chi_S + \frac{(\chi_T - \chi_S)}{1 + (i\omega\tau)^{1-\alpha}} \quad (1)$$

where $\omega = 2\pi\nu$, χ_T and χ_S are the isothermal and adiabatic susceptibilities *i.e.*, the susceptibilities observed in the two limiting cases $\nu \rightarrow 0$ and ∞, respectively. The α parameter (between 0 and 1) describes the distribution of relaxation times, wider distribution larger α. If α is equal to 0 only one single τ value. The frequency dependence[56,57] of χ_M' and χ_M'' can be split into:

$$\chi_M'(\omega) = \chi_S + \frac{(\chi_T - \chi_S)[1 + (\omega\tau)^{1-\alpha}\sin(\pi\alpha/2)]}{1 + 2(\omega\tau)^{1-\alpha}\sin\left(\frac{\pi\alpha}{2}\right) + (\omega\tau)^{2-2\alpha}} \quad (2)$$

$$\chi_M''(\omega) = \chi_S + \frac{(\chi_T - \chi_S)[(\omega\tau)^{1-\alpha}cos(\pi\alpha/2)]}{1 + 2(\omega\tau)^{1-\alpha}sin(\pi\alpha/2) + (\omega\tau)^{2-2\alpha}} \quad (3)$$

The relaxation process refers to the time a material spend to arrive to magnetic equilibrium after been applied a magnetic field and it was determinated by the equation 4.

$$\tau^{-1} = AH^4 + \frac{B_2}{1 + B_1H^2} + d\frac{1 + eH^2}{1 + fH^2}T^n \quad (4)$$

The terms of the equation refer to direct relaxation, quantum tunnelling and Raman, respectively. Once the data are represented, they can be fitted and the equation values obtained.

References:

(53) Y.-N. Guo, G.-F. Xu, Y. Guo and J. Tang, Relaxation dynamics of dysprosium (III) single molecule magnets, *Dalton Trans.*, **2011**, 40, 9953-9963.

(54) K. S. Cole and R. H. Cole, Dispersion and absorption in dielectrics I. Alternating current characteristics, *J. Chem. Phys.*, **1941**, 9, 341-351.

(55) C. Dekker, A. Arts, H. De Wijn, A. Van Duyneveldt and J. Mydosh, Activated dynamics in a two-dimensional Ising spin glass: Rb 2 Cu 1− x Co x F 4, *Phys Rev. B*, **1989**, 40, 11243.

(56) C. Benelli and D. Gatteschi, *Introduction to molecular magnetism: From transition metals to lanthanides*, John Wiley & Sons, **2015**.

(57) N. F. Chilton, R. P. Anderson, L. D. Turner, A. Soncini and K. S. Murray, PHI: A powerful new program for the analysis of anisotropic monomeric and exchange-coupled polynuclear d-and f-block complexes, *J. Comput. Chem.*, **2013**, 34, 1164-1175